

# **Flow-induced structuring of dense protein dispersions**

**Promotor**

Prof. dr. ir. R.M.Boom

Hoogleraar Levensmiddelenproceskunde, Wageningen Universiteit

**Co-promotor**

Dr. ir. A.J. van der Goot

Universitair docent, sectie Proceskunde, Wageningen Universiteit

**Promotiecommissie**

Prof. dr.-ing. H.P. Schuchmann

Universität Karlsruhe, Duitsland

Prof. dr. M.A. Cohen Stuart

Wageningen Universiteit

Prof. dr.ir. M.A.J.S. van Boekel

Wageningen Universiteit

Dr. T. Jongsma

Friesland Foods Corporate Research, Deventer

Dit onderzoek is uitgevoerd binnen de onderzoekschool VLAG.

Julita M. Manski

# **Flow-induced structuring of dense protein dispersions**

Proefschrift  
ter verkrijging van de graad van doctor  
op gezag van de rector magnificus  
van Wageningen Universiteit,  
Prof. dr. M.J. Kropff,  
in het openbaar te verdedigen  
op woensdag 16 mei 2007  
des namiddags te half twee in de Aula.

Julita M. Manski

Flow-induced structuring of dense protein dispersions

Thesis Wageningen University, The Netherlands, 2007 - with Dutch and Polish summary

Cover: Modified photograph of a fibrous macrostructure comprising calcium caseinate and palm fat after shearing and crosslinking (see also Figure 2A in Chapter 5).

ISBN 90-8504-610-6

*voor Babcia Leokadia*

*voor Ma en Pa*



*Een mens hoeft niet alles alleen te doen,  
hij moet alleen alles doen wat hij kan.*

Uit Bijdehandboekje voor jonge christenen (1997), naar Efeziërs 4:16.



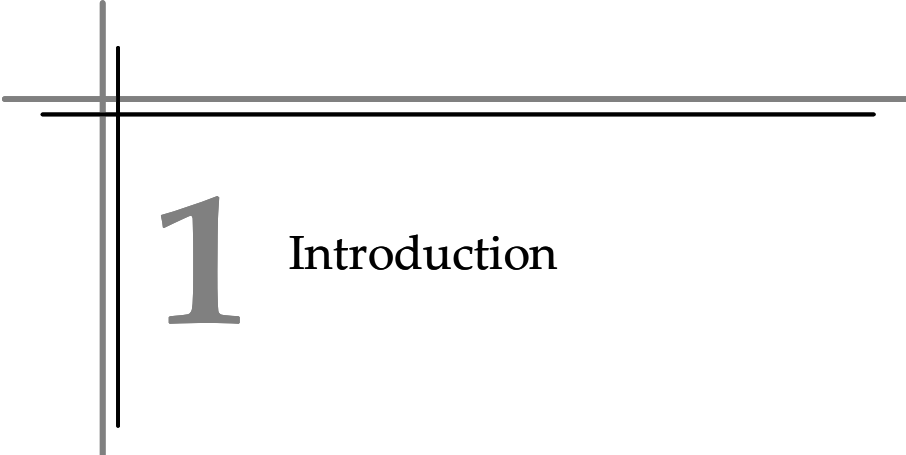


---

# Contents

1	Introduction	11
2	Influence of dispersed particles on small and large deformation properties of concentrated caseinate composites	23
3	Influence of mixing during enzymatic gelation of caseinate-water and caseinate-water-fat systems	53
4	Formation of fibrous materials from dense calcium caseinate dispersions	79
5	Influence of process parameters on formation of fibrous materials from dense calcium caseinate dispersions and fat	105
6	Factors influencing shear-induced anisotropy in dense caseinate dispersions	137
7	Advances in structure formation of anisotropic protein-rich foods through novel processing concepts	165
	Summary	195
	Streszczenie	201
	Samenvatting	207
	Dankwoord	215
	Publication List	219
	Training Activities	221
	Curriculum Vitae	222





# 1 Introduction

## 1. Protein-rich foods

Food products are made of a broad range of ingredients, of which the major categories are proteins, polysaccharides and lipids (fats and oils). Of these, proteins are major ingredients with respect to their nutritional value and their role in the formation of food textures.<sup>1</sup>

Recently, foods comprising a relatively high concentration of protein have gained increased interest with both the food industry and researchers. Consumption of protein-rich foods is associated with health benefits, such as reduction of food intake due to fast saturation<sup>2-4</sup> and prevention of muscle loss.<sup>5</sup> However, the implementation of high concentrations of protein imposes technological challenges to create tasteful and palatable products with attractive textures, preferably while preserving the nutritional value of the proteins. In addition, many protein-rich foods, such as meat, require a large investment of natural resources for their production. Preparation of similar products from alternative sources, for example vegetable proteins, would mean a step forward in sustainable food production.

Whether inspired by health or sustainability reasons, the creation of attractive, palatable and stable food textures is the key aspect in developing novel food products.

## 2. Food texture is the result of food structure

Food *texture* is manifested during consumption of foods where the complex interactions between various senses, such as vision, hearing and tasting, determine the sensory properties of products.<sup>1</sup> Therefore, food texture is a subjective perception. In contrast, food *structure* can be regarded as an objective feature of foods, namely the spatial organization of the building blocks present in foods. Food structures cover various length scales comprising a microscale ( $< 1 \mu\text{m}$ ), mesoscale ( $1\text{-}10^3 \mu\text{m}$ ) and macroscale ( $> 1 \text{mm}$ ).<sup>6</sup> The texture is strongly influenced by the structure on all these length scales. Not only should a product be visually appealing to consumers (macroscale), but also the meso- and microstructures are important as one can orally perceive particles from several micrometers in size and up.<sup>7</sup>

The relevance of the various length scales has large implications for the design and creation of novel food structures, and the characterization of food structures in general. The macrostructure is mainly determined by the processing conditions whereas the microstructure is mostly influenced by the ingredients. Both processing and the ingredients affect the mesostructure of foods. The evaluation of the final food product requires the use of various techniques to probe different length scales (Figure 1). Rheological, mechanical and microscopic techniques appear appropriate measuring methods.

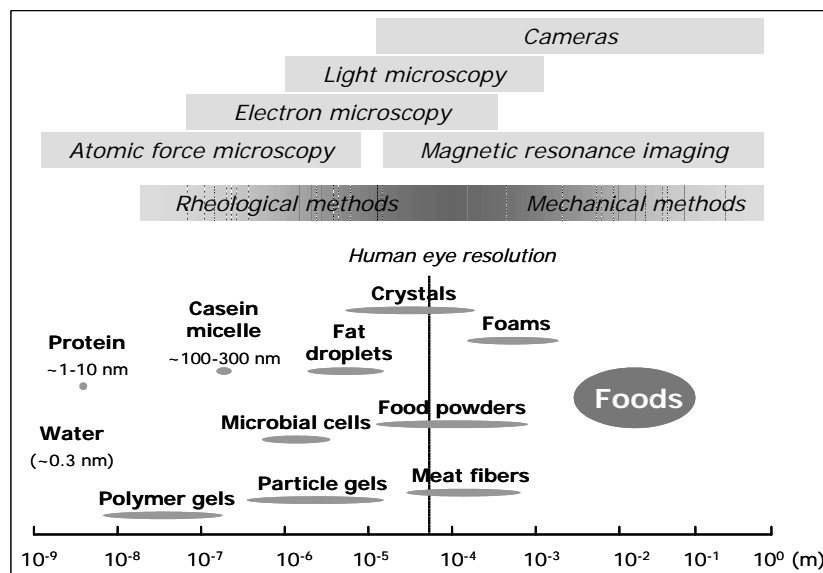


**Figure 1** Approximate length scales of structural elements used in foods and of possible techniques to probe food structures (figure adapted from Aguilera<sup>6</sup>).

In general, a distinction can be made between isotropic and anisotropic structures, where the former structures have equal properties in all directions (e.g. cheese) and the latter structures have different properties that depend on the orientation (e.g. meat). The microstructure of cheese can be classified as a bi-dispersed, almost bi-continuous, structure where both protein and fat are present as interconnected networks.<sup>8</sup> Meat has a highly fibrous structure, having alignment already at the

level of the size of proteins.<sup>9</sup> Figure 2 depicts schematically examples of isotropic and anisotropic structures that can be encountered in foods.

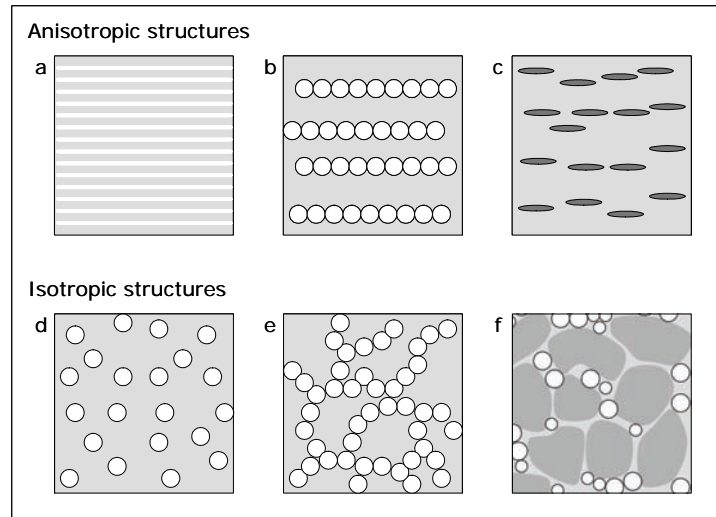


**Figure 2** Schematic examples of anisotropic and isotropic structures (micro/mesoscale) that can be encountered in systems based on oil-in-water (b, d, e, f) or water-in-water (a, f) emulsions or suspensions (c). In general, anisotropic structures are found in products like meat and fish whereas isotropic structures are encountered in emulsion-based products, such as mayonnaise, ice cream, and cheese.

### 3. Food structure formation

The formation of food structures involves the smart use of appropriate ingredients and processing to control the spatial arrangement of the building blocks of foods. An improved control of food structure may give opportunities for innovations in food products.

It is currently acknowledged that food texture should be the driver for the creation of novel foods.<sup>1,10</sup> This is in contrast with the traditionally used approach based on optimizing existing equipment or using new ingredients to obtain novel structures. Figure 3 illustrates this approach starting from defining the desired texture attributes for the new food product based on, for example, consumers' wishes. From there, the structure should be designed, and subsequently, created using the appropriate ingredients and processing conditions. Therefore, insights in the

relations between ingredient properties and processing are of utmost importance for designing food structures. This thesis focuses exactly on this aspect for the structure formation of protein-rich structures using a systematic approach (Figure 3).

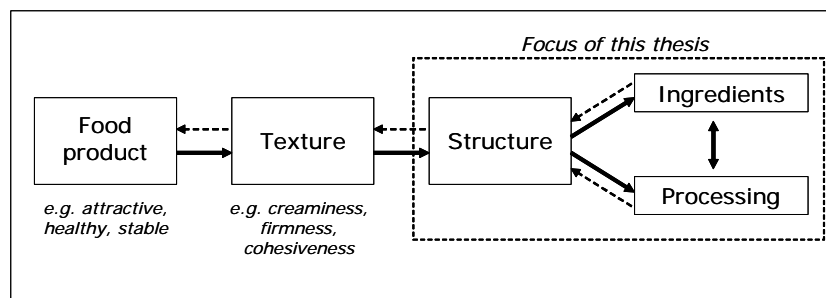


**Figure 3** Schematic overview of routes to develop new food products. The solid arrows indicate the new approach to design and create food products, which starts from the attributes of food products and textures. The dotted arrows denote the traditional route for creating foods, which is based on the optimization of equipment and ingredients. This thesis focuses on the interactions between ingredients (i.e. proteins) and processing conditions for the formation of novel food structures.

### 3.1 Food structuring processes

Food structure formation results from the interactions between ingredient properties and processing conditions. Till now, most research is focused on the development of ingredients rather than on the development of dedicated structuring processes.

The food processes traditionally used are often based on processes that are derived or adapted from the chemical industry<sup>7</sup>, such as mixing and extrusion. In these processes, ingredients are often treated in such a way that effective mixing is obtained using low energy inputs.

Nevertheless, applying flow that deforms a material and the structural elements inside the material is by far the most important way to induce structure in a material. The difference in processing between Gouda cheese and Mozzarella cheese may illustrate the effect of different flows on the spatial organization of protein and fat, thus structure formation of these cheeses. Cutting the curd after

coagulation, followed by pressing, yields a bi-continuous protein-fat structure after ripening as encountered in Gouda cheese, whereas stretching of the curd yields a fibrous structure as found in Mozzarella cheese.<sup>11</sup>

During extrusion, deformation of proteins is established in a very complex flow field comprising a variety of combinations of simple shear and elongational flow. Besides the presence of various flows, the occurrence of (irreversible) reactions in proteins at the extreme conditions employed during extrusion make obtaining systematic insight in structure formation mechanisms difficult.<sup>12</sup>

### ***3.2 Balancing deformation and solidification***

Even though deformation by flow can induce structure, this is not always sufficient. The structure that is induced has to be fixated, otherwise relaxation and diffusion processes will effectively undo the structure again.<sup>13</sup> In addition, solidification is required to stabilize food products.

Many researchers have focused on gelation of, often dilute, protein solutions by influencing non-covalent interactions or inducing covalent bonds as a means to create solid-like protein structures at quiescent conditions.<sup>14-17</sup> However, the combination of deformation and solidification is needed to entrap flow-induced structures. This implies that a compromise needs to be found between solidification and deformation as liquid materials are easy to process, but the end product should be a (soft) solid material. In addition, deformation of solidified, thus solid-like, materials can lead to breakage, therewith indicating that balancing deformation and solidification is essential. Figure 4 illustrates the role of these important steps in food structure formation.

Solidification in protein-rich systems during deformation can be achieved by controlling the temperature (for heating and/or cooling), while taking into account the possibility of inducing irreversible changes in proteins. The use of plasticizers, such as water or carbon dioxide, facilitates the deformation of biopolymers in general, for example during extrusion.<sup>18</sup> Evaporation of the plasticizer will yield a solidified product. Finally, enzymatic crosslinking of proteins offers a way to fixate structures. Transglutaminase is a well-known enzyme that crosslinks proteins.<sup>19</sup>



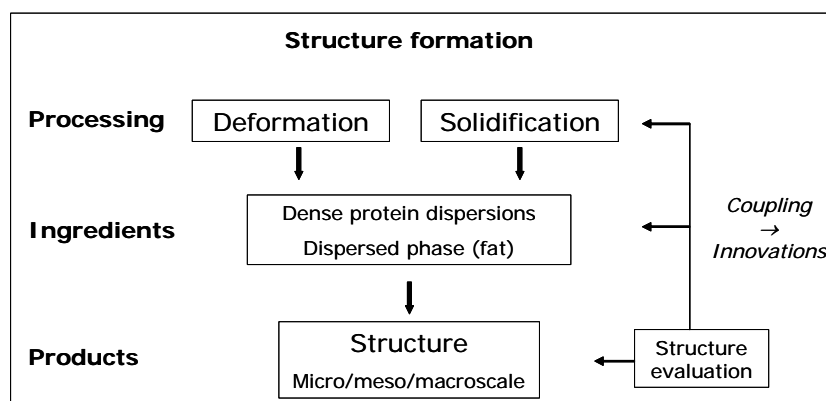


**Figure 4** Schematic representation of structure formation of dense protein dispersions in the presence of a dispersed phase as approached in this thesis. Both deformation and solidification are essential processing steps to obtain foods with a certain consistency. The structure formed should be assessed with respect to the micro-, meso-, and macroscale. Coupling between structural properties and the initial ingredients and processing will open the route to innovations.

### 3.3 Concluding remarks

The complexity of current processes, combined with the chemical changes occurring during processing of the biopolymers hinder innovation in this area severely. A systematic approach towards food structure formation is lacking, therewith explaining the absence of mechanistic models to describe and predict the behavior of ingredients, in particular proteins, during processing. Development of dedicated equipment for food structure formation could be a first step to increase understanding leading to new food products.

A promising approach to develop dedicated food structuring processes is found in isolating a specific mechanism leading to structuring, which usually occurs simultaneously with many other phenomena. Subsequent systematic investigation of solely this phenomenon will yield fundamental insight that in turn can be applied to improve the initial process, or that can even lead to an entirely new type of process (step).

Therefore, in addition to random flow (mixing), this thesis deals with structure formation of proteins at better-defined conditions comprising well-defined flow (shear flow), and both at moderate temperatures (40-50°C).

## 4. Dairy proteins

Proteins are essential nutrients that are found in animals and plants. Though the implementation of sustainable proteins derived from plants in novel foods is currently of high interest<sup>20</sup>, proteins from animal sources are still extensively applied due to their well-known functionality. Milk proteins for example have been used both in food applications and in food research for a long time now.

In general, proteins are versatile biomacromolecules that consist of a sequence of amino acids, which forms the primary structure of a protein. The secondary and tertiary structures are determined by the spatial arrangement of the amino acid chain(s). Proteins can have a random coil conformation or can be globular in shape. As proteins are electrolytes, they are sensitive to changes in pH and to the addition of ions.<sup>21</sup> The ability of proteins in solution to solidify and to form gels at specific conditions is one of many functionalities of proteins that makes them excellent structuring ingredients in foods.

The majority of the proteins present in milk consists of random coil caseins and an important minority consists of globular whey proteins. Four casein proteins are present in bovine milk, i.e.  $\alpha_{S1}$ -,  $\alpha_{S2}$ -,  $\beta$ - and  $\kappa$ -casein, which are assembled in milk in micelles that have a diameter of 100-300 nm.<sup>22</sup> In contrast to globular proteins, caseins are unable to denature upon heating due to the lack of a tertiary structure. In addition, caseins have specific interactions with divalent ions, such as calcium ions that are naturally present in milk.

Commercially relevant caseinates are manufactured using acidification and re-solubilization of the caseins. The acidification removes the (negative) charge on the caseins, which induces them to coagulate. During re-solubilization of the coagulated caseins, counter ions are introduced, such as sodium or calcium ions, therewith yielding the products sodium caseinate and calcium caseinate respectively.<sup>23</sup>

In this thesis, both sodium and calcium caseinate at high concentrations (> 10% w/w) are studied with respect to their structure formation capabilities. To mimic the complexity of foods, the structure formation of the caseinates is investigated in the presence of palm fat, which forms the dispersed phase in the model systems.

## 5. Objective and outline of thesis

The general objective of this thesis is to explore new processing routes based on flow to create innovative protein structures, and in parallel to gain insight in the relevant mechanisms. For this, the work is focused on the induction of a variety of structures in protein-rich (model) foods comprising a dispersed phase using random flow and well-defined flow, with the purpose to derive rules to design structured food materials that range from isotropic to anisotropic structures. In addition, the research aims at acquiring mechanistic insight in the structure formation of proteins by investigating parallels in adjacent research fields, such as structure formation in polymer systems. The structure of this thesis is outlined in Figure 5.

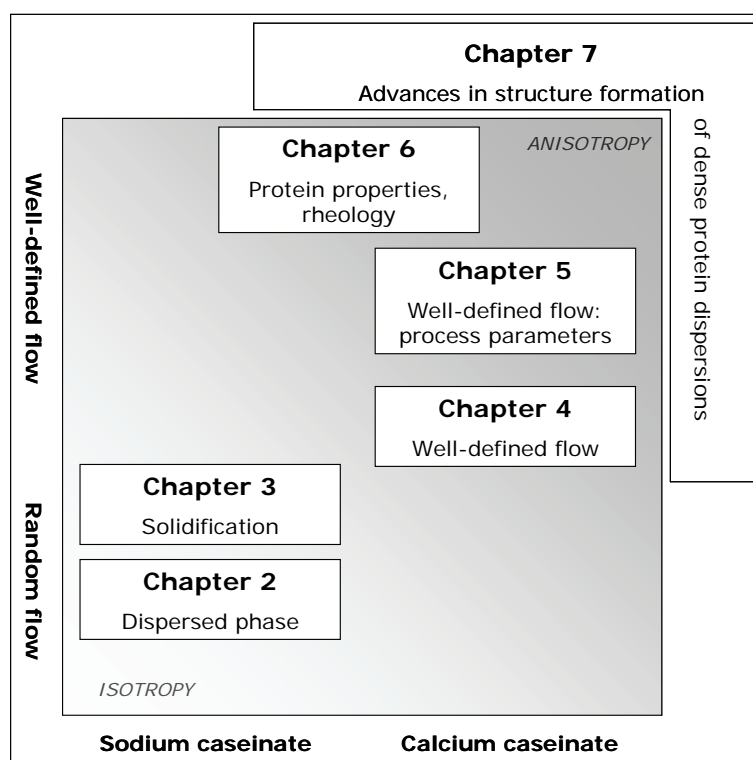


**Figure 5** Overview of the structure of this thesis and the coherence between the chapters.

**Chapter 2** describes the effect of dispersed particles, being palm fat and glass spheres, on the rheological properties of concentrated sodium caseinate gels, which are prepared by mixing and investigated using rheological and mechanical methods. Models usually applied to describe the effect of filler particles in composite materials proved useful to describe the rheological and mechanical parameters of the sodium caseinate structures as function of volume fraction of the various dispersed phases used.

**Chapter 3** introduces an important element in structure formation of soft solid foods, namely solidification. The structure formation of sodium caseinate in the presence of fat is established by combining mixing and solidification using enzymatic crosslinking of sodium caseinate. Changing the process in terms of the order of emulsification of the fat phase and solidification of the protein phase influences the resulting structural properties of the sodium caseinate emulsion gels to a large extent.

The use of well-defined flow, i.e. simple shear, for structure formation of proteins is introduced in **Chapter 4**. The effects of shear flow and solidification using enzymatic gelation on the structure formation of calcium caseinate are elucidated. In contrast to the previous chapters, Chapter 4 deals with protein structures in the absence of a dispersed phase. The calcium caseinate structures found are anisotropic in nature, since truly fibrous products are formed.

The novel structuring process based on well-defined flow and enzymatic crosslinking is further investigated for calcium caseinate in the presence of fat in **Chapter 5**. Insight is acquired in the effect of the shear rate on the structure formation of the fibrous protein structures. Chapter 5 concludes with identifying generic process parameters that are highly relevant for the structure formation of anisotropic protein structures.

**Chapter 6** unveils the uniqueness of the structuring process discussed in Chapters 4 and 5 by showing that sodium caseinate forms isotropic structures using the same process that yielded anisotropic structures for calcium caseinate. Rheological measurements of both caseinates and parallels found in the structure formation of polymer systems indicate that specific criteria need to be met for obtaining anisotropic protein-rich structures using shear flow.

Finally, **Chapter 7** provides an overview of advances in structure formation of anisotropic protein-rich foods. Current food structuring processes such as extrusion and spinning are discussed. As shown in the previous chapters, the use of well-defined flow appears promising for producing novel food structures and acquiring scientific understanding in food structure formation. The chapter concludes with highlighting the future possibilities for food structuring of concentrated protein systems, and the need for analyzing these systems and the resulting structures.

## References

- (1) Renard, D.; Van de Velde, F.; Visschers, R. W. **2006**. The gap between food gel structure, texture and perception. *Food Hydrocolloids* 20 (4): 423-431.
- (2) Antonio, J. **2006**. Body weight and protein. *Strength and Conditioning Journal* 28 (3): 28-29.
- (3) El Khoury, D. T. D.; Obeid, O.; Azar, S. T.; Hwalla, N. **2006**. Variations in postprandial ghrelin status following ingestion of high-carbohydrate, high-fat, and high-protein meals in males. *Annals of Nutrition and Metabolism* 50 (3): 260-269.
- (4) Lee, Y. P.; Mori, T. A.; Sipsas, S.; Barden, A.; Puddey, I. B.; Burke, V.; Hall, R. S.; Hodgson, J. M. **2006**. Lupin-enriched bread increases satiety and reduces energy intake acutely. *American Journal of Clinical Nutrition* 84 (5): 975-980.
- (5) Maughan, R. **2002**. The athlete's diet: Nutritional goals and dietary strategies. *Proceedings of the Nutrition Society* 61 (1): 87-96.
- (6) Aguilera, J. M. **2006**. Seligman lecture 2005 - food product engineering: Building the right structures. *Journal of the Science of Food and Agriculture* 86 (8): 1147-1155.
- (7) Aguilera, J. M. **2005**. Why food microstructure? *Journal of Food Engineering* 67 3-11.
- (8) Visser, J. **1991**. Factors affecting the rheological and fracture properties of hard and semi-hard cheese. *Bulletin of the International Dairy Federation* 268 49-61.
- (9) Aguilera, J. M.; Stanley, D. W. **1993**. The microstructure of food protein assemblies. *Food Reviews International* 9 (4): 527-550.
- (10) Norton, I.; Fryer, P.; Moore, S. **2006**. Product/process integration in food manufacture: Engineering sustained health. *Aiche Journal* 52 (5): 1632-1640.
- (11) Gunasekaran, S.; Ak, M. M. **2003**. *Cheese rheology and texture*; CRC Press, Boca Raton, FL.

- (12) Areas, J. A. G. **1992**. Extrusion of food proteins. *Critical Reviews in Food Science and Nutrition* 32 (4): 365-392.
- (13) Tolstoguzov, V. B. **1993**. Thermoplastic extrusion - the mechanism of the formation of extrudate structure and properties. *Journal of the American Oil Chemists Society* 70 (4): 417-424.
- (14) Chen, J. S.; Dickinson, E. **2000**. On the temperature reversibility of the viscoelasticity of acid-induced sodium caseinate emulsion gels. *International Dairy Journal* 10 (8): 541-549.
- (15) Pughaloni, L. A.; Matia-Merino, L.; Dickinson, E. **2005**. Microstructure of acid-induced caseinate gels containing sucrose: Quantification from confocal microscopy and image analysis. *Colloids and Surfaces B: Biointerfaces* 42 (3-4): 211-217.
- (16) Schorsch, C.; Carrie, H.; Clark, A. H.; Norton, I. T. **2000**. Cross-linking casein micelles by a microbial transglutaminase conditions for formation of transglutaminase-induced gels. *International Dairy Journal* 10 (8): 519-528.
- (17) Zhong, Q. X.; Daubert, C. R.; Velev, O. D. **2004**. Cooling effects on a model rennet casein gel system: Part 1. Rheological characterization. *Langmuir* 20 (18): 7399-7405.
- (18) Jeong, H. S.; Toledo, R. T. **2004**. Twin-screw extrusion at low temperature with carbon dioxide injection to assist expansion: Extrudate characteristics. *Journal of Food Engineering* 63 (4): 425-432.
- (19) De Jong, G. A. H.; Koppelman, S. J. **2002**. Transglutaminase catalyzed reactions: Impact on food applications. *Journal of Food Science* 67 (8): 2798-2806.
- (20) Linnemann, A. R.; Dijkstra, D. S. **2002**. Toward sustainable production of protein-rich foods: Appraisal of eight crops for western europe. Part 1. Analysis of the primary links of the production chain. *Critical Reviews in Food Science and Nutrition* 42 (4): 377-401.
- (21) Fennema, O. R. **1996**. *Food chemistry*; 3<sup>rd</sup> ed., Marcel Dekker, Inc., New York.
- (22) De Kruif, C. G. **1998**. Supra-aggregates of casein micelles as a prelude to coagulation. *Journal of Dairy Science* 81 (11): 3019-3028.
- (23) Aalbersberg, W. Y.; Hamer, R. J.; Jasperse, P.; De Jongh, H. H. J.; De Kruif, C. G.; Walstra, P.; De Wolf, F. A. **2003**. *Industrial proteins in perspective*; 1<sup>st</sup> ed. Vol. 23, Elsevier Science, Amsterdam.



# 2

## Influence of dispersed particles on small and large deformation properties of concentrated caseinate composites

---

This chapter is published as: Manski, J.M.; Kretzers, I.M.J.; Van Brenk, S.; Van der Goot, A.J.; Boom, R.M. **2007**. Influence of dispersed particles on small and large deformation properties of concentrated caseinate composites. *Food Hydrocolloids* 21 (1): 73-84.

## **Abstract**

Concentrated sodium caseinate composites (30% w/w in water), which contained either dispersed palm fat or glass spheres varying in size and surface properties were prepared in a Brabender Do-Corder kneader. The influence of the dispersed phase on the structural properties of the sodium caseinate composites was investigated using both small oscillating and large tensile deformations. Both experimental results and selected models showed that all measured properties were mainly influenced by the volume fraction of the dispersed particles. The type of filler, particle size and surface properties showed no differences in the small deformation properties, whereas the matrix-filler interaction played an important role in the large deformation properties. From the latter followed that sodium caseinate exhibited amphiphilic properties. Selected theoretical relations with the maximum volume packing fraction and the matrix-filler interaction as important parameters, agreed well with the experimental results. The relatively simple models can be applied as guidelines for designing composite food products.



## **1. Introduction**

Food products are generally composite materials consisting of biomaterials, such as proteins, carbohydrates and lipids that are arranged in a matrix phase and one or more dispersed phases.<sup>1-4</sup> A dairy food, such as cheese, often described as a soft solid, can be regarded as a composite with a continuous matrix of interconnected swollen casein particles and dispersed fat particles.<sup>5</sup> To improve the understanding of the structural properties of foods, various model systems comprising different matrices and dispersed particles have been investigated to elucidate the influence of the dispersed phase. Examples are gelatin (20% and 25% w/w) matrices with glass spheres<sup>6,7</sup> and soy protein (13% w/v) matrices with oil droplets.<sup>8</sup> Whey proteins have been applied as a matrix phase in a number of studies, such as whey gels (11-16% w/w) with oil droplets as filler<sup>1,9</sup>, glass spheres<sup>10</sup> or dextran particles.<sup>3</sup> The most important conclusion that follows from these studies is that adding a rigid dispersed phase at volume fractions of 0.10 and higher causes an increase in strength of the composite model system, either measured by small<sup>6,8,9</sup> or large deformations.<sup>1,3,7,8,10</sup> A prerequisite for increased strength of a composite with increasing volume fraction of filler was a good interaction between the matrix and filler phase.<sup>1,3,6,11</sup> However, a decrease in strength due to a presumed weak interaction between filler and matrix was only reported for a model system consisting of a gellan matrix and glass spheres<sup>12</sup> and an acidified milk gel containing washed milk fat droplets.<sup>11</sup> A small number of researchers reported on the effect of the particle size of various fillers on the composite strength, which increased with smaller-sized filler particles.<sup>1,8,10</sup> As shown, previous research on food composites has mainly been performed with whey matrices containing various fillers.

The structural properties of the discussed food model systems were typically investigated by either small or large deformations of which the latter were compression tests, except for the study with gelatin composites.<sup>7</sup> However, according to Luyten<sup>2</sup>, tensile tests are more accurate due to the pure uni-axial deformation in contrast to compression tests. Therefore, the use of tensile tests with large deformations in combination with small deformations seems to be a preferable method to characterize soft solid rheology.

In order to predict and to design structured foods, it is desirable to quantify the influence of a dispersed phase on the structural properties of food composites. Till now, quantitative models to describe the effect of a dispersed phase on the structural properties of model systems have only been applied in a few studies with food composites.<sup>7,10,11</sup> Van Vliet<sup>11</sup> applied Van der Poel's theory<sup>13</sup> describing an elastic medium with elastic inclusions to characterize filled polymer and casein gels. Van der Poel's theory was less appropriate to describe these filled gels, resulting in poor agreement with the data. Ross-Murphy and Todd derived and successfully applied an equation for the tensile strength of a filled gelatin system.<sup>7</sup> Langley and Green slightly modified this equation, which will be discussed later in this paper, for filled whey gels.<sup>10</sup>

Concentrated casein matrices with fillers have received little attention as a matrix phase in model systems, even though their applicability for cheese-like products is industrially relevant. To the best of our knowledge, the study of Van Vliet<sup>11</sup> with filled acidified milk gels (3% w/w casein) and the study of Zhou and Mulvaney<sup>14</sup> with rennet casein gels (26-45% w/w) filled with milk fat were the only reported studies containing casein. Therefore, the objective of the present study is to investigate the influence of the dispersed fat phase on the structural properties of a dairy food composite consisting of 30% (w/w in water) sodium caseinate by applying small oscillating as well as large tensile deformations. As an extension of the soft solid model system, glass spheres varying in size and surface properties were added to the sodium caseinate. Based on the results for the structural properties of the model system for a dairy soft solid, the applicability of selected models describing composite rheology will be discussed. Furthermore, quantitative design rules, which follow from these composite models, will be presented.

## 2. Theory

### 2.1 Small deformations

Several authors proposed an analogy between the rheology of suspensions and the elasticity of solid composites.<sup>15-19</sup> The majority of the models is deduced from Einstein's empirical relation for the viscosity of dilute suspensions with uniform,

monodisperse, rigid spheres.<sup>20,21</sup> Many authors extended Einstein's equation for higher volume fraction using the maximum packing fraction ( $\phi_{max}$ ) as an additional parameter.<sup>19,22,23</sup> Eilers' equation relates the complex modulus of the composite ( $G^*$ ) to that of the continuous matrix phase ( $G_c^*$ ) as a function of the volume fraction of dispersed particles ( $\phi$ ) in the following way<sup>22</sup>:

$$G^* = G_c^* \cdot \left( 1 + \frac{1.25 \cdot \phi}{1 - \frac{\phi}{\phi_{max}}} \right)^2 \quad [1]$$

Mooney<sup>24</sup> proposed an equation for concentrated suspensions with rigid particles by implementing the so-called crowding factor ( $k$ ):

$$G^* = G_c^* \cdot \exp\left(\frac{2.5 \cdot \phi}{1 - k \cdot \phi}\right) \quad [2]$$

For monodisperse spheres,  $k$  has an estimated value of 1.5 based on geometric packing. Pal<sup>19</sup> used equation 2 to describe  $G^*$  of concentrated viscoelastic suspensions containing rigid spheres with  $k$  replaced by  $1/\phi_{max}$ :

$$G^* \cdot H = G_c^* \cdot \exp\left(\frac{2.5 \cdot \phi}{1 - \frac{\phi}{\phi_{max}}}\right) \quad [3]$$

The variable  $H$  comprises the rigidity of the dispersed phase ( $G_d^*$ ) as follows<sup>19</sup>:

$$H = \left( \frac{G^* - G_d^*}{G_c^* - G_d^*} \right)^{-2.5} \quad [4]$$

In the case of rigid fillers ( $G_d^* \rightarrow \infty$ ), the value of  $H$  is one. Pal<sup>19</sup> proposed also a second relation, which is analogous to Krieger and Dougherty's<sup>23</sup> equation for the viscosity of suspensions:

$$G^* \cdot H = G_c^* \cdot \left( 1 - \frac{\phi}{\phi_{max}} \right)^{-2.5 \cdot \phi_{max}} \quad [5]$$

Equations 1 to 5 are applicable for fillers with volume fractions up to  $\phi_{max}$ . Theoretically, the value of  $\phi_{max}$  is either 0.64 for random close packing or 0.74 for a closest hexagonal packing of monodisperse rigid spheres.<sup>25</sup> As a comparison, Pal<sup>19</sup>

applied  $\phi_{max}$  values of 0.74 and 0.50 in equations 3 and 5, respectively, to describe  $G^*$  of suspensions of glass spheres in cellulose gum. Based on the different  $\phi_{max}$  values in equations 3 and 5 that Pal needed for the same suspension, combined with the fact that the  $\phi_{max}$  value obtained in equation 3 was rather high, we suspect that the physical interpretation of the crowding factor  $k$  in terms of  $\phi_{max}$  might be incorrect, as will be discussed later.

## 2.2 Large deformations

The large deformation properties of composites are characterized with the yield strain ( $\varepsilon$ ), yield stress ( $\sigma$ ) and the Young's modulus ( $E$ ). Besides the volume fraction and  $\phi_{max}$ , the interaction between filler and matrix plays an important role in models describing the large deformation properties of composites. Smith<sup>26</sup> and Nielsen<sup>27</sup> suggested the following relation for the yield strain  $\varepsilon$  of elastomeric composites:

$$\varepsilon = \varepsilon_c \cdot (1 - K \cdot \phi^{1/3}) \quad [6]$$

Smith<sup>26</sup> applied the value 1.105 for  $K$  based on the assumption that  $\varepsilon$  is zero when  $\phi_{max}$  equals 0.74, whereas Nielsen<sup>27</sup> used a value of one in the case of perfect adhesion between the continuous matrix and filler particles.

Ross-Murphy and Todd<sup>7</sup> derived an equation for the tensile yield stress  $\sigma$  of gelatin composites filled with glass beads, assuming perfect adhesion. Langley and Green<sup>10</sup> modified this equation with a parameter that approximated  $\phi_{max}$ , which resulted in the following equation for the tensile yield stress of the composite ( $\sigma$ ):

$$\sigma = \sigma_c \cdot \frac{1 - \left( \frac{\phi}{\phi_{max}} \right)^{1/3}}{\left( 1 - \frac{\phi}{\phi_{max}} \right)^{5/2}} \quad [7]$$

Turcsanyi<sup>28</sup> derived the following empirical model describing  $\sigma$  of filled polymers such as polypropylene and low-density polyethylene with an interaction parameter  $\beta$ :

$$\sigma = \sigma_c \cdot \left( \frac{1 - \phi}{1 + 2.5 \cdot \phi} \right) \cdot \exp(\beta \cdot \phi) \quad [8]$$

Turcsanyi showed that  $\beta$  is related to the interfacial properties between the matrix and filler, even though the parameter itself has no direct physical meaning. Also,  $\beta$  depends on the yield stress of the matrix. The interaction between polymer matrices and filler is positive when the value of  $\beta$  exceeds 3.<sup>28</sup>

Kerner<sup>29</sup> derived an equation for the bulk modulus for a suspension of grains with the assumption that the grains are spherical, randomly distributed across the suspending medium, and perfectly bonded to the medium. Lewis and Nielsen<sup>30</sup> modified the Kerner equation by implementing  $\phi_{max}$ . The modified Kerner equation for the Young's modulus of the composite ( $E$ ) comprising a matrix ( $E_c$ ) and a dispersed phase that is more rigid than the continuous phase reads:

$$E = E_c \cdot \frac{1 + A \cdot \phi}{1 - \psi \cdot \phi} \quad [9]$$

$A$  is a constant in which the Poisson ratio  $\nu$  is incorporated:

$$A = \frac{7 - 5\nu}{8 - 10\nu} \quad [10]$$

For incompressible materials,  $\nu$  has a value of 0.5. Variable  $\psi$  in equation 9 is related to  $\phi$  and  $\phi_{max}$  as follows<sup>30</sup>:

$$\psi = 1 + \phi \cdot \left( \frac{1 - \phi_{max}}{\phi_{max}^2} \right) \quad [11]$$

### 3. Materials and methods

#### 3.1 Composite materials

Sodium caseinate was acquired from DMV International (Veghel, The Netherlands). According to the manufacturer's specifications, the product contained at least 88% protein. Barentz Raw Materials (Hoofddorp, The Netherlands) provided palm fat (Table 1), which has a melt trajectory from 20°C to 37°C.

Three batches of glass spheres (coded 100HFL, 10HFL and 5HFB) with different sizes and surface properties were acquired from Pneumix (Son, The Netherlands), Potters Industries (Carlstadt, NJ, U.S.A.) and Potters Europe (Kirchheimbolanden,

Germany) respectively. Samples of the batches of glass spheres were analyzed with a Coulter Laser LS230 (Beckman Coulter Inc., Fullerton, CA, U.S.A.) to determine the average particle size distribution (PSD) based on the differential volume percentage (Figure 1) and the average particle diameter ( $d_{32}$ ). We assumed the surface properties based on the specified treatment of the glass spheres. Therefore, untreated glass spheres were assumed to be hydrophilic, whereas silane treated spheres were hydrophobic. Table 1 summarizes the properties of the glass spheres, including the particle and bulk densities ( $\rho$  and  $\rho_{bulk}$ ), which were determined in water ( $\rho$ ) and in air ( $\rho_{bulk}$ ). The quotient of these densities gives an indication of the value for  $\phi_{max}$  for each type of glass spheres. The 10HFL glass spheres were non-porous hollow spheres according to the manufacturer's specifications.

**Table 1** Properties of the fillers applied in the sodium caseinate composites. The density  $\rho$  and bulk density  $\rho_{bulk}$  were measured, the maximum volume packing fraction  $\phi_{max}$  is the quotient of these densities, and  $d_{32}$  is the measured average particle diameter.

Filler type	$\rho$ (g·mL <sup>-1</sup> )	$\rho_{bulk}$ (g·mL <sup>-1</sup> )	$\phi_{max}$ (-)	$d_{32}$ ( $\mu$ m)	Surface properties	Company and product name
100HFL	2.4	1.5	0.63	103.9	Hydrophilic	Pneumix (SMG-AF)
10HFL	1.1	0.7	0.64	9.7	Hydrophilic	Potters Industries (Spherigel 110P8)
5HFB	2.3	1.3	0.57	4.5	Hydrophobic	Potters Europe (Spheriglass 5000 CP03)
Fat	0.8	-	-	-	-	Barentz (Effekta Spezial)

### 3.2 Composite preparation

All produced composites were prepared with a sodium caseinate matrix of 30% (w/w in water), and volume fractions of filler increasing to 0.50. The composite preparation entailed firstly mixing sodium caseinate and water (ratio 3:7), and secondly mixing the caseinate matrix and filler. The 30% (w/w in water) caseinate matrix was prepared in a kitchen mixer (Philips, Amsterdam, the Netherlands) at low mixing rate. A Brabender Do-Corder 330 (Brabender OHG, Duisburg, Germany) with a mixing bowl (type W-50) was used to mix the caseinate matrix with a certain volume fraction of filler. The mixing profile of the Brabender Do-Corder 330 was set as follows: 4 min at 5 rpm, then an increase from 5 to 100 rpm in 1 min, and finally 16 min at 100 rpm. The filler was added in the first 4 minutes

of the mixing time. Fat was added at room temperature, thus in solid form. During mixing, the temperature was kept constant at 40°C with a water bath, and the torque was monitored. After mixing, the composite was collected in a mould of two square parallel plates (100 × 100 mm), which provided a controlled sample height of 3 mm. The sample was then stored in a refrigerator at 4°C for one day, until the small and large deformation tests were carried out.

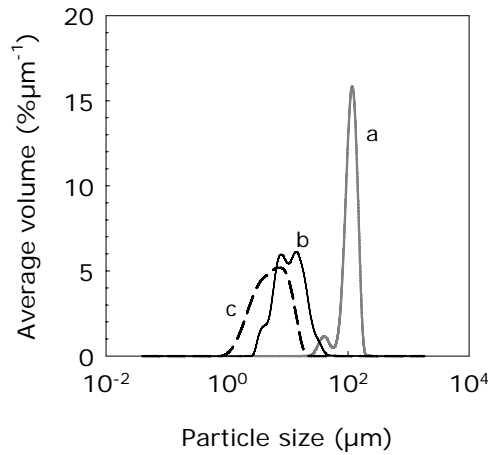


**Figure 1** Average particle size distribution of hydrophilic 100HFL (a) and 10HFL (b) glass spheres, and hydrophobic 5HFB (c) glass spheres that were used as filler particles in the sodium caseinate composites.

All composite materials with varying volume fractions of filler were prepared in at least two runs in the Brabender Do-Corder, as one mould filled with composite material provided insufficient material to perform all tests. The maximum and average errors were based on the steady state torque values between samples with identical composition, which were processed in different runs with the Brabender Do-Corder, and are listed in Table 2. The errors were calculated as follows:

$$Error = \left| \frac{\bar{x} - x_{sample}}{\bar{x}} \right| \cdot 100\% \quad [12]$$

In the above-mentioned equation,  $\bar{x}$  is the average value of dependent samples and  $x_{sample}$  is the single measured value of a sample.

The sodium caseinate samples without filler, and to a lesser extent the samples with filler, contained air bubbles, which were incorporated in the composites during mixing in the Brabender Do-Corder kneader. We estimated that the effect of the presence of non-rigid air bubbles on the sodium caseinate composites was only minor, using equations 4 and 5 with  $G_d^* \ll G_c^*$ . Assuming a maximum volume fraction of 0.05 of air bubbles in a sodium caseinate matrix resulted in a deviation of 8% in the complex modulus of the latter, which is in the range of the experimental error of the measurements. Therefore, air bubbles were not expected to affect the conclusions that were drawn about the influence of the dispersed phase.

**Table 2** Average and maximum errors, as defined in equation 12, of dependent samples during composite processing (s.s. *torque* = steady state torque), and during small ( $G^*$  and  $\tan\delta$ ) and large ( $\varepsilon$ ,  $\sigma$ , and  $E$ ) deformation measurements.

Error (%)	Variables processing	Variables small deformations		Variables large deformations		
	s.s.torque	$G^*$	$\tan\delta$	$\varepsilon$	$\sigma$	$E$
Average	8%	4%	1%	4%	10%	9%
Maximum	19%	17%	3%	12%	27%	24%

### 3.3 Small deformations

Small deformation tests were performed on a stress-controlled Bohlin CVO (Bohlin Instruments Ltd., Cirencester, U.K.). Composite samples with a thickness of 3 mm were taken from a double plate mould, and cut into a circular shape with a diameter of 25 mm. The geometry used for rheological analysis comprised two parallel discs (diameter 25 mm) with serrated surfaces in order to prevent slip, which are often used for cheese-like products.<sup>31</sup> After cutting, the composite samples were positioned between the two serrated discs, and the gap between the discs was set at 2 mm. Before measuring, the sample was rested for 15 min to relax built-up stresses due to previous handling.

Oscillatory amplitude sweeps were performed at a constant frequency of 1 Hz, at a temperature of 20°C and in duplicate. The resulting strain response and phase angle ( $\delta$ ) were measured. From the measurements, the complex ( $G^*$ ), the elastic ( $G'$ ) and viscous ( $G''$ ) moduli and the loss tangent ( $\tan\delta$ ) were calculated as a function



of the strain. The plots resulting from amplitude sweeps provided the linear viscoelastic (LVE) region and an indication of the critical strain limit ( $\gamma_c$ ) at which the LVE region ended. The measured moduli and  $\tan\delta$  were used in this study as rheological material properties to characterize and compare the various composites. The average and maximum errors of the duplicate small deformation measurements of  $G^*$  and  $\tan\delta$  from one sample are also given in Table 2. The measured properties of independently processed samples in the Brabender Do-Corder with the same composition are presented in the graphs.

### **3.4 Large deformations**

A Texture Analyzer T2 (Stable Micro Systems Ltd., Surrey, U.K.) was used for large deformation tests. Uni-axial tensile tests were conducted with a constant deformation rate of  $3 \text{ mm}\cdot\text{s}^{-1}$  at  $13^\circ\text{C} \pm 2^\circ\text{C}$ . Samples for the tensile tests, which were also taken from the double plate moulds, were cut in a dog bone shape with a total length of 90 mm. The width of the middle part of the samples was narrower (15 mm) than the outer parts (20 mm) to induce fracture in the middle of the dog bone-shaped samples. The length of the narrow part was 20 mm. The outer parts were broader to facilitate attachment to the grips of the Texture Analyzer. At least three samples per composite were tested.

The tensile curves were converted to stress-strain curves assuming a constant sample volume. The yield strain ( $\varepsilon$ ), which is the so-called Hencky strain, and the tensile yield stress ( $\sigma$ ) were calculated as described by Gunasekaran and Ak.<sup>31</sup> The Young's modulus ( $E$ ) was calculated from the initial linear slope of the stress-strain curve. Errors in the triplicate large deformation measurements of  $\varepsilon$ ,  $\sigma$  and  $E$  of one sample are listed in Table 2. Independently processed samples in the Brabender Do-Corder with the same composition are presented in the graphs.

### **3.5 Scanning electron microscopy**

The fracture surfaces of the sodium caseinate composites with glass spheres and fat as filler were analyzed with a scanning electron microscope (SEM). Composites containing 0.10 and 0.30 volume fractions of glass spheres and 0.10 and 0.20 volume fractions of fat droplets were fractured during the large tensile deformation tests. A sample of the fracture surface was carefully cut and glued into

a sample holder with TBS (tissue freezing medium, EMS, Ft. Washington, PA, U.S.A.), and subsequently frozen in liquid nitrogen. The sample holder was transferred under vacuum to the dedicated cryo-preparation chamber (Oxford cryo-system, CT 1500 HF, Eynsham, U.K.) onto a sample stage at  $-90^{\circ}\text{C}$  and subsequently freeze dried for 3 min at  $-90^{\circ}\text{C}$  at  $3 \cdot 10^{-7}$  Pa). After the sample surface was sputter coated with 10 nm platinum, it was transferred to the cold sample stage ( $-190^{\circ}\text{C}$ ) inside the Cryo-FESEM (JSM, JEOL 6300F Field Emission SEM, Tokyo, Japan) and subsequently analyzed with an accelerating voltage of 5 kV. Images of the fracture surfaces were digitally recorded (Orion, Brussels, Belgium).

### ***3.6 Confocal scanning laser microscopy***

To analyze the distribution of the dispersed phase across the sodium caseinate matrix, a confocal scanning laser microscope (CSLM) was used. A composite containing 0.10 volume fraction of hydrophobic beads (5HFB) was viewed, and composites with 0.10 and 0.19 volume fraction of fat droplets. Besides the spatial distribution, the typical size of fat droplets could be estimated.

All samples that were viewed with the CSLM contained  $3 \cdot 10^{-4}\%$  (w/w in protein) Rhodamine 110 (83695, Sigma Aldrich, Zwijndrecht, the Netherlands). The protein stain was added in the form of  $0.01 \text{ g} \cdot \text{L}^{-1}$  Rhodamine 110 in a phosphate buffered saline (PBS) solution. The fat phase comprised 50% (v/v) of a  $0.1 \text{ g} \cdot \text{L}^{-1}$  Nile Red (298395, Sigma Aldrich, Zwijndrecht, the Netherlands) in liquid palm fat solution. Consequently, the fat for these composites was added as a liquid in the Brabender Do-Corder. Experiments showed no differences between adding solid or liquid fat. After composite processing, the samples were transferred into 2-well chambered coverglasses (Nunc, Naperville, IL, U.S.A.) and stored in a refrigerator at  $4^{\circ}\text{C}$  for one day.

The samples with fat as filler were analyzed with a LSM 510 (Zeiss, Oberkochen, Germany) using an Ar-ion laser (wavelength 488 nm) and HeNe laser (wavelength 543 nm) with a 40x oil-immersion objective (Plan-Neofluar, Zeiss, Oberkochen, Germany). For the sodium caseinate phase, an emission filter of 505-550 nm was applied, whereas a 600-650 nm filter was used for the fat phase. For the composites with glass spheres, only the Ar-ion laser was used to view the sample. The pictures

taken of the samples were analyzed afterwards with the LSM Image Browser (Zeiss, Oberkochen, Germany).

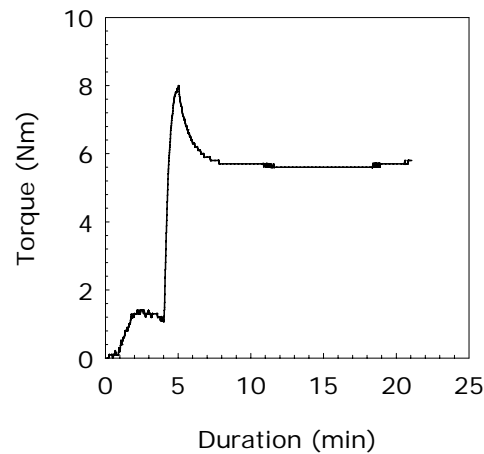


**Figure 2** Typical torque curve during processing in the Brabender Do-Corder kneader of a sodium caseinate composite with 0.35 volume fraction of 100HFL glass spheres. The composite components were added during the first 4 min, subsequently the mixing speed was increased from 5 to 100 rpm within 1 min, and finally the composite was mixed for 16 min at 100 rpm.

## 4. Results and discussion

### 4.1 Composite processing

The torque in time (Figure 2) showed a similar behavior for all sodium caseinate composites containing glass spheres during mixing in the Brabender Do-Corder kneader. The composite samples generated a maximum torque value after 5 min of mixing due to the increase in mixing rate from 5 to 100 rpm. After the maximum torque, the torque decreased until a steady state value was reached. The composites containing fat droplets as filler material did not show a clear maximum in torque. On-line torque measurements of samples with fat were at the low end of the measuring range of the Brabender Do-Corder (0 to 100 Nm). Also, the filling degree of the kneader influences the measured torque. Nevertheless, the steady state torque values were compared for the composites comprising increasing

volume fractions of various fillers. Figure 3 shows a more or less linear increase in steady state torque with increasing volume fraction of glass spheres. In contrast, the steady state torque of the composites with fat droplets decreased as the volume fraction increased, probably due to lubrication by the fat phase because the fat phase was liquid during mixing at 40°C. The steady state torque for the glass sphere composites seemed independent of the particle size. However, the hydrophobic glass spheres (5HFB) showed slightly lower torque values than the hydrophilic glass spheres, which may indicate lower interaction and friction with the sodium caseinate matrix compared to the hydrophilic spheres.

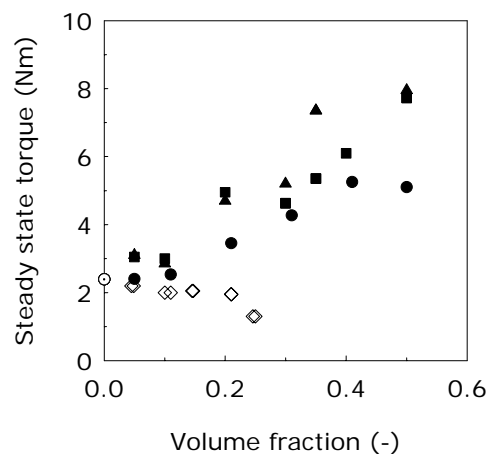


**Figure 3** Influence of the volume fraction of filler (■100HFL, ▲10HFL, ●5HFB, and ◇ fat) on the steady state torque during composite processing in the Brabender Do-Corder kneader at 40°C and 100 rpm. The sodium caseinate matrix is depicted with ○.

CSLM images (Figure 4) of composites containing either fat or hydrophobic glass spheres (5HFB) showed a random spatial distribution of the dispersed phase across the sodium caseinate matrix. From the CSLM images of composites containing fat, which also indicated a homogeneously distributed dispersed phase, most fat droplet diameters were estimated in the range of 1 to 5  $\mu\text{m}$ , and turned out to depend on the volume fraction of fat present in the composite (Figure 4A and 4B).

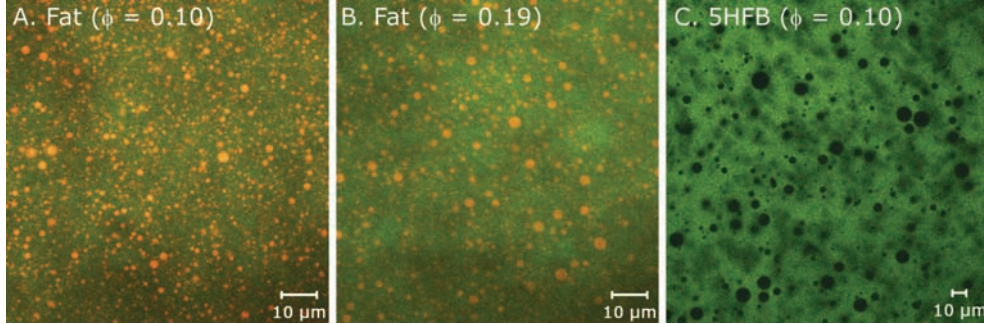


**Figure 4** CSLM images of sodium caseinate composites with (A) 0.10 and (B) 0.19 volume fraction of fat, and (C) 0.10 volume fraction of 5HFB. Each bar represents 10  $\mu\text{m}$ .

#### 4.2 Small deformations

The values for the complex modulus ( $G^*$ ) and the loss tangent ( $\tan\delta$ ) were determined at a constant strain of 0.01, which was in the LVE region of all composites except for the composites with the highest volume fraction of filler. Figure 5 illustrates the increase in  $G^*$  with increasing volume fraction of the dispersed phase up to 0.60, which is in agreement with previous research on food composites.<sup>6,8,9,14</sup> For a volume fraction larger than 0.40, both the  $G^*$  values at a strain of 0.01, and  $G^*$  values at the end of the LVE region are depicted in Figure 5. The latter estimated  $G^*$  values corresponded with the critical strain limit values  $\gamma_c$  that are shown in Table 3. The critical strain limit at a volume fraction of 0.50 filler decreased with increasing particle size (100HFL < 10HFL < 5HFB). Both at low (insert Figure 5) and high volume fractions (Figure 5), all filler types behaved similarly, which indicated that the volume fraction of filler was the important parameter for the rigidity increase of the composites. Obviously, both the surface properties and the particle sizes had no effect on  $G^*$ . From the observed similar reinforcement of  $G^*$  by adding either glass spheres or fat droplets, it can be concluded that rigid fillers enable the reinforcement of a composite; therefore, with the temperature applied, fat can be considered a rigid filler.

Figure 5 includes predictions by Eilers' model (equation 1) and by the two models by Pal (equations 3 and 5) for which a value of 0.6 was selected for  $\phi_{max}$  based on the measured particle densities and bulk densities of the glass spheres (Table 1). All three models gave reasonable but slightly higher predictions of  $G^*$  compared to our data up to 0.30 volume fraction (insert Figure 5). Pal's model based on

Mooney's equation (equation 3) started to deviate already from a volume fraction of 0.20 from the measured  $G^*$  values, and Figure 5 shows even a larger discrepancy between this model and the measured  $G^*$  in the high volume fraction regime. The measured  $G^*$  of the composites is described well when a  $k$  value of nearly 1 is chosen in the original Mooney equation (equation 2) based on fitting all data of the glass spheres with a least squares method. This leads to the conclusion that  $k \neq 1/\phi_{max}$ . Eilers' model (equation 1) and the model by Pal based on Krieger and Dougherty's derivation (equation 5) agree well with  $G^*$  at high volume fractions with  $\phi_{max} = 0.6$ .

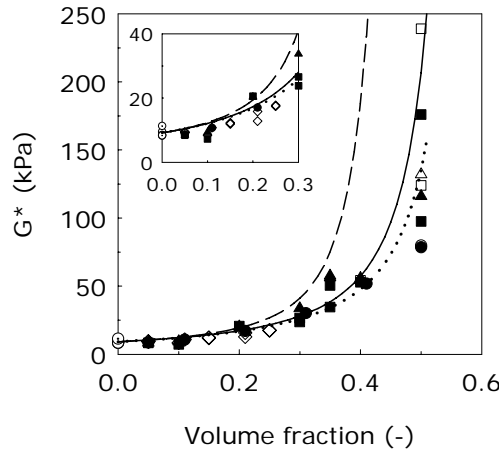


**Figure 5** Influence of the volume fraction (insert 0 to 0.30) of filler (■100HFL, ▲10HFL, ●5HFB, and ◇ fat) on the complex modulus ( $G^*$ ) of the sodium caseinate composites. The sodium caseinate matrix is depicted with ○. The upper line (dashed) is the Pal/Mooney model (equation 3), the middle line (solid) is the Pal/Krieger & Dougherty model (equation 5), and the lower line (dotted) is Eilers' model (equation 1). The  $\phi_{max}$  was set at 0.6 in all shown models.

Summarizing, the models that were initially developed for the viscosity of suspensions of rigid spheres agree well with  $G^*$  of the sodium caseinate composites containing either glass spheres or fat droplets at both low and high volume fractions. The discussed models explain the  $G^*$  behavior for a composite containing a rigid filler in terms of the volume fraction and the dependency on the particle size distribution that is included in  $\phi_{max}$ . Therefore, by varying the particle size

distribution of fillers, the composite rheology can be influenced.<sup>32</sup> It must be noted that in the rheological models for suspensions of rigid spheres, no-slip conditions are assumed between the continuous and dispersed phases. Several researchers interpreted this assumption as a strong interaction between matrix and filler.<sup>5,10,11,33</sup> However, the discussed models are able to describe the small deformation results well without the inclusion of an interaction parameter. Therefore, with only a known value of  $G^*$  for a continuous phase and an estimation of  $\phi_{max}$ , a prediction of  $G^*$  of a composite product as function of the volume fraction can be made by applying equations 1 or 5.

**Table 3** Critical strain limit values  $\gamma_c$ , which indicate the end of the LVE region, for independently processed composites containing  $\phi > 0.40$  of 100HFL, 10HFL and 5HFB glass spheres.

Filler type	$\phi$ (-)	$\gamma_c$ (-)
100HFL	0.40	$5.04 \cdot 10^{-3}$
	0.50	$9.61 \cdot 10^{-4}$
	0.50	$4.37 \cdot 10^{-4}$
10HFL	0.50	$1.02 \cdot 10^{-3}$
5HFB	0.50	$6.37 \cdot 10^{-3}$

Figure 6 shows  $\tan\delta$  as function of the volume fraction of filler.  $\tan\delta$  was independent of the volume fraction up to 0.15 for both glass spheres and fat droplets. At higher volume fractions ( $\phi > 0.15$ ), an increase in the volume fraction of large hydrophilic spheres (100HFL) had no effect on  $\tan\delta$  of the composites, whereas small hydrophilic (10HFL) spheres caused a significant decrease in  $\tan\delta$ , which implied a more solid-like behavior of the composites. Furthermore, the  $\tan\delta$  values indicated a difference in composite behavior between hydrophilic (10HFL) and hydrophobic (5HFB) spheres. The former caused a larger decrease in  $\tan\delta$  with increasing volume fraction. Based on theoretical considerations, both the presence of air bubbles, and inertia effects caused by density differences of the glass spheres are unlikely to account for the above-mentioned results. In contrast, Pal stated that  $\tan\delta$  is independent of the volume fraction of filler based on equations 3 and 4.<sup>19</sup> However, he also found a slightly decreasing  $\tan\delta$  with increasing volume fraction of glass spheres in cellulose gum.

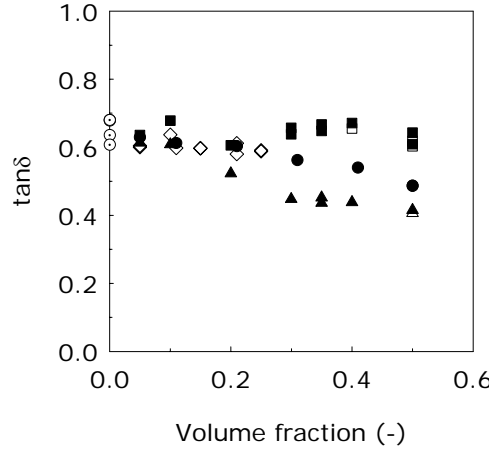


**Figure 6** Influence of the volume fraction of filler (■100HFL, ▲10HFL, ●5HFB, and ◇ fat) on the loss tangent ( $\tan\delta$ ) of the sodium caseinate composites. The sodium caseinate matrix is depicted with ○. The unfilled symbols at  $\phi > 0.40$  give an estimation of  $\tan\delta$  in the LVE region for which the strain value was lower than 0.01 as shown in Table 3.

### 4.3 Large deformations

The large tensile deformations showed more differences across the samples compared to the small deformations when looking at the influence of the volume. Figure 7 shows that the volume fraction up to 0.10 had no significant influence on the measured yield strain  $\varepsilon$ . Unfortunately, the results in the low volume fraction regime ( $0 < \phi < 0.15$ ) were affected by air inclusions. This is a known difficulty in performing large deformation tests.<sup>7,26</sup> The air inclusions were present after processing in the Brabender Do-Corder kneader, especially in the sodium caseinate samples without filler and in case of low volume fractions of large particles.

Figure 7 shows that  $\varepsilon$  decreased with increasing volume fraction ( $\phi > 0.10$ ) of the glass spheres. Further,  $\varepsilon$  was independent of filler size and type at higher volume fractions. The fat droplets showed no change in  $\varepsilon$  with increasing volume fraction, which may be due to the deformability of the fat droplets. Figure 7 includes the model by Nielsen (equation 6 with  $K = 1$ ), which was fitted to all measured data from  $\phi \geq 0.05$  using a least squares method to determine the value of  $\varepsilon$ . The theory agrees well with our measurements from  $\phi > 0.15$  but predicts much higher strain values in the low volume fraction regime. This difference is probably due to the



presence of air inclusions. The yield strain of the sodium caseinate matrix ( $\varepsilon_c$ ) as estimated by the model is a factor 3 higher than the measured value. Luyten and co-workers reported that inherent defects in Gouda cheese samples caused lower yield strain and yield stress values.<sup>2</sup> Stading and Hermansson observed the same effect for  $\beta$ -lactoglobulin gels.<sup>34</sup> Therefore, the present air inclusions accounted for the lower  $\varepsilon$  values measured in the low volume fraction regime. An interesting observation is that only the yield strain  $\varepsilon$  of the sodium caseinate composites ( $\phi < 0.15$ ) was influenced by the presence of air bubbles, and not the yield stress  $\sigma$  as can be seen in Figure 8. Summarizing, air inclusions as well as 100HFL spheres behaved as inherent defects leading to slightly lower  $\varepsilon$  values at low volume fractions. Based on the results and the applied model, the volume fraction of filler was the only parameter affecting  $\varepsilon$ . Furthermore, the model showed that already a small amount of filler caused a tremendous decrease in  $\varepsilon$  compared to  $\varepsilon_c$ . The fact that a low volume fraction of filler caused the largest change in  $\varepsilon$  is in contrast to previous observations with the small deformation property  $G^*$ , where high volume fractions of filler caused the largest change in  $G^*$ .

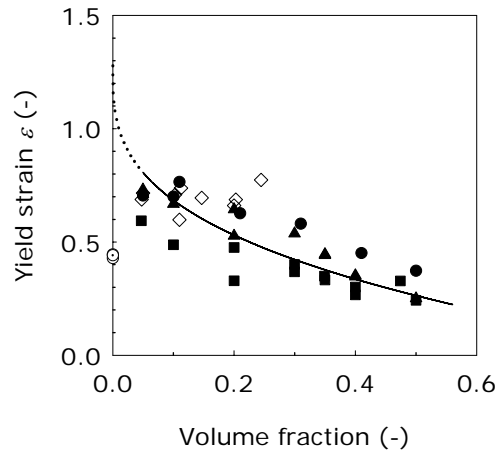


**Figure 7** Influence of the volume fraction of filler (■100HFL, ▲10HFL, ●5HFB, and ◇ fat) on the yield strain ( $\varepsilon$ ) measured with large tensile deformations. The sodium caseinate matrix is depicted with  $\odot$ . Nielsen's model (equation 6 with  $K = 1$ ) was fitted to the data with  $\phi \geq 0.05$  (leading to  $\varepsilon_c = 1.27$ ) using a minimal least squares method (solid line). The dotted line depicts extrapolation of the model for  $0 \leq \phi < 0.05$ .

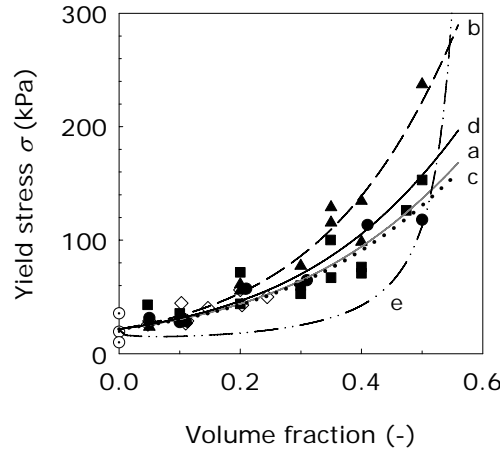


**Figure 8** Influence of the volume fraction of filler (■100HFL, ▲10HFL, ●5HFB, and ◇ fat) on the yield stress ( $\sigma$ ) measured with large tensile deformations. The sodium caseinate matrix is depicted with ○. Turcsanyi's model (equation 8) was fitted to the data to determine the interaction parameter  $\beta$  for each filler separately using a minimal least squares method and applying the average measured value of the yield stress of the matrix ( $\sigma_c$ ). The  $\beta$  values for the composites were (a)  $\beta = 6.70$  for 100HFL, (b)  $\beta = 7.67$  for 10HFL, (c)  $\beta = 6.61$  for 5HFB and (d)  $\beta = 6.98$  for fat. The  $\phi_{max}$  in Ross-Murphy's model (equation 7) was set at 0.6 (e).

Figure 8 shows the increasing yield stress  $\sigma$  with increasing volume fraction of the various fillers. From a volume fraction of 0.15, differences started to occur between the various glass sphere types. First, especially the hydrophilic 10HFL glass spheres showed larger  $\sigma$  values compared to the hydrophobic 5HFB glass spheres. Therefore, surface properties may have played a role at high volume fractions. An effect related to the surface properties was already indicated by the higher steady state torque values for the hydrophilic spheres compared to the hydrophobic spheres, as well as by the small deformation measurements ( $\tan\delta$ ). Second, 10HFL showed larger  $\sigma$  values compared to 100HFL, which might be explained by the higher specific surface area of the small spheres.<sup>35</sup> The same trend seems valid for the relatively small fat droplets compared to the relatively larger 5HFB spheres. When comparing the 10HFL and 100HFL glass spheres, the difference in specific surface area (i.e. surface area to volume ratio), which is directly proportional to the inverse of the sphere diameter, is approximately a factor 10. However, the results

showed that the largest variation in  $\sigma$  was less than a factor 2. Thus, the change in specific surface area is not the sole determining factor in the observed variation in  $\sigma$  when comparing small-sized and large-sized spheres. Therefore, we only expect an interaction effect related to the surface properties of the glass spheres and the fat droplets that affected the measured  $\sigma$ . Further, it must be noted that the samples with high volume fractions of filler tended to show more deviations as the difficulty of analyzing the samples increased.

Figure 8 includes the model of Ross-Murphy (equation 7), which shows a discrepancy with our measured values when  $\phi_{max}$  was set at 0.6. Ross-Murphy's model even predicts a minimum at a volume fraction of 0.07, which is not in agreement with our data.<sup>7</sup> Furthermore, our data suggests a finite value of  $\sigma$ , even at the densest sphere packing, which is in contrast to the model's prediction. The curvature of the model is not influenced when  $\phi_{max}$  is used as a fit parameter. Therefore, we can conclude that the use of  $\phi_{max}$  in equation 7 is incorrect. Langley and Green<sup>10</sup> applied the model by Ross-Murphy to explain particle size effects combined with strong interaction by assuming the existence of a whey protein layer around glass spheres, which increased the effective volume of the filler particles. They estimated effective  $\phi_{max}$  values that increased with increasing filler size, and calculated an adhering protein layer independently of the filler size.<sup>10</sup> The discrepancy of Ross-Murphy's model compared to our measurements did not allow such an approach. Moreover, the selected  $\phi_{max}$  with value 0.6 seems valid for our measured data in Figure 8, thus an effective  $\phi_{max}$  could not be deduced, which leads to the conclusion that the presence of such a protein layer was unlikely.

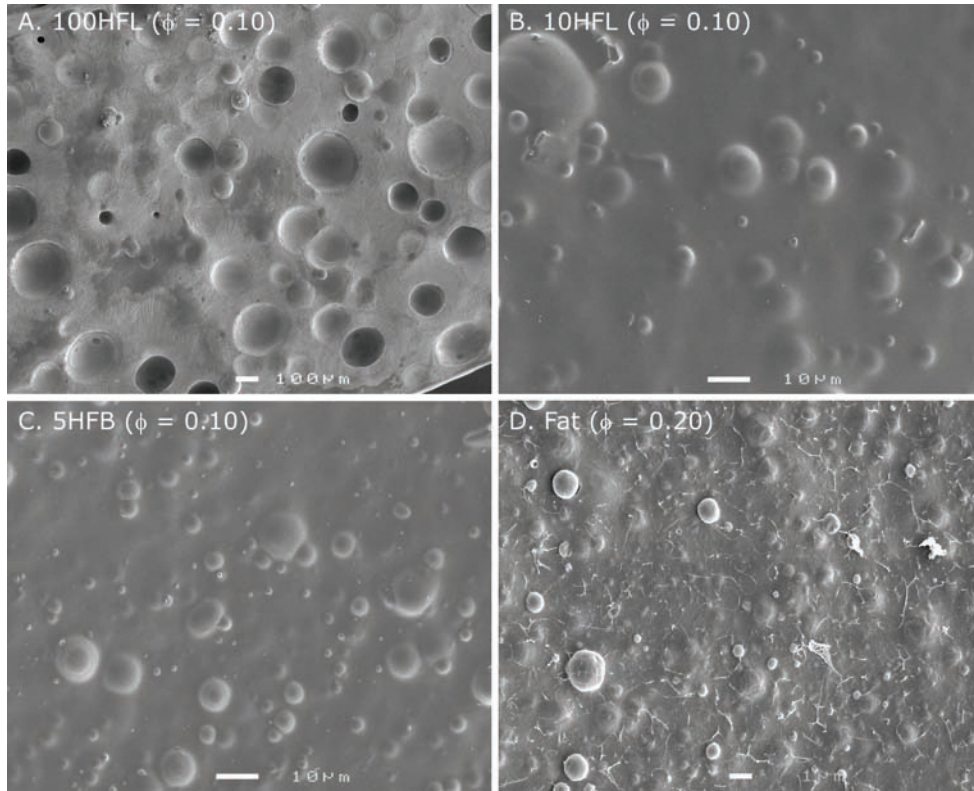
In contrast to the previous model, Turcsanyi's empirical model (equation 8), applied to our data showed excellent fits of the corresponding data using a minimal least squares method including the average measured value of  $\sigma$ . The fitted values of the interaction parameter  $\beta$  were 6.70 (100HFL), 7.67 (10HFL), 6.61 (5HFB) and 6.98 (fat), which indicate a positive and strong interaction between both a hydrophilic surface and sodium caseinate, and a hydrophobic surface and sodium caseinate. This confirms the amphiphilic character of the sodium caseinate protein.<sup>36,37</sup> Unfortunately, to our knowledge, no specific studies are known that elaborate on the degree of hydrophilicity of sodium caseinate or its components. Moreover, since  $\beta$  lacks a direct physical meaning<sup>28</sup>,  $\beta$  is not suited to predict the exact degree of interaction except for the indication of a weak ( $\beta < 3$ ) or strong ( $\beta >$

3) interaction with the matrix. However, Figure 8 shows that slight differences in  $\beta$  lead to large differences in  $\sigma$  at high volume fractions, indicating the sensitivity of the predictions of  $\beta$ . Therefore, since  $\sigma$  is increasing over the whole measured volume fraction range, including fat as filler, all applied fillers showed a positive interaction with the protein matrix, which resulted in more rigid structures. Moreover,  $\beta$  seems to be a sensitive parameter to characterize the slight differences in the type of glass surfaces of the fillers, as these were non-identical. The fact that the fat droplets showed a slightly higher interaction with the protein matrix than the hydrophobic 5HFB spheres might indicate a hydrophilic contribution of the fatty acid composition of palm fat to the protein-fat interaction. Overall, we can conclude that  $\sigma$  can be explained by taking into account the volume fraction and interaction between filler and matrix only.

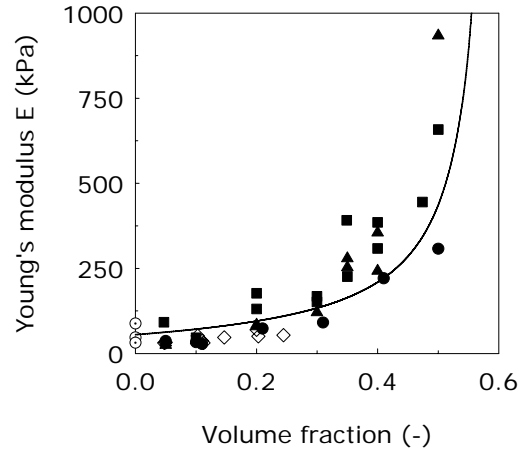
When a filler and matrix exhibit strong interaction, we expect that the fracture caused by the tensile deformation occurs through the matrix phase, which can be considered as the weak link in the composite.<sup>1,3,10</sup> SEM images (Figure 9) of the various sodium caseinate composites confirm that the fracture surface was located in the matrix phase as all filler particles were covered with protein matrix after the large tensile deformation. Only a few fat droplets were uncovered, which may be due to the shrinkage of fat during freezing of the composite samples after the tensile deformation (Figure 9D).

Figure 10 illustrates the increase of Young's modulus  $E$  due to an increasing volume fraction of filler. The  $E$ , which is the stiffness of the sodium caseinate composites, showed the largest increase at high volume fractions, which was similar to  $\sigma$  and  $G^*$ . The  $E$  values for 100HFL were higher for the whole volume fraction range compared to the other fillers. Researchers have reported on possible particle size effects on  $E$ <sup>35</sup>, or rejected these effects due to experimental errors<sup>30</sup>, or showed that  $E$  is not depending on particle size but on the aspect ratio of fillers.<sup>38</sup> Based on literature and our previous findings, we believe that the 100HFL fillers showed slightly higher  $E$  values due to a slightly different interaction with the matrix compared to the other fillers (based on  $\beta$  values). Further, the slight difference in interaction between hydrophilic and hydrophobic glass spheres came forward in  $E$  especially at high volume fractions. In Figure 10, the modified Kerner equation with a fixed  $\phi_{max}$  value of 0.6 and Poisson's ratio ( $\nu$ ) of 0.5 (equation 9) was found to be in agreement with the measured  $E$ . The model slightly overpredicted

our data up to a volume fraction of 0.30, which was mainly influenced by the choice of the average measured value for  $E_c$ . This value may have been affected by air inclusions to the same extent as the measured yield strain  $\varepsilon$  as  $E$  is the initial slope of the stress-strain curve. Further, the prediction by the model was found to be acceptable compared to data at high volume fractions. Summarizing, the modified Kerner equation agreed reasonably with the data; the prediction by the model may be improved by both the choice of  $E_c$  and  $\phi_{max}$ . The Young's modulus can be explained in terms of the volume fraction and  $\phi_{max}$ , and is independent of filler size and surface properties, which is in agreement with the model.



**Figure 9** SEM images of sodium caseinate composites containing 0.10 volume fraction of (A) 100HFL (bar 100  $\mu\text{m}$ ), (B) 10HFL (bar 10  $\mu\text{m}$ ), (C) 5HFB glass spheres (bar 10  $\mu\text{m}$ ) and 0.20 volume fraction of (D) fat droplets (bar 1  $\mu\text{m}$ ). In the sample of 100HFL (A) either air bubbles or holes, in which glass spheres were attached prior to the tensile deformation, are visible. Both 10HFL (B) and 5HFB (C) show fully covered glass spheres with protein matrix, whereas a few fat droplets (D) are uncovered.



**Figure 10** Influence of the volume fraction of filler (■100HFL, ▲10HFL, ●5HFB, and ◇ fat) on the Young's modulus ( $E$ ) measured with large tensile deformations. The sodium caseinate matrix is depicted with ○. The solid line represents the modified Kerner's equation (equation 9) in which  $\phi_{max}$  was set at 0.6 and the Poisson's ratio  $\nu$  at 0.5.

The large deformation measurements provided additional insight into the rheological behavior of the sodium caseinate composites during tensile fracture, indicating that interaction between filler and matrix plays a role in these composites. The tensile measurements showed slightly larger differences between the hydrophilic and hydrophobic glass spheres than the small deformation measurements, suggesting that hydrophilic fillers interacted slightly more strongly with sodium caseinate. However, the large deformation results confirmed the amphiphilic character of sodium caseinate, and the similarity in behavior of the hydrophobic glass spheres and fat droplets. Based on the results, the effect of particle size on the properties of the sodium caseinate composites is minor.

#### 4.4 Implications for design of composite foods

When designing new composite foods, we need to understand the quantitative influence of the various parameters on the rheology of the final product. In this work, we show that a dispersed phase largely influences the rigidity and strength of a sodium caseinate composite as indicated by increasing  $G^*$ ,  $E$  and  $\sigma$  values with

increasing volume fraction of either glass spheres or fat. A small amount of filler only caused the largest change in  $\varepsilon$ , which reflects the need for using both small and large deformations to fully characterize food composites. Table 4 summarizes the effects of the design parameters on the structural properties of caseinate composites. These design parameters are categorized in key parameters concerning the dispersed phase, and the interaction between this phase and the continuous phase.

The most crucial parameter in designing and predicting structural properties of food composites is the volume fraction of dispersed particles. The rheological properties of the continuous phase ( $G_c^*$ ,  $\varepsilon_c$ ,  $\sigma_c$  and  $E_c$ ), which are included as implicit design parameters in Table 4, also influence the structural properties of composites to a large extent. The particle size distribution of the dispersed phase plays a role in composites through  $\phi_{max}$ . The largest difference between the small and large deformation properties of composites is the influence of matrix-filler interaction on the latter properties. Especially  $\sigma$  was found to be sensitive to even slight differences in surface properties of fillers, which caused different matrix-filler interactions ( $\beta$ ). This implies that in case of fat as dispersed phase, the large deformation properties will be strongly affected by the fatty acid composition.

Table 4 is concluded with the predictive models from literature describing all effects on the structural properties of composite materials within 10% margins. The relatively simple models are reliable indicators for the design of composite foods. As an illustration, the predicted effect of 10 to 20% fat on the structural properties of cheese-like products is at the most a factor 2, which underlines the importance of the protein matrix properties.

**Table 4** Influence of design parameters on the final product properties of composite foods. Each product property is influenced by its respective continuous phase property as indicated in the equations. The investigated influences are denoted with + (increasing magnitude of the product property), – (decreasing magnitude of the product property), 0 (no influence).

Design parameters	Product properties				
	$G^*$	$\tan\delta$	$\varepsilon$	$\sigma$	$E$
$\phi$	++	0 <sup>a</sup>	--	++	++
(Rigid) dispersed phase properties					
$d_{32}$	0	0 <sup>a</sup>	0	0 <sup>b</sup>	0
PSD	+(via $\phi_{max}$ )	0	0	0	+(via $\phi_{max}$ )
Interaction matrix and filler					
$\beta$	0 <sup>c</sup>	0 <sup>c</sup>	+ <sup>d</sup>	++ <sup>e</sup>	+ <sup>d</sup>
Models <sup>f</sup>	$G_c^* \cdot \left( 1 + \frac{1.25 \cdot \phi}{1 - \phi_{max}} \right)^2$ or $G_c^* \cdot \left( 1 - \frac{\phi}{\phi_{max}} \right)^{-2.5 \cdot \phi_{max}}$				
	No model available	$\varepsilon_c \cdot (1 - K \cdot \phi^{1/3})$ with $K = 1$	$\sigma_c \cdot \left( \frac{1 - \phi}{1 + 2.5 \cdot \phi} \right) \cdot \exp(\beta \cdot \phi)$	$E_c \cdot \frac{1 + A \cdot \phi}{1 - \psi \cdot \phi}$ with $A = 1.5$ and $\psi = 1 + \phi \cdot \left( \frac{1 - \phi_{max}}{\phi_{max}^2} \right)$	

<sup>a</sup>Tan $\delta$  at high volume fractions ( $\phi \geq 0.25$ ) probably exhibited a particle size dependency.

<sup>b</sup>Besides the major influence of the matrix-filler interaction, the particle size may have a minor effect on  $\sigma$  of composites via the specific surface area.

<sup>c</sup>No-slip conditions are assumed when applying the rheological models for suspensions to composites.

<sup>d</sup>The models assume perfect adhesion to describe  $\varepsilon$  and  $E$  of composites.

<sup>e</sup>The interaction parameter  $\beta$  was found to be very sensitive.

<sup>f</sup>The equations are respectively from left to right from Eilers<sup>22</sup>, Pal<sup>19</sup>, Nielsen<sup>27</sup>, Turcsanyi<sup>28</sup>, and Lewis and Nielsen<sup>30</sup>.



## 5. Conclusions

A set of relatively simple equations, which have usually been applied for polymer suspensions and composites, could adequately predict the main structural properties of the investigated sodium caseinate composites comprising rigid fillers. These quantitative models provide guidelines to design new composite foods with merely a few design parameters that can be easily varied and measured.

Both results and selected models showed that the small and large deformation properties of composites largely depend on the volume fraction of the dispersed phase and the structural properties of the continuous phase. Most of the structural properties of the sodium caseinate composites were influenced with an order of magnitude by varying the key parameter  $\phi$  and showed the largest increase at high volume fractions of filler compared to the continuous phase properties. In contrast, low volume fractions of filler already caused a large decrease in  $\varepsilon$ .  $\tan\delta$  was expected to be independent of the volume fraction but showed a decreasing trend.

The particle size distribution in terms of  $\phi_{max}$  influenced  $G^*$  and  $E$  at high volume fractions of filler. The interaction between the continuous and dispersed phase plays an important role in the large deformation properties  $\varepsilon$ ,  $\sigma$  and  $E$ . This matrix-filler interaction is explicitly included in the model for  $\sigma$ . The strong interaction between sodium caseinate and both hydrophilic and hydrophobic glass spheres confirmed the amphiphilic behavior of sodium caseinate. Furthermore, the strong matrix-filler interaction generally leads to an increase in rigidity ( $G^*$  and  $E$ ). The particle size played no major role in the structural properties of the sodium caseinate composites.

## Acknowledgements

The authors wish to thank L. Hulshof for executing the first experiments in context of this research, A. van Aelst for preparing the SEM images, J. Champion for proofreading the manuscript, M. Paques and F.J.H. Jeurissen from Friesland Foods for the helpful discussions.

## References

- (1) Green, M. L.; Marshall, R. J.; Langley, K. R. **1989**. In *Structure and mechanical properties of model composite foods*. Annual Meeting of the British Society of Rheology, Warwick, Coventry; Carter, R. E., Ed. Elsevier Science: 1-12.
- (2) Luyten, H.; Van Vliet, T.; Walstra, P. **1992**. Comparison of various methods to evaluate fracture phenomena in food materials. *Journal of Texture Studies* 23 245-266.
- (3) Langley, K. R.; Martin, A.; Ogin, S. L. **1994**. The effect of filler volume fraction on the fracture-toughness of a model food composite. *Composites Science and Technology* 50 (2): 259-264.
- (4) Lee, C. M. **2002**. Role of hydrodynamically active biopolymeric ingredients in texture modification and physical stabilization of gel-based composite foods. *Journal of Food Science* 67 (3): 902-908.
- (5) Luyten, H.; Van Vliet, T. **1989**. In *Influence of a filler on the rheological and fracture properties of food materials.*, Annual Meeting of the British Society of Rheology, Warwick, Coventry; Carter, R. E., Ed. Elsevier Science: 43-56.
- (6) Richardson, R. K.; Robinson, G.; Ross-Murphy, S. B.; Todd, S. **1981**. Mechanical spectroscopy of filled gelatin gels. *Polymer Bulletin* 4 541-546.
- (7) Ross-Murphy, S. B.; Todd, S. **1983**. Ultimate tensile measurements of filled gelatin gels. *Polymer* 24 (4): 481-486.
- (8) Kim, K. H.; Renkema, J. M. S.; Van Vliet, T. **2001**. Rheological properties of soybean protein isolate gels containing emulsion droplets. *Food Hydrocolloids* 15 (3): 295-302.
- (9) Reiffers-Magnani, C. K.; Cuq, J. L.; Watzke, H. J. **1999**. Composite structure formation in whey protein stabilized o/w emulsions. I. Influence of the dispersed phase on viscoelastic properties. *Food Hydrocolloids* 13 (4): 303-316.
- (10) Langley, K. R.; Green, M. L. **1989**. Compression strength and fracture properties of model particulate food composites in relation to their microstructure and particle-matrix interaction. *Journal of Texture Studies* 20 (2): 191-207.
- (11) Van Vliet, T. **1988**. Rheological properties of filled gels. Influence of filler matrix interaction. *Colloid Polymer Science* 266 518-524.
- (12) Jampen, S.; Britt, I. J.; Yada, S.; Tung, M. A. **2001**. Rheological properties of gellan gels containing filler particles. *Journal of Food Science* 66 (2): 289-293.
- (13) Van der Poel, C. **1958**. On the rheology of concentrated dispersions. *Rheologica Acta* 1 (2-3): 198-205.
- (14) Zhou, N.; Mulvaney, S. J. **1998**. The effect of milk fat, the ratio of casein to water, and temperature on the viscoelastic properties of rennet casein gels. *Journal of Dairy Science* 81 (10): 2561-2571.

- (15) Goodier, J. N. **1933**. Concentration of stress around spherical and cylindrical inclusions and flaws. *Journal of Applied Mechanics A* 55: 39-44.
- (16) Hill, R.; Power, G. **1956**. Extremum principles for slow viscous flow and the approximate calculation of drag. *Quarterly Journal of Mechanical and Applied Mathematics* 9 (3): 313-319.
- (17) Uemura, S.; Takayanagi, M. **1966**. Application of the theory of elasticity and viscosity of two-phase systems to polymer blends. *Journal of Applied Polymer Science* 10: 113-125.
- (18) Palierne, J. F. **1990**. Linear rheology of viscoelastic emulsions with interfacial tension. *Rheologica Acta* 29 204-214.
- (19) Pal, R. **2002**. Complex shear modulus of concentrated suspensions of solid spherical particles. *Journal of Colloid and Interface Science* 245 (1): 171-177.
- (20) Einstein, A. **1906**. Eine neue Bestimmung der Molekuldimensionen. *Annalen der Physik* 19: 289-296.
- (21) Einstein, A. **1911**. Berichtigung zu meiner Arbeit: "Eine neue Bestimmung der Molekuldimensionen". *Annalen der Physik* 34: 591-592.
- (22) Eilers, H. **1941**. Die Viskosität von Emulsionen hochviskoser Stoffe als Funktion der Konzentration. *Kolloid Zeitschrift* 97: 313-321.
- (23) Krieger, I. M.; Dougherty, T. J. **1959**. A mechanism for non-Newtonian flow in suspensions of rigid spheres. *Transactions of the Society of Rheology* III: 137-152.
- (24) Mooney, M. **1951**. The viscosity of a concentrated suspension of spherical particles. *Journal of Colloid Science* 6 (2): 162-170.
- (25) Steinhaus, H. **1999**. In *Mathematical snapshots*; 3rd ed., Dover, New York: 202-203.
- (26) Smith, T. L. **1959**. Volume changes and dewetting in glass bead - polyvinyl chloride elastomeric composites under large deformations. *Transactions of the Society of Rheology* 3: 113-136.
- (27) Nielsen, L. E. **1966**. Simple theory of stress-strain properties of filled polymers. *Journal of Applied Polymer Science* 10 (1): 97-102.
- (28) Turcsanyi, B.; Pukanszky, B.; Tudos, F. **1988**. Composition dependence of tensile yield stress in filled polymers. *Journal of Materials Science Letters* 7: 160-162.
- (29) Kerner, E. H. **1956**. The elastic and thermo-elastic properties of composite media. *Proceedings of the Physical Society B* 8: 808-813.
- (30) Lewis, T. B.; Nielsen, L. E. **1970**. Dynamic mechanical properties of particulate-filled composites. *Journal of Applied Polymer Science* 14 (6): 1449-1471.
- (31) Gunasekaran, S.; Ak, M. M. **2003**. In *Cheese rheology and texture*; CRC Press, Boca Raton, FL: 437.

- (32) Servais, C.; Jones, R.; Roberts, I. **2002**. The influence of particle size distribution on the processing of food. *Journal of Food Engineering* 51 (3): 201-208.
- (33) Chen, J. S.; Dickinson, E. **1999**. Effect of surface character of filler particles on rheology of heat-set whey protein emulsion gels. *Colloids and Surfaces B-Biointerfaces* 12 (3-6): 373-381.
- (34) Stading, M.; Hermansson, A. M. **1991**. Large deformation properties of beta-lactoglobulin gel structures. *Food Hydrocolloids* 5 (4): 339-352.
- (35) Ahmed, S.; Jones, F. R. **1990**. A review of particulate reinforcement theories for polymer composites. *Journal of Materials Science* 25: 4933-4942.
- (36) Horne, D. S.; Leaver, J. **1995**. Milk proteins on surfaces. *Food Hydrocolloids* 9 (2): 91-95.
- (37) Horne, D. S. **1998**. Casein interactions: Casting light on the black boxes, the structure in dairy products. *International Dairy Journal* 8 (3): 171-177.
- (38) Verbeek, C. J. R. **2003**. The influence of interfacial adhesion, particle size and size distribution on the predicted mechanical properties of particulate thermoplastic composites. *Materials Letters* 57: 1919-1924.



# 3

## Influence of mixing during enzymatic gelation of caseinate-water and caseinate-water-fat systems

---

This chapter is published as: Manski, J.M.; Van der Goot, A.J.; Boom, R.M. **2007**. Influence of shear during enzymatic gelation of caseinate-water and caseinate-water-fat systems. *Journal of Food Engineering* 79 (2): 706-717.

## **Abstract**

Solidification, emulsification, and application of shear were combined to induce diversity and heterogeneity in the micro- and macrostructure of concentrated caseinate-based food matrices containing a dispersed fat phase. The products were evaluated with selected parameters from small-scale and large-scale deformations and confocal scanning laser microscopy. Sodium caseinate (10-30% w/w) was solidified with transglutaminase during mixing in a Brabender Do-Corder mixer, and palm fat (15% v/v) was emulsified either simultaneously during crosslinking, or after crosslinking. In absence of fat, granular caseinate structures were obtained. Adding fat prior to solidification and mixing resulted in strong homogeneous gels. Adding fat after solidification yielded protein granules surrounded by a concentrated fat phase. The structures were weaker and more brittle, and showed less strain hardening than the systems without fat, even though the linear viscoelastic properties were hardly different from the materials obtained by adding fat prior to mixing and solidification.

## 1. Introduction

One of the key aspects of food product design is creating new functional properties and novel food macro- and microstructures in order to provide tailored food characteristics desired by consumers. Texture and consistency of food products are major determinants of the overall properties of the products, including fracture properties during mastication. A food product fractures when local stresses exceed the cohesive stresses in a product.<sup>1</sup> By altering the spatial distribution and interaction of macrostructural elements in foods, we can influence the fracture pathways.

In addition to this, there is a trend to change the product formulation for health or sustainability reasons. Alternatively, ingredients of animal origin may be substituted for ingredients of vegetable origin. The challenge to be met is therefore to control the process of structuring food ingredients such that the same food microstructure is obtained for a range of ingredient formulations, or such that a range of microstructures can be obtained with one ingredient formulation only. Thus, it is important to investigate solidification and structuring as a function of the conditions during processing.

Enzymes can induce changes in texture, flavor, and nutritional values. Protein crosslinking enzymes have received much attention in recent years, especially  $\text{Ca}^{2+}$ -independent transglutaminase derived from *Streptoverticillium moberansae* (Tgase). Researchers have explored the potential of Tgase in diverse applications, such as cereals<sup>2,3</sup>, meat<sup>4-7</sup> and dairy products. Most studies focus on dairy applications in which Tgase influenced the protein network structure, leading to beneficial properties, such as reduced serum separation in yoghurt<sup>7,8</sup>, improved gelation and water binding properties of skim milk powder.<sup>9</sup> Kuraishi et al. found that Tgase increased curd yield.<sup>10</sup> An increased glass transition temperature of the gel<sup>11</sup> and improved water holding capacity<sup>9</sup> can explain most of the changes in product quality induced by Tgase. Furthermore, Tgase can be applied to control product rheology.<sup>12-15</sup>

Tgase catalyzes acyl-transfer reactions between  $\gamma$ -carboxamide groups of glutamine and the  $\epsilon$ -amino group of lysines in proteins, leading to inter- or intramolecular crosslinking. Sodium caseinate is reported to be a good substrate

for Tgase, mainly because of the open tertiary structure.<sup>16,17</sup> Lorenzen and co-workers studied the crosslinking of a sodium caseinate solution (15% w/w) and concluded that the crosslinking reaction was fast and that high degrees of crosslinking could be obtained.<sup>16</sup> Dickinson and Yamamoto showed that crosslinking of sodium caseinate before as well as after emulsification resulted in stable emulsions, indicating that crosslinking polymerization had no major effect on the emulsifying properties of casein (3% w/w).<sup>12</sup> However, the latter emulsions showed an increase in average droplet size with crosslinking time. Faergemand et al. confirmed these findings and concluded that the rate of development of surface viscoelasticity depended on the moment of crosslinking.<sup>18</sup> Tgase induced emulsion gels containing sodium caseinate (5% w/w) had similar values for the elastic ( $G'$ ) and viscous ( $G''$ ) moduli compared to more concentrated gels consisting of crosslinked protein only (9% w/w).<sup>12</sup> This could be attributed to the reinforcing effect of the dispersed phase.

For product applications, increased consistency might be desired by applying for example higher protein concentrations. The objective of the study reported here was to show the effect of processing on concentrated sodium caseinate solutions (up to 30% w/w) during Tgase catalyzed reactions and the resulting effects on selected rheological properties. Furthermore, the interaction between solidification of the concentrated sodium caseinate solutions and emulsification of added fat during processing was investigated with the goal to induce heterogeneity in the microstructure of the resulting soft solid products. The influence of processing on the behavior of crosslinked protein and the emulsification of fat was studied in a Brabender mixer (Duisburg, Germany), which is a well-accepted scale model of an extrusion process. Selected parameters from both small-scale and large-scale deformations and confocal scanning laser microscopy (CSLM) were used to reveal differences in macro- and microstructural properties of the highly concentrated protein and emulsion gels obtained after processing.



## 2. Materials and methods

### 2.1. Enzyme

Microbial  $\text{Ca}^{2+}$ -independent transglutaminase (protein-glutamine:amine  $\gamma$ -glutamyl-transferase, EC 2.3.2.13) derived from *Streptoverticillium moberansae* (1% Tgase, 99% maltodextrine) was obtained from Ajinomoto Co. Inc. (Tokyo, Japan). The enzyme activity was determined with the hydroxamate method.<sup>19</sup> The measured activity was 84 units $\cdot\text{g}^{-1}$ . A 20% (w/w in demineralized water) Tgase solution was prepared freshly every day prior to experimental runs by mechanical stirring for 1 h.

### 2.2 Preparation sodium caseinate gels

Sodium caseinate was obtained from DMV International (Veghel, The Netherlands). The product contained at least 88% protein according to the manufacturer's specifications. All protein concentrations used in this study are expressed as w/w. The concentrated sodium caseinate was either (1) crosslinked with Tgase during mixing in the Brabender mixer, or (2) only mixed without enzyme treatment, or (3) crosslinked with Tgase in an oven without mixing. Prior to a selected processing treatment, sodium caseinate was prepared as a solution, or as a premix, depending on the concentration used due to limited solubility of sodium caseinate at high concentrations in water:

- (i) 10% protein was dissolved in demineralized water at room temperature at least 12 h prior to an experimental run. The Tgase solution was added shortly before an experimental run so that the resulting enzyme-protein ratio was 1:10 (w/w), and the protein-enzyme solution was stirred for a few minutes at room temperature prior to further processing;
- (ii) 20% and 30% protein were mixed with demineralized water in a kitchen mixer at low mixing rate and at room temperature for a few minutes right before an experimental run. In the case of enzyme treatment, the Tgase solution (enzyme-protein ratio 1:10) was added to the kitchen mixer as well.

All sodium caseinate premixes (pH 6.8 - 7.0) contained a final concentration of 1% (w/w) sodium benzoate (Sigma Aldrich, Zwijndrecht, The Netherlands) that acted

as a preservative, and  $2 \cdot 10^{-4}\%$  (w/w) Rhodamine 110 (83695, Sigma Aldrich), which was added as a  $0.02 \text{ g} \cdot \text{L}^{-1}$  solution in phosphate buffered saline (PBS) prior to processing. Rhodamine 110 was used as a fluorescent protein dye for CSLM.

Crosslinked sodium caseinate samples during mixing were prepared by transferring the above-mentioned premixes to the mixing bowl (type W50) of the Brabender Do-Corder 330 (Brabender OHG, Duisburg, Germany), which was pre-heated and kept at a constant temperature of  $50^\circ\text{C}$  with a water bath. The mixing profile was set as follows: 4 min at 5 rpm, then an increase from 5 to 50 rpm in 1 min, and a selected duration at 50 rpm depending on the protein concentration (30 min for 20% and 30% protein; 60 min for 10% protein). The torque was monitored during mixing and crosslinking. For comparison, crosslinked sodium caseinate samples without mixing were heated in a  $50^\circ\text{C}$  oven with similar crosslinking reaction times as in the Brabender mixer. Further, 20%, 30% and 40% sodium caseinate premixes were prepared similarly to 20% premixes but without Tgase, and mixed in the Brabender mixer for 21 min at  $40^\circ\text{C}$ . After processing, the sodium caseinate gels were collected in a mould of two square parallel plates ( $100 \times 100 \text{ mm}$ ), which provided a controlled sample height of 3 mm. All samples were stored in a refrigerator at  $4^\circ\text{C}$  for one day, until further analysis.

### ***2.3 Preparation sodium caseinate emulsion gels***

Palm fat, with a melt trajectory from  $20^\circ\text{C}$  to  $37^\circ\text{C}$ , was acquired from Barentz Raw Materials (Hoofddorp, The Netherlands). All fat contents are expressed as volume fractions. Nile Red (72485, Sigma Aldrich), which is a fluorescent dye for fat for CSLM, was added to the melted palm fat in a concentration of  $0.1 \text{ g} \cdot \text{L}^{-1}$ . To each emulsion gel, 15% of the fat-Nile Red solution was added. The sodium caseinate premixes were prepared as previously described. Fat was added either:

- (i) during the first 4 min of the mixing time in the Brabender, which will be referred to as ' $t = 0$ ' in which crosslinking and emulsification occurred simultaneously;
- (ii) or at the moment that a minimal torque value was reached after having observed a torque maximum first, which will be referred to as ' $t =$  after torque peak (a.p.)' in which emulsification occurred after most of the protein was crosslinked.

The temperature during mixing, crosslinking and emulsification was kept constant at 50°C. After processing, the samples were collected and stored in the same way as the protein gels.

#### **2.4 Small-scale deformations**

Small-scale deformations were performed using dynamic strain amplitude tests on a stress-controlled Bohlin CVO (Bohlin Instruments Ltd., Cirencester, U.K.). Serrated parallel plates (diameter 25 mm, gap 2 mm) were used in order to prevent slip. A chamber covering the plates and the sample was used to prevent evaporation. Before measuring, samples were rested for 15 min to allow relaxation of the stresses induced by sample loading. Strain amplitude tests were performed in duplicate at a constant frequency of 1 Hz and at a temperature of 20°C. The rheological parameters to compare the structural properties of the protein and emulsion gels were the elastic modulus  $G'$  and  $\tan\delta$  within the linear viscoelastic (LVE) region. The coefficient of variance between independently produced samples in the Brabender mixer was 13% for  $G'$  and 3% for  $\tan\delta$ .

#### **2.5 Large-scale deformations**

A Texture Analyzer T2 (Stable Micro Systems Ltd., Surrey, U.K.) was used for large-scale deformation tests. Uni-axial tensile tests were conducted with a constant deformation rate of 3 mm·s<sup>-1</sup> at 14°C ± 2°C. Samples were cut into a dog bone shape with a total length of 90 mm. The width of the middle part of the samples was narrower (15 mm) than the outer parts (20 mm) to induce fracture in the middle of the dog bone-shaped samples. The length of the narrow part was 20 mm. Triplicate measurements were performed on a protein or emulsion gel sample.

The so-called Hencky strain ( $\varepsilon$ ), the tensile yield stress ( $\sigma$ ) and the Young's modulus ( $E$ ) were calculated as described by Gunasekaran and Ak.<sup>20</sup> The apparent strain hardening coefficient  $n$  was determined by applying a power law fit ( $\sigma = k \cdot \varepsilon^n$ ) on the  $\sigma$ - $\varepsilon$  curve in the measured  $\varepsilon$ -range of 30-100%, in order to provide additional information on the protein and emulsion gels. When  $n$  exceeds the value of 1, the sample exhibits strain hardening.<sup>21</sup> The coefficient of variance between

independently produced samples in the Brabender mixer was 7% for  $\sigma$ , 10% for  $\varepsilon$  and 3% for  $E$ .

## 2.6 CSLM and image analysis

After storing the sodium caseinate samples containing fat for one day at 4°C, samples were carefully cut, transferred to 2-well chambered coverglasses (Nunc, Naperville, IL, U.S.A.) and analyzed with an inverted LSM 510 (Zeiss, Oberkochen, Germany). An Ar-ion laser (488 nm) and HeNe laser (543 nm) were used to excitate the samples, and images were digitally recorded with a 10x dry objective (N.A. 0.3, zoom 2x and 4x) and for a few samples with a 40x oil immersion objective (N.A. 1.3). For the sodium caseinate phase, an emission filter of 505-530 nm was applied, whereas a 600-650 nm filter was used for the fat phase. CSLM images were analyzed using Image-J software<sup>22</sup>, in which the color responses for fat and protein were split. The resulting images were binarized and automatically thresholded. Pixels representing either fat or protein were counted and used for calculating the fat area fraction ( $A_{fat}$ ) per protein area fraction ( $A_{protein}$ ) to eliminate the influence of entrapped air. The average normalized fat area fraction ( $A_{fat}/A_{protein}$ ) was determined from 8 images (4 images at 20x and 40x magnification respectively) per sample.

## 2.7 Protein content

The protein contents of a selected number of sodium caseinate gels and emulsion gels were determined by the Dumas method using a NA2100 nitrogen and protein analyzer (CE Instruments, Milan, Italy). The nitrogen-protein conversion factor was 6.38.<sup>23, 24</sup> The added protein contents ( $x_{added}$ ) were confirmed with the measured protein values ( $y_{measured}$ ), which resulted in the following correlation:  $y_{measured} = 1.0049 \cdot x_{added}$  with  $R^2=0.9561$ . The following results will be discussed in terms of the protein content values that were aimed for in this study.

## 2.8 SDS-polyacrylamide gel electrophoresis

Sodium caseinate (10%, 20% and 30%) gels crosslinked in the Brabender mixer were first heated at 85°C for 6 min to inactivate Tgase, and subsequently

suspended in demineralized water to a final concentration of 10% (w/w) and stirred for 1 day using a magnetic stirrer. The suspending media were diluted 6x with SDS buffer, and SDS-polyacrylamide gel electrophoresis (SDS-PAGE) was performed with a mini-PROTEAN-3 electrophoresis system using Tris-HCl Ready Gel Precast 4-15% gradient gels (Biorad, Veenendaal, The Netherlands) according to the method of Laemmli.<sup>25</sup>

### 3. Results and discussion

#### 3.1 Sodium caseinate gels

##### 3.1.1 Processing aspects

Solidification of sodium caseinate solutions in the absence of shear transformed the protein solutions into homogeneous soft solids. Simultaneous solidification and mixing induced major structural changes, which were accompanied by typical torque responses as illustrated in Figure 1. After the increase to 50 rpm ( $t = 5$  min), the following stages in torque values could be distinguished: (a) a lag phase; (b) an increase to a maximum torque value; (c) followed by a decrease. The viscosity increase due to crosslinking caused the rise in torque during the first two stages, during which the protein premixes ( $\geq 20\%$ ) became considerably less gluey. The lag phase decreased in duration, whereas the maximum (peak) torque value increased with increasing protein content. At the peak torque, the crosslinked protein network started to lose its fluidity and solidified. This resulted in rupture of the network into soft protein granules with continued mixing. The Brabender mixer seemed to act as a mill, which accounts for the sudden decrease in torque observed following the peak torque. This effect was less pronounced for 10% protein. Once the minimum torque value (after peak) was reached ( $\sim 1$ -2 N·m), no change in macrostructure nor in torque was observed with continued mixing, even though further crosslinking was likely to occur based on reported Tgase rest-activity of 74% after 10 min at 50°C.<sup>26</sup>

After processing, 10% sodium caseinate resembled a soft gel without observable granules, whereas 20% and 30% sodium caseinate transformed into loosely bound,

dry-looking, irregularly shaped soft protein granules of 1-2 mm. It is likely that the smallest gap in the Brabender mixer, ca. 1.5 mm, determined the size-range of the protein granules. The formation of protein granules has been reported for whey proteins, where heat and shear were applied in the so-called microparticulation process to form whey protein aggregates, typically in the order of 5-10  $\mu\text{m}$ .<sup>27</sup> The granular macrostructure of crosslinked and mixed protein largely disappeared after overnight storage at 4°C in a mould, probably due to viscous behavior of the granules or to low Tgase activity causing assemblage of the protein granules.<sup>4,6</sup>

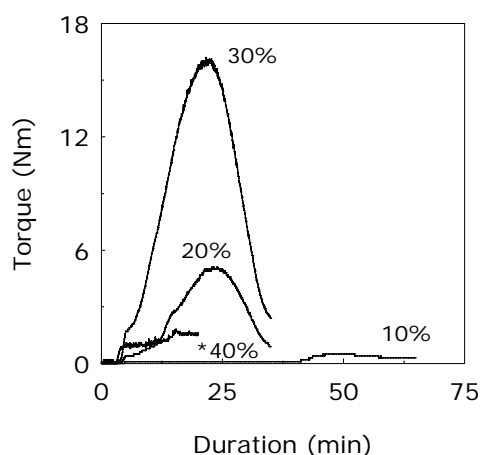


**Figure 1** Typical torque profiles during crosslinking and mixing of concentrated sodium caseinate premixes in the Brabender mixer. Sodium caseinate (10%, 20% and 30%) was crosslinked with Tgase (ration 1:10) at 50°C. Non-crosslinked sodium caseinate (\*40%) was mixed at 40°C. The mixing rate increased after 4 min within 1 min from 5 to 50 rpm, and remained at this rate for 30 min (20% and 30% protein), or 60 min (10% protein), or 16 min (40% protein).

### 3.1.2 Protein matrix properties

Sodium caseinate (30%) samples solidified with and without mixing were suspended in water, and subsequently analyzed using SDS-PAGE, as shown in Figure 2. Results from the non-mixed samples showed that more protein fragments were dissolved in water, but that all crosslinked protein samples clearly contained casein monomers (~ 25-30 kDa). The casein monomers were expected to play a role in emulsification when fat was added to the protein granules.

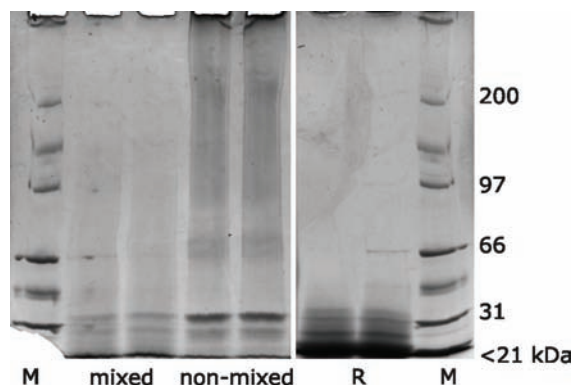


**Figure 2** SDS-PAGE gel of 30% crosslinked sodium caseinate, with or without mixing (duplicate lanes, denoted as mixed and non-mixed respectively). The protein samples were suspended in demineralized water for 1 day and the suspending medium was put on the gel. M = marker; R = reference 1% sodium caseinate in water.

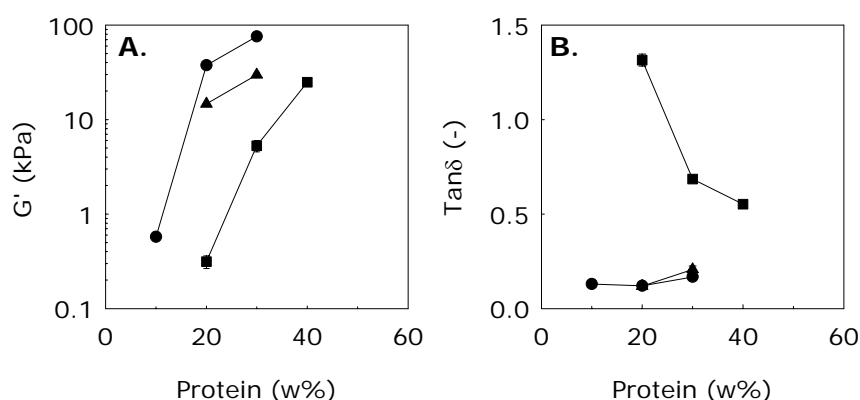


**Figure 3**  $G'$  (A) and  $\tan\delta$  (B) values of protein gels in the linear viscoelastic (LVE) region determined with strain amplitude sweeps. Sodium caseinate (10%, 20% and 30%) was either simultaneously mixed and crosslinked with Tgase (ratio 1:10), or only crosslinked, or only mixed.

Figure 3 and Figure 4 depict the influence of processing on the small-scale ( $G'$  and  $\tan\delta$ ) and the large-scale deformation properties (yield stress  $\sigma$ , Young's modulus  $E$  and yield strain  $\epsilon$ ) respectively. Mixing of sodium caseinate (20%, 30% and 40%) without enzymatic solidification resulted in protein gels with relatively low  $G'$  and high  $\tan\delta$  values. Simultaneous solidification and mixing of sodium caseinate

increased  $G'$  and decreased  $\tan\delta$  tremendously, which is typical for a polymer network with covalent bonds.<sup>28</sup> Mixing during solidification had an additional positive effect on  $G'$ , which rose by a factor 2.5 (based on 20% and 30% protein) when compared to solidification only, whereas  $\tan\delta$  remained unaffected. The fracture behavior of crosslinked and mixed protein matrices was influenced by mixing. These matrices were more brittle compared to only crosslinked protein as was shown by a decrease in  $\varepsilon$  (factor 1.4 and 2 for 20% and 30% protein respectively) that can be explained by the generated granular macrostructure. Mixing had no effect on yield stress  $\sigma$ , whereas the Young's modulus  $E$  increased after mixing and solidification (factor 2.6 and 1.8 for 20% and 30% protein respectively). However, the  $E$  values of the protein samples that were only crosslinked were probably lower due to insufficient homogeneous distribution of the enzyme at the start of the experiment, resulting in slightly weaker products.

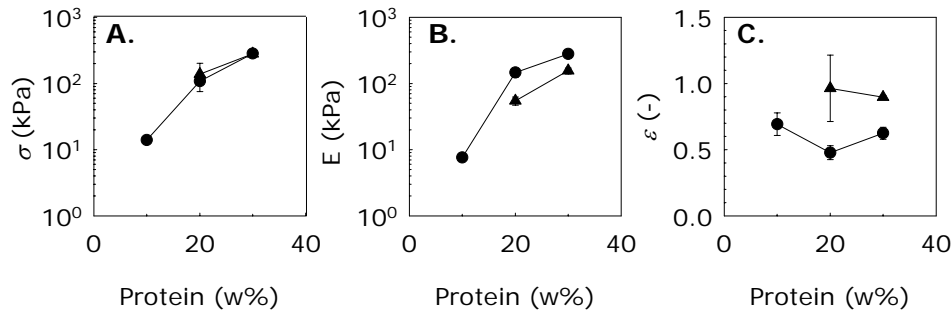


**Figure 4** Yield stress  $\sigma$  (A), Young's modulus  $E$  (B) and yield strain  $\varepsilon$  (C) of protein gels determined with tensile tests. Sodium caseinate (10%, 20% and 30%) was either simultaneously mixed and crosslinked (circle) with Tgase (ratio 1:10), or only crosslinked (triangle).

### 3.2 Sodium caseinate emulsion gels

Based on the typical torque profiles observed during processing sodium caseinate solutions (Figure 1), two moments were selected for addition of palm fat to investigate the interaction between solidification and emulsification during mixing, and for inducing heterogeneity in the microstructures. Emulsion gels were produced by adding 15% (v/v) fat, either at the start of mixing ( $t = 0$  min), or after formation of the granular protein macrostructure ( $t =$  after torque peak).



### 3.2.1 Macrostructural properties during processing

A comparison of Figure 1 and Figure 5 demonstrates that adding fat at the start of mixing ( $t = 0$  min) caused the torque to decrease relative to the situation without fat. Molten palm fat is likely to lubricate the more viscous protein phase, thus the torque of the protein-fat mixtures decreased. Compared to the systems without fat, the torque started to decrease at an earlier mixing time. Furthermore, no mechanical break-up of the protein-fat materials (i.e., formation of a granular texture) was observed during continued mixing after the torque peak. An onset of a granular structure was only evident for 30% sodium caseinate and fat. Apparently, the liquid fat droplets formed during emulsification and mixing absorbed the deformations exerted by the Brabender mixer, reducing the necessity for the protein network to fracture and form granules.

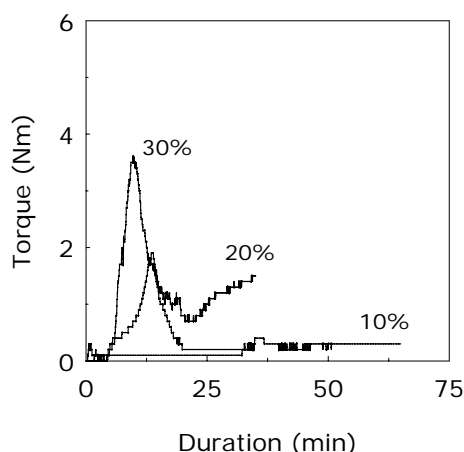


**Figure 5** Typical torque profiles during simultaneous crosslinking and emulsification of concentrated sodium caseinate premixes and palm fat in the Brabender mixer. Sodium caseinate (10%, 20% and 30%) was crosslinked with Tgase (ratio 1:10) at 50°C and 15% palm fat was added at  $t = 0$  min. The mixing rate increased after 4 min within 1 min from 5 to 50 rpm, and remained at this rate for 30 min (20% and 30% protein with 15% fat) or 60 min (10% protein with 15% fat).

Adding fat after attaining the torque peak (exactly the moment at which the measurement of the torque in Figure 1 was stopped) resulted in very different macrostructures. Upon fat addition, the measured torque dropped slightly and

increased slowly again until a stable torque value ( $\sim 1\text{-}2\text{ N}\cdot\text{m}$ ) was reached (data not shown). This response was independent of the sodium caseinate content. The resulting 10% sodium caseinate emulsion gel resembled a homogeneous soft gel, whereas the 20% and 30% sodium caseinate emulsion gels clearly retained the granular structure that we had previously observed for the protein matrices, resulting in brittle materials composed of protein granules encircled with fat. Contrary to the samples without fat, the brittle macrostructural appearance of the samples containing fat was preserved after storage.

### 3.2.2 Microstructural properties

Besides the macrostructures, the microstructures of the sodium caseinate emulsion gels obtained by changing the processing conditions, varied clearly. Figure 6 depicts a representative selection of CSLM images of the sodium caseinate emulsion gels with fat added at  $t = 0$  or at  $t =$  after torque peak. Further, a CSLM image of a 30% sodium caseinate matrix containing 15% palm fat without enzyme treatment is included to illustrate the effect of Tgase on the microstructure.

Firstly, the addition of Tgase clearly affected the (2D) spatial distribution and size of the fat droplets. In the absence of Tgase, the 30% sodium caseinate emulsion gel contained homogeneously and finely dispersed fat droplets. Secondly, the simultaneous solidification and emulsification ( $t = 0$ ) of the protein-fat mixtures yielded coarser fat droplets, which slightly increased in size with increasing protein content. The coarser droplets might be explained by the reduced availability of protein monomers due to crosslinking, leading to an increased interfacial tension. Thirdly, when fat was added after solidification ( $t =$  after torque peak), the fat did not have the possibility to penetrate the already formed protein granules. Thus, the fat was concentrated around the granules. In Figure 6, irregularly shaped protein domains ( $\geq 20\%$ ) can be distinguished with small fat droplets entrapped between the protein domains. In addition, air inclusion is seen (black areas), which was caused by milling and led to porous structures. For the 10% sodium caseinate emulsion gels, the fat distribution was hardly affected by adding fat at  $t = 0$  or at  $t =$  after torque peak due to the fact that crosslinked 10% sodium caseinate still behaved as liquid-like material. The small fat droplets, present in the 20% and 30% sodium caseinate emulsion gels, were possibly created due to shear forces between protein granules, which may be quite large locally.

Further, the crosslinked protein granules were large in size, and therefore limited in their diffusion rate to stabilize fat droplets. However, based on SDS-PAGE (Figure 2) we suggested that casein monomers were present after suspending protein granules in water. In an aqueous environment, these casein monomers may be considered as a third mobile phase that provided protein for forming an adsorption layer, and consequently for stabilizing small fat droplets.

**Table 1** Normalized fat area fraction ( $A_{fat}/A_{protein}$ ) with corresponding protein area fraction ( $A_{protein}$ ) of crosslinked sodium caseinate emulsion gels as determined from CSLM images using Image-J. Average normalized fat area fractions, determined from 8 images per sample (4 images at 20x magnification, and 4 at 40x), are presented with corresponding 95% confidence intervals ( $CI$ ). To compare, the added normalized fat area fraction, based on volume, was 0.176.

Added protein (%)	Fat added at t = 0		Fat added at t = after peak	
	$A_{fat}/A_{protein}$ (-)	$CI$ (-)	$A_{fat}/A_{protein}$ (-)	$CI$ (-)
10	0.11	0.02	0.13	0.03
20	0.22	0.04	0.12	0.02
30	0.30	0.05	0.07	0.02
30 (no Tgase)	0.23	0.02	-	-

Table 1 shows the amount of fat that is observed on the images expressed in area fractions, normalized on the area fractions found for protein. In principle, the value of the ratio of these two area fractions should be close to the ratio of the volume fractions that were used in the formulations.<sup>29</sup> The found values deviate from this. Especially in the samples where fat was added at a later stage in the process (t = after torque peak) lower apparent fat contents were found in the images. This difference might be explained by the presence of very small fat droplets that were not measured with the CSLM due to the limited resolution. Additionally, the heterogeneous distribution of fat over the samples might also have led to an underestimation of the fat content determined from the CSLM images.

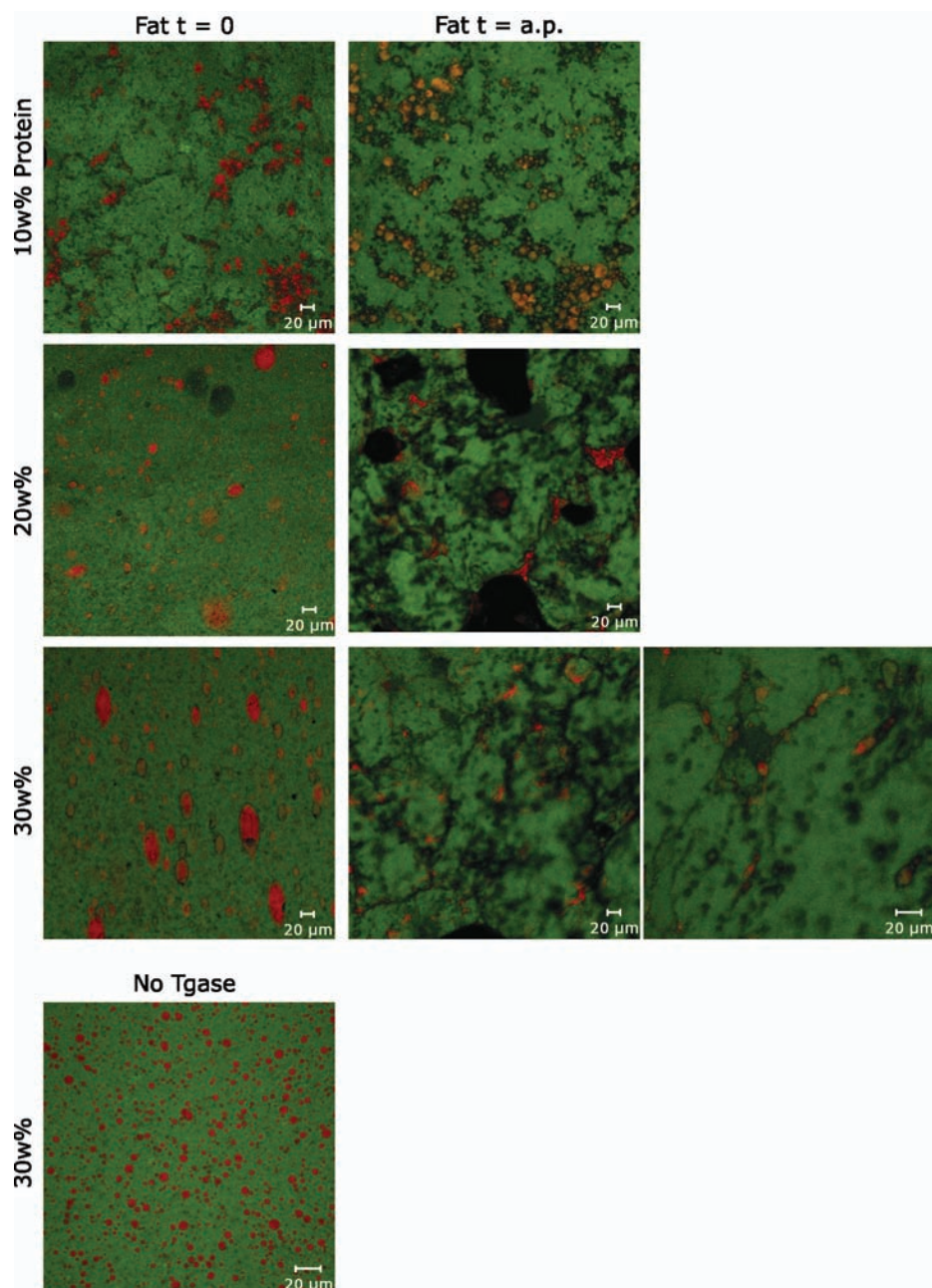


**Figure 6** CSLM images of sodium caseinate (10%, 20% and 30%) emulsion gels treated with Tgase (ratio 1:10) and of 30% sodium caseinate without Tgase. All samples contained 15% palm fat. The bars indicate a length of 20 μm.

### 3.2.3 Small-scale deformation properties

Rheological properties are directly connected to the microstructural properties of materials.<sup>30</sup> Figure 7 displays the normalized  $G'$  and  $\tan\delta$  values in the LVE region (based on mixed and crosslinked protein matrix values from Figure 3) of the sodium caseinate emulsion gels that were prepared by adding fat at  $t = 0$  or at  $t =$  after torque peak. The normalized LVE properties differed only slightly, even though we observed major differences between the macro- and microstructures of the two types of emulsion gels. Therefore, the LVE properties of the emulsion gels seem to depend on the product composition rather than on product structure.

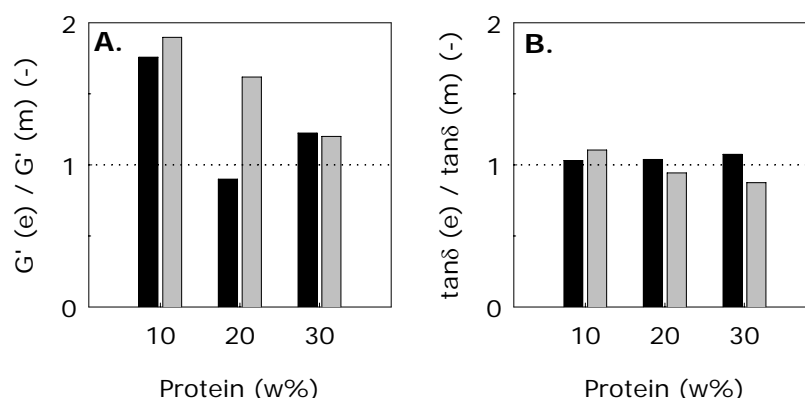


**Figure 7** Normalized  $G'$  (A) and  $\tan\delta$  (B) values of emulsion gels (denoted with 'e') in the linear viscoelastic region with the  $G'$  and  $\tan\delta$  values of the corresponding protein matrices (mixed & crosslinked; denoted with 'm') from Figure 3 as measured with strain amplitude sweeps. Sodium caseinate (10%, 20% and 30%) emulsion gels were treated with Tgase (ratio 1:10) and palm fat (15%) was added in the Brabender mixer at either  $t = 0$  (black bars) or at  $t =$  after the peak torque (a.p.) (grey bars).

Normalized values of  $G'$  that exceed the value of 1 indicate a reinforcement of the sodium caseinate matrix due to fat addition. Adding a dispersed phase that is rigid compared to the continuous phase will reinforce the latter phase.<sup>31-34</sup> Figure 7 illustrates that both 10% sodium caseinate emulsion gels ( $t = 0$  and  $t =$  after torque peak) clearly increased in  $G'$  value compared to the 10% protein matrix. Obviously, the fat phase behaved as a rigid filler in the relatively weak 10% sodium caseinate matrix. With increasing protein concentration, the reinforcing effect was expected

to decrease as the differences in the strength of the phases reduced<sup>35</sup>, which is in agreement with the measurements, except for the 20% sodium caseinate emulsion gel prepared by adding fat at  $t = 0$ , which showed no reinforcement at all.  $\tan\delta$  was not influenced by the addition of fat, which is in agreement with the theoretical finding that  $\tan\delta$  is independent of adding a rigid filler.<sup>36</sup> It is noteworthy that the reinforcement of protein matrices established by adding fat is slightly less compared to the positive effect of simultaneous mixing and crosslinking of protein on  $G'$ .

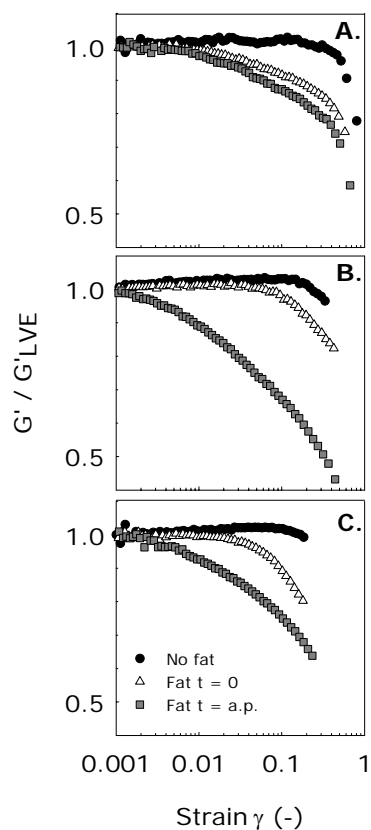


**Figure 8** Normalized  $G'$  values with the  $G'$  value in the linear viscoelastic (LVE) region as function of the strain  $\gamma$  as measured with strain amplitude sweeps. Sub figures **A**, **B** and **C** display the curves that are the average of duplicate measurements for materials containing 10%, 20% and 30% sodium caseinate respectively. All protein and emulsion gels were treated with Tgase (ratio 1:10). Palm fat (15%) was added in the Brabender mixer either at  $t = 0$  or at  $t =$  after the peak torque (a.p.).

In contrast to the LVE properties, the non-linear viscoelastic properties of the protein and emulsion gels showed clear differences. Figure 8 displays the  $G'$  values, normalized with  $G'$  from the LVE region, as function of the strain  $\gamma$  of both protein and emulsion gels. The addition of fat led to a decreased length of the LVE region (decrease of critical strain value which denotes the boundary of the LVE region), implying that especially the emulsion gels with fat added after the torque peak were more susceptible to fracture. All protein gels without fat started to show strain hardening at higher strain values, indicated by a slight increase of the normalized  $G'$  values.

Finally, when comparing the very differing microstructures of the 30% sodium caseinate emulsion gels (Figure 6:  $t = 0$  and  $t = \text{after peak}$ ) and their rather unchanged LVE properties (Figure 7), we may conclude that the structural elements of the protein phase, thus the granules with sizes in the order of mm, were at a scale that did not affect small-scale rheology in the LVE region. However, the moment of adding fat clearly affected the non-linear viscoelastic properties of the emulsion gels.

#### 3.2.4 Large-scale deformation properties

The macro- and microscopically differing emulsion gels also showed differences in large-scale tensile deformation properties as illustrated in Figure 9. Adding fat at  $t = 0$  provided macroscopically homogeneously mixed emulsion gels, which resulted in strong emulsion gels (10% and 20%), as indicated by an increase in yield stress  $\sigma$  and Young's modulus  $E$  compared to the corresponding protein matrices (normalized values  $> 1$ ). Remarkably, the 20% sodium caseinate emulsion gel was more ductile as indicated by an increase in normalized yield strain value, suggesting deformation of the fat phase. While the samples with 10 and 20% caseinate did not show the formation of a rigid, granular structure, the sample with 30% started to show evidence of such a structure. Thus, it is thought that the increase of (normalized) yield stress and Young's modulus is coupled to a homogeneous distribution of the fat phase. A concentration of the fat phase around protein granules instead leads to a reduction in strength.

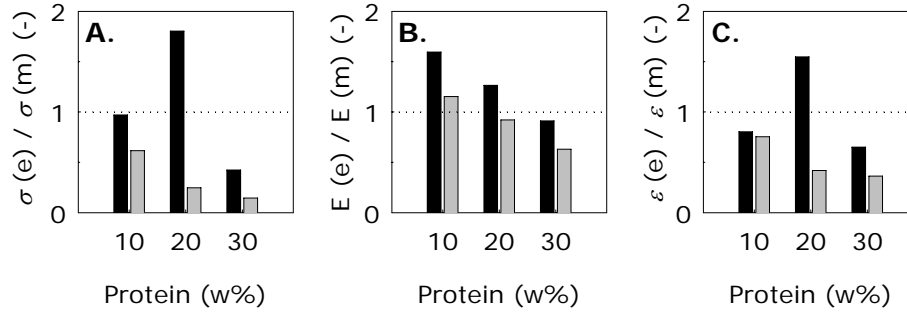


**Figure 9** Normalized yield stress  $\sigma$  (A), Young's modulus  $E$  (B) and yield strain  $\varepsilon$  (C) values of emulsion gels (denoted with 'e') with the  $\sigma$ ,  $E$  and  $\varepsilon$  values of the corresponding protein matrices (mixed & crosslinked; denoted with 'm') in Figure 4 as determined with tensile tests. Sodium caseinate (10%, 20% and 30%) emulsion gels were treated with Tgase (ratio 1:10) and palm fat (15%) was added in the Brabender mixer at either  $t = 0$  (black bars) or at  $t =$  after the peak torque (a.p.) (grey bars).

This was confirmed by the samples to which fat was added after the formation of protein granules. These emulsion gels fractured at lower yield stress  $\sigma$  values compared to the corresponding protein gels. With increasing protein content, the yield stress  $\sigma$  for fracturing the emulsion gels decreased due to the presence of protein granules, acting as relatively large inhomogeneities, and due to decreased cohesive forces between the protein granules. The same trend was observed for  $E$  and  $\varepsilon$ . The fat droplets act as a 'weak link' in the bi-dispersed microstructure when concentrated around protein-rich granules.

Finally, the apparent strain hardening coefficient  $n$  in Figure 10 shows that the sodium caseinate gels without fat clearly exhibited strain hardening ( $n > 1$ ), which is typical for polymer networks with covalent bonds.<sup>12</sup> Adding fat at  $t = 0$  caused a slight decrease of  $n$  due to the deformability of fat. Moreover, adding fat after the torque peak resulted in emulsion gels (20% and 30%) that exhibited no strain hardening ( $n < 1$ ) at all with increasing strain, which can be explained by the yielding behavior of the fat phase in combination with a diluted protein phase that acted as a weak semi-continuous phase through which fracture most likely propagated in these gels. Such a semi-continuous fat phase was not observed in the microstructure of the 10% sodium caseinate emulsion gel, and therefore, no effect on  $n$  was expected.



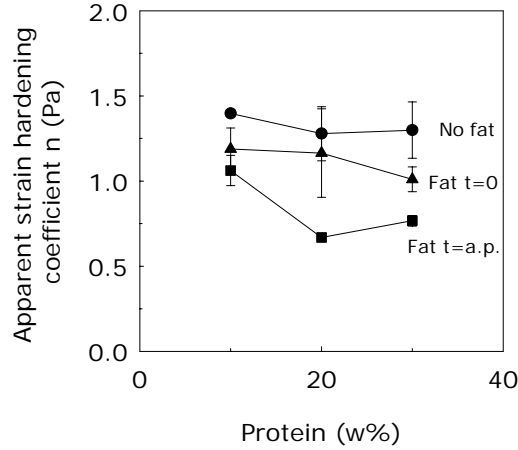


**Figure 10** Influence of adding fat (no fat, fat added at  $t = 0$  or at  $t =$  after torque peak) on apparent strain hardening coefficient  $n$ , which was determined from the tensile tests by fitting a power law relation to the  $\sigma$ - $\varepsilon$  curve ( $\sigma = k \cdot \varepsilon^n$ ).

Summarizing, we can conclude that the distribution of the protein and fat phase in the microstructures (continuous or dispersed) influenced the large-scale deformation properties to a large extent, while the small-scale deformation properties were not influenced so strongly. Further, the strain hardening behavior provided additional information on the microstructure of soft solids and correlated well with the microscopical observations with respect to the fat phase.

#### 4. Conclusions

Application of mixing during crosslinking of caseinate-based systems with Tgase was shown to strongly affect the structure of the resulting gels both on micro- and macro-scale. At low caseinate concentration, a homogeneous soft gel was obtained, whereas at concentrations of 20% (w/w) or higher, granular structures were obtained, formed by simultaneous solidification and rupturing of the gel. The size of the granules depended mainly on the geometry of the mixer used.

Adding fat prior to solidification and mixing resulted in homogeneous gels that were stronger (though more ductile) than the systems without fat added. Only with very high protein concentration (30%) was the on-set of a granular structure

observed. Weaker bi-dispersed structures were obtained when fat was added after the formation of a granular structure. These structures featured protein granules surrounded by a concentrated fat phase. They were more brittle and showed less strain hardening than the systems without fat, even though the LVE properties ( $G'$  and  $\tan\delta$ ) were hardly different from the materials obtained by adding the fat prior to mixing and crosslinking. Adding fat after protein crosslinking affected the fracture behavior ( $\sigma$ ,  $E$  and  $\varepsilon$ ) of the resulting bi-dispersed emulsion gels to a large extent, which correlated well with the microstructural observations, offering possibilities to influence fracture pathways by means of the distribution of the fat phase.

It is thus clear that by induction of crosslinking, and by changing the moment of addition of fat, one can easily induce large changes in micro- and macrostructural properties. Consequently, when applying these parameters for manipulating the product structure, without changing the overall formulation of the system, we expect to induce clear differences in sensory properties.

## Acknowledgements

The authors wish to thank M. Paques, F.J.H. Jeurissen and J. de Slegte from Friesland Foods for valuable discussions, and D. Peressini for critically reading sections concerning rheology.

## References

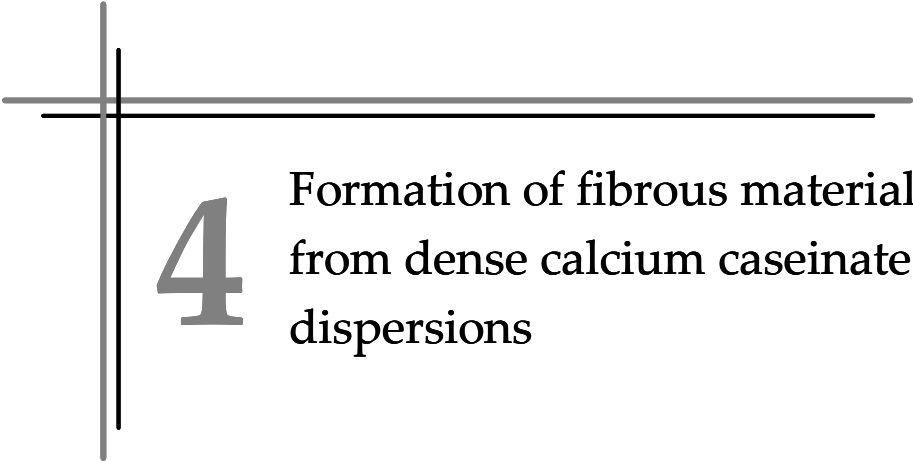
- (1) Luyten, H.; Van Vliet, T.; Walstra, P. **1992**. Comparison of various methods to evaluate fracture phenomena in food materials. *Journal of Texture Studies* 23: 245-266.
- (2) Basman, A.; Koksel, H.; Ng, P. K. W. **2002**. Effects of increasing levels of transglutaminase on the rheological properties and bread quality characteristics of two wheat flours. *European Food Research and Technology* 215 (5): 419-424.
- (3) Gerrard, J. A. **2002**. Protein-protein crosslinking in food: Methods, consequences, applications. *Trends in Food Science and Technology* 13 (12): 391-399.
- (4) Aktas, N.; Kilic, B. **2005**. Effect of microbial transglutaminase on thermal and electrophoretic properties of ground beef. *LWT - Food Science and Technology* 38 (8): 815.

- (5) Ramirez-Suarez, J. C.; Xiong, Y. L. **2002**. Transglutaminase cross-linking of whey/myofibrillar proteins and the effect on protein gelation. *Journal of Food Science* 67 (8): 2885-2891.
- (6) Serrano, A.; Cofrades, S.; Colmenero, F. J. **2004**. Transglutaminase as binding agent in fresh restructured beef steak with added walnuts. *Food Chemistry* 85 (3): 423-429.
- (7) Motoki, M.; Seguro, K. **1998**. Transglutaminase and its use for food processing. *Trends in Food Science and Technology* 9 (5): 204-210.
- (8) Lauber, S.; Henle, T.; Klostermeyer, H. **2000**. Relationship between the crosslinking of caseins by transglutaminase and the gel strength of yoghurt. *European Food Research and Technology* 210 (5): 305-309.
- (9) Imm, J. Y.; Lian, P.; Lee, C. M. **2000**. Gelation and water binding properties of transglutaminase-treated skim milk powder. *Journal of Food Science* 65 (2): 200-205.
- (10) Kuraishi, C.; Yamazaki, K.; Susa, Y. **2001**. Transglutaminase: Its utilization in the food industry. *Food Reviews International* 17 (2): 221-246.
- (11) Mizuno, A.; Mitsui, M.; Motoki, M. **1999**. Glass transition temperature of casein as affected by transglutaminase. *Journal of Food Science* 64 (5): 796-799.
- (12) Dickinson, E.; Yamamoto, Y. **1996**. Rheology of milk protein gels and protein-stabilized emulsion gels cross-linked with transglutaminase. *Journal of Agricultural and Food Chemistry* 44 (6): 1371-1377.
- (13) Menendez, O.; Schwarzenbolz, U.; Rohm, H.; Henle, T. **2004**. Casein gelation under simultaneous action of transglutaminase and glucono- $\delta$ -lactone. *Nahrung-Food* 48 (3): 165-168.
- (14) Schorsch, C.; Carrie, H.; Clark, A. H.; Norton, I. T. **2000**. Cross-linking casein micelles by a microbial transglutaminase conditions for formation of transglutaminase-induced gels. *International Dairy Journal* 10 (8): 519-528.
- (15) Schorsch, C.; Carrie, H.; Norton, I. T. **2000**. Cross-linking casein micelles by a microbial transglutaminase: Influence of cross-links in acid-induced gelation. *International Dairy Journal* 10 (8): 529-539.
- (16) Lorenzen, P. C.; Schlimme, E.; Roos, N. **1998**. Crosslinking of sodium caseinate by a microbial transglutaminase. *Nahrung-Food* 42 (3-4): 151-154.
- (17) Nonaka, M.; Sakamoto, H.; Toiguchi, S.; Kawajiri, H.; Soeda, T.; Motoki, M. **1992**. Sodium caseinate and skim milk gels formed by incubation with microbial transglutaminase. *Journal of Food Science* 57 (5): 1214-1218.
- (18) Faergemand, M.; Murray, B. S.; Dickinson, E. **1997**. Cross-linking of milk proteins with transglutaminase at the oil-water interface. *Journal of Agricultural and Food Chemistry* 45 (7): 2514-2519.

- (19) Yokoyama, K.; Ohtsuka, T.; Kuraishi, C.; Ono, K.; Kita, Y.; Arakawa, T.; Ejima, D. **2003**. Gelation of food protein induced by recombinant microbial transglutaminase. *Journal of Food Science* 68 (1): 48-51.
- (20) Gunasekaran, S.; Ak, M. M. **2003**. In *Cheese rheology and texture*; CRC Press, Boca Raton, FL: 60-64.
- (21) Sliwinski, E. L.; Kolster, P.; Van Vliet, T. **2004**. Large-deformation properties of wheat dough in uni- and biaxial extension. Part 1. Flour dough. *Rheologica Acta* 43 (4): 306-320.
- (22) Abramoff, M. D.; Magelhaes, P. J.; Ram, S. J. **2004**. Image processing with Image-J. *Biophotonics International* 11 (7): 36-42.
- (23) Grappin, R.; Lefier, D. **1993**. In *Reference and routine methods for the measurement of nitrogen fractions in milk and whey, cheese yields & factors affecting its control*, Proceedings of the International Dairy Federation Seminar, Cork.
- (24) Guo, M. R.; Fox, P. F.; Flynn, A.; Kindstedt, P. S. **1996**. Heat-induced modifications of the functional properties of sodium caseinate. *International Dairy Journal* 6 (5): 473-483.
- (25) Laemmli, U. K. **1970**. Cleavage of structural proteins during the assembly of the head of bacteriophage T14. *Nature* 227 (15): 680-685.
- (26) Ando, H.; Adachi, M.; Umeda, K.; Matsuura, A.; Nonaka, M.; Uchio, R.; Tanaka, H.; Motoki, M. **1989**. Purification and characteristics of a novel transglutaminase derived from micro-organisms. *Agricultural and Biological Chemistry* 53 (10): 2613-2617.
- (27) Spiegel, T.; Huss, M. **2002**. Whey protein aggregation under shear conditions - effects of pH-value and removal of calcium. *International Journal of Food Science and Technology* 37 (5): 559-568.
- (28) Dickinson, E. **1997**. Enzymatic crosslinking as a tool for food colloid rheology control and interfacial stabilization. *Trends in Food Science and Technology* 8 (10): 334-339.
- (29) Russ, J. C. **2005**. In *Image analysis of food microstructure*; CRC Press, Boca Raton, FL: 11.
- (30) Tunick, M. H. **2000**. Rheology of dairy foods that gel, stretch and fracture. *Journal of Dairy Science* 83: 1892-1898.
- (31) Manski, J. M.; Kretzers, I. M. J.; Van Brenk, S.; Van der Goot, A. J.; Boom, R. M. **2007**. Influence of dispersed particles on small and large deformation properties of concentrated caseinate composites. *Food Hydrocolloids* 21 (1): 73-84.
- (32) Kim, K. H.; Renkema, J. M. S.; Van Vliet, T. **2001**. Rheological properties of soybean protein isolate gels containing emulsion droplets. *Food Hydrocolloids* 15 (3): 295-302.

- (33) Reiffers-Magnani, C. K.; Cuq, J. L.; Watzke, H. J. **1999**. Composite structure formation in whey protein stabilized o/w emulsions. I. Influence of the dispersed phase on viscoelastic properties. *Food Hydrocolloids* 13 (4): 303-316.
- (34) Van Vliet, T. **1988**. Rheological properties of filled gels: Influence of filler matrix interaction. *Colloid Polymer Science* 266 518-524.
- (35) Aguilera, J. M.; Stanley, D. W. **1999**. In *Microstructural principles of food processing and engineering*; 2<sup>nd</sup> ed., Aspen Publishers, Inc.: 135.
- (36) Pal, R. **2002**. Complex shear modulus of concentrated suspensions of solid spherical particles. *Journal of Colloid and Interface Science* 245 (1): 171-177.





# 4

## Formation of fibrous materials from dense calcium caseinate dispersions

## **Abstract**

Application of shear and crosslinking enzyme transglutaminase (Tgase) induced fibrous hierarchical structures in dense (30% w/w) calcium caseinate (Ca-caseinate) dispersions. Using Tgase was essential for the anisotropic structure formation. The fibrous materials showed anisotropy on both micro- and macroscale as determined with scanning electron microscopy (SEM) and mechanical analyses, respectively. SEM revealed protein fibers with a diameter of ~100–200 nm; visually, we observed fibers of about 1 mm. Both shear and Tgase affected the reinforcement of the fibers to a large extent, whereas the mechanical properties in the direction perpendicular to the shear flow remained constant. Shearing Ca-caseinate without Tgase yielded a slightly anisotropic layered structure. Both crosslinking in the absence of shear and crosslinking during mixing resulted in gels without alignment. The formation of shear- and enzyme-induced anisotropic structures was explained by aligning of protein aggregates due to shear and concurrent solidification of the aligned protein aggregates.



## **1. Introduction**

The formation of fibrous food textures has received much interest from industry as well as food scientists for several decades. Replacing meat products with products from alternative protein sources is an important challenge. This implies creating meat-like structural and sensory properties with non-meat protein-based materials, that is, the formation of anisotropic structures at various length scales and in various concentration regimes.<sup>1,2</sup> Research on fibrous protein materials can be divided roughly into the self-assembly of proteins into fibrils, and the forced assembly of proteins into fibrous textures. Fibrillar self-assembly of various proteins, such as  $\beta$ -lactoglobulin, ovalbumin, and bovine serum albumin, has been achieved in diluted and semidiluted regimes under severe pH and temperature conditions.<sup>3,4</sup> These fibrils were in the order of nanometers thick and micrometers long. In contrast to self-assembly, forced assembly of protein solutions in the concentrated regime (e.g., >10% w/w protein) has been approached traditionally using extrusion or spinning techniques.

Extrusion cooking has been used to texturize proteins from various sources, such as soy flours, wheat, and dairy proteins.<sup>2,5</sup> Plasticization, melting, and break-up of proteins occur in the extruder barrel, and fibrous textures can be formed due to alignment of the proteins in long cooling dies.<sup>2,5</sup> Cheftel obtained fibrous structures only from soy concentrate; soy isolates could not be transformed into anisotropic structures.<sup>5</sup> Typical values of ratio of the longitudinal and transverse resistance to stretching are 1-4 for fibrous extrudates from defatted soy flour, depending on the barrel temperature and pH.<sup>6</sup> This ratio, indicative of fiber quality<sup>7</sup>, was 1-2 for extrudates of defatted soy flour and pork as determined by cutting.<sup>8</sup> Tolstoguzov underlined that incompatible biopolymers are required to form anisotropic structures during extrusion.<sup>9</sup> In general, the shortcomings of extrusion are the use of high temperatures for protein denaturation, inducing uncontrollable chemical reactions, and the presence of high shear forces during extrusion, which can lead to break-up of structural elements,<sup>10</sup> even at a molecular level.<sup>11</sup>

Spinning of biopolymers is based on aligning macromolecules due to shear and elongational flow in a spinneret and during coagulation.<sup>12</sup> Typically, the resulting fibers (~100  $\mu$ m) are coagulated in baths containing acid and salt solutions, and

then washed. Hydrocolloids, such as carrageenan<sup>13,14</sup> and alginate,<sup>15,16</sup> or vegetable proteins, such as soy<sup>17</sup> or field bean protein,<sup>18</sup> were used in combination with casein in a two-phase blend to decrease the solubility in water of the casein-based fibers produced. In the case of spun pea and fababean protein, fibers with a granular core and strand-like cortex were formed.<sup>12</sup> Edible films prepared using wet spinning of soy protein isolate did not reveal any macromolecular orientation of the proteins.<sup>19</sup> The disadvantages of spinning are the large waste streams of water from the coagulation and washing baths. In addition, the necessity for low pH, high salt concentrations, and chemical additives to coagulate the fibers makes the design of a process for production of fibers suitable for consumption a complex matter.

In this paper, we present a novel technology based on application of simple shear flow and concurrent enzymatic crosslinking to induce an anisotropic fibrous structure in concentrated calcium caseinate without the necessity for coagulation baths, washing steps, high temperatures, or high shear forces.

Casein consists mainly of  $\alpha_{S1}$ -,  $\alpha_{S2}$ -,  $\beta$ -, and  $\kappa$ -casein in the ratio 4:4:2:1. The serine and threonyl phosphates of  $\alpha$ - and  $\beta$ -caseins can interact with calcium ( $\text{Ca}^{2+}$ ) and other di- and trivalent ions.<sup>20</sup> Because of this interaction, calcium caseinate (Ca-caseinate) dispersions contain protein aggregates<sup>21,22</sup> that are comparable with casein micelles (~100–300 nm) in milk.<sup>23,24</sup> Sodium caseinate, dialyzed with ionic  $\text{Ca}^{2+}$  at various concentrations, featured a hydrodynamic radius in the range of ~100–300 nm, which indicates the presence of aggregates of at least hundreds of protein molecules.<sup>24</sup> The enzyme transglutaminase (Tgase) has been used mainly to crosslink sodium caseinate.<sup>25–27</sup> We examined the susceptibility of Ca-caseinate to alignment by shear and solidification by Tgase, because Ca-caseinate dispersions comprise larger protein aggregates than sodium caseinate (~50 nm).<sup>28</sup> To our knowledge, the enzymatic gelation of Ca-caseinate has not been studied before.

In this paper, we show that simple shear and enzymatic crosslinking induces a novel fibrous protein structure based on Ca-caseinate only. The resulting microstructural properties were studied with SEM analysis. The structural characteristics are revealed with small and large deformations leading to the linear viscoelastic properties and the mechanical properties, respectively, of the Ca-caseinate structures.

## 2. Materials and methods

### 2.1 Materials

The measured activity of microbial  $\text{Ca}^{2+}$ -independent transglutaminase (protein-glutamine:amine  $\gamma$ -glutamyl-transferase, EC 2.3.2.13) derived from *Streptoverticillium moberansae* (1% Tgase, 99% maltodextrine, Ajinomoto Co. Inc., Tokyo, Japan) was 117 units $\cdot\text{g}^{-1}$  using the hydroxamate method.<sup>29</sup> Tgase catalyzes acyl-transfer reactions between  $\gamma$ -carboxyamide groups of glutamine and the  $\epsilon$ -amino group of lysines in proteins. A 20% (w/w in demineralized water) Tgase solution was freshly prepared prior to the experimental runs by mechanical stirring at room temperature for 1 h.

Ca-caseinate contained at least 88% protein according to the manufacturer's specifications (DMV International, Veghel, The Netherlands). A protein premix (pH 6.8–7.0) consisting of 30% w/w Ca-caseinate, Tgase (enzyme/protein (E:P) ratio 1:20 based on weight), and demineralized water was prepared in a kitchen mixer at low speed and at room temperature prior to processing. Some minor components were added for preservation and further analysis (confocal scanning laser microscopy: data not shown), such as 1% (w/w) sodium benzoate (Sigma Aldrich, Zwijndrecht, The Netherlands) and  $2\cdot 10^{-4}\%$  (w/w) Rhodamine 110 (83695, Sigma Aldrich), added as a 0.02 g $\cdot\text{L}^{-1}$  solution in phosphate buffered saline (PBS).

Dimethylsulfoxide (DMSO) and ethanol used for the preparation of samples for SEM were of analytical grade (Sigma Aldrich).

### 2.2 Shear cell device

A well-defined flow was applied by using the shear cell device developed in house (Wageningen University, The Netherlands), based on a rheometer concept<sup>30</sup> and depicted in Figure 1A. In the shear cell device ( $V = 70 \text{ mL}$ ), biopolymers are subjected to a simple linear shear profile, which is established between the plate (i.e. the bottom cone) and the cone (angle  $\alpha_{\text{plate}} = 105^\circ$ ,  $\alpha_{\text{cone}} = 100^\circ$ ) as shown in the schematic drawing (Figure 1B). The rotating plate and stationary cone are heated (or cooled) with water. The temperature of the material is measured with a thermo

couple located in the cone. The device is attached to a Brabender Do-Corder 330 (Brabender OHG, Duisburg, Germany) to enable shear rate control, and torque and temperature readings.

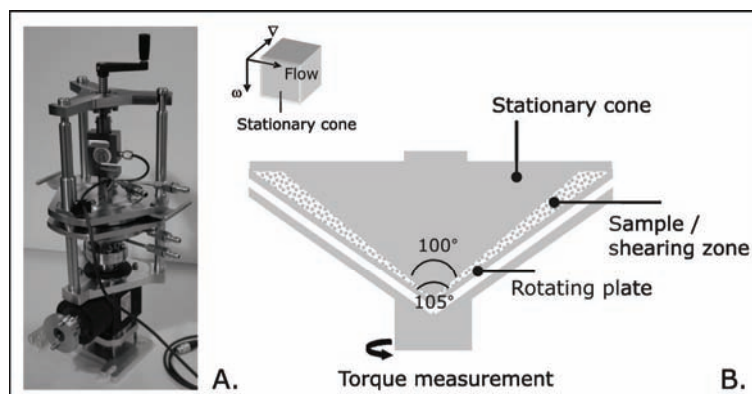


**Figure 1** Picture (A) and schematic overview (B) of the shear cell device. The cone angle =  $100^\circ$ ; the angle between the cone and the plate (shearing zone) =  $2.5^\circ$ ;  $R_{\text{plate}} = 0.08508$  m;  $R_{\text{cone}} = 0.07638$  m. The stationary cone and rotating plate are heated/cooled with water.

### 2.3 Sample preparation in the shear cell device

The Ca-caseinate premix prepared in the kitchen mixer was transferred to the pre-heated ( $50^\circ\text{C}$ ) shear cell device. After the shear cell was filled, the mixture was subjected to the following shear treatment: 4 min at 5 rpm ( $12\text{ s}^{-1}$ ), then an increase from 5 to 50 rpm ( $12$  to  $120\text{ s}^{-1}$ ) in 1 min, and then 30 min at 50 rpm ( $120\text{ s}^{-1}$ ). In the case of a quiescent treatment, the mixture was subjected to 5 rpm for 30 s, and subsequently the shear cell was stopped (0 rpm) for 35 min. In addition, a Ca-caseinate sample was prepared in a mixing bowl (W-50, Brabender OHG) with counter rotating elements, which was attached to the Brabender Do-Corder, at the same rotational speed as the sheared samples prepared in the shear cell device. After processing, the material was cooled in the stationary shear cell to approximately  $12^\circ\text{C}$  in  $\sim 10$  min. The mixed material was not cooled, but a sample was taken immediately at  $50^\circ\text{C}$ . The processed materials were transferred to moulds consisting of two square parallel plates. Part of the material was used within 2 h for further analysis (tensile tests and sample preparation for SEM), and

some was stored in a refrigerator for 1 day at 4°C until further analysis (protein content and linear viscoelastic (LVE) measurements). The time between creating the materials and performing specific measurements was kept constant.

## ***2.4 Scanning electron microscopy***

Micro- and nanostructural aspects of the Ca-caseinate materials were observed with a field emission scanning electron microscope (FESEM) at ambient temperature. Dry samples were prepared according to the modified method described by Muller et al.<sup>31</sup> to observe the protein network without interference of the water phase. Sheared Ca-caseinate samples were carefully cut into squares (<10 × 10 mm) and immersed in DMSO (concentration range 15%, 30%, and 50% v/v in demineralized water) for 60 min each. Excess 50% DMSO was removed from the samples with filter paper. Slow freezing of the samples was performed in cold gaseous nitrogen above liquid nitrogen. Subsequently, the samples were immersed in liquid nitrogen, and freeze fractured on a brass table with a razorblade (single edge carbon steel, EMS, Washington USA) and a hammer. Freeze fracturing was performed parallel and perpendicular to the shear flow that was exerted on the samples in the shear cell device (based on the shear flow–vorticity plane). The resulting fracture planes were the velocity gradient–shear flow plane and velocity gradient–vorticity plane, respectively. In this paper, we define the directions and resulting fracture planes as parallel and perpendicular, respectively. The mixed sample, having no clear shear direction, was treated similarly after defining a random plane (plane 1), and a plane perpendicular to this plane (plane 2). All of the Ca-caseinate samples exhibited brittle fracture. After fracturing, samples were thawed in 50% DMSO for >60 min, and subsequently re-hydrated with water through the reverse DMSO concentration range (60 min each). The samples were dehydrated in graded series of ethanol (10%, 30%, 50%, 70%, 90% v/v) to 100% ethanol (20 min each). Samples in 100% ethanol were critical point dried with carbon dioxide (CPD 020, Balzers, Liechtenstein) and examined with a stereomicroscope to identify the fracture planes. Subsequently, the samples were glued on a sample holder using conductive carbon cement (Leit-C, Neubauer Chemicalien, Germany), and sputter coated with 20 nm platinum (JFC 1200, JEOL, Japan). The fractured surfaces were analyzed with a FESEM (JEOL 6300 F, Tokyo, Japan) at room temperature at a working distance of 8 mm, with SE detection at

3.5–5 kV. All images were recorded digitally (Orion, 6 E.L.I. sprl., Belgium) at a scan rate of 100 s (full frame) at a size of  $2528 \times 2030$ , 8 bit. Noise reduction and resizing of the images were done using Adobe Photoshop CS.

### ***2.5 Rheological properties***

The LVE properties ( $G'$  and  $\tan\delta$ ) were determined in duplicate with dynamic oscillating strain amplitude tests with a stress-controlled Bohlin CVO (Bohlin Instruments Ltd., Cirencester, UK) at a constant frequency of 1 Hz and at a temperature of 20°C. Serrated parallel plates (diameter 25 mm, gap 2 mm) were used to prevent slipping. A chamber covering the sample was used to prevent evaporation. Before measuring, the samples were rested for 15 min to allow relaxation of the stresses induced by sample loading.

### ***2.6 Mechanical properties***

A Texture Analyzer T2 (Stable Micro Systems Ltd., Surrey, UK) was used for large deformation tests. Uni-axial tensile tests were conducted with a constant deformation rate of  $3 \text{ mm}\cdot\text{s}^{-1}$  at room temperature within 2 h after creating the Ca-caseinate materials. Samples were cut into a rectangular shape ( $30 \times 12 \text{ mm}$ ) with a thickness of 3–5 mm (measured for each individual sample). The length of the to-be-extended part was 15.2 mm. At least three measurements were performed on a fibrous protein sample in each direction, parallel and perpendicular to the shear flow (based on the shear flow–vorticity plane, thus the resulting fracture planes were the same planes as viewed by SEM). The fibrous structure led inevitably to variations between measurements because fracture sometimes occurred at once, and sometimes in multiple stages. Based on the measured force–distance curves, the Hencky strain ( $\varepsilon$ ), tensile yield stress ( $\sigma$ ), and Young's modulus ( $E$ ) were calculated.<sup>32</sup>

### ***2.7 Protein content***

The protein content of the processed samples was determined by the Dumas method using a NA2100 nitrogen and protein analyzer (CE Instruments, Milan, Italy). The nitrogen-protein conversion factor was 6.38.<sup>33</sup> The average measured

protein content was  $28.4 \pm 1.1\%$  within a 95% confidence interval. The mixed and crosslinked Ca-caseinate sample had a higher protein content of 35.4%, which was attributed to syneresis.

### 3. Results and discussion

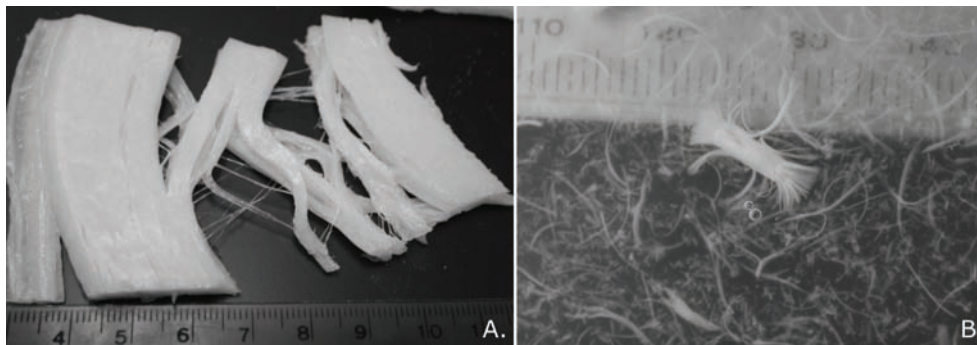


**Figure 2** Picture of fibrous 30% Ca-caseinate after shearing and crosslinking (A). After suspending a piece of the same sample in demi-water for 1 day, distinct fibers were visible (B). The scale in pictures A is in centimeters and in picture B in millimeters.

#### 3.1 Macrostructural aspects

Crosslinking with Tgase during shearing led to real fibrous macrostructures that could be torn apart along the direction of shear flow as shown in Figure 2A. The structures obtained were white and shiny. Individual macroscopic fibers, typically about 1 mm, could be observed after dispersing a piece of sample for 1 day in demineralized water (Figure 2B). Shearing of 30% Ca-caseinate without Tgase resulted in a remarkably layered structure with a subtle anisotropic character. After only the protein matrix was sheared, the opaque white structure could be peeled off in the direction of the shear flow over length scales in the order of centimeters. Ca-caseinate that was crosslinked under quiescent conditions resulted in a firm protein gel without any observable alignment. Finally, mixing of Ca-caseinate and Tgase for 35 min led to syneresis and resulted in a compact protein gel. After syneresis, the protein content of the remaining sample was 35% instead of the added 30%. Based on the macrostructural observations, it could be concluded that shear and crosslinking with Tgase appeared to be essential for creating an anisotropic fibrous Ca-caseinate structure.



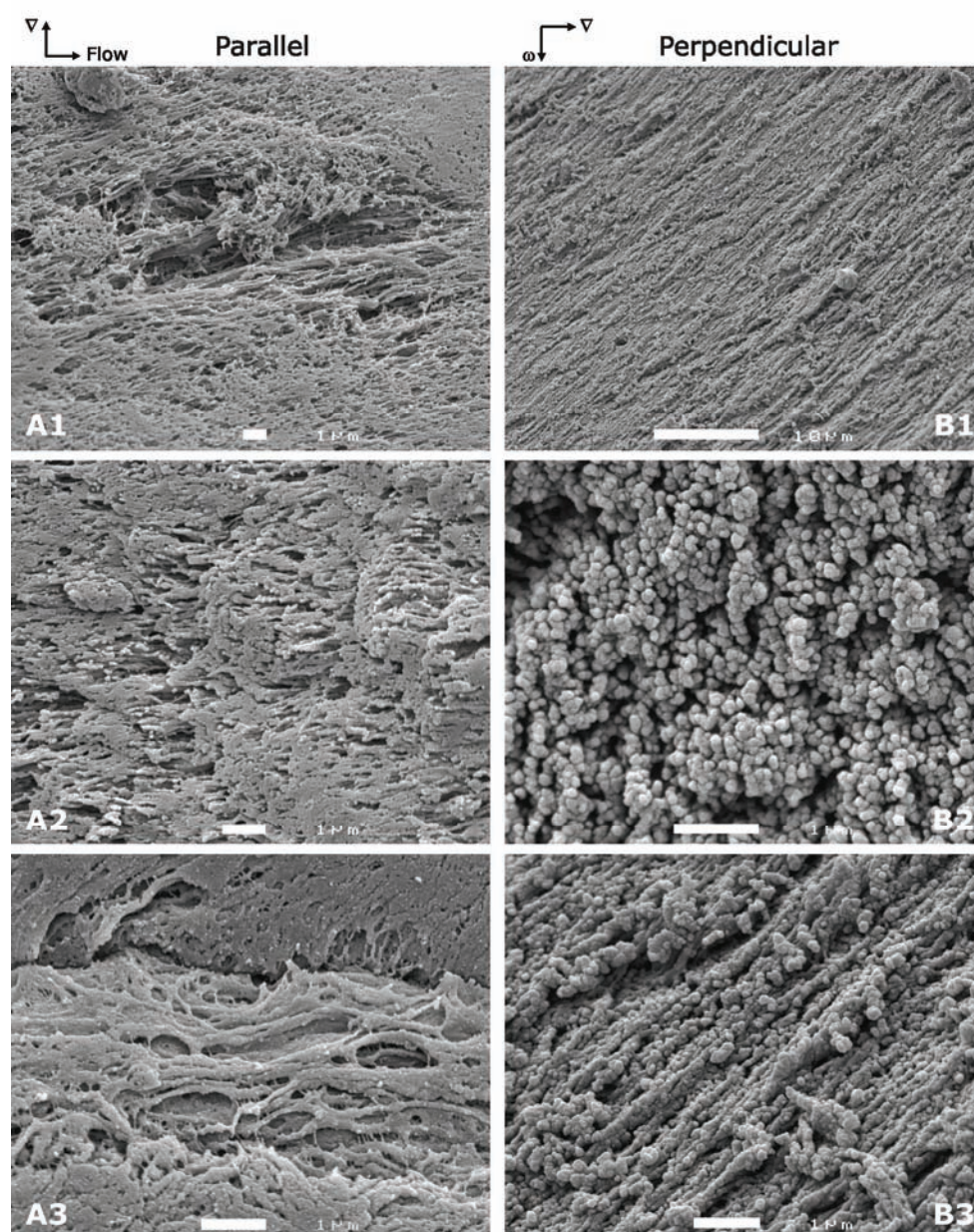


**Figure 3** SEM images of fractured surfaces parallel (**A**) and perpendicular (**B**) to the shear flow exerted in the shear cell device of 30% Ca-caseinate and Tgase (E:P = 1:20) sheared at 50°C and 50 rpm ( $= 120 \text{ s}^{-1}$ ) during 35 min. The scale bars denote 1  $\mu\text{m}$  except for the scale bar in **B1**, being 10  $\mu\text{m}$ . The images were acquired at the following magnifications: **A1** at 5000 $\times$ , **A2** at 10000 $\times$ , **A3** and **B3** at 15000 $\times$ , **B1** at 2500 $\times$  and **B2** at 20000 $\times$ .

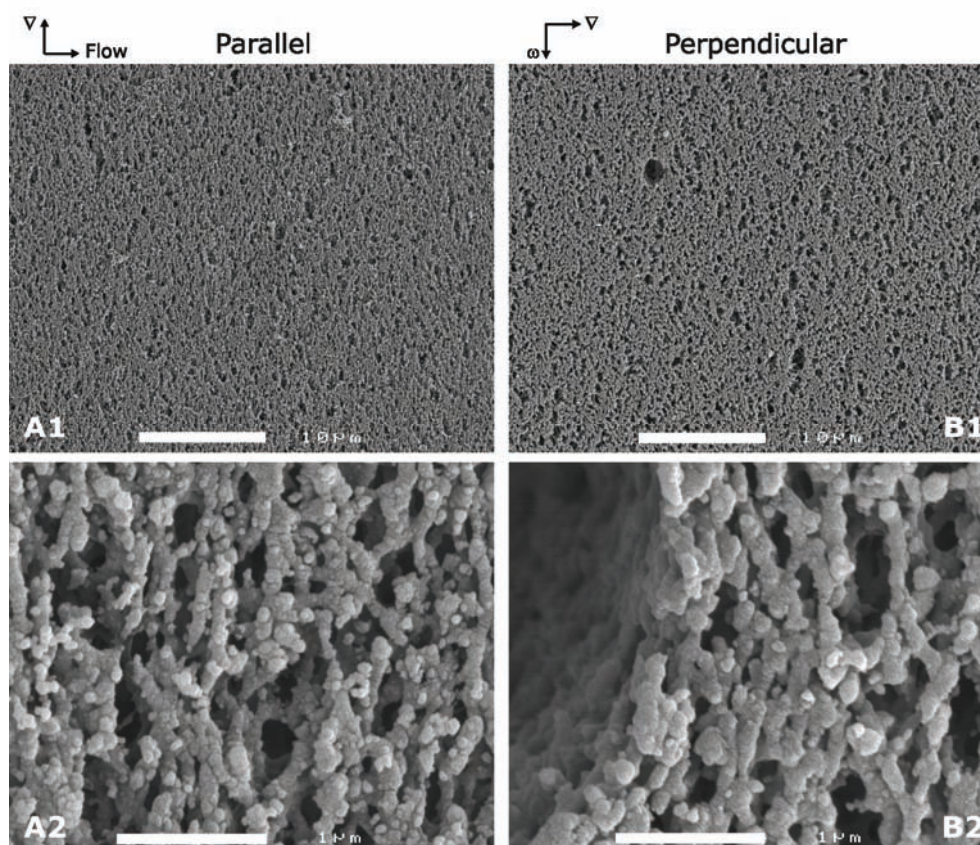


### **3.2 Microstructure: effect of shear and crosslinking**

The micro- and nanoscale structures of the processed Ca-caseinate materials were studied with SEM. The SEM images of sheared and crosslinked Ca-caseinate are shown in Figure 3. Shear-induced alignment is visible in the microstructures parallel to the shear flow (Figure 3A). To give a good impression we displayed several SEM images obtained at different magnifications and locations within the sample (Figure 3A.1, 3A.2 and 3A.3). Because of the compact microstructure, the alignment could not be observed throughout the sample. The sheared and crosslinked protein structures also contained open spaces and air bubbles, which enabled us to view fibers with a clear orientation. Those disturbances probably explain why the fiber orientation deviated from the shear direction in some cases. Figure 3A.3 shows an example of fibers at the surface of an air bubble. Obviously, the fibers viewed with SEM were on a totally different scale from the fibers observed visually in the macrostructure, that is, nanometers versus millimeters, which indicates a hierarchical fibrous structure. Based on the images, a typical fiber diameter of ~100–200 nm could be deduced.

Perpendicular to the shear flow, two types of microstructures were observed, spherical domains of dense protein (Figure 3B.2), which may represent the cross-sections of fibers, and again aligned protein structures (Figure 3B.1 and 3B.2). The latter alignment might be caused by chained protein particles, or by an optically deceiving projection of the observed velocity gradient–vorticity plane.

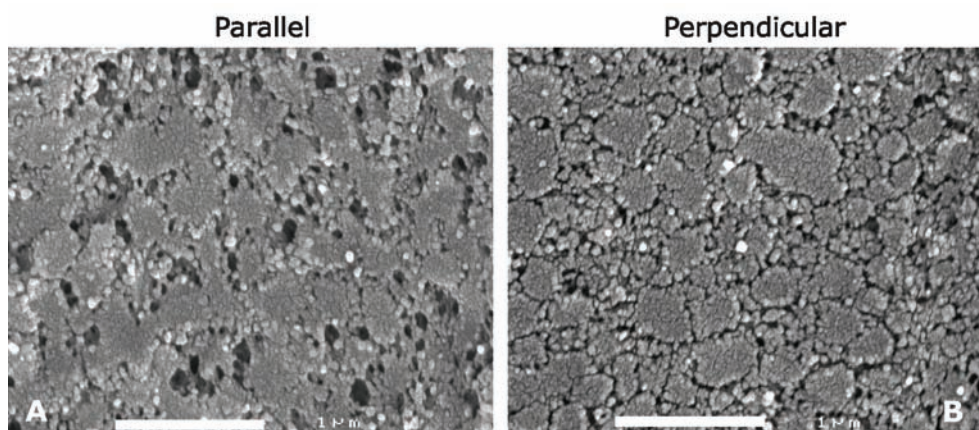
The microstructure of sheared calcium caseinate without use of Tgase showed large differences as compared to the sheared and simultaneously crosslinked protein microstructures. On a macroscale, no fibers were visible, but a layered structure was formed that could be peeled off. At a microscale, a subtle orientation could be deduced from the plane parallel to the shear flow (Figure 4A.1), which was less clear for the plane perpendicular to the shear flow (Figure 4B.1). The protein network appeared more porous as compared to the crosslinked protein network (Figure 4A.2 and 4B.2), which may suggest that free water was located in those pores. The size of the protein domains was comparable to the size of the spheres that were present in the crosslinked protein network (~100–200 nm).



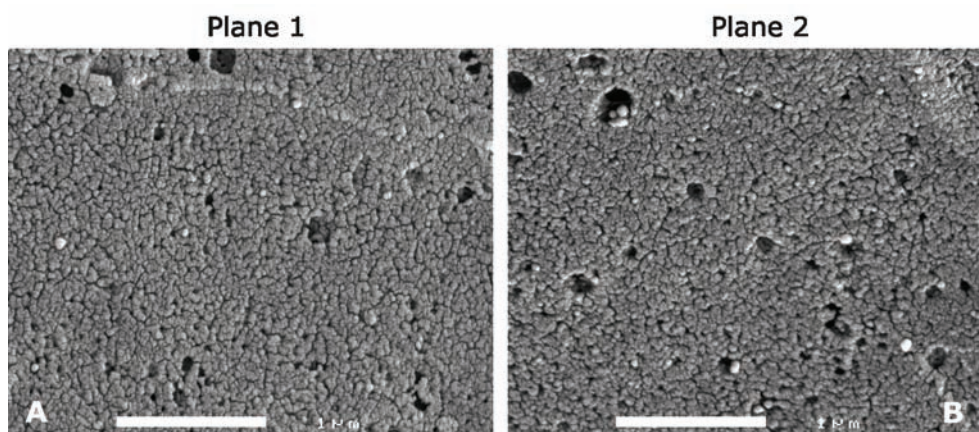
**Figure 4** SEM images of fractured surfaces parallel (**A**) and perpendicular (**B**) to the shear flow exerted in the shear cell device of 30% Ca-caseinate sheared at 50°C and 50 rpm ( $= 120 \text{ s}^{-1}$ ) during 35 min. The scale bars denote 10  $\mu\text{m}$  (**A1** and **B1** acquired at 3000 $\times$ ) and 1  $\mu\text{m}$  (**A2** and **B2** acquired at 35000 $\times$ ).

Figure 5 shows the SEM images of crosslinked Ca-caseinate under quiescent conditions. The microstructures of the fracture planes parallel to the shear cell surface (Figure 5A) and perpendicular to it (Figure 5B) resembled each other. Subtle differences between these two planes could be caused by natural inhomogeneities in the material. One can observe compact areas ( $\sim 0.5 \mu\text{m}$ ) surrounded by less compact areas containing protein domains. Tgase may have been present in these compact areas, and crosslinking could have led to such

compactness accompanied by expulsion of free water, leading to slightly swollen and porous protein structures between the compact areas.



**Figure 5** SEM images of parallel (**A**) and perpendicular (**B**) fractured surfaces of 30% Ca-caseinate, crosslinked by Tgase (E:P = 1:20) under quiescent conditions at 50°C. Both images were acquired at 35000x and the scale bars denote 1 μm.



**Figure 6** SEM images of fractured surfaces of 30% Ca-caseinate and Tgase (E:P = 1:20) mixed in a mixer at 50°C and 50 rpm for 35 min. Plane 1 (**A**) was randomly chosen, and plane 2 (**B**) was perpendicular to plane 1. Both images were acquired at 35000x and the scale bars denote 1 μm.

Finally, mixed and crosslinked Ca-caseinate yielded a compact microstructure consisting of protein spheres of ~100 nm (Figure 6). The compactness can be explained by the syneresis that occurred during mixing. No differences were observed between the randomly chosen plane 1 (Figure 6A), and the corresponding plane perpendicular to plane 1, that is, plane 2 (Figure 6B).

Summarizing, in the presence of Tgase, simple shear induced strong anisotropy on a macroscale. Alignment on a microscale was also observed, but it was not always consistent with the direction of shear flow. Only the combined action of shear and Tgase yielded anisotropic Ca-caseinate structures.

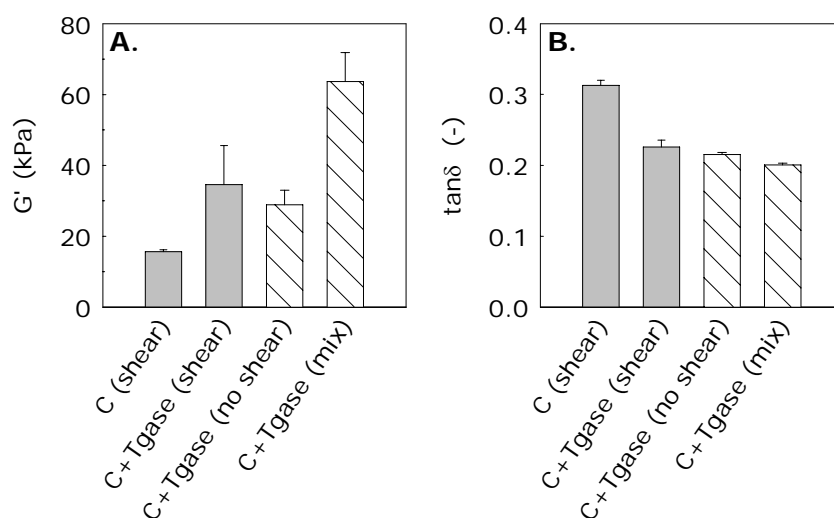
### **3.3 Material properties**

The material properties of the sheared and crosslinked Ca-caseinate structures are discussed in terms of their rheological and mechanical properties. The latter will reveal the anisotropic properties of the processed protein materials.

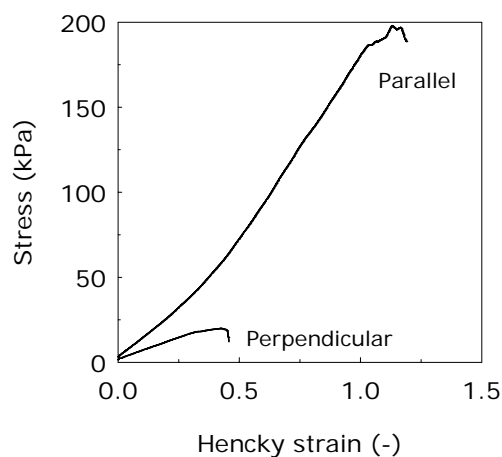
#### **3.3.1 Rheological properties**

Figure 7 displays  $G'$  and  $\tan\delta$  within the LVE region of the various Ca-caseinate samples. Typically, the rheological properties of caseinate gels are determined by noncovalent interactions, such as electrostatic and hydrophobic interactions. The formation of covalent bonds will dominate the interactions present and will largely determine the rheological properties. Therefore, enzymatic crosslinking increased  $G'$ , whereas  $\tan\delta$  was decreased, which is typical of structures where covalent bonds are introduced.<sup>25,34</sup> No difference in  $G'$  and  $\tan\delta$  between shearing and quiescent treatment of crosslinked Ca-caseinate was found. Thus, shearing did not affect the formation of covalent bonds. The mixed and crosslinked Ca-caseinate sample showed a larger  $G'$  and slightly lower  $\tan\delta$  value, which can be explained by an effective higher protein concentration.

The anisotropic behavior of the sheared and crosslinked Ca-caseinate samples was not found in the LVE properties. Only the presence of Tgase resulted in distinct differences in  $G'$  and  $\tan\delta$ . Therefore, we can conclude that the anisotropic fibers acted as an isotropic continuum at the length scale probed with small deformations.



**Figure 7** LVE properties  $G'$  (A) and  $\tan\delta$  (B) with 95% confidence intervals of the various 30% Ca-caseinate structures. C, Ca-caseinate; Tgase, crosslinked using Tgase; (no) shear, (un)sheared in the shear cell device; mix, mixed in mixer. Grey bars denote anisotropic materials whereas the shaded bars denote isotropic materials.



**Figure 8** Typical stress–strain curves of 30% Ca-caseinate and Tgase (E:P = 1:20) sheared at 50°C and 50 rpm ( $= 120 \text{ s}^{-1}$ ) for 35 min, elongated in the parallel and perpendicular directions to the shear flow.

### 3.3.2 Mechanical properties

Figure 8 depicts typical stress–strain curves of the tensile behavior of sheared and crosslinked Ca-caseinate in the two directions relative to the applied shear flow on the sample during processing. It is immediately clear that both the yield (maximum) stress and the yield strain in the parallel direction, thus in the direction of the fibers, were much larger as compared to the values in the perpendicular direction. Further, the curvature of the stress–strain curve for the sample elongated in the parallel direction showed strain hardening behavior<sup>10</sup>; this was not the case for the sample elongated in the other direction.

Figure 9 illustrates the tensile properties (yield stress  $\sigma$ , yield strain  $\varepsilon$  and Young's modulus  $E$ ) for the various Ca-caseinate samples that were extended until fracture. On the basis of these tensile properties, we can conclude that Ca-caseinate that was both crosslinked and sheared showed a significant degree of anisotropy because of the large differences between the properties measured in the direction parallel and perpendicular to the shear flow. Sheared Ca-caseinate behaved anisotropically, which is evident by differences in  $\sigma$  and  $\varepsilon$  (the difference in  $E$  was not significant). Crosslinked Ca-caseinate under quiescent conditions was not anisotropic based on the tensile tests; this was also observed visually and by SEM (Figure 5). When comparing the sheared Ca-caseinate sample with the sample that was crosslinked while shearing, we think that no significant amount of crosslinks was formed in the direction perpendicular to the shear flow. However, these average perpendicular values of  $\sigma$ ,  $\varepsilon$ , and  $E$  (Figure 9) also coincide with the perpendicular values of the quiescently crosslinked Ca-caseinate material. Apparently, the absence of mixing during the quiescently crosslinked Ca-caseinate resulted in a lack of coherence in the material. Mixed and crosslinked Ca-caseinate showed no differences in the measured stress–strain curves of the samples elongated in the two random directions perpendicular to each other. The average values of  $\sigma$ ,  $\varepsilon$ , and  $E$  indicate that the material was highly elastic (high  $E$  value) and ductile (high  $\sigma$  value).

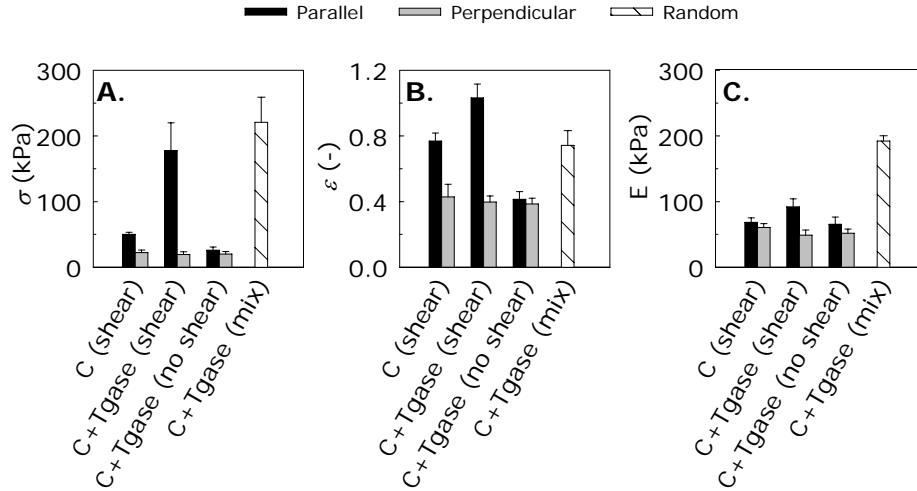


**Figure 9** Tensile properties (yield stress  $\sigma$  (A), yield strain  $\varepsilon$  (B) and Young's modulus  $E$  (C)) with 95% confidence intervals of the various 30% Ca-caseinate materials. C, Ca-caseinate; Tgase, crosslinked using Tgase (E:P = 1:20); (no) shear, (un)sheared in the shear cell device; mix, mixed in a mixer.

Table 1 summarizes the ratios between the tensile properties measured in the direction parallel and perpendicular to the shear flow. As already shown, the anisotropic fibrous samples were much stronger in the parallel direction as compared to the perpendicular direction, which was especially reflected in the high yield stress ratio  $\sigma_{\parallel}/\sigma_{\perp}$  (i.e.,  $\sim 9$ ). The ratios of the yield strain and Young's modulus were  $\sim 2$ – $3$  for the anisotropic Ca-caseinate structures. Based on the values of the ratios of the tensile properties, the sheared Ca-caseinate in the absence of Tgase showed slight anisotropy.

**Table 1** Ratio of the tensile properties (yield stress  $\sigma$ , yield strain  $\varepsilon$  and Young's modulus  $E$ ) measured parallel and perpendicular to the shear flow. The anisotropic 30% Ca-caseinate samples are sheared and crosslinked 30% Ca-caseinate (C + TG + shear) and sheared 30% Ca-caseinate (C + shear).

	Ratio parallel/perpendicular		
	$\sigma$	$\varepsilon$	$E$
C + TG + shear	9.2	2.6	1.9
C + shear	2.3	1.8	1.1



Table 2 lists the values of the tensile properties, normalized with the corresponding values of the Ca-caseinate samples so that the effect of shear (sheared and crosslinked Ca-caseinate normalized with crosslinked Ca-caseinate under quiescent conditions), and of Tgase (sheared and crosslinked Ca-caseinate normalized with sheared Ca-caseinate without Tgase) could be deduced. Both shear and Tgase affected the tensile properties in the parallel direction to a large extent, that is, in the direction of the anisotropic microstructures. Moreover, considering the normalized yield stress values, the reinforcing effect of shear (in the presence of Tgase) was almost twice as large as the effect of Tgase only. This may be explained by a synergistic effect of shear and Tgase. Unfortunately, we could not determine the effect of shear in non-crosslinked Ca-caseinate, as the mechanical properties of Ca-caseinate without shearing and crosslinking could not be measured due to the weak structure. The effects of both shear and Tgase were negligible for the normalized tensile properties in the perpendicular direction, because the normalized values were close to 1.

**Table 2** Normalized tensile properties (yield stress  $\sigma$ , yield strain  $\varepsilon$  and Young's modulus  $E$ ) for the measured parallel and perpendicular directions. The sheared and crosslinked 30% Ca-caseinate sample ( $[C+TG]_{\text{shear}}$ ) was normalized with crosslinked 30% Ca-caseinate under quiescent conditions ( $[C+TG]_{\text{no shear}}$ ), and with the sheared 30% Ca-caseinate ( $[C]_{\text{shear}}$ ), leading to the effect of shear and Tgase, respectively.

		Parallel, normalized			Perpendicular, normalized		
		$\sigma$	$\varepsilon$	$E$	$\sigma$	$\varepsilon$	$E$
Effect shear	$\frac{[C+TG]_{\text{shear}}}{[C+TG]_{\text{noshear}}}$	7.7	2.6	1.6	0.8	1.0	0.8
Effect Tgase	$\frac{[C+TG]_{\text{shear}}}{[C]_{\text{shear}}}$	3.5	1.3	1.4	0.9	0.9	0.8

Table 3 provides an overview of the most important macro-, microstructural and mechanical features of the Ca-caseinate structures discussed, indicating that both shear and enzymatic crosslinking were essential for the formation of fibrous Ca-caseinate materials.



**Table 3** Overview of the macro-, microscale and mechanical characteristics of 30% Ca-caseinate samples after shearing, mixing, or quiescent treatment, with or without Tgase.

	Property	Ca-caseinate	Ca-caseinate + Tgase
Shearing	Macro <sup>a</sup>	Layered	Fibers <1 mm
	Micro <sup>b</sup>	Little orientation, protein domains ~60–120 nm	Fibers ~100–200 nm
	Mechanical <sup>c</sup>	Slightly anisotropic	Highly anisotropic
Quiescent	Macro <sup>a</sup>	Isotropic, grainy <sup>d</sup>	Isotropic
	Micro <sup>b</sup>	-	Protein domains ~50–100 nm and patches ~200–700 nm
	Mechanical <sup>c</sup>	-	Isotropic
Mixing	Macro <sup>a</sup>	-	Isotropic
	Micro <sup>b</sup>	-	Protein domains ~100 nm
	Mechanical <sup>c</sup>	-	Isotropic

<sup>a</sup>Macro denotes the macrostructural properties of the Ca-caseinate materials after processing.

<sup>b</sup>Micro denotes the microstructural characteristics as observed with SEM.

<sup>c</sup>Mechanical denotes the behavior of the Ca-caseinate materials during tensile tests (i.e. isotropic or anisotropic).

<sup>d</sup>Sample was not cohesive enough to perform SEM and mechanical analysis.

### 3.4 Structure formation by shear and crosslinking

When a concentrated Ca-caseinate dispersion was sheared, a layered structure was found (Figure 10). Enzymatic crosslinking during shearing changed the morphology of Ca-caseinate into fibers. On the basis of the observed phenomena, we consider some factors that may account for the shear- and enzyme-induced effects.

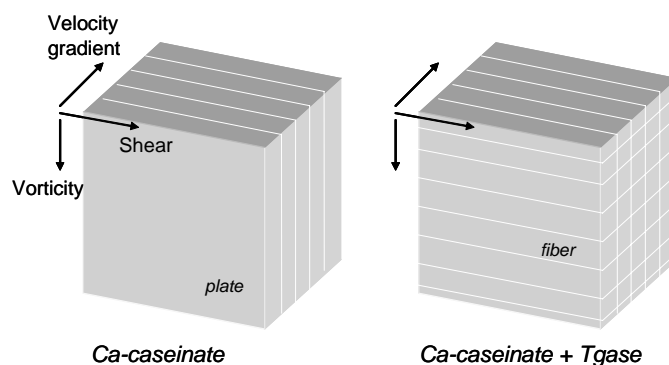


**Figure 10.** Schematic overview of shear- and enzyme-induced anisotropy in the dense Ca-caseinate: layered structure as observed after shearing Ca-caseinate (**A**) and the fibrous structure as observed after shearing Ca-caseinate in the presence of Tgase (**B**).

Ca-caseinate forms aggregates of ~100–300 nm that are stabilized due to strong interactions with  $\text{Ca}^{2+}$ -ions.<sup>24</sup> We assume that these structural elements are susceptible to ordering but not to breaking up. Therefore, we consider the Péclet number, which gives the ratio between convective and Brownian motion:<sup>35</sup>

$$Pe = \frac{6\pi a^3 \dot{\gamma} \eta_m}{kT} \quad [1]$$

where  $a$  denotes the particle radius,  $\dot{\gamma}$  is the shear rate ( $120 \text{ s}^{-1}$ ),  $\eta_m$  is the viscosity of the protein medium (~40 Pa·s at the relevant shear rate, based on a measured flow curve, data not shown),  $k$  is Boltzmann's constant and  $T$  is the temperature. When we assume a minimum protein sphere radius of 50 nm,  $Pe$  exceeds the critical value of 1, implicating that shear dominates in the system. Thus, alignment imposed by shear cannot be undone by diffusion. Inertia of the system is negligible for particles in the order of nanometers.

The anisotropic microstructures induced by shear and enzymatic crosslinking can be explained by phase separation of the structural elements in Ca-caseinate. It must be noted that we used a highly concentrated system, in which the casein aggregates are closely packed or in a jammed state.<sup>36</sup> Nevertheless, we think that local phase separation into a protein-rich and protein-poor phase with a low interfacial tension, which might have already been present in the system at rest, was enhanced by shearing resulting in alignment of these phases.

In the absence of Tgase, the combined effects of shear and  $\text{Ca}^{2+}$ -interactions led to a layered Ca-caseinate macrostructure, which showed anisotropic behavior during the tensile tests. Vermant found that shear banding occurring in worm-like micelle solutions yields structures that align parallel to a Couette cell wall.<sup>37</sup> This would result in a layered structure, similar to Figure 10A, although Vermant reported only two or three layers.<sup>37</sup> We suspect that due to the close packing of the Ca-caseinate micelles, diffusion is severely hindered, which will lead to an increased number of layers. In contrast, the microstructures as observed with SEM seem to be hardly affected by shear in terms of orientation, although it is likely that alignment in Ca-caseinate at a microscale was present due to phase separation and shear. The fact that Ca-caseinate was not quenched during shearing could cause the structure to re-order due to relaxation of the aligned protein assemblies.

Relaxation of dense colloidal microstructures upon cessation of shear was described for a silica-polymer system.<sup>38</sup>

In the presence of Tgase, crosslinking possibly increased the size of the Ca-caseinate aggregates, making them even more susceptible to alignment by shearing ( $a$  increases, consequently  $Pe$  increases). In addition, in the phase-separated protein-rich phase, Tgase induced covalent bonds in the direction of the flow. Shear-induced anisotropy in polystyrene particle suspensions was attributed to the directional dependence of break-up and reformation of aggregates.<sup>39</sup> Because solidification occurred at a shorter time scale than relaxation, the fibrous micro- and macrostructures were preserved after cessation of shear. On the basis of these considerations, we think that the anisotropy in the samples starts at the molecular level. Enhanced anisotropy as a result of enzymatic action eventually leads to macroscopical anisotropy.

### 3.5 Process prospective

In this paper, we used an in house developed shearing device to be able to use shear rate as a process parameter. Although the use of simple shear is well-known in rheological studies, it is rare in conventional processing. Our results, however, show that it may be interesting to consider the use of simple shear in processes, as it leads to the creation of novel structures that can be used in novel food products. This leads to the question of whether such a shearing device can be scaled up to an industrial process.

A constant shear profile can be obtained or approached using a cone and plate configuration, but also in a Couette configuration. The latter configuration may be more appropriate for scaling up, as the outer cylinder resembles current industrial vessels. By changing the conventional stirrer, one could possibly obtain a neat shear field inside the reactor. The process that we present in this paper is carried out at constant temperature. Therefore, we do not impose any limitations concerning heating or cooling to the process, which will ease the scale up to industrial scale.

To conclude, development of new processing equipment seems essential for making the fibrous structures presented here. Fortunately, the conditions used in this study may be applicable at industrial scale.

## 4. Conclusions

We have shown that an anisotropic fibrous Ca-caseinate structure was formed using a novel technology based on shear-induced structure formation and concurrent solidification. Enzymatic crosslinking during shearing proved to be essential for the anisotropic structure formation. The simplicity of the method combined with the high anisotropy obtained show the potential of the technology for novel food structures and applications.

After shearing and enzymatic crosslinking using Tgase, anisotropic fibrous structures were formed in a concentrated Ca-caseinate matrix on the macroscale and the microscale. We visually observed fibers of about 1 mm, and the SEM images revealed protein fibers with a diameter of ~100–200 nm, which were composed of chained protein domains. The LVE properties showed an increase in  $G'$  and a decrease in  $\tan\delta$  due to addition of Tgase. These properties were isotropic (i.e., independent of the direction of strain). In contrast, tensile properties confirmed the presence of anisotropic structures, especially based on large differences between the yield stress values in the parallel and perpendicular directions as compared to the applied shear flow. Shear affected the reinforcement of the anisotropic fibers to a large extent, whereas the properties in the perpendicular direction remained constant. Tgase also significantly influenced the structure formation in the shear direction.

Phase separation of protein aggregates at a molecular level due to shear was proposed as the mechanism leading to shear- and enzyme-induced anisotropic structures. Enzymatic crosslinking is needed to solidify the aligned protein aggregates, which may relax on cessation of shear when no solidification agent is present. Therefore, we conclude that macroscopic alignment is due to phenomena at a molecular scale.

## Acknowledgement

We are grateful to A. van Aelst from the Wageningen Electron Microscopy Centre for preparing the SEM images. M. Paques, F.J.H. Jeurissen and J. de Slegte from Friesland Foods are thanked for valuable discussions.

## References

- (1) Aguilera, J. M. **2005**. Why food microstructure? *Journal of Food Engineering* 67: 3-11.
- (2) Aguilera, J. M.; Stanley, D. W. **1993**. The microstructure of food protein assemblies. *Food Reviews International* 9 (4): 527-550.
- (3) Akkermans, C.; Venema, P.; Rogers, S. S.; Van der Goot, A. J.; Boom, R. M.; Van der Linden, E. **2006**. Shear pulses nucleate fibril aggregation. *Food Biophysics* 1 (3): 144-150.
- (4) Veerman, C.; Sagis, L. M. C.; Venema, P.; van der Linden, E. **2005**. The effect of shear flow on the percolation concentration of fibrillar protein assemblies. *Journal of Rheology* 49 (2): 355-368.
- (5) Cheftel, J. C.; Kitagawa, M.; Queguiner, C. **1992**. New protein texturization processes by extrusion cooking at high moisture levels. *Food Reviews International* 8 (2): 235-275.
- (6) Noguchi, A. **1989**. Extrusion cooking of high-moisture protein foods. In *Extrusion cooking*; Mercier, C.; Linko, P.; Harper, J. M., Eds., American Association of Cereal Chemists, Inc., St. Paul, Minnesota: 343-370.
- (7) Thiebaud, M.; Dumay, E.; Cheftel, J. C. **1996**. Influence of process variables on the characteristics of a high moisture fish soy protein mix texturized by extrusion cooking. *Food Science and Technology-Lebensmittel-Wissenschaft und Technologie* 29 (5-6): 526-535.
- (8) Liu, S. X.; Peng, M.; Tu, S.; Li, H.; Cai, L.; Yu, X. **2005**. Development of a new meat analog through twin-screw extrusion of defatted soy flour-lean pork blend. *Food Science and Technology International* 11 (6): 463-470.
- (9) Tolstoguzov, V. B. **1993**. Thermoplastic extrusion - the mechanism of the formation of extrudate structure and properties. *Journal of the American Oil Chemists Society* 70 (4): 417-424.
- (10) Peighambardoust, S. H.; Van der Goot, A. J.; Van Vliet, T.; Hamer, R. J.; Boom, R. M. **2006**. Microstructure formation and rheological behaviour of dough under simple shear flow. *Journal of Cereal Science* 43: 183-197.
- (11) Van den Eijnde, R.; Van der Linden, E.; Van der Goot, A. J.; Boom, R. **2004**. A mechanistic model of the relation between molecular structure of amylopectin and macromolecular degradation during heating-shearing processes. *Polymer Degradation and Stability* 85 (1): 589-594.
- (12) Gallant, D. J.; Bouchet, B.; Culioli, J. **1984**. Ultrastructural aspects of spun pea and fababean proteins. *Food Microstructure* 3 175-183.

- (13) Downey, G.; Burgess, K. J. **1979**. Texture studies on edible protein fibers produced by a wet spinning technique: 1. Fibers produced from casein and carrageenan. *Journal of Food Technology* 14 (1): 21-31.
- (14) Downey, G.; Burgess, K. J. **1979**. Texture studies on edible protein fibers produced by a wet spinning technique: 2. Fibers produced from casein and alginate. *Journal of Food Technology* 14 (1): 33-40.
- (15) Antonov, Y. A.; Zhuravskaya, N. A.; Tolstoguzov, V. B. **1985**. Solubility of protein fibers obtained from casein solutions and liquid two-phase water-casein-sodium alginate systems. *Die Nahrung* 29 (1): 39.
- (16) Suchkov, V. V.; Grinberg, V. J.; Tolstoguzov, V. B. **1980**. Study of the spinnability of emulsions based on a 2-phase water-casein sodium alginate system. *Nahrung-Food* 24 (9): 893-897.
- (17) Suchkov, V. V.; Grinberg, V. Y.; Bikbov, T. M.; Muschiolik, G.; Schmandke, H.; Tolstoguzov, V. B. **1988**. Non-spinneret formation and functional-properties of fibrous texturates based on a liquid 2-phase system water-casein-soya protein isolate. *Nahrung-Food* 32 (7): 669-678.
- (18) Suchkov, V. V.; Popello, I. A.; Bikbov, T. M.; Grinberg, V. Y.; Dianova, V. T.; Polyakov, V. I.; Muschiolik, G.; Schubring, R.; Schmandke, H.; Tolstoguzov, V. B. **1988**. Non-spinneret formation and functional-properties of fibrous textures based on a liquid 2-phase system water-casein-field bean protein isolate. *Nahrung-Food* 32 (7): 679-689.
- (19) Rampon, V.; Robert, R.; Nicolas, N.; Dufour, E. **1999**. Protein structure and network orientation in edible films prepared by spinning process. *Journal of Food Science* 64 (2): 313-316.
- (20) Aalbersberg, W. Y.; Hamer, R. J.; Jasperse, P.; De Jongh, H. H. J.; De Kruif, C. G.; Walstra, P.; De Wolf, F. A. **2003**. In *Industrial proteins in perspective*; 1<sup>st</sup> ed., Vol. 23, Elsevier Science, Amsterdam.
- (21) Moughal, K. I.; Munro, P. A.; Singh, H. **2000**. Suspension stability and size distribution of particles in reconstituted, commercial calcium caseinates. *International Dairy Journal* 10: 683-690.
- (22) Srinivasan, M.; Singh, H.; Munro, P. A. **1999**. Adsorption behaviour of sodium and calcium caseinates in oil-in-water emulsions. *International Dairy Journal* 9 (3-6): 337-341.
- (23) De Kruif, C. G. **1998**. Supra-aggregates of casein micelles as a prelude to coagulation. *Journal of Dairy Science* 81 (11): 3019-3028.
- (24) Dickinson, E.; Semenova, M. G.; Belyakova, L. E.; Antipova, A. S.; Il'in, M. M.; Tsapkina, E. N.; Ritzoulis, C. **2001**. Analysis of light scattering data on the calcium

- ion sensitivity of caseinate solution thermodynamics: Relationship to emulsion flocculation. *Journal of Colloid and Interface Science* 239 (1): 87-97.
- (25) Manski, J. M.; Van der Goot, A. J.; Boom, R. M. **2007**. Influence of shear during enzymatic gelation of caseinate-water and caseinate-water-fat systems. *Journal of Food Engineering* 79 (2): 706-717.
- (26) Lorenzen, P. C.; Schlimme, E.; Roos, N. **1998**. Crosslinking of sodium caseinate by a microbial transglutaminase. *Nahrung-Food* 42 (3-4): 151-154.
- (27) Nonaka, M.; Sakamoto, H.; Toiguchi, S.; Kawajiri, H.; Soeda, T.; Motoki, M. **1992**. Sodium caseinate and skim milk gels formed by incubation with microbial transglutaminase. *Journal of Food Science* 57 (5): 1214-1218.
- (28) Lucey, J. A.; Srinivasan, M.; Singh, H.; Munro, P. A. **2000**. Characterization of commercial and experimental sodium caseinates by multiangle laser light scattering and size-exclusion chromatography. *Journal of Agricultural and Food Chemistry* 48 (5): 1610-1616.
- (29) Yokoyama, K.; Ohtsuka, T.; Kuraishi, C.; Ono, K.; Kita, Y.; Arakawa, T.; Ejima, D. **2003**. Gelation of food protein induced by recombinant microbial transglutaminase. *Journal of Food Science* 68 (1): 48-51.
- (30) Peighambaroust, S. H.; Van der Goot, A. J.; Hamer, R. J.; Boom, R. M. **2004**. A new method to study simple shear processing of wheat gluten-starch mixtures. *Cereal Chemistry* 81 (6): 714-721.
- (31) Muller, W. H.; Van Aelst, A. C.; Humbel, B. M.; Van der Krift, T. P.; Boekhout, T. **2000**. Field-emission scanning electron microscopy of the internal cellular organization of fungi. *Scanning* 22: 295-303.
- (32) Gunasekaran, S.; Ak, M. M. **2003**. In *Cheese rheology and texture*; CRC Press, Boca Raton, FL: 437.
- (33) Guo, M. R.; Fox, P. F.; Flynn, A.; Kindstedt, P. S. **1996**. Heat-induced modifications of the functional properties of sodium caseinate. *International Dairy Journal* 6 (5): 473-483.
- (34) Dickinson, E.; Yamamoto, Y. **1996**. Rheology of milk protein gels and protein-stabilized emulsion gels cross-linked with transglutaminase. *Journal of Agricultural and Food Chemistry* 44 (6): 1371-1377.
- (35) Larson, R. G. **1999**. In *The structure and rheology of complex fluids*; Oxford University Press, New York: 664.
- (36) Panouille, M.; Durand, D.; Nicolai, T. **2005**. Jamming and gelation of dense  $\beta$ -casein micelle suspensions. *Biomacromolecules* 6: 3107-3111.
- (37) Vermant, J. **2001**. Large-scale structures in sheared colloidal dispersions. *Current Opinion in Colloid and Interface Science* 6 (5-6): 489-495.

- (38) Ramakrishnan, S.; Gopalakrishnan, V.; Zukoski, C. F. **2005**. Clustering and mechanics in dense depletion and thermal gels. *Langmuir* 21 (22): 9917-9925.
- (39) Hoekstra, H.; Vermant, J.; Mewis, J. **2003**. Flow-induced anisotropy and reversible aggregation in two-dimensional suspensions. *Langmuir* 19: 9134-9141.





# 5

## Influence of process parameters on formation of fibrous materials from dense calcium caseinate dispersions and fat

## **Abstract**

Concentrated calcium caseinate (Ca-caseinate) in the presence of palm fat forms hierarchical fibrous materials after enzymatic crosslinking under well-defined deformation. The presence of fat induces the protein fibers to be arranged in bundles of  $\sim 200$  fibers, separated by layers that are concentrated in fat. We investigated the effect of shear rate, shear time and protein concentration on the formation of fibrous materials in the two-phase protein-fat system. The ratio between crosslinking rate and shear rate determined whether a fibrous structure was formed or not, indicating a subtle interplay between material properties and process conditions. Prolonged shear time influenced the transition from fibrous materials into damaged structures accompanied by syneresis. The experimental results are concluded in a generalized diagram, which provides an initial explanation of the structural transitions induced by solidification and shear.

## **1. Introduction**

Both food industry and food scientists have been interested in creating fibrous food textures for several decades now. Especially the use of alternative protein sources for meat-like products is widely investigated. With respect to product applications, structure formation of multi-phase systems can be even more relevant.

Traditional processes to create fibrous structures such as spinning and extrusion are often performed with multi-phase systems.<sup>1</sup> Spinning of for example casein and sodium alginate solutions results in fibers with a thickness in the order of hundreds of micrometers.<sup>2,3</sup> In the case of spun pea and fababean protein, fibers with a granular core and strand-like cortex were formed.<sup>4</sup> However, no evidence of macromolecular orientation was found after wet spinning of soy protein isolate.<sup>5</sup> The difficulty of assembling single fibers into a food macrostructure on production scale and the necessity of coagulation chemicals and acids are some of the disadvantages when considering spinning as a food structuring process.

Extrusion of proteins at high temperatures (100-180°C) is said to result in fibrous extrudates.<sup>6,7</sup> The presence of polysaccharides can be a prerequisite for protein fiber formation during extrusion, which is attributed to the prevention of transversal protein aggregation due to phase separation.<sup>8</sup> Extrusion of defatted soy flour (150°C) resulted in protein filaments (~10-50 µm) between which polysaccharides were accumulated, yielding tensile stress ratios parallel and perpendicular to the fiber direction of 1-4.<sup>9</sup> In the case of dairy protein-fat systems, extrusion (80-120°C) was applied to blend and emulsify ingredients into cheese analogs. An increase in screw speed yielded smaller fat droplets<sup>8,10</sup> whereas a rise in temperature caused more casein aggregation.<sup>8</sup> Fibrousness in a dairy protein-fat system is only reported for Mozzarella cheese, which is produced by a cooking and stretching process.<sup>11</sup> Confocal scanning laser microscopy (CSLM, order of 100 µm) showed alignment of the protein phase<sup>12</sup>, therewith indicating the length scale of alignment in Mozzarella cheese. Further, scanning electron microscopy (SEM, order of 1 µm) did not reveal anisotropy at this scale.<sup>11</sup> The fracture stress of Mozzarella cheese parallel to the protein alignment was about a factor 2 higher compared with the fracture stress perpendicular to the fibers.<sup>13</sup> Studies concerning

extrusion processes indicate that anisotropy could be induced in biopolymer mixtures; however, the anisotropy in terms of fracture stress ratios was fairly limited. Moreover, the use of high temperatures could be a disadvantage for protein structure formation.

When the above-mentioned approaches are compared to studies using model materials, an important difference can be observed. For structuring model systems comprising proteins and polysaccharides, researchers often use idealized flow patterns (i.e. shear rate and shear stress) as occurring in rheometers in combination with well selected ingredient properties, generally using dilute systems. Dilute protein-polysaccharide systems for example formed elongated and even anisotropic structures by applying deformation.<sup>14,15</sup>

In the present paper, we will show the effects of shear parameters on the formation of anisotropic structures in a two-phase system, i.e. protein and fat, using a novel technology for creating fibrous materials from dense protein dispersions.<sup>16</sup> We used well-defined shear flow as a mild structuring process at moderate temperature (50°C) to create fibrous materials from concentrated calcium caseinate (Ca-caseinate) dispersions and palm fat. The use of fat as a second phase allows structuring the fibers at an additional length scale into bundles surrounded by a phase rich in fat. Concurrent enzymatic crosslinking using transglutaminase (Tgase) entrapped the shear-induced structure. The Ca-caseinate-fat structures were investigated with CSLM and SEM. Small and large deformation tests provided insight in the linear viscoelastic properties (LVP) and tensile properties respectively of the unique Ca-caseinate-fat materials.

## 2. Materials and methods

### 2.1 Materials

The activity of microbial  $\text{Ca}^{2+}$ -independent transglutaminase (protein-glutamine:amine  $\gamma$ -glutamyl-transferase, EC 2.3.2.13) derived from *Streptovorticilium moberansae* (1% Tgase, 99% maltodextrine, Ajinomoto Co. Inc., Tokyo, Japan) was 81-135 units·g<sup>-1</sup> according to the manufacturer's specification. Tgase catalyzes acyl-transfer reactions between  $\gamma$ -carboxyamide groups of

glutamine and the  $\epsilon$ -amino group of lysines in proteins. A 20% (w/w in demineralized water) Tgase solution was prepared freshly prior to experimental runs by mechanical stirring at room temperature for 1 h.

Ca-caseinate contained at least 88% protein according to the manufacturer's specifications (DMV International, Veghel, The Netherlands). A protein premix (pH 6.8-7.0) consisting of 25% or 30% (w/w) Ca-caseinate, Tgase and demineralized water was prepared in a kitchen mixer at low speed and at room temperature prior to processing. The absolute enzyme concentrations  $[E_0]$  were equal for both Ca-caseinate concentrations, leading to enzyme-protein (E:P) ratios of 1:20 and 1:17 for 30% and 25% Ca-caseinate respectively. Several minor components were added for preservation and CSLM analysis, being 1% (w/w) sodium benzoate (Sigma Aldrich, Zwijndrecht, The Netherlands) and  $2 \cdot 10^{-4}$ % (w/w) Rhodamine 110 (83695, Sigma Aldrich) respectively. The latter was added to the protein-premix as a  $0.02 \text{ g} \cdot \text{L}^{-1}$  solution in phosphate buffered saline (PBS).

Palm fat, which was acquired from Barentz Raw Materials (Hoofddorp, The Netherlands), has a melt trajectory from  $20^\circ\text{C}$  to  $37^\circ\text{C}$ , implying that the fat was liquid during processing ( $50^\circ\text{C}$ ), and solid during further analysis ( $20^\circ\text{C}$ ). Nile Red (72485, Sigma Aldrich), a fluorescent dye for fat for CSLM, was added to the melted palm fat in a concentration of  $0.2 \text{ g} \cdot \text{L}^{-1}$ . Of this undiluted solution, 15% v/v was for a short time mixed by hand with an appropriate amount of the protein premix prior to transferring the protein-fat mixture to the shear cell device.

Dimethylsulfoxide (DMSO) and ethanol, used for preparation of samples for SEM, were of analytical grade (Sigma Aldrich).

## **2.2 Sample preparation**

The combined protein-fat premix was transferred to the pre-heated ( $50^\circ\text{C}$ ) shear cell device (Wageningen University, The Netherlands), which is depicted in Figure 1. Inside the in house developed shear cell ( $V = 70 \text{ mL}$ ), the mixture is subjected to a simple linear shear profile, which is established between the plate (i.e. bottom cone) and cone (angle  $\alpha_{\text{plate}} = 105^\circ$ ,  $\alpha_{\text{cone}} = 100^\circ$ ). The rotating plate and stationary cone are temperature controlled with water. The temperature of the material is measured with a thermo couple located in the cone. The device is attached to a Brabender Do-Corder 330 (Brabender OHG, Duisburg, Germany) to enable shear

rate control, and torque (maximum torque value is 100 Nm) and temperature readings.

After filling the shear cell, the mixture was subjected to the following shear treatment: 4 min at 5 rpm ( $12 \text{ s}^{-1}$ ), then an increase in one minute from 5 rpm to the desired rpm value (10, 50 or 100 rpm, which are equivalent to 24, 120 and  $240 \text{ s}^{-1}$  respectively) for a set duration. This set duration will be referred to as the shear time. After processing, the material was cooled in the stationary shear cell to approximately  $12^\circ\text{C}$  in  $\sim 10$  min. The measured torque curves were calibrated relative to the measured torque value at  $t = 0$ .

The processed materials were transferred to moulds consisting of two square parallel plates ( $100 \times 100 \text{ mm}$ ). Part of the material was used within 2 h for further analysis (tensile tests and sample preparation for SEM), and a part was stored at  $4^\circ\text{C}$  for 1 day (LVP and creep measurements) and to a maximum of 6 days (CSLM) prior to further analysis.

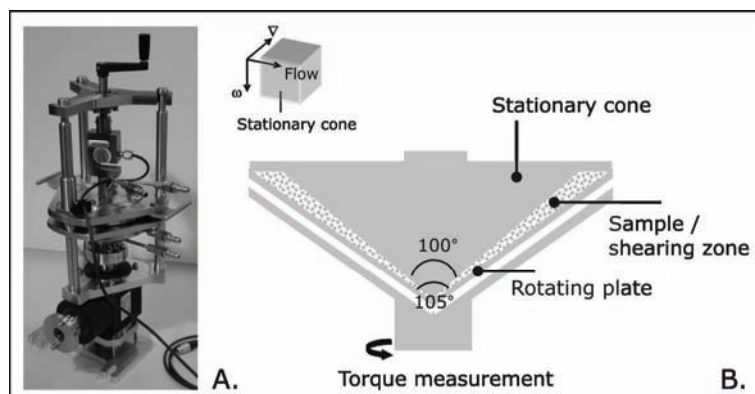


**Figure 1** Picture (A) and schematic overview (B) of shear cell device. The cone angle =  $100^\circ$ ; angle between cone and plate (shearing zone) =  $2.5^\circ$ ;  $R_{\text{plate}} = 0.08508 \text{ m}$ ;  $R_{\text{cone}} = 0.07638 \text{ m}$ . The stationary cone and rotating plate are temperature controlled with water.

### 2.3 Confocal scanning laser microscopy

The mesostructure of the processed Ca-caseinate-fat materials was observed with CSLM in the vorticity – shear flow plane. After storage at  $4^\circ\text{C}$ , protein-fat samples taken from the middle section of the shear cell were carefully cut, transferred to 2-

well chambered coverglasses (Nunc, Naperville, IL, U.S.A.) and analyzed with an inverted LSM 510 (Zeiss, Oberkochen, Germany). An Ar-ion laser (488 nm) and HeNe laser (543 nm) were used to excite the samples. For the protein phase, an emission filter of 505-530 nm was applied, whereas a 600-650 nm filter was used for the fat phase. Images were digitally recorded with a 10x dry objective (N.A. 0.3, zoom 2x and 4x) and a 40x oil immersion objective (N.A. 1.3).

Image analysis of the raw data images (512 x 512 pixels) of the fat phase was performed using the Image Toolbox of Matlab 7.0 (The Mathworks Inc., Natick MA, U.S.A.). At least 6 images per sample obtained at 10x magnification were used to determine the diameter size based on pixel area ( $d = \sqrt{4\pi / \text{area}}$ ). Also, the deformation parameter  $D$  was calculated from the length of maximum axis ( $L_{max}$ ) and the minimum axis length ( $L_{min}$ ) of an ellipsoidal:

$$D = \frac{(L_{max} - L_{min})}{(L_{max} + L_{min})} \quad [1]$$

Based on cumulative distributions of the fat droplet diameter and  $D$ , average cumulative distributions were constructed.

## 2.4 Scanning electron microscopy

The micro- and nanostructures of the sheared and crosslinked Ca-caseinate-fat materials were observed with a field emission scanning electron microscope (FESEM) at ambient temperature. Dry samples were prepared according to the method described by Muller et al.<sup>17</sup> and modified by Manski et al.<sup>16</sup> Ca-caseinate-fat samples (< 10 x 10 mm) were immersed in DMSO and slowly frozen in liquid nitrogen. Freeze fracturing was performed parallel and perpendicular to the shear flow that was exerted on the samples in the shear cell device (based on the shear flow – vorticity plane). The resulting fracture planes were the velocity gradient–shear flow plane and velocity gradient – vorticity plane respectively. In this paper, we will define the directions and resulting fracture planes as parallel and perpendicular respectively. After fracturing, samples were thawed in DMSO, subsequently re-hydrated to water, and then dehydrated in ethanol. Critical point drying with carbon dioxide (CPD 020, Balzers, Liechtenstein) was performed, and after completing drying, the pressure was reduced to atmospheric pressure within 2 hours, minimizing sample artifacts. After identifying the fracture planes with a

stereomicroscope, the samples were glued on a sample holder using conductive carbon cement (Leit- C, Neubauer Chemicalien, Germany), and sputter coated with 20 nm platinum (JFC 1200, JEOL, Japan). The fractured surfaces were analyzed with a FESEM (JEOL 6300 F, Tokyo, Japan) at room temperature at a working distance of 8 mm, with SE detection at 3.5-5 kV. All images were recorded digitally (Orion, 6 E.L.I. sprl., Belgium) at a scan rate of 100 seconds (full frame) at a size of 2528 x 2030, 8 bit. Noise reduction and resizing of the images was done with Adobe Photoshop CS.

### 2.5 Linear viscoelastic properties

Linear viscoelastic properties (LVP) of the processed materials were determined in duplicate with dynamic oscillating strain amplitude tests with a controlled stress Bohlin CVO (Bohlin Instruments Ltd., Cirencester, U.K.) at a constant frequency of 1 Hz and at a temperature of 20°C. Single frequency sweeps (0.01-100 Hz) were performed at a constant strain within the linear viscoelastic region at 20°C. Creep tests were conducted in duplicate at 20°C at a stress within the linear viscoelastic region (< 350 Pa). The creep time was 2000 s. Serrated parallel plates (diameter 25 mm, gap 2 mm) were used in all cases to prevent slip. A chamber covering the sample was used to prevent evaporation. Before measuring, samples were rested for 5-15 min to allow relaxation of the stresses induced by sample loading.

The mechanical spectra obtained were analyzed with a power law fit to the  $G'$ -frequency curves ( $G' \propto \omega^n$ ). Creep curves were analyzed with the 6-element Burgers model, which proved to be suitable to describe the viscoelastic properties of soft solid materials.<sup>18</sup> The model comprises a Maxwell element with two Kelvin-Voigt elements in series:

$$J(t) = \frac{1}{G_1} + \frac{1}{G_2} \left[ 1 - \exp\left(\frac{-tG_2}{\eta_2}\right) \right] + \frac{1}{G_3} \left[ 1 - \exp\left(\frac{-tG_3}{\eta_3}\right) \right] + \frac{t}{\eta_1} \quad [2]$$

The instantaneous compliance  $J_1$  equals  $1/G_1$ , viscous flow is represented by  $t/\eta_1$ , and the rest of the equation (two Kelvin-Voigt elements) stands for the retarded compliance. We focused on  $J$ ,  $\eta_1$  and the retardation times  $\tau_2 (= G_2/\eta_2)$  and  $\tau_3 (= G_3/\eta_3)$  to discriminate between the various sheared and crosslinked materials.



## 2.6 Tensile properties

A Texture Analyzer T2 (Stable Micro Systems Ltd., Surrey, U.K.) was used for large deformation tests. Uni-axial tensile tests were conducted with a constant deformation rate of  $3 \text{ mm}\cdot\text{s}^{-1}$  at room temperature within 2 h after creating the Ca-caseinate-fat materials. Samples were cut into a rectangular shape ( $30 \times 12 \text{ mm}$ ) having a thickness of 3-5 mm (measured for each individual sample). The length of the to-be-extended part was 15.2 mm. At least three measurements were performed on a fibrous protein sample in each direction, parallel and perpendicular to the shear flow (with respect to the shear flow-vorticity plane, thus the resulting fracture planes were the same planes as viewed with SEM). Due to the fibrous character of the samples, fracture occurred sometimes at once, and sometimes in a multi-stage way indicative of the fibrous structure, inevitably leading to variations between measurements. The tensile yield stress ( $\sigma$ ) and Hencky strain ( $\epsilon$ ), calculated from the measured force-distance curves<sup>19</sup>, were used to compare the various processed materials.

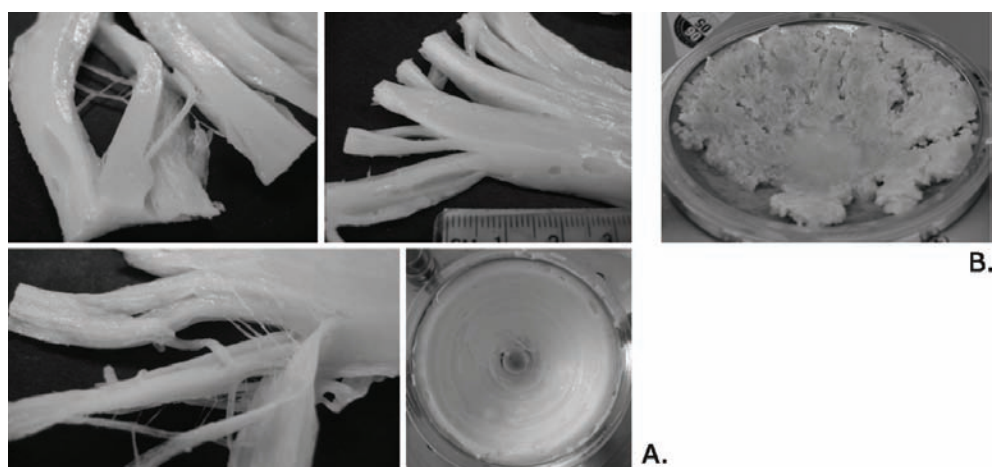


**Figure 2** **A.** Fibrous macrostructure of sheared and crosslinked 30% Ca-caseinate, 15% palm fat and Tgase (1:20) at  $120 \text{ s}^{-1}$  for 30 min (order of scale in cm); **B.** Damaged macrostructure in the shear cell (diameter shear cell is  $\sim 15 \text{ cm}$ ) with the same composition obtained at  $120 \text{ s}^{-1}$  for 60 min.

### 3. Results

#### 3.1 Processing and macrostructure

Shearing of 30% Ca-caseinate and 15% fat in the presence of Tgase at a fixed shear rate and shear time ( $120\text{ s}^{-1}$  and 30 min) resulted in a fibrous macrostructure as shown in Figure 2A. The fibers in the material could be separated easily by hand (fibers  $\sim 1\text{ mm}$ ). Shearing at  $240\text{ s}^{-1}$  resulted in a fibrous material that appeared qualitatively more fibrous compared to the material sheared at intermediate shear rate ( $120\text{ s}^{-1}$ ). In contrast, when Ca-caseinate and fat were sheared in the absence of Tgase, a homogenous macrostructure was observed without any orientation induced by the shear flow. A decrease in protein content (25% Ca-caseinate) also yielded a fibrous structure.

The formation of fibrous structures was accompanied by a constant torque evolution as illustrated in Figure 3 for 30% Ca-caseinate-fat sheared at  $120\text{ s}^{-1}$  (up to 30 min), which was also observed for  $240\text{ s}^{-1}$  but at higher torque values. In the absence of Tgase or at lower protein content, the torque response was lower due to the decreased viscosity of the protein phase (data not shown). The torque curves showed some variation at constant process conditions, possibly due to the use of the lower end of the torque range.

Prolonged shearing (60 min) of 30% Ca-caseinate and fat at  $120\text{ s}^{-1}$  resulted in a damaged structure, probably caused by disruption of the fibrous material after formation, which was broken down into small fragments. Expelled liquid (syneresis) was present as displayed in Figure 2B. After careful examining, some fibrous pieces could still be observed. In all cases, break-up was accompanied by a torque increase (Figure 3,  $*120\text{ s}^{-1}$ ). Shearing and crosslinking of 25% Ca-caseinate showed a similar rise in torque after 30 min and a damaged structure. The process time at which the transition occurred could vary in each experiment, which may be accounted to the stochastic formation of covalent bonds perpendicular to the shear flow.

Applying a low shear rate ( $24\text{ s}^{-1}$ ) also caused a sudden increase in the torque curve (Figure 3). However, shearing for 30 min at  $24\text{ s}^{-1}$  resulted in an isotropic macrostructure accompanied by some expelled fat and subtle syneresis. Probably

no alignment was induced in the Ca-caseinate-fat material at low shear rate. Concluding, fiber formation yielded a constant torque response, whereas a sudden increase in torque indicated either break-up during prolonged shearing, or the formation of an isotropic structure accompanied by a rise in viscosity.

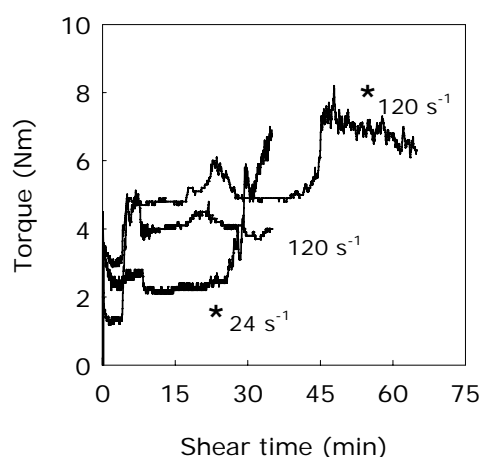


**Figure 3** Typical torque curves as function of shear time at selected shear rates (24 and 120 s<sup>-1</sup>) during shearing in the shear cell device of 30% Ca-caseinate and Tgase (1:20). All samples contained 15% palm fat. The asterisk (\*) denotes the materials that were not fibrous after shearing.

### 3.2 Microstructure

The SEM images in Figure 4 illustrate the microstructure of 30% Ca-caseinate and fat after shearing and crosslinking using Tgase (1:20). The differences between the planes parallel (Figure 4.A1-A2) and perpendicular (Figure 4.B1-2) to the shear flow are very distinct for the simultaneously sheared and crosslinked material. Compact fibers were formed in the direction parallel to the shear flow with a typical fiber diameter of ~100-200 nm. At open spaces in the structure or in the inner surface of air bubbles, the fibers could be better distinguished. The direction of fibers in the inner surface of air bubbles sometimes differed from the shear direction indicating local disturbances of the shear flow, as shown in Figure 4.A2. Perpendicular to the shear flow, we observed 'molten' structures (Figure 4.B2) in which the protein seemed covered by the fat phase.

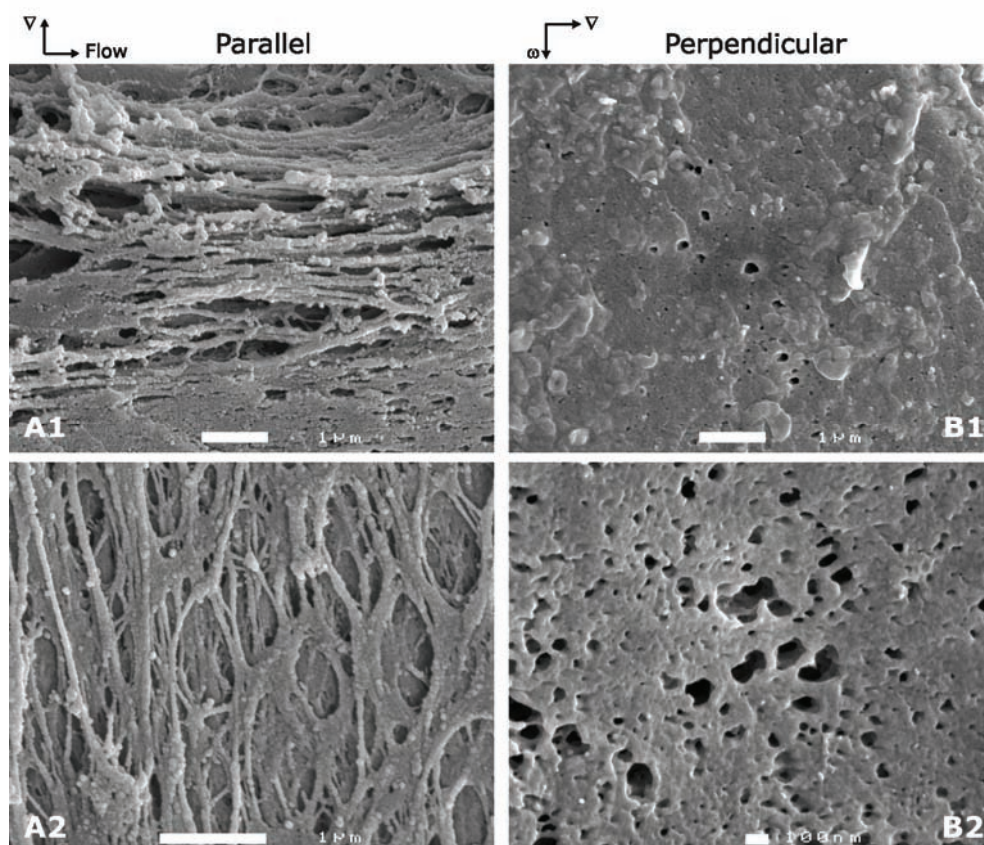


**Figure 4** SEM images of fractured surfaces parallel (**A**) and perpendicular (**B**) to the shear flow exerted in the shear cell device of 30% Ca-caseinate and 15% palm fat crosslinked with Tgase (1:20). All scale bars indicate 1  $\mu\text{m}$ , except for Fig. 4.B2, which is 100 nm.

### 3.3 Mesostructure

CSLM images of sheared and crosslinked 30% Ca-caseinate reveal that the presence of the fat phase induced anisotropy at an additional length scale, by arranging the fibers into bundles. Figure 5.A3 gives evidence of two types of fat structures in the 30% Ca-caseinate-fat materials obtained after 30 min shearing at  $120\text{ s}^{-1}$ . Relatively small and large dispersed fat droplets were observed as well as fat layers elongated in the shear direction. Based on several independently processed samples, we observed that fat was mostly present in droplet form, but also in a deformed state (based on the deformation ( $D$ ) values in Figure 5.B3-4).

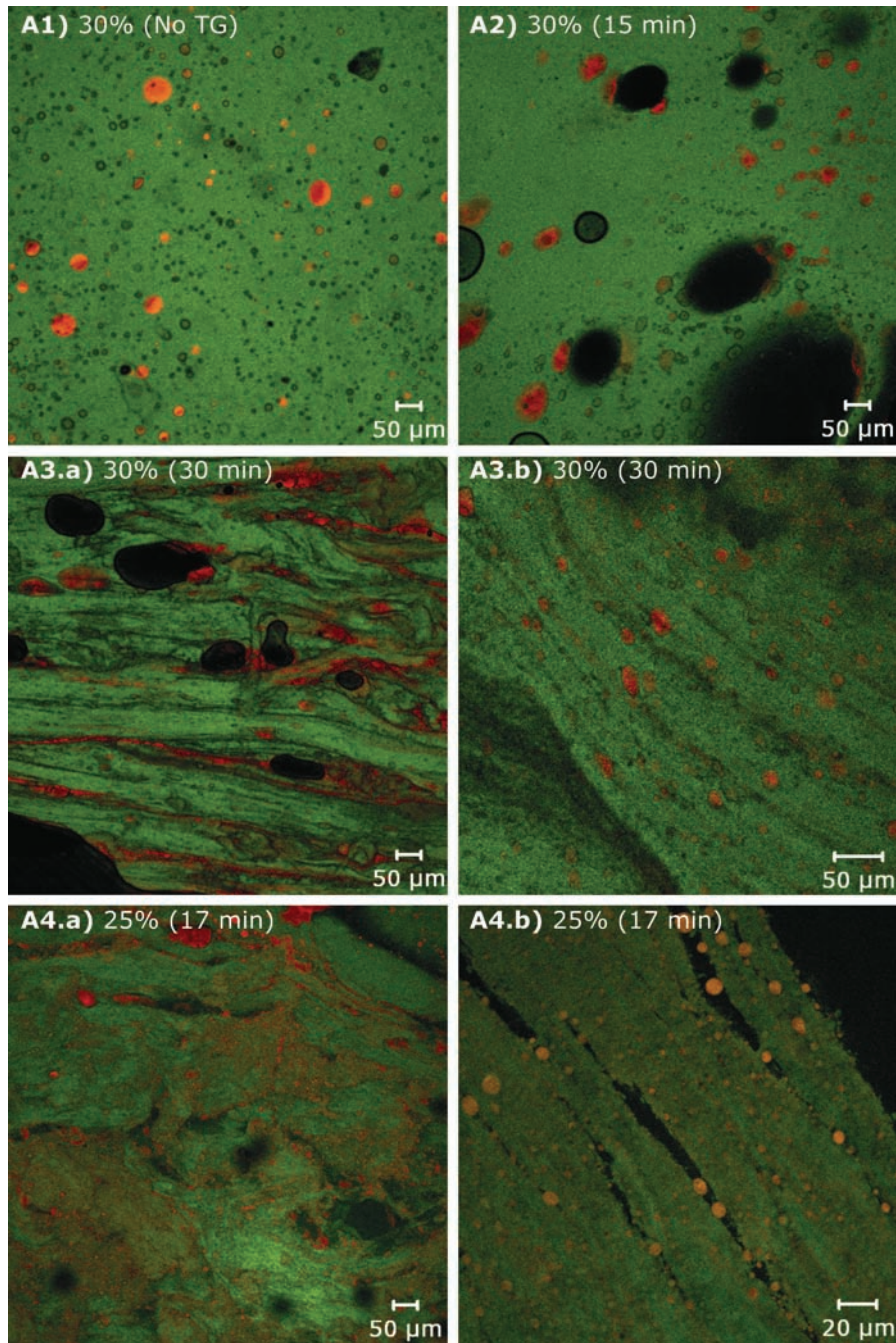
Very small fat droplets caused a certain degree of structure in the protein phase with an orientation parallel or inclined to the shear direction. A typical protein layer thickness of  $\sim 40\ \mu\text{m}$  (thus consisting of  $\sim 200$  single protein fibers), and a fat layer thickness of  $\sim 10\ \mu\text{m}$  could be estimated.

Figure 5.A1 shows the isotropic mesostructure of sheared 30% Ca-caseinate and fat without Tgase consisting of a continuous protein phase with dispersed fat droplets. The average cumulative distributions of the fat droplet diameter and deformation  $D$  indicate that without Tgase, the fat droplets were larger in size and less deformed compared to the fibrous structures formed with Tgase (Figure 5.B2-4).

The effect of shear time (15 and 30 min) at a constant shear rate of  $120\ \text{s}^{-1}$  for 30% Ca-caseinate is illustrated in Figure 5.A2-3. The black areas in the CSLM images indicate that air inclusions were present in this sample. After 5 and 15 min of shearing of 30% Ca-caseinate and fat, fibrous macrostructures were already observed by eye. However, except for some fat droplet orientation this is not evident from the CSLM image as shown for 15 min of shearing, compared to the reference sample that was sheared for 30 min. The fat droplet diameter decreased with increased shearing time, whereas  $D$  showed little variation (Figure 5.B1-3). Apparently, fat layer formation is a result of protein fiber formation. A protein content of 25% (E:P increased to 1:17) led already to a fibrous macrostructure after 17 min of shearing, which exhibited alignment of finely dispersed fat droplets as shown in Figure 5.A4. The droplets were smaller compared to droplets in the structures with higher protein content (Figure 5.B1), and no fat layers were observed.

The isotropic mesostructure obtained at low shear rate ( $24\ \text{s}^{-1}$ ) contained smaller sized fat droplets compared to the intermediate shear rate ( $120\ \text{s}^{-1}$ ), whereas the average cumulative curves of the  $D$  parameter were the same (Figure 5.B2-4). The mesostructure obtained at the highest shear rate of  $240\ \text{s}^{-1}$  showed dispersed structures with random fat droplets as well as fat structures aligned in layers ( $\sim 10\ \mu\text{m}$  thick) in the shear flow direction.





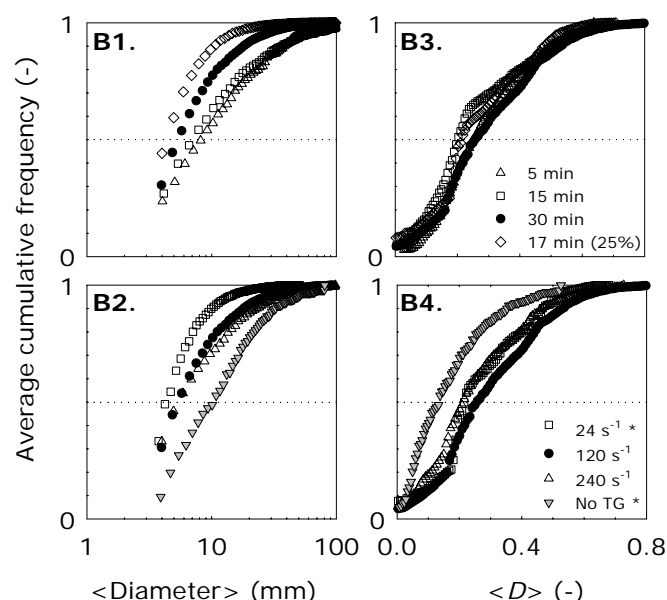


**Figure 5 A.** Selected CSLM images of sheared and crosslinked Ca-caseinate-fat materials containing 25% or 30% protein (Tgase 1:17 and 1:20 respectively) and 15% palm fat and obtained after shearing at various times at  $120 \text{ s}^{-1}$ . No TG indicates the non-crosslinked 30% Ca-caseinate material without Tgase. The images are taken from the vorticity – shear flow plane. All scale bars indicate  $50 \mu\text{m}$ , except for Fig. 5A.4b, which is  $20 \mu\text{m}$ . **B.** Average cumulative frequencies of the fat droplet diameter and deformation parameter  $D$  of selected Ca-caseinate-fat samples as determined with image analysis using at least 6 images at a magnification of 10x.

### 3.4 Rheological properties

The LVP ( $G'$  and  $\tan\delta$ ) of the Ca-caseinate-fat materials are plotted in Figure 6 as function of shear time. For the fibrous 30% Ca-caseinate-fat structures, a moderate increase in  $G'$  was measured as function of shear time, thus crosslinking reaction time. The increase in  $G'$  can be explained by the increase in the density of the covalent bonds.<sup>20</sup> Decrease in protein content to 25% Ca-caseinate resulted in a slightly lower value of  $G'$ . The sheared Ca-caseinate-fat structure in absence of Tgase showed a lower  $G'$  and higher  $\tan\delta$  value compared to the samples crosslinked with Tgase. The  $\tan\delta$  of the sample that was sheared for only 5 minutes was clearly lower than the value obtained for the sample that was not crosslinked, indicating that the sample sheared for 5 min is more solid-like than the sample

without Tgase. Remarkably, the initial decrease of  $\tan\delta$  ends after 5 min due to the fact that  $G''$  also starts to increase after 5 min. The LVP of the fibrous materials were not affected by the shear rate (data not shown), suggesting that the number of covalent bonds was equal for each shear rate as the reaction time was constant. At low shear rate ( $24\text{ s}^{-1}$ ), the isotropic material obtained had a slightly higher  $G'$  value, which may be explained by the presence of a more interconnected protein network as not all crosslinks were created in the shear flow direction.

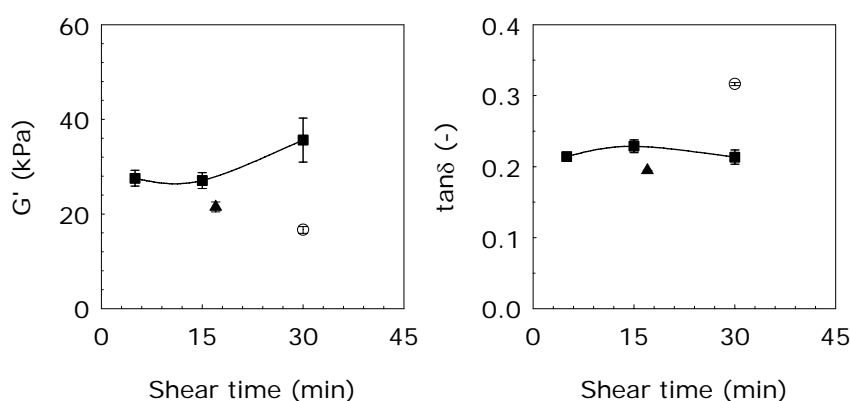


**Figure 6** Effect of shear time on the LVP,  $G'$  and loss tangent ( $\tan\delta$ ), with 95% confidence intervals of 30% Ca-caseinate and Tgase (1:20) (denoted with ■), 25% Ca-caseinate and Tgase (1:17) (denoted with ▲), and 30% Ca-caseinate without Tgase (no TG) (denoted with ○). All samples contained 15% palm fat. Open symbols denote samples that were not fibrous after shearing.

The so-called mechanical spectra (i.e. log-log plots of  $G'$ -frequency, not shown) were hardly influenced by shear time or shear rate when considering the slope of the log-log plots ( $n$  determined as  $G' \propto \omega^n$ ). Only the composition (i.e. presence of Tgase) of the materials affected the  $n$  value when comparing the crosslinked samples ( $n \sim 0.13$ - $0.15$ ) with the non-crosslinked 30% Ca-caseinate sample ( $n \sim 0.22$ ), which behaved less like a solid material.

Figure 7 depicts the effect of shear time and shear rate on the normalized  $G'$  curves as function of strain, normalized with the corresponding  $G'$  values from the linear viscoelastic region for 30% Ca-caseinate-fat samples. For the fibrous samples based on 30% Ca-caseinate, no clear trend can be deduced for the limit of the linear



viscoelastic region as function of shear time. The non-crosslinked homogeneous 30% Ca-caseinate sample showed a steeper decrease in the non-linear regime compared to the fibrous samples, which indicates that the homogeneous material was affected more abruptly at high strain values probably due to the presence of weaker (non-covalent) interactions. The limit of the linear viscoelastic region of the non-fibrous sample obtained at low shear rate ( $24 \text{ s}^{-1}$ ) was much higher compared to the linear viscoelastic limit of the fibrous samples ( $120$  and  $240 \text{ s}^{-1}$ ), which suggests that the strain limiting the linear viscoelastic region could be used as a measure for anisotropy.

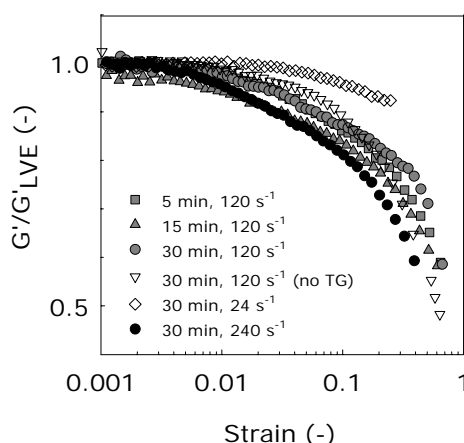


**Figure 7** Effect of shear time and shear rate on  $G'/G'_{LVE}$  ( $G'$  values normalized with the  $G'$  value in the linear viscoelastic (LVE) region) as function of the strain  $\gamma$  as measured with strain amplitude sweeps of the materials consisting of 30% Ca-caseinate, 15% palm fat and Tgase (1:20). The normalized curves are the average of duplicate measurements. Open symbols denote samples that were not fibrous after shearing. The sample denoted with 'no TG' was not crosslinked with Tgase.

The creep curves representing the total compliance, including the fits with the 6-element Burgers model, of the Ca-caseinate-fat materials are shown in Figure 8. The increase in crosslinking time resulted in a decrease of the total compliance, which is inversely proportional to the elastic modulus. Further, non-crosslinked but sheared Ca-caseinate and fat behaved more viscous compared to the crosslinked materials (insert Figure 8).

Table 1 summarizes the fitted parameters  $J_1$ ,  $\eta_1$  and the retardation times  $\tau_2$  and  $\tau_3$  from the Burgers model. The large decrease in  $J_1$  and retardation times, and increase in  $\eta_1$  after 5 min of shearing and crosslinking compared to the non-crosslinked material clearly indicates that the presence of Tgase had the largest effect on the creep parameters. The steep decline in retardation times shows that the Ca-caseinate matrix was rapidly transformed by the enzyme from a more or less viscous protein matrix into an elastic material. Obviously, the presence of covalent bonds resulted in less mobile molecules within the structures, and a larger resistance to flow at longer time scales as reflected by a rise in  $\eta_1$ . Further increase in shear (reaction) time had a subtle decreasing effect on  $J_1$ ,  $\tau_2$  and  $\tau_3$ . It must be noted that the parameters  $G_2$ ,  $G_3$ ,  $\eta_2$  and  $\eta_3$ , which determine the retardation times, increased with increasing shearing time. The shear rate itself hardly affected the creep parameters (Table 1).

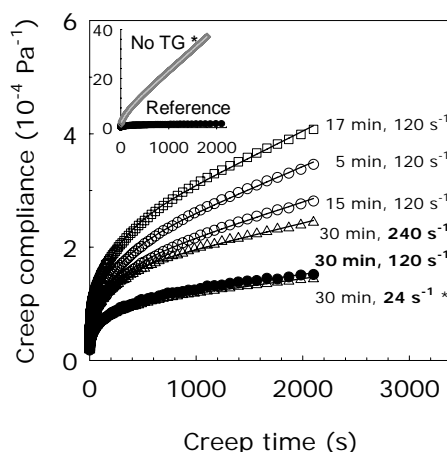


**Figure 8** Effect of shear time (open circles) and shear rate (open triangles) on creep curves (total compliance) of 30% Ca-caseinate, 15% palm fat and Tgase (1:20) obtained after processing. Also, a creep curve is shown for 25% Ca-caseinate, 15% palm fat and Tgase (1:17) (open squares). The lines represent the fitted curves with the 6-element Burgers model. The inserted graph displays non-crosslinked sheared 30% Ca-caseinate-fat (denoted with 'No TG') and crosslinked sheared 30% Ca-caseinate-fat (denoted with 'Reference' and filled circles). Non-fibrous samples are denoted with an asterisk.

**Table 1** Fitted creep-parameters including the standard deviations from the 6-element Burgers model (equation 2). The model was fitted to the creep curves that were measured at 20°C within the linear viscoelastic region. Non-fibrous samples are denoted with an asterisk.

Cacas (%)	E:P	$t_{shear}$ (min)	$\dot{\gamma}$ (s <sup>-1</sup> )	$J_1$ (10 <sup>-5</sup> Pa <sup>-1</sup> )	$\eta_1$ (10 <sup>6</sup> Pa·s)	$\tau_2$ (=G <sub>2</sub> /η <sub>2</sub> ) (s)	$\tau_3$ (=G <sub>3</sub> /η <sub>3</sub> ) (s)
30	-	30*	120*	15.9 ± 0.7*	0.8 ± 0.4*	6122 ± 8241*	127 ± 15*
30	1:20	5	120	4.0 ± 0.2	11.3 ± 1.7	260 ± 11	11 ± 1
30	1:20	15	120	4.0 ± 0.5	15.5 ± 0.9	256 ± 13	10 ± 1
30	1:20	30	120	3.2 ± 0.9	27.7 ± 16	214 ± 17	8 ± 1
25	1:17	17	120	5.5 ± 0.05	10.1 ± 0.9	261 ± 12	9 ± 1
30	1:20	30*	24*	2.3 ± 0.4*	29.6 ± 11.9*	210 ± 34*	8 ± 1*
30	1:20	30	240	3.5 ± 0.5	26.0 ± 6.1	200 ± 28	8 ± 1

### 3.5 Mechanical properties

#### 3.5.1 Effect shear time and protein concentration

Figure 9 depicts the mechanical properties (yield stress  $\sigma$  and yield strain  $\varepsilon$ ) as function of the shear time for fibrous 25% and 30% Ca-caseinate-fat materials. The large 95% confidence intervals can be explained by a step-wise and gradual fracture of fibrous samples, especially parallel to the fiber direction. The mechanical properties of the non-crosslinked 30% Ca-caseinate-fat material are also included in Figure 9. Already after 5 min of shearing at 120 s<sup>-1</sup>, anisotropy was observed in the 30% Ca-caseinate-fat material as the mechanical properties parallel and perpendicular to the fiber direction showed differences. The mechanical properties measured in the perpendicular direction remained more or less constant as function of shear time. This indicates that reinforcement of the fibrous structures through covalent binding occurred mainly in the flow direction. The anisotropy, characterized by the yield stress in the parallel direction, increased drastically with increasing shear time for 30% Ca-caseinate and fat. The mechanical properties of 25% Ca-caseinate and fat, sheared for 17 min, were more or less similar to the properties of the 30% Ca-caseinate sample sheared for 15 min. The non-crosslinked material based on 30% Ca-caseinate and fat behaved as an isotropic material for all tensile parameters. Remarkably, the mechanical properties of the non-crosslinked isotropic material equaled more or less the mechanical properties of the fibrous

materials measured perpendicular to the shear flow. This suggests that no significant amount of covalent bonds was formed perpendicular to the shear flow.

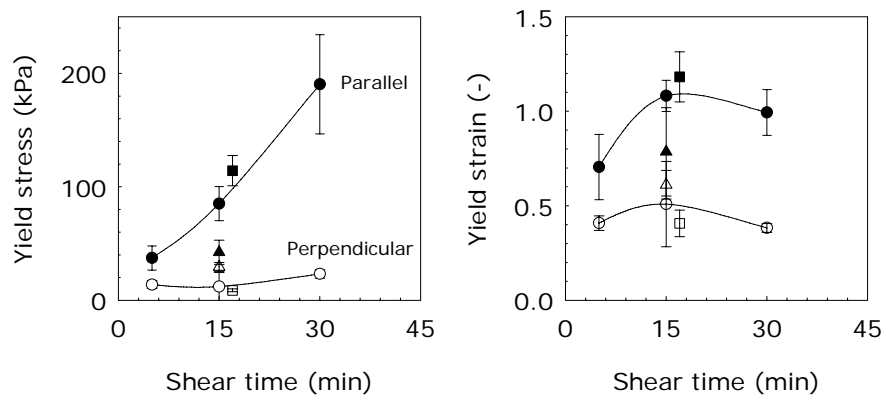


**Figure 9** Effect of shear time on tensile properties yield stress  $\sigma$  and yield strain  $\varepsilon$  with 95% confidence intervals of 25% Ca-caseinate and Tgase (1:17) (denoted with ■), 30% Ca-caseinate and Tgase (1:20) (denoted with ●) or without Tgase (no TG; denoted with ▲). All samples contained 15% palm fat. The tensile properties were measured parallel (filled symbols) and perpendicular (open symbols) to the shear flow exerted in the shear cell device.

Table 2 summarizes the effect of the shear time on the ratio of the mechanical properties measured parallel and perpendicular to the fiber direction, which can be interpreted as a measure of the fiber quality.<sup>21</sup> An increase in shear time affected all four mechanical parameters of the fibrous 30% Ca-caseinate materials positively, of which the yield stress increased mostly. The largest yield stress ratio (i.e.  $\sigma_{\parallel}/\sigma_{\perp} = 13$ ) was found for the fibrous structure with lower protein content (25% Ca-caseinate).

### 3.5.2 Effect shear rate

The shear rate proved to be an excellent process parameter to control the extent of fibrousness of sheared and crosslinked protein-fat materials. Figure 10 summarizes the effect of shear rate on the mechanical properties. Based on the mechanical properties measured parallel and perpendicular to the shear flow, we conclude that the 30% Ca-caseinate-fat material obtained at a low shear rate ( $24 \text{ s}^{-1}$ ) behaved

as an isotropic material. The yield stress and yield strain measured parallel to the fiber direction increased with increasing shear rate. The mechanical properties determined perpendicular to the flow direction first decreased with increasing shear rate in the transition from isotropic to anisotropic materials (i.e. between 24 and 120 s<sup>-1</sup>), which suggests a critical range of shear rates for fiber formation. Once fibers were formed, the shear rate hardly affected the mechanical properties of the anisotropic materials determined perpendicular to the fiber direction. When considering all process parameters (shear rate and shear time), we can conclude that the mechanical properties of the anisotropic fibrous materials measured perpendicular to the shear flow were similar and independent of the treatment. Moreover, these mechanical properties equaled those of the isotropic non-crosslinked 30% Ca-caseinate-fat material (Figure 9). This implies that no significant amount of covalent bonds was created in the vorticity – shear flow plane in the fibrous materials, which is partly hindered by the presence of fat.

Table 2 summarizes the ratios of the mechanical properties of the fibrous materials measured parallel and perpendicular to the fiber direction. Based on these ratios, the 30% Ca-caseinate-fat material formed at the highest shear rate (240 s<sup>-1</sup>) was the most fibrous ( $\sigma_{||}/\sigma_{\perp} = 14.2$ ), thereby indicating that the shear rate can be used successfully to control the degree of fibrousness.

**Table 2** Effect of shear time and shear rate on the ratio of the tensile properties of fibrous and non-fibrous Ca-caseinate-fat materials measured parallel and perpendicular to the shear flow (at 120 s<sup>-1</sup>) exerted in the shear cell device. Non-fibrous samples are denoted with an asterisk.

Ca-cas (%)	Ratio E:P	Shear rate (s <sup>-1</sup> )	Shear time (min)	Yield stress $\sigma_{  }/\sigma_{\perp}$ (-)	Yield strain $\varepsilon_{  }/\varepsilon_{\perp}$ (-)
30	-	120 *	30 *	1.4 *	1.3 *
30	1:20	120	5	2.7	1.7
30	1:20	120	15	7.0	2.1
30	1:20	120	30	8.2	2.6
25	1:17	120	17	13.0	2.9
30	1:20	24 *	30 *	1.2 *	1.1 *
30	1:20	240	30	14.2	3.6

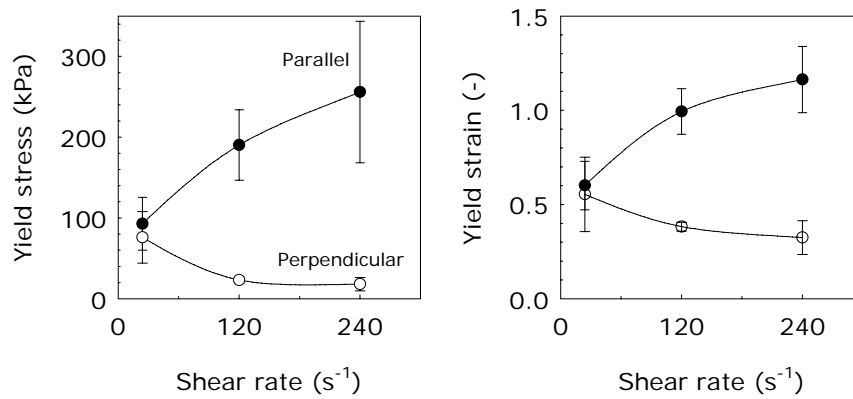


**Figure 10** Effect of shear rate on tensile properties yield stress  $\sigma$  and yield strain  $\varepsilon$  with 95% confidence intervals of 30% Ca-caseinate with Tgase (1:20) and without Tgase (no TG). All samples contained 15% palm fat. The tensile properties were measured parallel (filled symbols) and perpendicular (open symbols) to the shear flow exerted in the shear cell device.

#### 4. Discussion

Fibrous materials were found in a specific window of process conditions and composition. This study focuses on the effect of shear time, shear rate and protein concentration. Only enzymatic crosslinking in combination with shearing led to fibrous Ca-caseinate-fat structures. The presence of fat induced the fibers to be arranged in bundles surrounded by fat, thus yielding so-called hierarchical protein-fat structures. The shear rate appeared to be a process parameter for controlling both the formation of fibrous structures and the degree of fibrousness. The formation of fibrous structures was time-dependent, showing a gradual transition from a fibrous structure into a damaged structure accompanied by syneresis.

We will now discuss the interplay between the investigated process parameters and (1) the fat phase and (2) the protein matrix properties with respect to the structure formation of fibrous structures.

#### 4.1 Role of fat during structure formation

The SEM images show little difference between the sheared and crosslinked fibrous Ca-caseinate structures containing fat compared to the previously fibrous structures without fat.<sup>16</sup> The estimated fiber thickness was more or less similar (~100-200 nm). However, with CSLM, we observed an additional length scale in the Ca-caseinate-fat materials where protein bundles and deformed fat structures were visible. Our results indicate that it is likely that bonds are created mostly in the direction of the shear flow. The presence of fat further hinders the formation of covalent bonds in the direction perpendicular to the flow, thereby possibly enhancing the fibrous character of the material. This is in line with the role of fat globules in Mozzarella cheese, which are accumulated between protein strands and are said to prevent fusion of these strands.<sup>22</sup>

The values of the mechanical properties of the fibrous sample containing fat were slightly higher compared to the fibrous protein sample without fat<sup>16</sup>, suggesting reinforcement of the structure by the solid fat phase.<sup>23</sup> The ratios of the mechanical properties measured parallel and perpendicular to the shear flow were similar to the fibrous sample without fat, having both a high yield stress ratio of 8-9, suggesting a similar degree of anisotropy.

In the absence of Tgase, the fat droplets were larger and less deformed in the isotropic Ca-caseinate-fat material compared to the fat droplets present in the fibrous structures containing Tgase. This is probably due to lower viscous forces in the absence of Tgase, as indicated with the Capillary number ( $Ca$ ):

$$Ca = \frac{\eta_{matrix} \dot{\gamma} R_0}{\sigma_{Int}} \quad [3]$$

The  $Ca$  number gives the ratio between viscous ( $\eta_{matrix}$  is the viscosity of the matrix,  $\dot{\gamma}$  is the shear rate, and  $R_0$  is the initial droplet size), and interfacial forces ( $\sigma_{Int}$  is the interfacial tension). The initial fat droplet size in the protein-fat premix prior to shearing is unknown, but presumably large as a result of the preparation. In the presence of Tgase,  $\eta_{matrix}$  will increase with increasing shearing time, leading to large viscous forces and consequently to droplet break-up. However, an increase in matrix elasticity will enhance elongation of the dispersed phase, and temporarily even orientation towards the flow direction.<sup>24</sup> The viscosity ratio ( $\lambda = \eta_{dispersed} / \eta_{matrix}$ ) of the phases also influences structure formation during well-defined deformation:

when  $\lambda < 1$ , which is likely the case during shearing and crosslinking Ca-caseinate and fat, droplets will get elongated during shearing.<sup>25</sup> Also,  $\lambda$  decreases with increasing  $\eta_{matrix}$ , thereby shifting the critical  $Ca$  number at which break-up occurs to a higher value<sup>26</sup>, and as a result favoring elongated deformation of the fat droplets. As the surfaces of fat droplets are stabilized by casein molecules during shearing and crosslinking, elongation of the fat droplets will enhance as well.

The slightly smaller and rounder fat droplets present in the microstructure of 25% Ca-caseinate-fat compared to 30% Ca-caseinate-fat structures suggest an increase in fat droplet stabilization by casein molecules in the initially lower viscous protein matrix of 25% compared to 30% Ca-caseinate.

#### ***4.2 Role of protein properties during structure formation***

Ca-caseinate dispersions comprise protein aggregates<sup>27, 28</sup> that are comparable to casein micelles (~100-300 nm) in milk.<sup>29</sup> These structural elements are most likely susceptible for alignment by shear when hydrodynamic forces dominate. This can be illustrated with a shear-based form of the Péclet number, which represents the ratio between shearing motion (towards aligning) and diffusion (towards randomization)<sup>25</sup>:

$$Pe = \frac{\dot{\gamma}R}{D} \approx \frac{6\pi\eta_{matrix}\dot{\gamma}R^3}{kT} \quad [4]$$

The diffusion coefficient  $D$  of the aggregate was based on the Stokes-Einstein approximation (i.e.  $kT/6\pi\eta_{matrix}R$ ) with Boltzmann's constant  $k$ , temperature  $T$  and viscosity of the matrix  $\eta_{matrix}$ . At a low  $Pe$ , the shear rate ( $\dot{\gamma}$ ) is not sufficient to overcome the dispersing effect of diffusion, and therefore the aggregate will not be lined up. As crosslinking increases the aggregate size ( $R$ ), the  $Pe$  will rise strongly and the particles will be aligned more effectively. Therefore, crosslinking may be an effective tool to promote alignment.

Based on the fact that after shearing at  $24 \text{ s}^{-1}$  an isotropic material was formed, we think that the applied shear rate was too low to align the structural elements, i.e. the casein aggregates. Shearing at relatively high shear rates was needed for alignment and the creation of fibers. When the shear rate is low, the protein matrix is more viscous due to shear thinning behavior (data not shown). Therefore, it is likely that a more random covalent network is being formed, which will reach a



percolated state rapidly. Shearing at a high shear rate ( $240 \text{ s}^{-1}$ ) resulted in enhanced fibrousness as reflected by the mechanical properties. This can be explained by an increase in micro phase separation due to the high shear rate, leading to more fibers, and the presence of small fat droplets in thin layers. Summarizing, the shear rate appears to be an essential tool to influence the creation and degree of fibrousness of fibrous materials based on Ca-caseinate and fat.

Based on Michaelis-Menten kinetics, an equal initial and maximum crosslinking rate was present in the 25% and 30% Ca-caseinate systems, since the initial absolute enzyme concentration was constant. An excess of substrate ( $[P_0] \gg [E_0]$ ,  $[P_0] \gg K_m$  based on the model substrate Z-Gln-Gly<sup>30</sup>) reduces the Michaelis-Menten equation to a proportional relation between the maximum reaction rate and enzyme concentration ( $v_{max} \propto [E_0]$ ). This results in a higher effective crosslinking rate  $[E/P]$  in the 25% Ca-caseinate system compared with 30% Ca-caseinate (i.e.  $[E/P]$  values of 0.06 and 0.05 respectively), which could explain the superior yield stress properties (i.e. higher  $\sigma_{||}/\sigma_{\perp}$  value) of the fibrous material based on 25% Ca-caseinate compared to 30% Ca-caseinate.

The higher crosslinking rate also explains the reduction in shear time before break-up of the 25% Ca-caseinate-fat structure compared to the 30% Ca-caseinate-fat system. In the former case, a lower protein concentration requires less crosslinks to form a complete network, which are formed in a shorter time compared to a higher protein concentration. After a certain shear time, the fibrous structures probably reached their maximum strength, and consequently disorientation and even break-up occurred. The formation of covalent bonds perpendicular to the flow direction could have resulted in the same behavior, i.e. break-up of the aligned structures.

### 4.3 Effect of process parameters on structure formation in Ca-caseinate-fat systems

Based on the results, we can deduce that interplay between crosslinking rate and shear rate determines the formation of fibrous structures. We summarize the results in a diagram (Figure 11) in order to provide an overview of the types of structures that can be obtained. On the y-axis the solidification rate ( $r_s$ ) and shear rate, yielding  $r_s / \dot{\gamma}$ , are plotted as function of process time. In the case of enzymatic crosslinking,  $r_s$  scales with  $[E/P]$ , whereas the shear rate is interpreted as a measure

of alignment. All experimental data points for 30% Ca-caseinate-fat materials are displayed in the diagram. The 25% Ca-caseinate-fat materials were excluded because the lower protein concentration did not only influence  $[E/P]$ , but also the viscosity. The latter effects are expected to be highly non-linear and require further investigation. Based on the experimental data and theoretical considerations, four structural regions can be constructed in the diagram: (1) fibrous structures denoted with  $F$ , (2) 'granular' structures, which are the damaged and broken-down structures after over-shearing, denoted with  $G$ , (3) isotropic solid materials that are crosslinked into a solid but not aligned denoted with  $I_s$ , and (4) isotropic liquid materials, which are materials that contain the same consistency as the starting material, denoted with  $I_l$ .

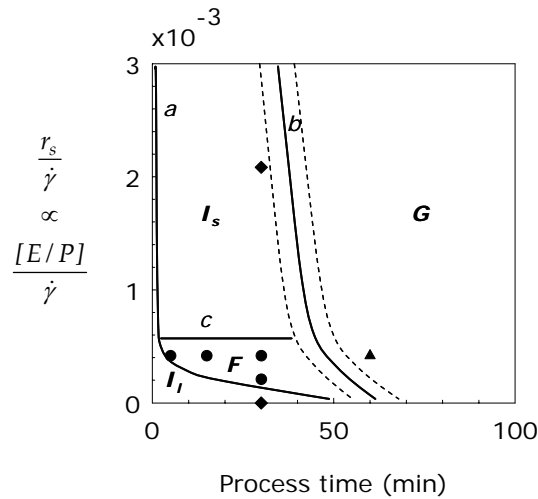


**Figure 11** Diagram based on the ratio of solidification rate and shear rate as function of process time. Lines  $a$ ,  $b$  and  $c$  represent transitions to four structural regions: (1) isotropic liquid materials ( $I_l$ ), (2) fibrous materials ( $F$ ), (3) isotropic solid materials ( $I_s$ ) and (4) damaged 'granular' materials ( $G$ ). Circles, triangles and diamonds represent fibrous, granular and isotropic materials respectively based on 30% Ca-caseinate, 15% palm fat and Tgase (1:20) obtained at various process conditions.

At a fixed  $[E/P]/\dot{\gamma}$  ratio  $< \sim 6 \cdot 10^{-4}$  (arbitrary units), three structural transitions can occur with increased process time. First, an isotropic liquid is formed at short process times when either  $\dot{\gamma} \rightarrow \infty$  or  $[E/P] \rightarrow 0$ . Structural elements, which are

prone to shear alignment when hydrodynamic forces dominate, will align at high shear rates, but will lose their orientation when no solidification is applied. The process time needed for fixation of the structure depends on the solidification rate, explaining the shape of the transition line *a*. At longer process times the aligned structure breaks, resulting in a 'granular' structure accompanied with syneresis. This is depicted with the time-dependent transition line *b*.

When the solidification rate dominates the shear rate ( $[E/P]/\dot{\gamma} > \sim 8 \cdot 10^{-4}$ ), a time-independent transition occurs, illustrated by line *c*. No anisotropic materials will be formed in that case. Above transition line *c*, when solidification dominates alignment, three time-dependent transitions exist as well. At very short time scales an isotropic liquid is formed, which rapidly transforms into an isotropic solid with a random highly percolated network (line *a*). As the network strength increases with process time, the transition to the granular region (line *b*) can be expected due to break-down of the structure. With increased solidification rate, the transition from an isotropic solid into a granular material will occur earlier, which explains the asymptotic behaviour of line *b*. Similarly, we think that line *a* is also an asymptote towards the y-axis. It must be noted that the values of  $[E/P]/\dot{\gamma}$  are arbitrary and specific for the system under investigation. Nevertheless, the existence of two time-dependent (*a*, *b*) and one time-independent (*c*) transition dividing the structural diagram into four distinct regions, of which the fibrous region is the narrowest one, may be generic for the structuring process based on well-defined flow and solidification.

The proposed diagram provides an explanation why structuring processes, other than well-defined flow processes, do not result in highly aligned and fibrous structures. During mixing, biopolymers are subjected to relatively low shear rates, and occasionally to high peak shear rates.<sup>31</sup> Due to the motion inherent during mixing, the macromolecules are continuously re-oriented, and eventually the total material will be treated at these high peak stresses, which can result in break-up of the structure. Therefore, during mixing, the material will never reach the fibrous region as an isotropic solid (region *I<sub>s</sub>*), or even a granular structure (region *G*), will be formed rapidly.

In case of extrusion, a slit die is used to align biopolymers. Shear flow, in combination with solidification due to disulfide bonds and hydrophobic interactions during cooling can lead to a certain extent of anisotropy.<sup>7,32</sup> However,

to our best of knowledge, alignment at smaller spatial scales (i.e. 50 – 500 nm) was not reported for extruded fibrous materials. Besides, fibers produced through extrusion are always composed of two or more phases. Nevertheless, Figure 11 can be used to explain that the extrusion process will enter the fibrous region as defined in the diagram when the cooling rate, shear rate, and length of the die are balanced correctly.

Further investigation should elucidate the dependence of the structuring process on material properties in terms of rheological behavior, which may yield an extended expression for the balance between solidification rate and shear rate including product properties such as viscosity and initial protein cluster size. Only then more complete insight will be obtained in the generic mechanism of the formation of fibrous structures with ingredients other than casein proteins.

## 5. Conclusion

A novel structuring process based on well-defined shear flow and enzymatic crosslinking using Tgase yields highly anisotropic structures on micro-, meso- and macroscale in case of dense Ca-caseinate-fat dispersions. The formation of anisotropic materials depends on the interplay between on the one hand ingredient properties, in particular the rheological behavior and the presence of structural elements, and on the other hand process parameters. Prolonged shear time influenced the transition from fibrous materials in damaged structures accompanied by syneresis. The effect of shear rate and solidification rate on structure formation of Ca-caseinate-fat materials was summarized in a diagram, indicating that the process window for the formation of anisotropic structures is narrow. This study stresses that shear rate is an effective parameter to control both the formation and the degree of fibrousness in Ca-caseinate-fat materials. Therefore, the shear rate will prove useful as a design parameter in equipment based on well-defined flow patterns for the creation of novel foods and materials.

## Acknowledgements

The authors wish to thank A. van Aelst from the Wageningen Electron Microscopy Centre for preparing the SEM images, and M. Paques, F.J.H. Jeurissen and J. de Slegte from Friesland Foods for valuable discussions.

## References

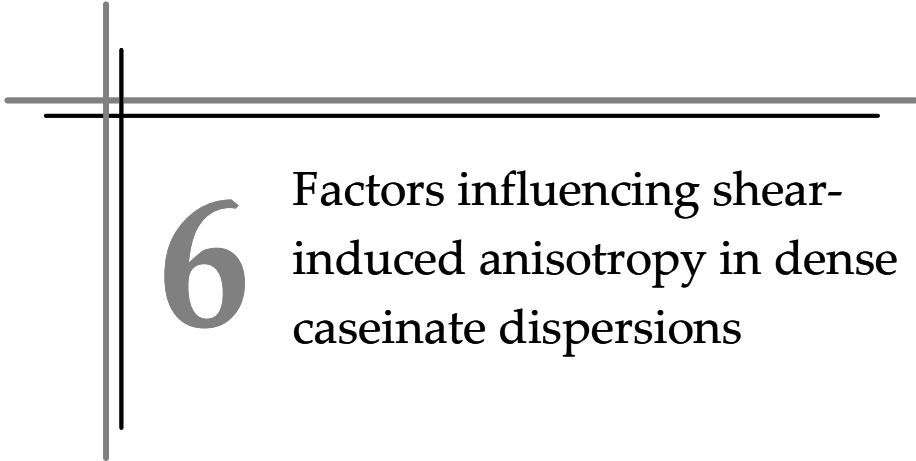
- (1) Tolstoguzov, V. B. **1993**. Thermoplastic extrusion - the mechanism of the formation of extrudate structure and properties. *Journal of American Oil Chemists Society* 70 (4): 417-424.
- (2) Antonov, Y. A.; Zhuravskaya, N. A.; Tolstoguzov, V. B. **1985**. Solubility of protein fibers obtained from casein solutions and liquid two-phase water-casein-sodium alginate systems. *Die Nahrung* 29 (1): 39.
- (3) Suchkov, V. V.; Grinberg, V. J.; Tolstoguzov, V. B. **1980**. Study of the spinnability of emulsions based on a 2-phase water-casein sodium alginate system. *Nahrung-Food* 24 (9): 893-897.
- (4) Gallant, D. J.; Bouchet, B.; Culioli, J. **1984**. Ultrastructural aspects of spun pea and fababean proteins. *Food Microstructure* 3: 175-183.
- (5) Rampon, V.; Robert, R.; Nicolas, N.; Dufour, E. **1999**. Protein structure and network orientation in edible films prepared by spinning process. *Journal of Food Science* 64 (2): 313-316.
- (6) Areas, J. A. G. **1992**. Extrusion of food proteins. *Critical Reviews in Food Science and Nutrition* 32 (4): 365-392.
- (7) Aguilera, J. M.; Stanley, D. W. **1993**. The microstructure of food protein assemblies. *Food Reviews International* 9 (4): 527-550.
- (8) Cheftel, J. C.; Kitagawa, M.; Queguiner, C. **1992**. New protein texturization processes by extrusion cooking at high moisture levels. *Food Reviews International* 8 (2): 235-275.
- (9) Noguchi, A. **1989**. Extrusion cooking of high-moisture protein foods. In *Extrusion cooking*; Mercier, C.; Linko, P.; Harpo, J. M., Eds., American Association of Cereal Chemists, Minnesota: 343-370.
- (10) Zuber, F.; Megard, D.; Cheftel, J. C. **1987**. Continuous emulsification and gelation of dairy ingredients by HTST extrusion cooking: Production of processed cheeses. *International Journal of Food Science and Technology* 22 (6): 607-626.

- (11) McMahon, D. J.; Paulson, B.; Oberg, C. J. **2005**. Influence of calcium, pH, and moisture on protein matrix structure and functionality in direct-acidified nonfat Mozzarella cheese. *Journal of Dairy Science* 88: 3754-3763.
- (12) O'Reilly, C. E.; Murphy, P. M.; Kelly, A. L.; Guinee, T. P.; Auty, M. A. E.; Beresford, T. P. **2002**. The effect of high pressure treatment on the functional and rheological properties of Mozzarella cheese. *Innovative Food Science and Emerging Technologies* 3: 3-9.
- (13) Ak, M. M.; Gunasekaran, S. **1997**. Anisotropy in tensile properties of Mozzarella cheese. *Journal of Food Science* 62 (5): 1031-1033.
- (14) Wolf, B.; Frith, W. J. **2003**. String phase formation in biopolymer aqueous solution blends. *Journal of Rheology* 47 (5): 1151-1170.
- (15) Wolf, B.; Scirocco, R.; Frith, W. J.; Norton, I. T. **2000**. Shear-induced anisotropic microstructure in phase-separated biopolymer mixtures. *Food Hydrocolloids* 14 (3): 217-225.
- (16) Manski, J. M.; Van der Goot, A. J.; Boom, R. M. **2007**. Formation of fibrous materials from dense calcium caseinate dispersions. *Biomacromolecules*, in press.
- (17) Muller, W. H.; Van Aelst, A. C.; Humbel, B. M.; Van der Krift, T. P.; Boekhout, T. **2000**. Field-emission scanning electron microscopy of the internal cellular organization of fungi. *Scanning* 22: 295-303.
- (18) Edwards, N. M.; Peressini, D.; Dexter, J. E.; Mulvaney, S. J. **2001**. Viscoelastic properties of durum wheat and common wheat dough of different strengths. *Rheologica Acta* 40: 142-153.
- (19) Gunasekaran, S.; Ak, M. M. **2003**. In *Cheese rheology and texture*; CRC Press, Boca Raton, FL: 437.
- (20) Dickinson, E.; Yamamoto, Y. **1996**. Rheology of milk protein gels and protein-stabilized emulsion gels cross-linked with transglutaminase. *Journal of Agricultural and Food Chemistry* 44 (6): 1371-1377.
- (21) Thiebaud, M.; Dumay, E.; Cheftel, J. C. **1996**. Influence of process variables on the characteristics of a high moisture fish soy protein mix texturized by extrusion cooking. *Food Science and Technology-Lebensmittel-Wissenschaft and Technologie* 29 (5-6): 526-535.
- (22) McMahon, D. J.; Oberg, C. J. **1998**. Influence of fat, moisture and salt on functional properties of Mozzarella cheese. *Australian Journal of Dairy Technology* 53 (2): 98-101.
- (23) Manski, J. M.; Kretzers, I. M. J.; Van Brenk, S.; Van der Goot, A. J.; Boom, R. M. **2007**. Influence of dispersed particles on small and large deformation properties of concentrated caseinate composites. *Food Hydrocolloids* 21 (1): 73-84.
- (24) Sibillo, V.; Simeone, M.; Guido, S. **2004**. Break-up of a Newtonian drop in a viscoelastic matrix under simple shear flow. *Rheologica Acta* 43 (5): 449-456.

- (25) Larson, R. G. **1999**. In *The structure and rheology of complex fluids*; Oxford University Press, New York: 664.
- (26) Migler, K. B.; Hobbie, E. K.; Qiao, F. **1999**. In line study of droplet deformation in polymer blends in channel flow. *Polymer Engineering Science* 39 (11): 2282-2291.
- (27) Moughal, K. I.; Munro, P. A.; Singh, H. **2000**. Suspension stability and size distribution of particles in reconstituted, commercial calcium caseinates. *International Dairy Journal* 10: 683-690.
- (28) Srinivasan, M.; Singh, H.; Munro, P. A. **1999**. Adsorption behaviour of sodium and calcium caseinates in oil-in-water emulsions. *International Dairy Journal* 9 (3-6): 337-341.
- (29) De Kruif, C. G. **1998**. Supra-aggregates of casein micelles as a prelude to coagulation. *Journal of Dairy Science* 81 (11): 3019-3028.
- (30) Ohtsuka, T.; Umezawa, Y.; Nio, N.; Kubota, K. **2001**. Comparison of deamidation activity of transglutaminases. *Journal of Food Science* 66 (1): 25-29.
- (31) Peighambardoust, S. H.; Van der Goot, A. J.; Hamer, R. J.; Boom, R. M. **2005**. Effect of simple shear on the physical properties of glutenin macro polymer (GMP). *Journal of Cereal Science* 42 (1): 59-68.
- (32) Ledward, D. A.; Tester, R. F. **1994**. Molecular transformations of proteinaceous foods during extrusion processing. *Trends in Food Science and Technology* 5 117-120.







# 6 Factors influencing shear-induced anisotropy in dense caseinate dispersions

---

This chapter is submitted as: Manski, J.M.; Van Riemsdijk, L.E.; Van der Goot, A.J.; Boom, R.M. 2007. Factors influencing shear-induced anisotropy in dense caseinate dispersions.

## **Abstract**

Rheological measurements of dense calcium caseinate and sodium caseinate dispersions ( $\geq 15\%$ ) provided insight in the factors determining shear-induced structure formation in caseinates. Calcium caseinate at sufficiently high concentration (30%) was shown to form highly anisotropic structures during shearing and concurrent enzymatic crosslinking. In contrast, sodium caseinate formed isotropic structures using similar processing conditions. The main difference between the two types of caseinates is the counter ion present, and as a consequence, the size of structural elements and their interactions. The rheological behavior of calcium caseinate and sodium caseinate reflected these differences, yielding non-monotonic and shear thinning flow behavior for calcium caseinate whereas sodium caseinate behaved almost as a Newtonian fluid. The coupling and the non-monotonic behavior of the shear stress and normal stress in calcium caseinate showed resemblance to shear-induced concentration fluctuations, which are often seen in polymeric and micellar model systems. Shear-induced concentration fluctuations, leading to phase separation, are thought to be the underlying mechanism for anisotropic structure formation in calcium caseinate.

## **1. Introduction**

Shear-induced structuring of proteins is of high interest for the development of novel products, such as meat analogs. Recently, we showed that well-defined flow and concurrent enzymatic crosslinking led to anisotropic materials based on dense calcium caseinate (Ca-caseinate) dispersions.<sup>1</sup> The study reported here demonstrates that the shear-induced structure formation as reported for Ca-caseinate is not generic yet. Dense sodium caseinate (Na-caseinate) dispersions formed isotropic materials using exactly the same processing conditions as for dense Ca-caseinate dispersions. Therefore, in this paper, we report on the difference between Ca-caseinate and Na-caseinate using rheological measurements to identify relevant prerequisites for the shear-induced formation of anisotropic structures in caseinate dispersions.

Shear-induced structure formation is widely investigated in polymer and micellar solutions and colloidal suspensions using rheometers. The effects of shear flow can be summarized as the induction of three types of structures ranging from small distortions of the equilibrium structure, orientation in flow direction, and concentration fluctuations.<sup>2,3</sup> Viscoelasticity in terms of normal stresses as well as shear thinning behavior was thought to play an important role for shear-induced string formation of macroscopic particle dispersions.<sup>4-7</sup> Bundle-like ordering of dense colloidal latex dispersions was strongly affected by particle interactions and particle concentration.<sup>8</sup> The critical stress needed for inducing ordering depended on the particle size of the latex dispersions used. Concentration fluctuations yielding shear bands have mainly been studied for wormlike micellar solutions, which show shear thinning or shear thickening behavior.<sup>9-12</sup>

To our knowledge, research on concentrated caseinate systems is scarce. Several studies focused on the rheological behavior of concentrated Na-caseinate<sup>13</sup>, casein<sup>14,15</sup> and milk<sup>16-18</sup> in order to couple shear viscosity with physical properties of the protein micelles, such as voluminosity and interaction potentials. Concentrated Na-caseinate dispersions above 10% (w/v) were found to behave as closely packed spheres exhibiting soft sphere interactions.<sup>13</sup> Similarly, jamming of  $\beta$ -casein above 10% (w/v) was reported to cause a strong increase in viscosity reflecting the closely packed character of the dispersions.<sup>15</sup> The micelles present in caseinate dispersions

range from 20-50 nm for Na-caseinate<sup>19</sup> and 100-300 nm for Ca-caseinate in diameter.<sup>20,21</sup> The difference in micelle size is attributed to the presence of calcium ions that provide interaction with casein proteins leading to larger micelle sizes.<sup>22</sup>

In this paper, we combine insights from literature with data from our own measurements of the rheological behavior of dense Ca-caseinate and Na-caseinate dispersions. Many studies, concerned with structure evolution under shear, relate the macroscale phenomena (structuring) to rheological behavior. In line with this, the objective of the study reported here was to link the rheological properties of the concentrated starting materials with the structure formation of these caseinates at macroscale. The structure formation of both caseinates (30%) in the presence of a dispersed phase (fat) was investigated in a shear cell device providing well-defined flow fields, followed by structure analysis using mechanical tests and microscopy (SEM and CSLM). The rheological behavior of both caseinates (15-30%) was characterized using steady shear and small amplitude oscillatory shear.

## 2. Materials and methods

### 2.1 Materials

Both Ca-caseinate and Na-caseinate contained at least 88% protein according to the manufacturer's specifications (DMV International, Veghel, The Netherlands). Depending on the concentration used, protein dispersions (pH 6.8 - 7.0) were either prepared by mechanical stirring overnight (protein concentration  $\leq 20\%$  w/w), or by preparing a so-called premix (protein concentration  $> 20\%$  w/w). The premix of caseinate and demineralized water was prepared in a kitchen mixer at low speed and room temperature prior to processing. Several minor components were added for preservation and CSLM analysis, being 1% (w/w) sodium benzoate (Sigma Aldrich, Zwijndrecht, The Netherlands) and  $2 \cdot 10^{-4}\%$  (w/w) Rhodamine 110 (83695, Sigma Aldrich) respectively. The latter was added to the protein-premix as a  $0.02 \text{ g} \cdot \text{L}^{-1}$  solution in phosphate buffered saline (PBS).

In case of an enzyme treatment, microbial  $\text{Ca}^{2+}$ -independent transglutaminase (Tgase: protein-glutamine:amine  $\gamma$ -glutamyl-transferase, EC 2.3.2.13) derived from *Streptoverticillium moberansae* (1% Tgase, 99% maltodextrine, Ajinomoto Co. Inc.,

Tokyo, Japan) was added to the aqueous part of the premix (expressed as enzyme-protein ratios E:P = 1:20). For this purpose, a 20% (w/w in demineralized water) Tgase stock solution was prepared freshly prior to the experimental runs by mechanical stirring at room temperature for 1 h. The measured activity of Tgase was 117 units·g<sup>-1</sup> using the hydroxamate method.<sup>23</sup>

Palm fat, acquired from Barentz Raw Materials (Hoofddorp, The Netherlands), was used as a dispersed phase in selected protein materials. Nile Red (72485, Sigma Aldrich), a fluorescent dye for fat for CSLM, was added to the melted palm fat in a concentration of 0.2 g·L<sup>-1</sup>. Of this undiluted solution, 15% v/v was shortly mixed by hand with an appropriate amount of the protein premix prior to transferring the protein-fat mixture to the shear cell device.

Dimethylsulfoxide (DMSO) and ethanol, used for preparation of samples for SEM, were of analytical grade (Sigma Aldrich).

## ***2.2 Preparation and analysis of caseinate materials***

Dense Na-caseinate dispersions (30%) were sheared in the shear cell device in the absence or presence of the crosslinking enzyme transglutaminase (E:P = 1:20), similarly to the methods that were used for preparing dense Ca-caseinate materials.<sup>24</sup> After preparing the Na-caseinate materials in the shear cell device, tensile tests were performed to determine the yield stress and yield strain measured parallel and perpendicular to the shear flow. The samples were analyzed using confocal scanning laser microscopy (CSLM) and scanning electron microscopy (SEM) as described elsewhere.<sup>24</sup>

## ***2.3 Rheological characterization of dense caseinate dispersions***

### ***2.3.1 Steady shear measurements***

Shear rate sweeps including the measurement of normal forces were performed for Ca- and Na-caseinate at various concentrations (15%, 20% and 30%) with a Paar MCR 301 rheometer (Anton Paar, Graz, Austria) at 50°C using cone/plate geometries (i.e. angle 4°/diameter 50 mm for 15% and 20% protein and angle 2°/diameter 20 mm for 30% protein due to the large viscosity spectrum). All

dispersions contained 1% sodium benzoate. The 15% and 20% protein dispersions were liquid when loaded to the rheometer, whereas 30% protein dispersions were soft solids, which became liquid upon heating. Shortly before the rheological characterization, the soft solids were prepared in a Brabender Do-Corder mixer (type W50) at 50°C and 50 rpm for 20 min (of which the first 5 min were mixed at 5 rpm) in order to obtain well-dispersed starting materials. The 15% and 20% protein dispersions were dispersed overnight prior to the rheological measurements, and kept at ~40°C. Water evaporation during the measurements was minimized by using a solvent trap. After temperature equilibration (2 min), duplicate (except for 30% caseinates) shear rate sweeps were performed in the range of 1-300 s<sup>-1</sup>. Each shear rate was applied for 10 s (total measure time 210 s). After applying increasing shear rates (up sweep), the shear rate was decreased to measure the down sweep. For 30% Ca-caseinate and 30% Na-caseinate, the effect of pre-shear (5 s<sup>-1</sup> and 25 s<sup>-1</sup> for 2 min) was investigated and the effect of a resting time (7 min followed by pre-shear) before applying a new shear rate sweep on the same sample.

The transient viscosity behavior of the same protein dispersions was measured at constant shear rates (24, 50 and 120 s<sup>-1</sup>) for > 1000 s. Prior to the transient measurements at these constant shear rates, the shear rate was increased stepwise: 1, 10 s<sup>-1</sup> (followed by 24 or 50 s<sup>-1</sup>) and 100 s<sup>-1</sup> (followed by 120 s<sup>-1</sup>), each applied for 100 s. The shear stress and first normal stress difference ( $N_1$ ) determined after 60 s of shearing at these shear rates (average values of at least duplicates) were compared to the measured values obtained during the shear rate sweeps.

The difficulty of measuring dense protein systems is reflected in the maximum values of the coefficient of variation (CV, defined as the ratio of standard deviation and mean value multiplied by 100%) for the measured stress values. The maximum CV for shear rate sweeps as well as transient measurements was 9% for 15% and 20% Na-caseinate; 30% Na-caseinate showed a maximum CV of 30% for transient stress values. The CV values for the shear rate sweeps of 15% Ca-caseinate were <125% for shear rates below 10 s<sup>-1</sup> and a maximum CV of 13% for shear rates exceeding 10 s<sup>-1</sup>. The maximum CV for 20% Ca-caseinate was 39%. The maximum CV for the measured transient stress values were 32%, 28% and 54% for 15%, 20% and 30% Ca-caseinate respectively.

### 2.3.2 Small amplitude oscillatory shear measurements

Duplicate frequency sweeps (angular frequency  $\omega$  range of 1-628 s<sup>-1</sup>) were performed at a constant strain of 1% (based on strain amplitude sweeps performed at 1 Hz) at 50°C using a stress-controlled Paar MCR 301. The serrated parallel-plate geometry (diameter 25 mm, gap 1 mm) was used, since parallel plates are the preferred geometry for small strain measurements of high viscous materials.<sup>25</sup> The CV in the  $G'$  measurements for Na-caseinate was below 10% for  $\omega < 300$  s<sup>-1</sup> and the maximum CV was 23%. The maximum CV for Ca-caseinate was 45%.

## 3. Results

This section will show the difference in structure formation of Na-caseinate and Ca-caseinate, and in their rheological properties.

### 3.1 Effect of shear on structure formation of dense Ca- and Na-caseinate dispersions

As shown previously, 30% Ca-caseinate dispersions form highly anisotropic materials under shear flow.<sup>1,24</sup> Figure 1 provides an overview of the anisotropic structures that were formed after shearing 30% Ca-caseinate, i.e. layered and fibrous structures. In the current paper, we show that dense 30% Na-caseinate dispersions remained isotropic after identical processing (shearing at 120 s<sup>-1</sup> and crosslinking with Tgase 1:20 for 30 min). A homogeneous macrostructure was observed, both in the absence and in the presence of fat. Tensile tests of sheared and crosslinked Na-caseinate confirmed that the material behaved as an isotropic material when comparing the yield stress and yield strain values parallel and perpendicular to the exerted shear flow in the shear cell device. These are shown in Table 1. The mesostructure of sheared and crosslinked Na-caseinate-fat material showed that fat was present as droplets, randomly located in the matrix, as displayed in Figure 2. SEM images of the microstructure parallel (Figure 3A) and perpendicular (Figure 3B) to the shear flow proved that no molecular or mesoscale alignment was achieved in the sheared and crosslinked Na-caseinate-fat material.

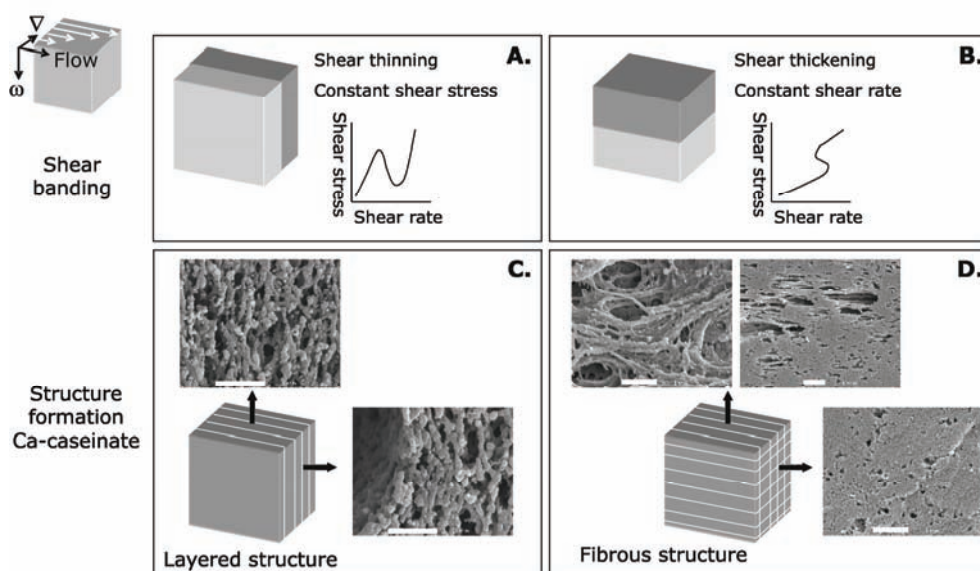


**Figure 1** Schematic representation of shear-induced structures, i.e. shear bands, found in polymer systems (**A.** bands perpendicular to velocity gradient and **B.** bands perpendicular to vorticity direction). The schematic structures formed after shearing dense (30%) Ca-caseinate dispersions both in absence (**C.** layered structure) and presence of crosslinking enzyme transglutaminase (**D.** fibrous structure, also containing 15% palm fat) are shown as well. SEM images obtained at various planes display the microstructures of these sheared Ca-caseinate dispersions, which are described in detail elsewhere.<sup>1,24</sup> The scale bars denote 1  $\mu\text{m}$ .

**Table 1** Ratio of tensile properties measured parallel and perpendicular to the shear flow of sheared and crosslinked Ca- and Na-caseinate materials (Tgase 1:20), with or without palm fat (15%), including 95% confidence intervals. The materials were prepared by shearing at  $120 \text{ s}^{-1}$  for 30 min.

Material	Yield stress $\sigma_{  }/\sigma_{\perp}$ (-)	Yield strain $\varepsilon_{  }/\varepsilon_{\perp}$ (-)
30% Na + Fat	$0.8 \pm 46\%$	$0.9 \pm 16\%$
30% Na	$1.1 \pm 85\%$	$1.0 \pm 42\%$
30% Ca + Fat <sup>ref. 24</sup>	$8.2 \pm 38\%$	$2.6 \pm 18\%$
30% Ca <sup>ref. 1</sup>	$9.2 \pm 24\%$	$2.6 \pm 8\%$

Table 2 summarizes the various observations with respect to dense caseinate systems and the effect of shear and crosslinking on the resulting structures. These experiments indicate that the alignment was specific for the protein Ca-caseinate,



and was influenced by protein concentration, since shearing and crosslinking of 20% Ca-caseinate yielded an isotropic material. The presence of a dispersed phase did not alter the structure formation of the protein phase.

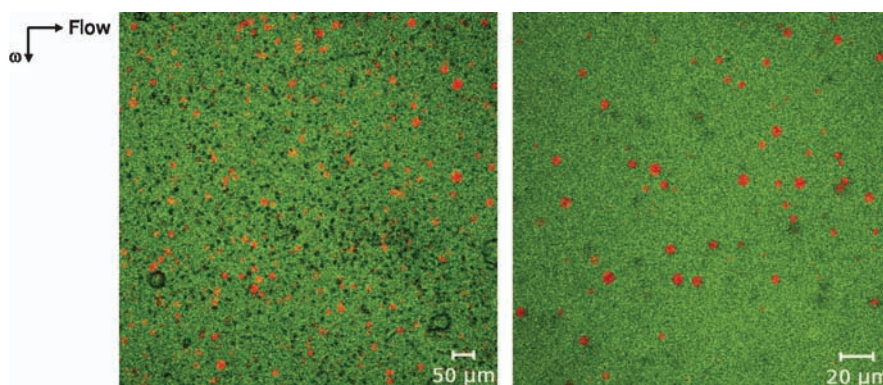


**Figure 2** CSLM images of sheared and crosslinked 30% Na-caseinate and 15% fat (Tgase 1:20,  $120 \text{ s}^{-1}$ , 30 min,  $50^\circ\text{C}$ ) obtained at two magnifications (10x, scale bar  $50 \mu\text{m}$  and 40x, scale bar  $20 \mu\text{m}$ ).

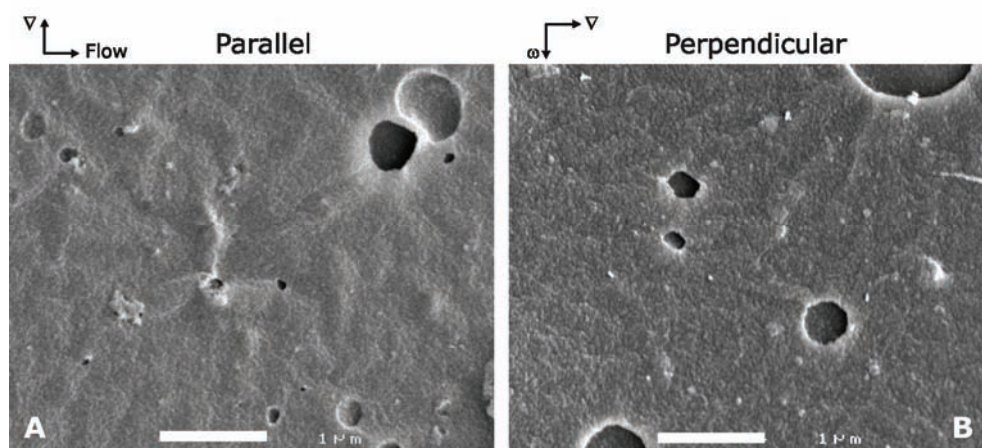


**Figure 3** SEM images of sheared and crosslinked 30% Na-caseinate and fat (Tgase 1:20,  $120 \text{ s}^{-1}$ , 30 min) parallel (A) and perpendicular (B) to the shear flow exerted in the shear cell device. The scale bars denote  $1 \mu\text{m}$ .

**Table 2** Overview of observations of the structural properties of Ca-caseinate and Na-caseinate materials after shearing ( $120 \text{ s}^{-1}$ ) and crosslinking using Tgase for 30 min (unless stated otherwise).

Protein	Concentration (%)	E:P (-)	Dispersed phase	Structural properties
Ca-caseinate	30	1:20	15% Fat	Anisotropic (fibers) <sup>ref. 24</sup>
		1:20	-	Anisotropic (fibers) <sup>ref. 1</sup>
		-	-	Anisotropic (layers) <sup>ref. 1</sup>
	25	1:17	15% Fat	Anisotropic <sup>ref. 24</sup>
	20	1:10	-	Isotropic (syneresis) <sup>a</sup>
		1:20	10% Fat	Isotropic
Na-caseinate	30	1:10	10% Fat	Isotropic
		1:20	15% Fat	Isotropic
		1:20	-	Isotropic <sup>b</sup>
	20	1:20	10% Fat	Isotropic <sup>c</sup>

<sup>a</sup> 60 min of shearing.<sup>b</sup> Isotropic after applying  $120 \text{ s}^{-1}$  and  $360 \text{ s}^{-1}$ .<sup>c</sup> 40 min of shearing.

## 3.2 Rheology of dense Ca- and Na-caseinate dispersions

### 3.2.1 Effect of steady shear on shear stress

Figure 4 depicts the shear stress as function of shear rate, of Ca- and Na-caseinate at three concentrations (i.e. 15%, 20% and 30%) in the range of  $1\text{--}300 \text{ s}^{-1}$ . The main difference between the shear stresses of Ca- and Na-caseinate is that the shear stress is much smoother for Na-caseinate at all concentrations. Further, Ca-caseinate shows shear-thinning behavior, whereas Na-caseinate behaves almost as a Newtonian liquid at the concentrations and shear rates measured. This difference between Ca- and Na-caseinate is persistent but diminishes when the concentration is increased to 30%. However, at the relevant shear rates used in the shear cell device ( $10\text{--}150 \text{ s}^{-1}$ ), 30% Ca-caseinate is still clearly shear thinning, whereas the viscosity of 30% Na-caseinate appears to level off (see also insert Figure 4).

At all three concentrations, Ca-caseinate exhibits fluctuations in shear stress with increasing shear rate. First, a shear thickening behavior is observed, and when the shear rate exceeds approximately  $10 \text{ s}^{-1}$ , the curves for all Ca-caseinate concentrations become monotonic; they all show shear thinning behavior. An increase in stress may reflect build-up of structure, whereas the stress decrease

indicates break-up of this structure. The non-monotonic evolution of the stress is often explained by transition(s) in 'structure' of micellar dispersions.<sup>26</sup>

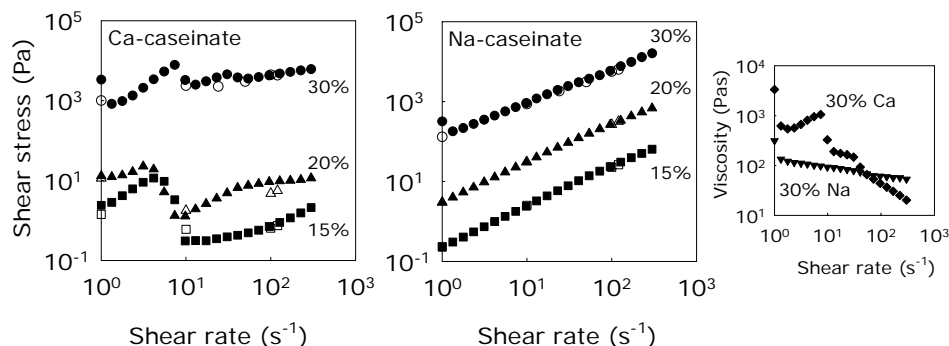


**Figure 4** Shear stress as function of shear rate (up sweep) of Ca-caseinate and Na-caseinate (15%, 20% and 30%) measured at 50°C. Each shear rate was applied for 10 s (closed symbols; squares, triangles and circles for 15%, 20% and 30% caseinate respectively). Transient measurements (data points taken at shear rates that were applied for 60 s; open symbols) are included as well. The insert shows the viscosity as function of shear rate for 30% Ca-caseinate and 30% Na-caseinate.

Based on preliminary shear rate sweeps that were performed using various measure times, as well as transient measurements at fixed shear rates, we can conclude that the shear stresses of both caseinates depended on the shear time applied. A too short shear time, i.e. less than 5 s, led to deviating flow curves, suggesting that no steady state was reached (data not shown). A good resemblance was found between transient flow data (data taken at  $t = 60$  s) and shear rate sweeps where a constant shear rate sweep of 10 s per shear rate was applied, which is shown in Figure 4. It must be noted that the transient shear stress showed an overshoot during the start-up flow for dense Ca-caseinate (20%, 30%) dispersions, whereas no such overshoot was observed for Na-caseinate. This suggests again that some form of structure was present in the dense Ca-caseinate dispersions.

Various pre-shear treatments ( $5 s^{-1}$  and  $25 s^{-1}$  for 2 min) did not result in the break-down of the structure present in 30% Ca-caseinate, as we still observed an initial increase in shear stress, which implies shear thickening behavior. Subsequently, a decrease in shear stress occurred with increasing shear rate (i.e. up sweep), which

is shown in Figure 5. The shear thickening is more pronounced for a pre-shear treatment at  $25\text{ s}^{-1}$  compared to  $5\text{ s}^{-1}$ . In addition, the stress curves did not exhibit such a maximum anymore when the shear rate was decreased (down sweep). A similar observation was done for dilute wormlike micelles, which was attributed to the fact that a banded structure already existed during the down sweep, which had been formed during the up sweep.<sup>27</sup> Obviously, the initial structure could not be reformed within the time scale of the down sweep.

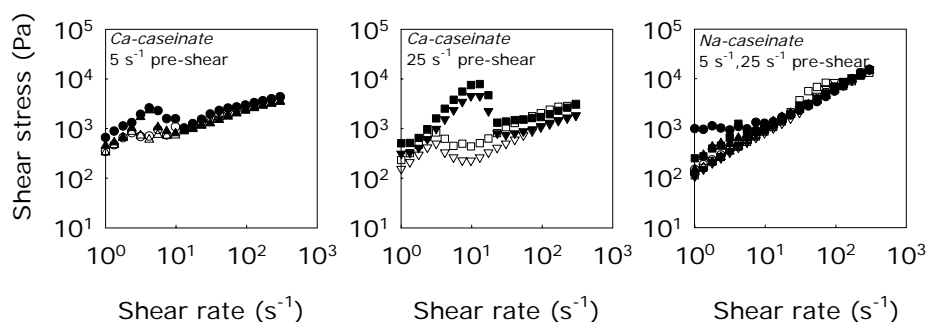


**Figure 5** Shear stress as function of shear rate of 30% Ca-caseinate and 30% Na-caseinate measured at  $50^{\circ}\text{C}$  after applying a pre-shear treatment at  $5\text{ s}^{-1}$  (circles) and  $25\text{ s}^{-1}$  (squares) for 2 min. The effect of a resting time of 7 min followed by again a pre-shear treatment at  $5\text{ s}^{-1}$  (triangles up) and  $25\text{ s}^{-1}$  (triangles down) for 2 min is also displayed. The flow curves for increasing (up sweep) and decreasing (down sweep) shear rates (each applied for 10 s) are denoted with closed and open symbols respectively.

In addition, hysteresis effects were observed for Ca-caseinate when comparing the shear stress curves obtained with increasing shear rates and decreasing shear rates. This implies that structural changes may have taken place due to the shear history. A resting time of 7 min resulted in the same shear stress curves, thus exhibiting shear thickening during the up sweep, and hysteresis based on the down sweep, albeit both at slightly lower absolute shear stress values. This indicates that the caseins were able to turn to their initial situation at least to a certain extent, and therewith showing a subtle time-dependency. Dense Na-caseinate behaved in all cases almost as a Newtonian fluid, independent of either a pre-shear applied, or resting time. These results suggest that 30% Na-caseinate exhibits an almost time-independent flow behavior, in contrast to 30% Ca-caseinate.

When considering the shear rate range of 10-300 s<sup>-1</sup>, power law fits ( $\sigma = K\dot{\gamma}^n$ ) can be applied to the shear stress-shear rate curves of the caseinate dispersions, yielding low shear-thinning indices ( $n$ ) for Ca-caseinate as shown in Table 3. Therefore, in the relevant range of shear rates that is applied in the shear cell device to create anisotropic structures, Ca-caseinate is highly shear-thinning. Power-law fits of the stress-shear rate curves of Na-caseinate (Figure 4 and Table 3) reveal that Na-caseinate starts to become shear-thinning with increasing concentration. The measured flow curves do not allow the determination of the shear rate at which shear thinning starts to occur. However, this shear rate is presumably a few orders of magnitude lower for Ca-caseinate compared to the shear rate for Na-caseinate when considering the measured flow curves. The inverse of this so-called critical shear rate reflects a system-specific relaxation time  $\tau_{rel}^{14, 28}$ , and therefore, our results suggest that  $\tau_{rel, Na} \ll \tau_{rel, Ca}$ .

**Table 3** Power law fit values ( $\sigma = K\dot{\gamma}^n$ ) to the shear stress-shear rate curves of dense Ca-caseinate (in shear rate range of 10-300 s<sup>-1</sup>) and Na-caseinate (in shear rate range of 1-300 s<sup>-1</sup>) dispersions, which are shown in Figure 4.

Protein	Concentration (%)	$K$ (Pa·s <sup><math>n</math></sup> )	$n$ (-)	$R^2$
Ca-caseinate	15	0.05	0.61	0.94
	20	0.68	0.54	0.88
	30	1628.20	0.22	0.81
Na-caseinate	15	0.24	1.00	0.99
	20	3.22	0.96	0.99
	30	158.09	0.79	0.99

Finally, during the transient measurements at various shear rates, we observed a fluctuating behavior of the shear stress for 30% Ca-caseinate, implying instable flow behavior, whereas no such fluctuations were observed for 30% Na-caseinate.

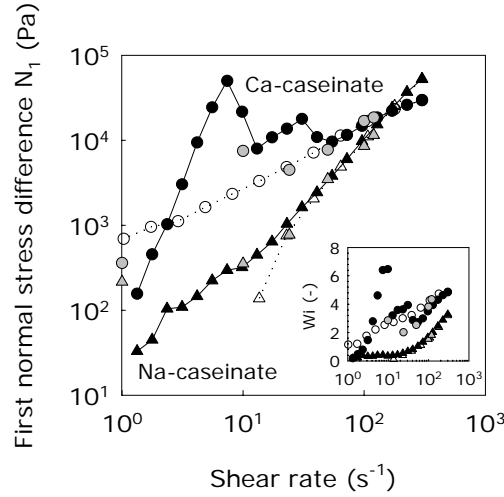


**Figure 6** First normal stress difference  $N_1$  as function of shear rate of 30% Ca-caseinate (circles) and 30% Na-caseinate (triangles) measured at 50°C. The curves for both increasing (up sweep) and decreasing (down sweep) shear rates are denoted with closed and open symbols respectively. The insert depicts the Weissenberg number as function of the shear rate for Ca-caseinate and Na-caseinate (the same symbols are used as for  $N_1$ ).

### 3.2.2 Effect of steady shear on first normal stress difference

Normal forces varying between  $10^{-2}$  and 10 N were found for 30% Ca-caseinate and 30% Na-caseinate in the shear rate range of 1-300  $s^{-1}$ , whereas 20% Na-caseinate exhibited normal forces only at shear rates larger than 50  $s^{-1}$ . Figure 6 displays the first normal stress difference  $N_1$  as function of the shear rate obtained from both shear rate sweeps and transient measurements for the 30% caseinates. Ca-caseinate showed slightly higher values compared to Na-caseinate. The measured  $N_1$  for 30% Ca-caseinate also displays non-monotonic behavior with increasing shear rate, similarly as we observed for the shear stress. With decreasing shear rates (down sweep) we observe a nearly perfect power law behavior of  $N_1$ . In contrast,  $N_1$  for 30% Na-caseinate shows a power law behavior with both increasing and decreasing shear rate. The measured curves for the two caseinates show a cross-over around 120  $s^{-1}$ , after which  $N_{1,Na} > N_{1,Ca}$ . The transient  $N_1$  values coincide best for 30% Na-caseinate as displayed in Figure 6. The resulting Weissenberg number ( $Wi = N_1/\sigma$ ), often used to quantify the viscoelasticity of solutions, of 30% Ca-caseinate was higher compared to 30% Na-caseinate for the whole shear rate range,

but the difference decreased to a factor 2 at the high shear rates ( $Wi$  of 4 and 2 respectively for  $120 \text{ s}^{-1}$ ), as depicted in Figure 6 (insert).

Figure 7 shows the effect of a pre-shear treatment of the evolution of  $N_1$  as function of increasing and decreasing shear rate for both caseinates. Again,  $N_1$  of 30% Ca-caseinate shows non-monotonic behavior with increasing shear rate, whereas such behavior is not observed when the shear rate is decreased. The highest shear rate used for the pre-shear treatment resulted in the strongest increase in  $N_1$ . There is hardly an effect of resting time on  $N_1$ , confirming that the structures in the Ca-caseinate dispersion were able to quickly recover to their initial state. With exception of the low shear rates ( $< 10 \text{ s}^{-1}$ ), 30% Na-caseinate shows a power law relation of  $N_1$  with the shear rate. The down sweeps deviate slightly from the up sweeps, and similarly to Ca-caseinate, no time-dependent effect on  $N_1$  was observed for Na-caseinate.

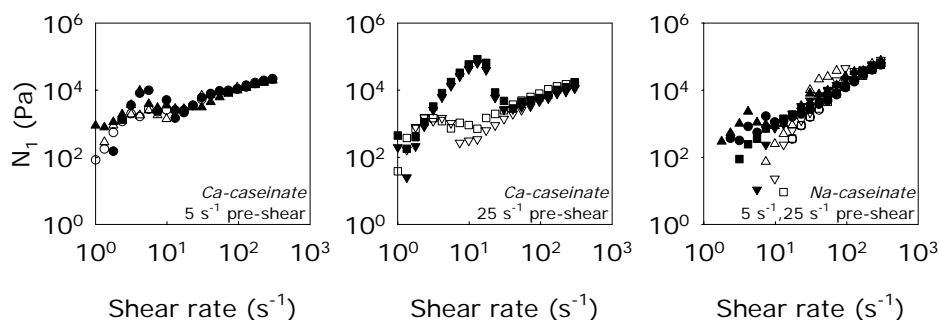


**Figure 7** First normal stress difference  $N_1$  as function of shear rate of 30% Ca-caseinate and 30% Na-caseinate measured at  $50^\circ\text{C}$  after applying a pre-shear treatment at  $5 \text{ s}^{-1}$  (circles) and  $25 \text{ s}^{-1}$  (squares) for 2 min. The effect of a resting time of 7 min followed by again a pre-shear treatment at  $5 \text{ s}^{-1}$  (triangles up) and  $25 \text{ s}^{-1}$  (triangles down) for 2 min is also displayed. The flow curves for increasing (up sweep) and decreasing (down sweep) shear rates (each applied for 10 s) are denoted with closed and open symbols respectively.

We also observed fluctuations in normal stress during transient measurements of 30% Ca-caseinate, whereas 30% Na-caseinate did not show these strong irregular fluctuations (data not shown). Transient shear stress and normal stress were found to exhibit coupled oscillating behavior in micellar solutions in their non-linear

region<sup>9,29</sup>, which might indicate that a comparable mechanism caused these oscillations in Ca-caseinate.

### 3.2.3 Linear viscoelastic properties

Figure 8 displays the frequency dependency of  $G'$  and  $G''$  of 30% Ca- and Na-caseinate dispersions measured at 50°C. Both dense caseinates show a cross-over of  $G''$  and  $G'$  ( $\tan\delta = 1$ ), which falls in the low frequency range for Ca-caseinate ( $\omega \approx 2 \text{ s}^{-1}$ ) and in the high frequency range for Na-caseinate ( $\omega \approx 200 \text{ s}^{-1}$ ). Therefore, Ca-caseinate behaved mostly as a solid material at 50°C throughout the probed frequency range, which was also reflected by a rather low  $\tan\delta$  value of  $\sim 0.35$ . Na-caseinate is much more frequency dependent compared to Ca-caseinate. The lowest  $\tan\delta$  value that was measured for Na-caseinate was  $\sim 0.67$ . Obviously, Ca-caseinate features stronger physical interactions compared to Na-caseinate due to the presence of divalent calcium ions.<sup>22</sup> In addition, the fact that 30% Ca-caseinate tended to show a plateau in  $G'$  implies that this system is stronger 'entangled' and less transient compared to Na-caseinate.<sup>13</sup>

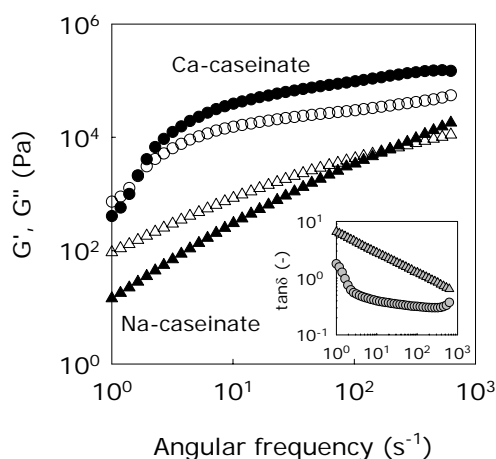


**Figure 8** Mechanical spectra comprising  $G'$  (closed symbols),  $G''$  (open symbols) and  $\tan\delta$  (inserted graph) as function of angular frequency  $\omega$  of 30% Ca-caseinate (circles) and 30% Na-caseinate (triangles) measured at 50°C.



It is noteworthy that the Cox-Mertz rule (i.e.  $\eta(\dot{\gamma}) = \eta^*(\omega)$ )<sup>30</sup> is not valid for Ca-caseinate, whereas Na-caseinate appears to obey this empirical scaling law when considering the absolute viscosity values. In both cases, the slopes of the  $\eta^*-\omega$  curves resemble the slopes of the flow curves obtained with steady shear measurements. In general, the invalidity of the Cox-Mertz rule indicates a more complex behavior, and in this case it confirms the previously discussed rheological behavior of 30% Ca-caseinate.<sup>30,31</sup>

## 4. Discussion

Section 3.1 showed that shearing dense Ca-caseinate and Na-caseinate flow and concurrent enzymatic crosslinking resulted in different macro- and microstructures. We hypothesize that the cause for this difference lays in the fundamental differences of the physical properties of the starting materials. Dense Ca-caseinate dispersions behave as dispersions having strong attractive forces between its building blocks, relative to Na-caseinate dispersions. In other words, the thermodynamic stability of the Ca-caseinate dispersions is lower: in the phase diagram they are probably situated closer to the region of demixing. Therefore, the random concentration fluctuations are much larger than in Na-caseinate dispersions. Shear flow further enhances these concentration fluctuations due to a lowering of the entropy of mixing. These enhanced concentration fluctuations imply the existence of regions with higher and lower viscosity, yielding phase separated bands that become aligned due to the shear flow. The presence of concentration fluctuations is reflected in the rheological behavior of Ca-caseinate, which shows non-monotonic flow behavior. Solidification of the aligned concentration fluctuations using enzymatic crosslinking results in fibrous structures. In contrast, dense Na-caseinate dispersions are more stable (further away from the demixing region in the phase diagram) due to the weaker interactions, and therefore, less affected by shear. Consequently, no structure formation at a micro- and mesoscale can be discerned in Na-caseinate.

To support this hypothesis, we will discuss the following aspects: first, we will provide theoretical considerations for structure formation of Na-caseinate, which are supported by the rheological differences between Ca-caseinate and Na-caseinate due to their different nature (4.1). Then, we will discuss the parallels in

the case of Ca-caseinate that can be drawn with other, often polymeric and micellar, complex fluids under shear flow (4.2).

#### ***4.1 Theoretical process conditions for shear-induced structure formation of Na-caseinate***

Shear can only induce structure in these systems if its effect cannot be compensated by the mobility of the system. Therefore, our hypothesis is that the intrinsic physical properties of Ca-caseinate are such that shear-induced structure formation is favored at the time scales that we investigated. Obviously, Na-caseinate possesses structural elements that are not influenced by shear at the selected time scales. The question that arises is which process conditions are required to lead to shear-induced structure formation in Na-caseinate.

In general, shear flow induces alignment of structural elements towards the shear flow direction when the hydrodynamic forces dominate the Brownian motion. This is expressed by the Péclet number<sup>25</sup>:

$$Pe = \frac{6\pi a^3 \dot{\gamma} \eta}{kT} \gg 1 \quad [1]$$

The radius of the structural elements is denoted with  $a$ ,  $\dot{\gamma}$  is the shear rate,  $\eta$  is the (shear) viscosity of the solutions,  $k$  is Boltzmann's constant and  $T$  is the temperature. The  $Pe$  number summarizes the main parameters (i.e. particle size and shear rate) that are relevant for shear-induced alignment of particles, or in this case micellar proteins. Here, we can apply  $Pe$  as a scaling rule to estimate the shear rate at which Na-caseinate will be influenced by shear flow, by relating it to the shear rate at which alignment takes place in Ca-caseinate:

$$\eta_{Na}(\dot{\gamma}) a_{Na}^3 \dot{\gamma}_{Na} \cong \eta_{Ca}(\dot{\gamma}) a_{Ca}^3 \dot{\gamma}_{Ca} \quad [2]$$

Though the typical domain sizes in dense Ca-caseinate and Na-caseinate are unknown in the experimental window studied, a first estimate can be based on the micelle sizes of Na-caseinate and Ca-caseinate in dilute solutions, leading to the assumption that the size of Na-caseinate micelles  $a_{Na}$  is a factor 5 smaller than the size of Ca-caseinate micelles  $a_{Ca}$  (assuming  $a_{Na} \sim 25$  nm and  $a_{Ca} \sim 125$  nm<sup>19-21</sup>). Further, the shear viscosity of Ca-caseinate was approximately a factor 2 higher compared

to the shear viscosity of Na-caseinate ( $\eta_{Ca} \approx 2 \cdot \eta_{Na}$  at a shear rate of  $\sim 120 \text{ s}^{-1}$ ; see Figure 4). From these estimated values, we find that the shear rate needed to induce alignment in Na-caseinate is approximately a factor  $3 \cdot 10^2$  larger compared to Ca-caseinate. A shear rate in the order of  $10^4 \text{ s}^{-1}$  cannot be applied in the shear cell device.

The analysis discussed above shows that the larger aggregates present in Ca-caseinate are more likely to be influenced by shear flow. However,  $Pe$  does not include all information about the strength of physical bonds yet, although the presence of interactions affects the aggregate size. The difference in interactions between Ca- and Na-caseinate can be derived from the inverse of the angular frequency at which  $G''$  and  $G'$  show a crossover, which is the longest relaxation time  $\tau$ .<sup>32</sup> From Figure 8 we can roughly estimate that  $\tau_{Ca} \approx 100 \cdot \tau_{Na}$ , which confirms that much stronger interactions are present in 30% Ca-caseinate compared to Na-caseinate, most likely caused by the calcium ions.

Subsequently, another criterion for shear-induced alignment is based on the Deborah number ( $De$ ), i.e. the product of the characteristic material time ( $\tau$ ) and the characteristic process time (shear rate), which should exceed the value of 1 ( $\tau\dot{\gamma} \gg 1$ ).<sup>33</sup> When comparing these parameters of Ca- and Na-caseinate dispersions, the following scaling rule follows:

$$\tau_{Na} \dot{\gamma}_{Na} \cong \tau_{Ca} \dot{\gamma}_{Ca} \quad [3]$$

Using the  $De$  number as a scaling rule for Ca- and Na-caseinate, we can also conclude that the shear rate necessary to induce alignment in Na-caseinate is two orders in magnitude ( $10^2$ ) larger compared to the shear rate needed for Ca-caseinate, which is in line with the prediction based on the  $Pe$  number. In addition, the fact that  $De$  yields a slightly lower value for the estimation of the shear rate compared to  $Pe$  suggests that the interactions between the proteins, which result in a system-specific relaxation time  $\tau$  used in  $De$ , are accounted for implicitly in  $Pe$ . Obviously, these interactions also determine the size of the structural elements present in the dispersion. It is noteworthy that it is difficult to define exactly the nature of the interactions as included in these dimensionless numbers, since the effect of interactions in a system is noticeable at various length scales (e.g. micelles, aggregates of micelles or a network of aggregates).

## 4.2 Explaining the effect of shear on Ca-caseinate dispersions

The structure formation that we found for dense Ca-caseinate dispersions seems analogous to the structure formation in polymer (micellar) solutions and colloidal suspensions that is related to flow-induced formation of concentration fluctuations, and the occurrence of phase separation. In this section, we will show that the measured rheological properties and the intrinsic physical properties of Ca-caseinate provide indications that shear-induced concentration fluctuations and phase separation have resulted in the formation of anisotropic structures.

Wormlike micelle solutions, often studied at semi-dilute concentrations, exhibit a non-monotonic flow behavior as a consequence of concentration fluctuations. These solutions can form shear bands perpendicular to the velocity gradient (having a constant stress) or perpendicular to the vorticity direction (having a constant shear rate), which is schematically illustrated in Figure 1.<sup>29,34,35</sup> Based on the theory for the coupling of concentration and flow, it was proposed that shear bands with the former orientation are created in shear thinning solutions whereas bands with the latter orientation are encountered in shear thickening solutions.<sup>36</sup> Besides non-monotonic flow behavior, fluctuations in both shear stress and normal stress were observed in these solutions exhibiting shear-induced concentration fluctuations.<sup>9,29</sup> In the case of a side-chain liquid crystal polymer melt, time periodic shear stress oscillations were attributed to the formation of a long-range ordered structure (i.e. nematic phase).<sup>37</sup>

Shear-induced phase separation can be closely connected to shear-induced concentration fluctuations.<sup>3,10,27</sup> Shear-induced phase separation was coupled to the presence of a second overshoot in both transient stress and normal stress at longer time scales in wormlike micelle solutions.<sup>38,39</sup> High shear rates induced demixing in concentrated temperature-sensitive poly(N-isopropylacrylamide) microgel suspensions, which showed slightly attractive interactions. Shear flow enhanced the concentration fluctuations along the flow direction leading to solvent being squeezed out of the microgel particles until phase separation occurred finally.<sup>40</sup> This behavior was not observed for repulsive interactions or for lower particle concentration, which was attributed to the lack of elasticity and of close packing.<sup>41</sup> Bundle-like ordering in dense latex dispersions due to shear-induced concentration fluctuations also depended on the particle-particle interactions and particle

concentration.<sup>8</sup> Apparently, the occurrence of shear-induced concentration fluctuations and phase separation leading to structure formation depends on the rheological properties (e.g. flow curves and transient (normal) stress behavior) and the physical properties (e.g. interactions) of the polymers or colloids in solution. In addition, the shear-induced phenomena are concentration dependent due to the close relation between density and interactions. The role of viscoelasticity in these systems has not been conclusive yet, and might as well be the result of structure formation.

The investigated Ca-caseinate dispersions exhibited non-monotonic flow behavior in terms of reproducible shear thickening followed by shear thinning, which obviously gives rise to structural changes. Shear thickening prior to shear thinning, observed for dense  $\beta$ -casein suspensions, was related by Panouillé et al.<sup>15</sup> to the presence of an attractive force between the closely packed micelles. In Ca-caseinate dispersions, calcium ions provide strong interactions between proteins.<sup>22</sup> These interactions can lead to gradual protein aggregation, which can be considered as the formation of random concentration fluctuations, and calcium-bridge formation. The absence of a zero-shear viscosity plateau indicates that large aggregates are present in Ca-caseinate dispersions.<sup>41</sup> A similar observation was done for closely packed latex suspensions.<sup>2</sup>

In general, electrostatic interactions and the presence of counter-ions determine the stability of protein dispersions towards phase separation based on their contributions in the free energy.<sup>42</sup> The Derjaguin-Landau-Verweij-Overbeek (DLVO) theory uses electrostatic repulsion and van der Waals attractive interactions to estimate the free energy that is required to bring two particles together.<sup>43</sup> The stability (i.e. against aggregation of the proteins) of caseins decreases with decreasing voluminosity (thus increasing protein concentration), which positively affects the attractive van der Waals interaction. Based on the available water in the investigated 30% Ca-caseinate dispersion, we can estimate a maximum voluminosity of  $2.3 \text{ mL}\cdot\text{g}^{-1}$ . In contrast, casein micelles in milk have a voluminosity of  $3.9 \text{ mL}\cdot\text{g}^{-1}$ .<sup>44</sup> The strong short-range attractive and weak long-range repulsive interactions indicate that dense Ca-caseinate systems are prone to phase separate.<sup>45</sup>

In addition, due to the attractive interactions, dense Ca-caseinate dispersions are presumably close to the spinodal in the phase diagram. In general, the depth of

concentration fluctuations is strongly dependent on the distance to the spinodal and becomes infinitely large on the spinodal.<sup>46</sup> Therefore, a flow-induced shift of the demixing region will affect dense Ca-caseinate dispersions. Consequently, dense Ca-caseinate dispersions may be susceptible for shear-induced phase separation, or at least shear-induced formation of concentration fluctuations.

The susceptibility of Ca-caseinate dispersions towards phase separation will depend on the protein concentration. We observed that a 20% Ca-caseinate dispersion did not show anisotropic structure formation. This may be explained by the fact that this dispersion with lower protein content is further away from the demixing region due to altered interactions as the proteins are less closely packed. One might speculate however that reduction of the stability of the dispersion or the reduction of the solvent quality might result in shear-induced structure formation in these dispersions as well.

Besides layered structures, we found highly fibrous structures for sheared and crosslinked Ca-caseinate (Figure 1). Covalent bonds in Ca-caseinate were mainly created in the direction of the shear flow, therewith inducing discontinuities in the vorticity direction.<sup>1</sup> Besides the decrease in entropy due to the alignment of closely packed proteins (concentration fluctuations), enzymatic crosslinking of casein both increases the size of protein clusters and the rigidity of these clusters, and consequently, phase separation becomes even more favorable.<sup>42</sup> Also, crosslinking decreases the diffusion coefficient of the caseinates as the molecular weight of the protein clusters increases, therewith hindering mobility through the micro-phases formed, which may result in fibers that remain after cessation of the flow. The combined effects of initial alignment of concentration fluctuations due to attractive particle interactions, and the additional creation of covalent bonds on the entropy in the Ca-caseinate system are likely to have resulted in fibrous structures.

## 5. Conclusions

A detailed investigation of the properties of dense Ca- and Na-caseinate dispersions has led to the following conclusions concerning shear-induced structure formation in industrially relevant materials:

1. Fiber formation due to shearing and enzymatic crosslinking is not a generic feature of caseinates yet, as we found isotropic materials for dense Na-caseinate

and highly anisotropic materials for dense Ca-caseinate at similar processing conditions. This study reveals the importance of the counter ion present and the protein concentration for obtaining anisotropic structures, which affect the rheological behavior to a large extent.

2. We think that shear-induced structure formation only occurs if the starting material is susceptible for ordering by shear. Larger micellar structural elements and pronounced attractive interactions in Ca-caseinate compared to Na-caseinate account for the differences found in structure formation.

3. The industrially relevant protein mixtures seem to show similarities with model materials often used to study shear-induced structure formation, such as the types of structures and the rheological behavior. The main similarities observed in the latter behavior were non-monotonic flow behavior, significant normal stresses, and the presence of attractive interactions.

4. Based on our experimental data and insights from literature, we hypothesize that shear-induced concentration fluctuations can lead to anisotropic structure formation in protein systems that are close to the point of demixing. A high protein concentration, strong attractive interactions and shear flow enhance the concentration fluctuations. Fixation of the aligned concentration fluctuations results in a fibrous structure.

## Acknowledgements

The authors wish to thank A. van Aelst from the Wageningen Electron Microscopy Centre for preparing the SEM images, C. Klein for input on the rheological measurements, and M. Paques from Friesland Foods for fruitful discussions.

## References

- (1) Manski, J. M.; Van der Goot, A. J.; Boom, R. **2007**. Formation of fibrous materials from dense calcium caseinate dispersions. *Biomacromolecules*: in press.
- (2) Belzung, B.; Lequeux, F.; Vermant, J.; Mewis, J. **2000**. Flow-induced anisotropy in mixtures of associative polymers and latex particles. *Journal of Colloid and Interface Science* 224 (1): 179-187.

- (3) Wang, S. Q. **1991**. Growth of dynamic polymers (micelles) in shear flow. *Macromolecules* 24 (10): 3004.
- (4) Lyon, M. K.; Mead, D. W.; Elliott, R. E.; Leal, L. G. **2001**. Structure formation in moderately concentrated viscoelastic suspensions in simple shear flow. *Journal of Rheology* 45 (4): 881-890.
- (5) Michele, J.; Patzold, R.; Donis, R. **1977**. Alignment and aggregation effects in suspensions of spheres in non-Newtonian media. *Rheologica Acta* 16: 317-321.
- (6) Scirocco, R.; Vermant, J.; Mewis, J. **2004**. Effect of the viscoelasticity of the suspending fluid on structure formation in suspensions. *Journal of Non-Newtonian Fluid Mechanics* 117 (2-3): 183-192.
- (7) Won, D.; Kim, C. **2004**. Alignment and aggregation of spherical particles in viscoelastic fluid under shear flow. *Journal of Non-Newtonian Fluid Mechanics* 117: 141-146.
- (8) Vermant, J.; Raynaud, L.; Mewis, J.; Ernst, B.; Fuller, G. G. **1999**. Large-scale bundle ordering in sterically stabilized latices. *Journal of Colloid and Interface Science* 211 (2): 221-229.
- (9) Azzouzi, H.; Decruppe, J. P.; Lerouge, S.; Greffier, O. **2005**. Temporal oscillations of the shear stress and scattered light in a shear-banding-shear-thickening micellar solution. *European Physical Journal E* 17 (4): 507-514.
- (10) Fischer, P.; Wheeler, E. K.; Fuller, G. G. **2002**. Shear-banding structure orientated in the vorticity direction observed for equimolar micellar solution. *Rheologica Acta* 41 (1-2): 35-44.
- (11) Lopez-Gonzalez, M. R.; Holmes, W. M.; Callaghan, P. T. **2006**. Rheo-NMR phenomena of wormlike micelles. *Soft Matter* 2 (10): 855-869.
- (12) Schubert, B. A.; Wagner, N. J.; Kaler, E. W.; Raghavan, S. R. **2004**. Shear-induced phase separation in solutions of wormlike micelles. *Langmuir* 20 (9): 3564-3573.
- (13) Farrer, D.; Lips, A. **1999**. On the self-assembly of sodium caseinate. *International Dairy Journal* 9 (3-6): 281-286.
- (14) Panouille, M.; Benyahia, L.; Durand, D.; Nicolai, T. **2005**. Dynamic mechanical properties of suspensions of micellar casein particles. *Journal of Colloid and Interface Science* 287 468-475.
- (15) Panouille, M.; Durand, D.; Nicolai, T. **2005**. Jamming and gelation of dense  $\beta$ -casein micelle suspensions. *Biomacromolecules* 6: 3107-3111.
- (16) Karlsson, A. O.; Ipsen, R.; Schrader, K.; Ardo, Y. **2005**. Relationship between physical properties of casein micelles and rheology of skim milk concentrate. *Journal of Dairy Science* 88 (11): 3784-3797.



- (17) Solanki, G.; Rizvi, S. S. H. **2001**. Physico-chemical properties of skim milk retentates from microfiltration. *Journal of Dairy Science* 84: 2381-2391.
- (18) Velez-Ruiz, J. F.; Barbosa-Canovas, G. V. **2000**. Flow and structural characteristics of concentrated milk. *Journal of Texture Studies* 31 (3): 315-333.
- (19) Lucey, J. A.; Srinivasan, M.; Singh, H.; Munro, P. A. **2000**. Characterization of commercial and experimental sodium caseinates by multiangle laser light scattering and size-exclusion chromatography. *Journal of Agricultural and Food Chemistry* 48 (5): 1610-1616.
- (20) De Kruif, C. G. **1998**. Supra-aggregates of casein micelles as a prelude to coagulation. *Journal of Dairy Science* 81 (11): 3019-3028.
- (21) Dickinson, E.; Semenova, M. G.; Belyakova, L. E.; Antipova, A. S.; Il'in, M. M.; Tsapkina, E. N.; Ritzoulis, C. **2001**. Analysis of light scattering data on the calcium ion sensitivity of caseinate solution thermodynamics: Relationship to emulsion flocculation. *Journal of Colloid and Interface Science* 239 (1): 87-97.
- (22) Aalbersberg, W. Y.; Hamer, R. J.; Jasperse, P.; De Jongh, H. H. J.; De Kruif, C. G.; Walstra, P.; De Wolf, F. A. **2003**. *Industrial proteins in perspective*; 1st ed., Vol. 23, Elsevier Science, Amsterdam.
- (23) Yokoyama, K.; Ohtsuka, T.; Kuraishi, C.; Ono, K.; Kita, Y.; Arakawa, T.; Ejima, D. **2003**. Gelation of food protein induced by recombinant microbial transglutaminase. *Journal of Food Science* 68 (1): 48-51.
- (24) Manski, J. M.; Van der Zalm, E. E. J.; Van der Goot, A. J.; Boom, R. **2007**. Influence of process parameters on formation of fibrous materials from dense caseinate dispersions and fat. *Food Hydrocolloids*: in press.
- (25) Macosko, C. W. **1994**. In *Rheology: Principles, measurements, and applications*; Wiley-VCH, New York: 550.
- (26) Acharya, D. P.; Sharma, S. C.; Rodriguez-Abreu, C.; Aramaki, K. **2006**. Viscoelastic micellar solutions in nonionic fluorinated surfactant systems. *Journal of Physical Chemistry B* 110 (41): 20224-20234.
- (27) Grand, C.; Arrault, J.; Cates, M. E. **1997**. Slow transients and metastability in wormlike micelle rheology. *Journal De Physique II* 7 (8): 1071-1086.
- (28) Menjivar, J. A.; Rha, C. K. **1980**. Viscoelastic effects in concentrated protein dispersions. *Rheologica Acta* 19 (2): 212-219.
- (29) Fischer, P. **2000**. Time dependent flow in equimolar micellar solutions: Transient behaviour of the shear stress and first normal stress difference in shear induced structures coupled with flow instabilities. *Rheologica Acta* 39 (3): 234-240.
- (30) Larson, R. G. **1999**. In *The structure and rheology of complex fluids*; Oxford University Press, New York: 664.

- (31) Ikeda, S.; Nishinari, K. **2000**. Intermolecular forces in bovine serum albumin solutions exhibiting solidlike mechanical behaviors. *Biomacromolecules* 1 (4): 757-763.
- (32) Ponche, A.; Dupuis, D. **2005**. On instabilities and migration phenomena in cone and plate geometry. *Journal of Non-Newtonian Fluid Mechanics* 127 (2-3): 123-129.
- (33) Forster, S.; Konrad, M.; Lindner, P. **2005**. Shear thinning and orientational ordering of wormlike micelles. *Physical Review Letters* 94 (1): 17803-1-4.
- (34) Radulescu, O.; Olmsted, P. D.; Decruppe, J. P.; Lerouge, S.; Berret, J. F.; Porte, G. **2003**. Time scales in shear banding of wormlike micelles. *Europhysics Letters* 62 (2): 230-236.
- (35) Vermant, J. **2001**. Large-scale structures in sheared colloidal dispersions. *Current Opinion in Colloid and Interface Science* 6 (5-6): 489-495.
- (36) Schmitt, V.; Marques, C. M.; Lequeux, F. **1995**. Shear-induced phase-separation of complex fluids - the role of flow-concentration coupling. *Physical Review E* 52 (4): 4009-4015.
- (37) Pujolle-Robic, C.; Noirez, L. **2003**. Identification of nonmonotonic behaviors and stick-slip transition in liquid crystal polymers. *Physical Review E* 68 (6): (061706-)1-5.
- (38) Magda, J. J.; Lee, C. S.; Muller, S. J.; Larson, R. G. **1993**. Rheology, flow instabilities, and shear-induced diffusion in polystyrene solutions. *Macromolecules* 26 (7): 1696-1706.
- (39) Saito, S.; Hashimoto, T. **2001**. Critical conditions for structure formation in semidilute polymer solutions induced under continuous shear flow. *Journal of Chemical Physics* 114 (23): 10531-10543.
- (40) Stieger, M.; Lindner, P.; Richtering, W. **2004**. Small-angle neutron scattering study of shear-induced phase separation in aqueous poly(n-isopropylacrylamide) solutions. *E-Polymers* 046: 1-10.
- (41) Stieger, M.; Richtering, W. **2003**. Shear-induced phase separation in aqueous polymer solutions: Temperature-sensitive microgels and linear polymer chains. *Macromolecules* 36 (23): 8811-8818.
- (42) Semenova, M. G. **2007**. Thermodynamic analysis of the impact of molecular interactions on the functionality of food biopolymers in solution and in colloidal systems. *Food Hydrocolloids* 21 (1): 23-45.
- (43) Walstra, P. **1990**. On the stability of casein micelles. *Journal of Dairy Science* 73 1965-1979.
- (44) Walstra, P. **1979**. Voluminosity of bovine casein micelles and some of its implications. *Journal of Dairy Research* 46 (2): 317-323.

- (45) Stradner, A.; Sedgwick, H.; Cardinaux, F.; Poon, W. C. K.; Egelhaaf, S. U.; Schurtenberger, P. **2004**. Equilibrium cluster formation in concentrated protein solutions and colloids. *Nature* 432 (7016): 492-495.
- (46) Scholte, T. G. **1972**. Light-scattering of concentrated polydisperse polymer-solutions. *Journal of Polymer Science Part C-Polymer Symposium* (39): 281-291.





# 7

## Advances in structure formation of anisotropic protein-rich foods through novel processing concepts

---

This chapter is submitted as: Manski, J.M.; Van der Goot, A.J.; Boom, R.M. 2007. Advances in structure formation of anisotropic protein-rich foods through novel processing concepts.

## **Abstract**

Protein-rich foods are of high interest due to health benefits and sustainability. For obtaining attractive products, technological challenges are posed in optimal structuring of foods containing more than 10% (w/w) protein. Structure formation of anisotropic soft solid foods comprises deformation and solidification. Current processes for producing fibrous protein-rich products, such as extrusion and spinning, seem to have reached a limit in development, due to their complexity in flow patterns. Model studies on simpler polymer systems show that well-defined flow and interactions between structural elements are important for obtaining anisotropic structures. Recently, highly fibrous products were produced from dense protein dispersions using well-defined flow and concurrent enzymatic crosslinking. This seems to be closely related to the phenomena found in the simpler polymer systems, and is probably related to the thermodynamic state of the system combined with well-definiteness of the flow field. This underlines that new steps in structuring can be taken when the design of the equipment will be based on the utilization of the desired structuring mechanism, instead of adapting existing types of equipment.

## **1. Introduction**

Protein-rich foods have recently gained increased interest due to health benefits involved in the consumption of proteins. Foods with high protein content induce fast saturation, which in turn has been shown to reduce people's food intake.<sup>1-3</sup> Consumption of protein-rich foods can also prevent muscle loss.<sup>4</sup> Creating tasteful and palatable protein-rich products using proteins from various sources imposes technological challenges. The implementation of for example proteins derived from plants in novel foods is of high interest.<sup>5</sup> Anisotropic structures are often encountered in protein-rich foods, such as meat and fish. In the case of imitating meat, a key success factor appears to be the formation of an attractive fibrous structure.<sup>6</sup>

In general, controlling the spatial organization of structural elements, such as proteins, using appropriate processing is an important aim of food structuring in order to create products with attractive textures.<sup>7</sup> Due to the nature of the building blocks of foods, structuring at micro- and mesoscale is of high interest.<sup>8</sup> Structure formation of proteins can be divided in a low and a high concentration regime, with a rough transition point around 10% protein where the viscosity increases rapidly due to close packing of the proteins.<sup>9</sup> In the current paper, we will focus on structure formation of protein systems with concentrations exceeding 10%.

Traditionally, processes used in chemical engineering have been adapted for food structuring purposes even though there is a large difference in aims and applications.<sup>7</sup> Equipment in the chemical industry is often focused on effective mixing of ingredients using low energy inputs. Relatively few innovations in *dedicated* food structuring processes have been reported over the last years, in spite of the advantages that can be attained when applying processes that maximize the potential use of ingredients without loosing nutritional quality. To illustrate this, patents for the creation of fibrous protein textures that have been filed or issued since the 1990's mostly cover traditional processes, such as extrusion (e.g.<sup>10-12</sup>). Most industrial processes for food ingredients comprise complex, relatively undefined flow, whereas analytical methods to assess the rheological properties of food ingredients are based on the application of well-defined flow.<sup>13</sup>

Food structure formation comprises a deformation and solidification step of biopolymers.<sup>14</sup> The rate of deformation and solidification should be carefully balanced. Once a material is solidified, additional deformation will damage the structure. But too slow solidification can lead to relaxation and subsequent loss of the structure formed.

In this review, we will elaborate on future possibilities for dedicated structuring processes of anisotropic protein-rich foods. A framework for food structuring based on solidification and deformation of biopolymers will be applied to analyze current food structuring processes. Parallels between structure formation of food ingredients and structure formation of polymeric materials are presented, which may co-direct future developments in food structuring. We conclude that innovation of novel foods will benefit tremendously from the use of more dedicated structuring processes that are tailor-made to benefit from food ingredient properties. In addition, well-defined structuring processes will allow a more scientific approach related to the physical properties of ingredients to structures formed.

## **2. Traditional processes for fibrous protein-rich foods**

Extrusion and spinning are traditional processes to create anisotropic protein-rich foods such as meat and sea-food analogs from proteins of both animal and non-animal sources. In this section, we give a brief overview of recent developments.

### **2.1 Extrusion**

Extrusion is a thermo-mechanical process that has been applied for almost 70 years to produce low-moisture products, such as pasta, snacks, and breakfast cereals.<sup>15</sup> Since 1975, extrusion has been used to texturize plant proteins, often leading to porous protein products, which after rehydration resembled meat-like structures.<sup>16</sup> Subsequently, protein extrusion evolved to high-moisture conditions, often exceeding 40%, which has led to the development of new extruder designs.<sup>17</sup>

Texturization of plant proteins comprises protein denaturation at relatively high temperatures (100-200°C), high pressures (17-60 atm) and moderate mechanical shear rates (120-180 s<sup>-1</sup>) in order to obtain a molten mass that can be deformed.<sup>6,18</sup> In



contrast to synthetic polymers, both reversible and non-reversible reactions occur in protein systems, which have large implications on the functional properties of the resulting products.<sup>18</sup> After a typical residence time of several minutes in the extruder, the molten protein mass is pushed through a cooling die to obtain protein alignment.<sup>6,18,19</sup> Solidification results from cooling, non-covalent interactions and additional disulphide bond formation.<sup>18-20</sup>

Table 1 provides an overview of various ingredients, mostly mixtures of proteins and polysaccharides, and extrusion conditions that have been applied to texturize products. The formation of fibrous structures during extrusion has frequently been attributed to the deformation of these intrinsically phase separated systems, which are water-in-water emulsions that can form aligned structures.<sup>14</sup> Based on various products, ranging from extruded defatted soy flour<sup>21</sup>, a salmon fish-soy protein blend<sup>19</sup> and a zein protein-wheat starch mixture<sup>22</sup>, we can deduce that elongated domains or fiber-like structures were found in the order of 0.1-100 micrometers in thickness (Table 1). No evidence of molecular orientation was found in extruded soy protein isolate and maltodextrin products.<sup>23</sup> Cheftel<sup>19</sup> found that extrusion of soy protein with high protein purity did not result in a fibrous texture. It is argued that at the high temperatures used during extrusion, only a homogeneous phase can exist, even when proteins and polysaccharides are present<sup>20</sup>, therewith explaining the formation of structures that were not very fibrous. Table 1 shows that not all extruded products are assessed on their microstructural properties with microscopic techniques or on their degree of fibrousness using mechanical tests.

Besides the production of meat analogs, extrusion (80-120°C) has been applied to blend and emulsify dairy ingredients for the production of cheese analogs<sup>19,24</sup> and for the production of microparticles, which can be used as fat substitutes.<sup>25,26</sup> In general, homogeneous gelled materials were obtained as shown in Table 1. Fibrousness in a dairy protein-fat system is only reported for Mozzarella cheese, which is produced by a cooking and stretching process.<sup>27</sup> The fibrousness is caused by the presence of protein strands in the order of ~10 micrometers<sup>28</sup>, which are separated by fat globules.<sup>29</sup>

Overall, it seems that most studies concerning the effect of process parameters on the structure formation of protein-rich extrudates are rather empirical. Often ingredient composition, moisture content, screw speed and temperature along the extruder barrel are varied (Table 1), therewith making comparisons between

processes and products complicated, let alone providing insight in structure formation mechanisms. The concept of solidification and deformation explains the limitations of extrusion to produce fibrous products. Due to sequential locally high and low shear rates in the extruder barrel, random re-orientation of the proteins takes place, undoing any orientation and yielding an isotropic material. The fact that a certain degree of alignment is achieved in the cooling die can be attributed to the better defined flow in the die (i.e. laminar flow), and often the presence of a phase separated system.

## 2.2 Spinning

Spinning is another technique employed to induce alignment in biopolymer solutions based on deformation and solidification. Similarly to extrusion, alignment during spinning is promoted by the use of intrinsically phase separated systems.<sup>14, 30</sup> While pushing the viscous biopolymer solution through a spinneret, the water-in-water emulsion is aligned, and the resulting fibers are stretched.<sup>31</sup> Solidification is achieved using coagulation agents, such as salts, acid or alkali solutions or non-food grade glutaraldehyde or formaldehyde. After coagulation, the spun fibers are washed. The resulting fibers have a thickness in the order of the size of the spinneret holes, usually hundreds of micrometers.<sup>14,31</sup> Non-spinneret spinning has also been applied to produce protein fibers. In this case, the biopolymer solution is extruded through shaping nozzles, resulting in many fibers per nozzle.<sup>14</sup>

Various milk proteins, plant proteins and polysaccharides have been used for spinning, which is summarized in Table 1. The use of protein-polysaccharide mixtures was found to reduce the water-solubility of the produced fibres.<sup>32-34</sup> Spun pea protein fibers were reported to have an aligned cortex and a granular core.<sup>31</sup> Similarly to extrusion, no evidence of molecular orientation was found after spinning of soy protein isolate.<sup>35</sup>

The use of spinning as a process to produce food fibers involves disadvantages, such as generating large waste streams from the coagulation and washing baths, the use of chemical coagulants and the difficulty of assembling single fibers into a food product on an industrial scale. The fact that research on spinning for food

applications has been scarce since 1999 probably indicates that the drawbacks of the process may outweigh the benefits.

### ***2.3 Need for new approach for food structuring processes***

The previous sections indicate that developments in extrusion and spinning in the past have been spectacular. But, it seems that the extreme complexity of the conditions during processing hinders further developments. We think that advances can be attained by increased control over flow patterns in structuring processes.

With respect to deformation, both shear flow and elongational flow are applied in the traditional protein structuring processes, therewith inducing a high level of complexity. Focusing on one type of deformation would help in acquiring knowledge about the fundamentals of these processing steps in relation to the formation of anisotropic foods. Subsequent (re-)design of dedicated equipment for structuring based on this knowledge then can lead to a next step in structuring of concentrated protein foods. In addition, the trend towards product diversity will probably induce a new interest for batch processes. Deformation applied in a batch process offers the advantage of uncoupling flow (shear) rate and process time, which may prove more useful for food structuring.

The fact that protein foods are just one (albeit very complex) type of polymeric solution leads to the insight that studies into simpler solutions of for example synthetic polymers may indicate a direction for development into new structuring processes. Formation of anisotropic structures is often encountered in polymeric systems, ranging from polymer melts to liquid crystals. Relevant parameters for structure formation as well as tools to study structure formation can be deduced from these model studies. The following section will focus on these aspects.

**Table 1** Examples of traditional food structuring processes (i.e. extrusion, spinning, mixing) and a novel process based on well-defined flow for the formation of protein-rich foods comprising high moisture contents (> 40% in most cases). The main ingredients, the obtained structural properties in the products, and the methods to assess the structures are listed. The following abbreviations are used: F, fibrous structures; I, isotropic structures; SPI, soy protein isolate; SPC, soy protein concentrate; WPI, whey protein isolate; WPC, whey protein concentrate.

Main ingredients	Structures
<b>EXTRUSION</b>	
Soy flour <sup>21</sup>	F (protein filaments of 10-50 µm) <sup>a,b</sup>
SPI, maltodextrin <sup>23</sup>	F (no molecular orientation) <sup>a,c,d</sup>
SPI, SPC <sup>19</sup>	F, I (only for SPI, SPC yielded isotropic structures) <sup>e</sup>
SPC, fish surimi <sup>36</sup>	F (enhanced when screw speed ↑) <sup>b</sup>
SPI, wheat starch <sup>37</sup>	F (no molecular orientation, enhanced when water content ↓) <sup>a,f</sup>
SPI, wheat gluten, wheat starch <sup>38</sup>	F (correlation fibrousness and polarization spectroscopy data) <sup>e,g,h</sup>
Soy flour, lean pork <sup>39</sup>	F <sup>e,i</sup>
Wheat gluten <sup>19</sup>	F (continuous or shredded product depending on temperature) <sup>e</sup>
Zein protein, corn starch <sup>22</sup>	F, I (fibrils in order of few 100 nm, but at low specific mechanical energy aggregates) <sup>j</sup>
Calcium caseinate, butter oil <sup>19</sup>	I <sup>e</sup>
WPI, WPC, whey albumin <sup>26</sup>	I (texturized, new functionality, closely packed protein particles in the order of nm) <sup>i,j,k,l,n</sup>

<b>MIXING</b>	
Mozzarella cheese (commercial) <sup>40,28</sup>	<b>F</b> (protein strands of several $\mu\text{m}$ in thickness) <sup>b</sup>
<b>SPINNING</b>	
Casein, alginate <sup>32</sup>	<b>F</b> (water-in-water emulsion, droplets of 20-30 $\mu\text{m}$ prior to spinning; monofibers filled with many thinner fibers (2-5 $\mu\text{m}$ )) <sup>n</sup>
Casein, SPI <sup>41</sup>	<b>F</b> <sup>f</sup>
Pea protein; fababean protein <sup>31</sup>	<b>F</b> (fibers ~ 50-70 $\mu\text{m}$ thick, stranded cortex, granular inner structure) <sup>ab,ij</sup>
SPI <sup>35</sup>	<b>I</b> (no molecular orientation in spun film) <sup>b,c</sup>
Non-food: SPI, glycerol <sup>42</sup>	<b>F</b> (stretching and solidification improved fiber strength) <sup>b</sup>
Soybean protein, polyvinyl-alcohol <sup>43</sup>	<b>F</b> (crystallinity depended on PVA content) <sup>b,f,d</sup>
<b>WELL-DEFINED FLOW</b>	
Calcium caseinate, palm fat <sup>44, 45</sup>	<b>F</b> (orientation on macro- and microscale, fibers of 100-200 nm in thickness) <sup>b,e,f,n</sup>
Sodium caseinate, palm fat <sup>46</sup>	<b>I</b> (homogeneous dispersed fat-in-protein structures) <sup>b,e,f,o</sup>

<sup>a</sup> Optical (light) microscopy. <sup>b</sup> Mechanical (tensile) tests; tensile strength ratio is the ratio of the tensile strengths measured parallel and perpendicular to the fiber direction. <sup>c</sup> IR-spectroscopy. <sup>d</sup> X-ray diffraction. <sup>e</sup> Visual observations. <sup>f</sup> Scanning electron microscopy. <sup>g</sup> Fluorescence polarization spectroscopy. <sup>h</sup> High resolution imaging. <sup>i</sup> Mechanical (cutting) tests. <sup>j</sup> Transmission electron microscopy. <sup>k</sup> Mechanical (compression) tests. <sup>l</sup> Functionality tests. <sup>m</sup> Laser diffraction. <sup>n</sup> Solubility tests. <sup>o</sup> Confocal scanning laser microscopy (CSLM).

**Table 2** Selection of various model systems where anisotropic structure formation was observed using well-defined shear flow (in rheometers), including the key phenomena for the structure formation. Vorticity and velocity gradient directions are denoted with  $\omega$  and  $\nabla$  respectively.

Model system	Structures	General remarks about phenomena
<b>WORMLIKE MICELLE SOLUTIONS</b>		
Cetylpyridinium chloride and sodium salicylate (CPyCl-NaSal) <sup>47, 48,49,50,51</sup>	Shear bands <sup>a,b,c,d</sup>	<ul style="list-style-type: none"> <li>- Semi-dilute concentrations</li> <li>- Non-monotonic stress-shear rate curves</li> <li>- Flow instabilities</li> <li>- Usually 2-3 bands, perpendicular to <math>\nabla</math> or <math>\omega</math></li> </ul>
Cetyltrimethylammonium bromide (CTAB) and NaSal or KBr <sup>52, 53</sup>	Shear bands <sup>a,c,e,f</sup>	<ul style="list-style-type: none"> <li>- Oscillations in stress and normal stress</li> <li>- Shear-induced concentration fluctuations</li> <li>- Phase separation (accompanied by turbidity)</li> <li>- Shear thinning, shear thickening</li> </ul>
<b>POLYMER SOLUTIONS</b>		
Polystyrene/diethyl malonate solution <sup>54</sup>	Elongated structures in flow direction ( $\perp \nabla$ ) <sup>b,c</sup>	
High molecular weight ( $M_w$ ) deuterated polystyrene in dioctyl phthalate <sup>55</sup>	Structures ( $\perp \nabla$ ) <sup>a,b,g</sup>	<ul style="list-style-type: none"> <li>- Semi-dilute concentrations</li> <li>- Spinodal decomposition and demixing</li> <li>- Shear-induced concentration fluctuations</li> </ul>
Aqueous solutions of linear poly(N-isopropylacrylamide) and PNIPAM microgel particles <sup>56, 57</sup>	Lamellar structures (closely packed), demixing <sup>a,e,g,i</sup>	<ul style="list-style-type: none"> <li>- Butterfly and streak patterns in SALS/SANS</li> <li>- Shear thinning</li> <li>- Structures disappear after cessation flow</li> </ul>
Ultrahigh $M_w$ polyethylene in paraffin wax as solvent <sup>58, 59</sup>	Optically anisotropic fibrils in flow direction <sup>a,b,c,e</sup>	

<b>COLLOIDAL SUSPENSIONS</b>	
Polystyrene latex dispersions, charge stabilized by sulfate surface groups (92, 120, 143 nm) <sup>60</sup>	Layers (hexagonal) <sup>g</sup>
Two aqueous poly(butylacrylate-styrene) lattices (average diameter 127, 254 nm) <sup>61</sup>	Bundle-like structures in flow direction <sup>a,b,e</sup>
Poly(butylacrylate-styrene) latex particles (83 nm) and two telechelic polymers based on polyacrylamide and polyacrylic acid <sup>62</sup>	Aligned particles in flow direction and in $\omega$ direction <sup>a,b</sup>
	<ul style="list-style-type: none"> <li>- Dense colloidal dispersions</li> <li>- Structures depend on particle concentration</li> <li>- Structures disappear after cessation flow</li> <li>- Long-range interactions favor bundle formation</li> <li>- Shear thinning (alignment in flow direction)</li> <li>- Shear-induced concentration fluctuations</li> <li>- Interactions (particle, depletion) important</li> </ul>
<b>MACROSCOPIC PARTICLE SUSPENSIONS</b>	
Polyacrylamide solution in water-glycerol; polymethyl-methacrylate (PMMA) spheres (126-150 and 53-63 $\mu\text{m}$ ) <sup>63</sup>	String formation in flow direction <sup>a,c</sup>
Glycerin, ethylene glycol, polyacrylamide; xanthan-sucrose solutions ; PMMA spheres (300-355 $\mu\text{m}$ ) <sup>64</sup>	String formation in flow direction <sup>a,c</sup>
Polyisobutylene (PIB) in polybutene; PIB in decalin; hydroxypropylcellulose and carboxymethylcellulose sodium salt; polystyrene spheres (2.7 $\mu\text{m}$ ) <sup>65</sup>	String formation in flow direction <sup>a,b,c</sup>
	<ul style="list-style-type: none"> <li>- Coarser strings when particle concentration <math>\uparrow</math></li> <li>- Shear thinning essential</li> <li>- <math>Wi</math> not only determining for particle string formation (no criterion possible)</li> <li>- Bulk phenomenon</li> </ul>

POLYMER EMULSIONS		
Polybutadiene, polystyrene in dioctylphthalate as solvent <sup>66</sup>	Emulsion strings in flow direction <sup>b,c</sup>	
Aqueous gelatin-dextran blends in sucrose solution <sup>67</sup>	Emulsion strings in flow direction <sup>a,c</sup>	- Spinodal decomposition - Filament thickness depends on phase volumes used, which in turn depends on the viscosity ratio between the two solutions - Phase transition at critical shear rate - Viscoelasticity (influenced through $M_w$ ) plays role in orientation in $\omega$ direction
Polydimethylsiloxane (minor component) and polyisobutylene <sup>68</sup>	Emulsion strings in flow direction <sup>c</sup>	
Polystyrene and polyethylene <sup>69</sup>	Emulsion strings in flow direction ( $140 \text{ s}^{-1}$ ); elongated droplets in $\omega$ direction ( $455 \text{ s}^{-1}$ ) <sup>a,c</sup>	
Water dispersed in lubricant oil with sorbitan monooleate <sup>70</sup>	Aligned cylindrical aggregates in $\omega$ direction <sup>a,c</sup>	

<sup>a</sup> Rheology. <sup>b</sup> Small-angle light scattering (SALS) under flow. <sup>c</sup> Light microscopy or video imaging under flow. <sup>d</sup> Nuclear magnetic resonance (NMR spectroscopy) and NMR velocimetry. <sup>e</sup> Birefringence, dichroism under flow. <sup>f</sup> Light scattering. <sup>g</sup> Small-angle neutron scattering (SANS) under flow. <sup>h</sup> Small-angle X-ray scattering (SAXS) under flow. <sup>i</sup> Static light scattering (SLS).



### **3. Structure formation in polymer model systems**

In contrast to the processes described in the previous section, structure formation of complex polymeric fluids has been studied extensively with respect to deformation, usually under well-defined flow conditions using rheometers. Flow-induced structures encountered in complex fluids are often anisotropic in nature, although these are not fixed. We will focus on the flow-induced formation of anisotropic (i.e. lamellar and bundle-like) structures in various systems, which have the common features that they are phase separated on a microscopic or macroscopic scale, and that they comprise structural elements that can be affected by flow. The relevance of the phenomena involved for structure formation of anisotropic protein-rich foods in terms of process conditions and mechanistic insight will be highlighted.

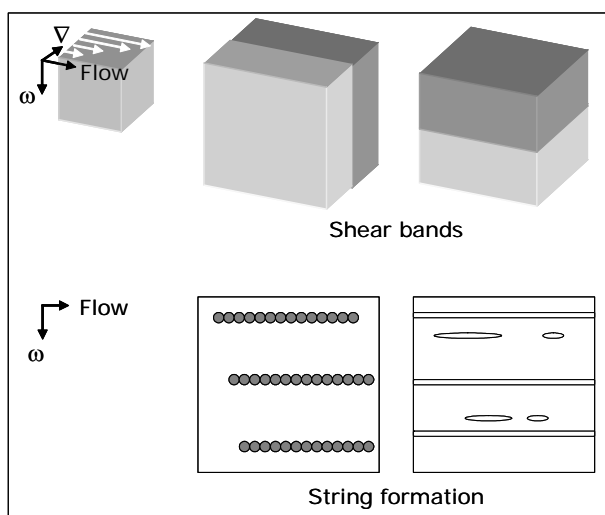
#### **3.1 Anisotropic structures**

Table 2 provides examples of wormlike micelle solutions, polymers solutions, colloidal and non-colloidal suspensions where anisotropic structures as a result of shearing have been observed.

Lamellar structures with different viscosities, so-called shear bands, are encountered in semi-dilute wormlike micelle solutions that show a non-monotonic flow behavior (i.e. shear stress as function of shear rate<sup>71</sup>). Depending on the flow behavior of the solutions, i.e. shear thinning or shear thickening, shear bands can be formed perpendicular to the velocity gradient or perpendicular to the vorticity direction respectively, which is depicted in Figure 1.<sup>47,72,73</sup> The formation of shear bands, of which usually a few are formed, is attributed to the coupling between fluctuating concentrations in the sheared solution and generated stresses, also referred to as shear-induced concentration fluctuations.<sup>62,74</sup>

Various concentrated systems with shear thinning flow behavior form closely packed lamellar structures during shearing, such as polycrystalline cubic crystals<sup>75</sup> and electrostatically stabilized dense colloids<sup>60,76</sup> (Table 2). The formation of sliding lamellar structures was proposed to be a generic feature of colloidal dispersions independent of the internal particle structure.<sup>56</sup>

Shear flow affects phase transitions in near-critical solutions, which can lead to changes in structure.<sup>77,78</sup> Phase separation induced by shear flow, for example through spinodal decomposition, is closely related to concentration fluctuations.<sup>48,79,80</sup> Therefore, susceptibility to shear-induced phase separation depends on the thermodynamic state of the solutions. Attractive interactions in microgels of dense polymer particles lead to demixing as a result of shear-induced concentration fluctuations whereas repulsive interactions yield closely packed lamellar structures.<sup>56</sup>



**Figure 1** Schematic overview of shear-induced phenomena in complex polymeric fluids: shear bands due to shear-induced concentration fluctuations in for example wormlike micelle solutions, and so-called string formation in macroscopic particle suspensions (i.e. chaining of particles) and emulsions (i.e. elongation of emulsion droplets). The flow, vorticity and velocity gradient directions are denoted with 'Flow', ' $\omega$ ' and ' $\nabla$ ' respectively.

The formation of bundle-like structures in dense latex suspensions oriented in the flow direction depended on the presence of long-range interactions and on the particle concentration.<sup>61</sup> Weakly aggregating colloidal particles formed banded structures in the vorticity direction rather than in the flow direction.<sup>62,81</sup> Ordering of colloidal aggregates in the vorticity direction increased with increasing shear rate and particle concentration.<sup>81</sup> The structures formed were also related to shear-induced concentration fluctuations.

On a macroscopic scale, alignment of solid particles and emulsion droplets was obtained in viscoelastic solutions. So-called string formation of solid particles was accompanied by the presence of normal stresses in the viscoelastic suspensions, expressed as the Weissenberg number ( $Wi$ ), and shear thinning.<sup>63,64,82</sup> However, the effect of viscoelasticity (through  $Wi$ ) on aligning particles could not be proven, which led to the conclusion that string formation is mainly a hydrodynamically driven phenomenon.<sup>65</sup>

Bi-continuous string formation oriented in the flow direction has been observed in various two-phase systems (Table 2). A polymer blend showed string formation under strong shear flow, which was related to spinodal decomposition of the system.<sup>66</sup> A biopolymer mixture of gelatin and dextran also exhibit similar anisotropic structures, which were stable under steady shear flow.<sup>67</sup> The string formation depended on the viscosity ratio, shear rate and phase volumes used. Well-defined deformation and simultaneous solidification through cooling of a dilute polysaccharide mixture of gellan and  $\kappa$ -carrageenan also yielded elongated structures.<sup>83</sup> Confinement accounted for a transition of droplets into strings for concentrated polymer blends.<sup>68</sup>

Emulsion droplets in polymer blends were reported to form structures in the vorticity direction at high shear rates ( $> 450 \text{ s}^{-1}$ ), which was explained by the viscoelasticity of the phases involved.<sup>69</sup> A shear thinning emulsion with attractive interactions formed cylindrical aggregates in the vorticity direction, which was accompanied by negative normal stresses.<sup>70</sup>

### ***3.2 Factors relevant for anisotropic structure formation***

In all studies, the thermodynamic and rheological properties of the systems were important for obtaining anisotropic shear-induced structures. The investigated systems were either close to the point of phase separation or intrinsically phase separated.

In case of wormlike micelles, the time scale of the formation and breakage of entanglements, therewith influencing the micellar length, is important for structure formation under shear.<sup>84,85</sup> For colloidal suspensions, long-range electrostatic interactions and short-range van der Waals interactions<sup>61</sup>, or depletion interactions in the presence of a polymer<sup>62</sup> can affect structure formation. Therefore,

interactions between the structural elements in the model systems cause structure formation. These interactions are affected by the concentration used, the presence of ions, or other components that can induce interactions, and temperature.

The role of viscoelasticity during structure formation is not clear yet. Many shear-induced structural changes are accompanied by the presence of normal stresses (Table 2). However, it may as well be a result of ordering of structural elements, suggesting that cause and result are not clear in the various systems.

#### **4. Structure formation of protein-rich systems using well-defined flow**

In the light of the studies concerning polymer model systems, it seems logical to start with the fundamental mechanisms of structure formation identified in the previous sections, and from this, define conditions that lead to the same type of structure formation in concentrated protein foods. This first necessitates the discussion of the influence of well-defined flow on structuring in protein-rich foods.

##### ***4.1 Fibrous protein-rich structures formed using well-defined flow***

Figure 2 illustrates the type of structures that were obtained after shearing solely dense calcium caseinate dispersions (30% w/w), and a two-phase system comprising the same protein and palm fat (13% w/w) in a shear cell device, which was developed based on a rheometer concept.<sup>44,86</sup> Shear flow was essential to align the dense calcium caseinate dispersions into macroscopic layers. Simultaneous shearing and crosslinking using the enzyme transglutaminase of calcium caseinate was required to obtain fibers (~100-200 nm) in both the one- and two-phase system.<sup>44,45</sup> The degree of fibrousness in the products was high, based on the ratio of the yield stresses measured parallel and perpendicular to the fiber direction, which varied between 8 and 14 depending on process conditions and composition. The layered calcium caseinate product resulted in a yield stress ratio of 2.

Shear rate was found to be an important process parameter to control both the formation of fibrous structures and the degree of anisotropy. Based on the process

parameters involved, we concluded that the crosslinking rate and shear rate should be balanced to successfully obtain fibrous products.<sup>45</sup>

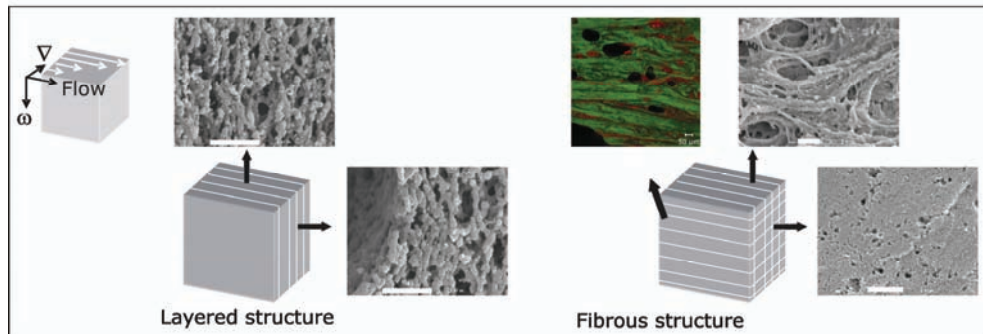


**Figure 2** Microstructures (scanning electron microscopy (SEM) images), mesostructures (confocal scanning laser microscopy (CSLM) images) and schematic representations of dense (30%) calcium caseinate materials after shearing. Layered structures were formed in the absence of the crosslinking enzyme transglutaminase. The SEM images of this structure show subtle orientation of the protein phase. Fibrous structures were formed in the presence of transglutaminase. The SEM images show fibers in the plane parallel to flow, and isotropic structure in the plane perpendicular to the flow. The CSLM image depicts a multi-layered structure of protein and fat at a mesoscale. The formation of both structures is described in detail elsewhere.<sup>44,45</sup> The scale bars in the SEM images denote 1  $\mu\text{m}$  and the width of the CSLM image is  $\sim 0.9$  mm. The flow, vorticity and velocity gradient directions are denoted with 'Flow', ' $\omega$ ' and ' $\nabla$ ' respectively.

#### 4.2 Structure formation is a mutual effort of protein properties and processing

Recent research showed that the formation of the fibrous protein-rich structures using well-defined flow and enzymatic crosslinking is dependent on the precise properties of the system and does not occur in any system. After processing dense sodium caseinate dispersions (30% w/w) at similar process conditions as calcium caseinate, isotropic materials without any observable orientation at macro- or microscale were obtained.<sup>46</sup>

The different behavior of calcium caseinate and sodium caseinate under shear flow could be related to the difference in structural elements present. The dimensionless

numbers Péclet ( $\frac{6\pi a^3 \dot{\gamma} \eta}{kT}$ ;  $a$ , particle radius;  $\dot{\gamma}$ , shear rate;  $\eta$ , viscosity, the solutions;  $k$ , Boltzmann's constant;  $T$ , temperature) and Deborah ( $\tau \dot{\gamma}$ ;  $\tau$ , relaxation time) indicate that the presence of structural elements with a certain size or relaxation time is essential for shear-induced ordering.<sup>87</sup> Calcium caseinate dispersions comprised both larger protein aggregates (100-300 nm<sup>88,89</sup>) and stronger attractive interactions due to the presence of calcium ions compared to sodium caseinate (20-50 nm<sup>90</sup>), therewith favoring shear-induced ordering.

Structure formation induced by shear flow was proposed to be a generic property of near-critical and phase separated systems.<sup>77,91</sup> We rationalized that the closely packed calcium caseinate system with strong attractive interactions was thermodynamically close to instability, resulting in shear-induced micro phase separation in protein-rich and protein-poor phases, which led to layer formation. In addition, the rheological behavior of dense calcium caseinate was non-monotonic and shear-thinning, in contrast to sodium caseinate, and resembled the rheological behavior of polymer model systems that exhibited shear-induced concentration fluctuations. Presumably, in the presence of the crosslinking enzyme, fixation of the shear-induced structures can occur, resulting in a fibrous structure.

Decreasing the calcium caseinate concentration from 30% to 20% did not result in the formation of an anisotropic structure after shearing and crosslinking.<sup>46</sup> Obviously, a lower protein concentration results in a less closely packed dispersion, therewith affecting the interactions and the thermodynamics of the system, and in turn the susceptibility to shear-induced structure formation. This illustrates the subtlety in finding the correct combination of formulation and process conditions.

### ***4.3 Effect of well-defined flow on protein molecules***

The physical properties of proteins determine to a large extent the structure obtained using well-defined flow. In high shear processes, such as extrusion or mixing, proteins can be altered as a result of breakage or crosslinking<sup>18,20</sup>, though it must be noted that these processes are often performed at high temperatures. Nevertheless, it is valid to raise the question to what extent shear flow can affect

proteins. Systematic studies concerning the effect of shear rate and shear stress on concentrated protein systems are scarce. A few studies have been conducted to study molecular changes of proteins in dilute and viscous media using various shear devices. Small globular proteins (< 40 kDa) in dilute water solutions were not affected by shear rates up to  $10^5 \text{ s}^{-1}$ .<sup>92,93</sup> In contrast, the shear stresses applied during shearing of the enzyme  $\alpha$ -amylase (48 kDa) in viscous starch dispersions were thought to reduce the thermo-stability of the enzyme. Inactivation of  $\alpha$ -amylase was reported to occur only at very high shear stresses exceeding 50 kPa.<sup>94</sup>

Glutenin macropeptide aggregates, which are an important fraction of the protein gluten, were shown to stay intact during shearing of wheat dough, while the aggregates do break up during conventional mixing. At similar levels of specific mechanical energy (SME), which is typically used in mixing processes to determine the energy input per kilogram material, shearing (<  $50 \text{ s}^{-1}$ ) appeared a much milder processes compared to mixing of various types of wheat dough.<sup>95,96</sup> In addition, the maximum shear stress (time-independent) occurring during shearing of low-moisture starch appeared to determine the breakage of starch molecules rather than the energy input (time-dependent) during shearing.<sup>97,98</sup>

Concluding, the physical properties of proteins are not expected to alter in well-defined flow due to their small molecular size. Therefore, the use of well-defined flow at moderate temperatures can preserve protein functionality, which is in contrast with the effect of a thermo-mechanical treatment such as extrusion.

#### ***4.4 Challenges for research on structure formation in protein-rich systems***

Creation of novel protein structures requires in-depth knowledge of protein interactions (thermodynamic state) and rheological properties in concentrated systems. This imposes challenges to current analytical methods to study these properties and structure formation capabilities of concentrated protein systems, as these methods are often only suited to analyze properties of dilute systems.

Studies on the interactions in dense protein systems are scarce. A few researchers used osmotic measurements and rheology to study concentrated sodium caseinate and bovine serum albumin dispersions, which were regarded as glassy

materials.<sup>99,100</sup> In general, dense protein systems pose limitations to the geometries and shear rates that are accessible with rheometers due to their high viscoelasticity.<sup>87</sup> Improved design of geometries is needed to prevent expulsion of viscoelastic materials at high shear rates.

Small angle light, neutron or x-ray scattering (SALS, SANS or SAXS) have frequently been applied to study polymer model systems under flow (Table 2). These techniques probe structures at various length scales, being 0.2-100  $\mu\text{m}$  using light, 1-100 nm using x-rays and 1-20 nm using neutrons respectively.<sup>101</sup> In dense food systems, length scales of 0.2-100  $\mu\text{m}$  are interesting for probing, which is usually performed using optical techniques. However, light cannot be applied to opaque samples. Therefore, developments are needed with respect to techniques that can probe relevant length scales in food, preferably on-line, as the phenomena tend to be time-dependent. Finally, to investigate structure formation capabilities of highly viscous or viscoelastic materials such as protein-rich dispersions, the development of new structuring equipment needs to be stimulated, including pilot-scale equipment to test the industrial applicability.

## 5. Conclusions and future outlook

Structuring is considered an important activity in food engineering.<sup>102</sup> However, traditional processes to produce fibrous protein-rich products limit innovations in anisotropic structures due to the design of the current equipment. When considering deformation and solidification as key processes in structure formation of soft solid foods, it is clear that we need to start with good fundamental insight in those phenomena and characteristics that lead to the formation of the desired structure. Instead of adapting existing, proven equipment, it is important to take the step to design new equipment solely based on optimally achieving the specific structuring mechanism. In this light, equipment based on well-defined flow, therewith enabling the use of shear rate as design parameter, appears promising. In addition, novel technologies based on mild processing can increase the functionality of ingredients, since the native functionality of the ingredients may be preserved in a better way.

Research and innovation in food structuring will benefit tremendously by matching the use of well-defined flow and specific initial ingredient properties



(Figure 3). The rheological properties and the interactions present in the starting ingredients appear successful tools to estimate the performance of these ingredients during processing. Therefore, research should be devoted to understand the effect of interactions in concentrated protein systems on structure formation capabilities. Parallels between protein systems and polymer model systems are useful to interpret these relations, and therefore, the existence of these parallels should be explored further. Besides experimental insight, the acquired knowledge can be applied in developing numerical models to describe the structure formation of dense protein dispersions as function of interactions, concentration and deformation.

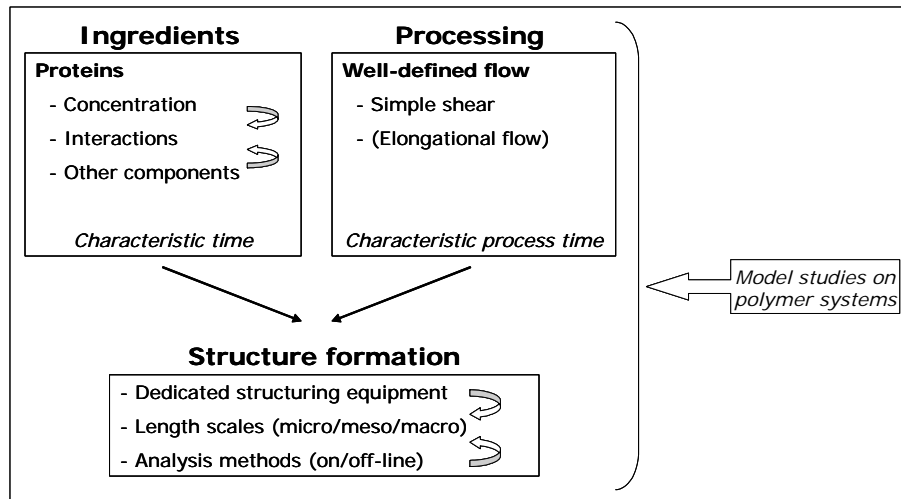


**Figure 3** Schematic overview of interplay between ingredients and processing for structure formation. The concentration and interactions present in protein dispersions determine the characteristic time (e.g. diffusion time, relaxation time) of the starting ingredients. Well-defined flow also has a characteristic process time (e.g. shear rate). To obtain anisotropic structures, both characteristic times should be in balance, which is reflected in the dimensionless numbers Péclet and Deborah. To induce diversity in food structures, developments are needed in structuring equipment and analysis methods to create and analyze structures respectively at the relevant length scales. Insights from model studies may contribute to developments in food structure formation.

Both the increasing interest to implement high concentrations of proteins in novel foods and the relevance of concentrated protein dispersions for shear-induced

structure formation demand a new approach towards investigating protein systems. It is important that in future the thermodynamic and rheological aspects in concentrated protein (food) systems can be better characterized and quantified. This requires developments in analytical techniques. Finally, introducing the concept of well-defined flow in processing can result in highly relevant and valuable scientific insight in structure formation of complex materials like foods, which will stimulate innovations in that area.

## Acknowledgements

The authors wish to thank M. Paques from Friesland Foods for fruitful discussions.

## References

- (1) Antonio, J. **2006**. Body weight and protein. *Strength and Conditioning Journal* 28 (3): 28-29.
- (2) El Khoury, D. T. D.; Obeid, O.; Azar, S. T.; Hwalla, N. **2006**. Variations in postprandial ghrelin status following ingestion of high-carbohydrate, high-fat, and high-protein meals in males. *Annals of Nutrition and Metabolism* 50 (3): 260-269.
- (3) Lee, Y. P.; Mori, T. A.; Sipsas, S.; Barden, A.; Puddey, I. B.; Burke, V.; Hall, R. S.; Hodgson, J. M. **2006**. Lupin-enriched bread increases satiety and reduces energy intake acutely. *American Journal of Clinical Nutrition* 84 (5): 975-980.
- (4) Maughan, R. **2002**. The athlete's diet: Nutritional goals and dietary strategies. *Proceedings of the Nutrition Society* 61 (1): 87-96.
- (5) Linnemann, A. R.; Dijkstra, D. S. **2002**. Toward sustainable production of protein-rich foods: Appraisal of eight crops for Western Europe. Part 1. Analysis of the primary links of the production chain. *Critical Reviews in Food Science and Nutrition* 42 (4): 377-401.
- (6) Aguilera, J. M.; Stanley, D. W. **1993**. The microstructure of food protein assemblies. *Food Reviews International* 9 (4): 527-550.
- (7) Aguilera, J. M. **2005**. Why food microstructure? *Journal of Food Engineering* 67: 3-11.
- (8) Aguilera, J. M. **2006**. Seligman lecture 2005 - food product engineering: Building the right structures. *Journal of the Science of Food and Agriculture* 86 (8): 1147-1155.
- (9) Panouille, M.; Durand, D.; Nicolai, T. **2005**. Jamming and gelation of dense  $\beta$ -casein micelle suspensions. *Biomacromolecules* 6: 3107-3111.

- (10) Brown, D. W.; Yakabu, P. I.; Paulsen, P. V.; Baumer, C. R.; Solorio, S. **2005**. High soy protein nuggets and applications in food products. WO/2005/096834.
- (11) Eastman, J.; Lee, G.; Wochok, Z. S. **2006**. Textured food product. WO/2006/130713.
- (12) Giffard, C. **2004**. Meat analogue of authentic appearance. WO/2004/045301.
- (13) Tabilo-Munizaga, G.; Barbosa-Canovas, G. V. **2005**. Rheology for the food industry. *Journal of Food Engineering* 67 (1-2): 147-156.
- (14) Tolstoguzov, V. B. **1993**. Thermoplastic extrusion - the mechanism of the formation of extrudate structure and properties. *Journal of the American Oil Chemists Society* 70 (4): 417-424.
- (15) Harper, J. M. **1989**. Food extruders and their applications. In *Extrusion cooking*; Mercier, C.; Linko, P.; Harpo, J. M., Eds., American Association of Cereal Chemists: Minnesota: 1-15.
- (16) Campbell, M. F. **1981**. Processing and product characteristics for textured soy flours, concentrates and isolates. *Journal of the American Oil Chemists Society* 58 (3): 336-338.
- (17) Akdogan, H. **1999**. High moisture food extrusion. *International Journal of Food Science and Technology* 34 (3): 195-207.
- (18) Areas, J. A. G. **1992**. Extrusion of food proteins. *Critical Reviews in Food Science and Nutrition* 32 (4): 365-392.
- (19) Cheftel, J. C.; Kitagawa, M.; Queguiner, C. **1992**. New protein texturization processes by extrusion cooking at high moisture levels. *Food Reviews International* 8 (2): 235-275.
- (20) Ledward, D. A.; Tester, R. F. **1994**. Molecular transformations of proteinaceous foods during extrusion processing. *Trends in Food Science and Technology* 5 117-120.
- (21) Noguchi, A. **1989**. Extrusion cooking of high-moisture protein foods. In *Extrusion cooking*; Mercier, C.; Linko, P.; Harpo, J. M., Eds., American Association of Cereal Chemists, Minnesota: 343-370.
- (22) Batterman-Azcona, S. J.; Lawton, J. W.; Hamaker, B. R. **1999**. Microstructural changes in zein proteins during extrusion. *Scanning* 21 (3): 212-216.
- (23) Yuryev, V. P.; Zasytkin, D. V.; Ghenin, Y. V.; Zhukov, V. A.; Alexeyev, V. V.; Tolstoguzov, V. B. **1991**. Role of maltodextrin in promoting structure formation in extruded soya isolate. *Carbohydrate Polymers* 15 (3): 243-253.
- (24) Zuber, F.; Megard, D.; Cheftel, J. C. **1987**. Continuous emulsification and gelation of dairy ingredients by HTST extrusion cooking: Production of processed cheeses. *International Journal of Food Science and Technology* 22 (6): 607-626.
- (25) Cheftel, J. C.; Dumay, E. **1993**. Microcoagulation of proteins for development of creaminess. *Food Reviews International* 9 (4): 473-502.

- (26) Onwulata, C. I.; Konstance, R. P.; Cooke, P. H.; Farrell, H. M. **2003**. Functionality of extrusion - texturized whey proteins. *Journal of Dairy Science* 86 (11): 3775-3782.
- (27) McMahon, D. J.; Paulson, B.; Oberg, C. J. **2005**. Influence of calcium, pH, and moisture on protein matrix structure and functionality in direct-acidified nonfat Mozzarella cheese. *Journal of Dairy Science* 88: 3754-3763.
- (28) O'Reilly, C. E.; Murphy, P. M.; Kelly, A. L.; Guinee, T. P.; Auty, M. A. E.; Beresford, T. P. **2002**. The effect of high pressure treatment on the functional and rheological properties of Mozzarella cheese. *Innovative Food Science and Emerging Technologies* 3: 3-9.
- (29) Paulson, B. M.; McMahon, D. J.; Oberg, C. J. **1998**. Influence of sodium chloride on appearance, functionality, and protein arrangements in nonfat Mozzarella cheese. *Journal of Dairy Science* 81 (8): 2053-2064.
- (30) Ledward, D. A. **1993**. Creating textures from mixed biopolymer systems. *Trends in Food Science and Technology* 4 (12): 402-405.
- (31) Gallant, D. J.; Bouchet, B.; Culioli, J. **1984**. Ultrastructural aspects of spun pea and fababean proteins. *Food Microstructure* 3: 175-183.
- (32) Antonov, Y. A.; Zhuravskaya, N. A.; Tolstoguzov, V. B. **1985**. Solubility of protein fibers obtained from casein solutions and liquid two-phase water-casein-sodium alginate systems. *Die Nahrung* 29 (1): 39.
- (33) Downey, G.; Burgess, K. J. **1979**. Texture studies on edible protein fibers produced by a wet spinning technique. 1. Fibers produced from casein and carrageenan. *Journal of Food Technology* 14 (1): 21-31.
- (34) Downey, G.; Burgess, K. J. **1979**. Texture studies on edible protein fibers produced by a wet spinning technique. 2. Fibers produced from casein and alginate. *Journal of Food Technology* 14 (1): 33-40.
- (35) Rampon, V.; Robert, R.; Nicolas, N.; Dufour, E. **1999**. Protein structure and network orientation in edible films prepared by spinning process. *Journal of Food Science* 64 (2): 313-316.
- (36) Thiebaud, M.; Dumay, E.; Cheftel, J. C. **1996**. Influence of process variables on the characteristics of a high moisture fish soy protein mix texturized by extrusion cooking. *Food Science and Technology-Lebensmittel-Wissenschaft and Technologie* 29 (5-6): 526-535.
- (37) Lin, S.; Huff, H. E.; Hsieh, F. **2002**. Extrusion process parameters, sensory characteristics, and structural properties of a high moisture soy protein meat analog. *Journal of Food Science* 67 (3): 1066-1072.
- (38) Yao, G.; Liu, K. S.; Hsieh, F. **2004**. A new method for characterizing fiber formation in meat analogs during high-moisture extrusion. *Journal of Food Science* 69 (7): E303-E307.

- (39) Liu, S. X.; Peng, M.; Tu, S.; Li, H.; Cai, L.; Yu, X. **2005**. Development of a new meat analog through twin-screw extrusion of defatted soy flour-lean pork blend. *Food Science and Technology International* 11 (6): 463-470.
- (40) Ak, M. M.; Gunasekaran, S. **1997**. Anisotropy in tensile properties of Mozzarella cheese. *Journal of Food Science* 62 (5): 1031-1033.
- (41) Suchkov, V. V.; Grinberg, V. Y.; Bikbov, T. M.; Muschiolik, G.; Schmandke, H.; Tolstoguzov, V. B. **1988**. Non-spinneret formation and functional-properties of fibrous texturates based on a liquid 2-phase system water-casein-soya protein isolate. *Nahrung-Food* 32 (7): 669-678.
- (42) Huang, H. C.; Hammond, E. G.; Reitmeier, C. A.; Myers, D. J. **1995**. Properties of fibers produced from soy protein isolate by extrusion and wet-spinning. *Journal of the American Oil Chemists Society* 72 (12): 1453-1460.
- (43) Zhang, X. F.; Min, B. G.; Kumar, S. **2003**. Solution spinning and characterization of poly(vinyl alcohol)/soybean protein blend fibers. *Journal of Applied Polymer Science* 90 (3): 716-721.
- (44) Manski, J. M.; Van der Goot, A. J.; Boom, R. M. **2007**. Formation of fibrous materials from dense calcium caseinate dispersions. *Biomacromolecules*: in press.
- (45) Manski, J. M.; Van der Zalm, E. E. J.; Van der Goot, A. J.; Boom, R. M. **2007**. Influence of process parameters on formation of fibrous materials from dense caseinate dispersions and fat. *Food Hydrocolloids*: in press.
- (46) Manski, J. M.; Van Riemsdijk, L. E.; Van der Goot, A. J.; Boom, R. M. **2007**. Factors influencing shear-induced anisotropy in dense caseinate dispersions. *Submitted*.
- (47) Fischer, P. **2000**. Time dependent flow in equimolar micellar solutions: Transient behaviour of the shear stress and first normal stress difference in shear induced structures coupled with flow instabilities. *Rheologica Acta* 39 (3): 234-240.
- (48) Fischer, P.; Wheeler, E. K.; Fuller, G. G. **2002**. Shear-banding structure orientated in the vorticity direction observed for equimolar micellar solution. *Rheologica Acta* 41 (1-2): 35-44.
- (49) Mendez-Sanchez, A. F.; Lopez-Gonzalez, M. R.; Rolon-Garrido, V. H.; Perez-Gonzalez, J.; de Vargas, L. **2003**. Instabilities of micellar systems under homogeneous and non-homogeneous flow conditions. *Rheologica Acta* 42 (1-2): 56-63.
- (50) Herle, V.; Fischer, P.; Windhab, E. J. **2005**. Stress driven shear bands and the effect of confinement on their structures - a rheological, flow visualization, and rheo-SALS study. *Langmuir* 21 (20): 9051-9057.
- (51) Lopez-Gonzalez, M. R.; Holmes, W. M.; Callaghan, P. T. **2006**. Rheo-NMR phenomena of wormlike micelles. *Soft Matter* 2 (10): 855-869.

- (52) Azzouzi, H.; Decruppe, J. P.; Lerouge, S.; Greffier, O. **2005**. Temporal oscillations of the shear stress and scattered light in a shear-banding-shear-thickening micellar solution. *European Physical Journal E* 17 (4): 507-514.
- (53) Lerouge, S.; Decruppe, J. P.; Olmsted, P. **2004**. Birefringence banding in a micellar solution or the complexity of heterogeneous flows. *Langmuir* 20 (26): 11355-11365.
- (54) Endoh, M. K.; Takenaka, M.; Hashimoto, T. **2006**. Effects of shear flow on a semidilute polymer solution under phase-separating condition. *Polymer* 47 (20): 7271-7281.
- (55) Saito, S.; Hashimoto, T.; Morfin, I.; Lindner, P.; Boue, F. **2002**. Structures in a semidilute polymer solution induced under steady shear flow as studied by small-angle light and neutron scattering. *Macromolecules* 35 (2): 445-459.
- (56) Stieger, M.; Lindner, P.; Richtering, W. **2004**. Small-angle neutron scattering study of shear-induced phase separation in aqueous poly(n-isopropylacrylamide) solutions. *E-Polymers* 046: 1-10.
- (57) Stieger, M.; Richtering, W. **2003**. Shear-induced phase separation in aqueous polymer solutions: Temperature-sensitive microgels and linear polymer chains. *Macromolecules* 36 (23): 8811-8818.
- (58) Murase, H.; Kume, T.; Hashimoto, T.; Ohta, Y. **2005**. Shear-induced structures in semidilute solution of ultrahigh molecular weight polyethylene at temperature close to equilibrium dissolution temperature. *Macromolecules* 38 (15): 6656-6665.
- (59) Murase, H.; Kume, T.; Hashimoto, T.; Ohta, Y. **2005**. Time evolution of structures under shear-induced phase separation and crystallization in semidilute solution of ultrahigh molecular weight polyethylene. *Macromolecules* 38 (21): 8719-8728.
- (60) Dux, C.; Musa, S.; Reus, V.; Versmold, H.; Schwahn, D.; Lindner, P. **1998**. Small angle neutron scattering experiments from colloidal dispersions at rest and under sheared conditions. *Journal of Chemical Physics* 109 (6): 2556-2561.
- (61) Vermant, J.; Raynaud, L.; Mewis, J.; Ernst, B.; Fuller, G. G. **1999**. Large-scale bundle ordering in sterically stabilized latices. *Journal of Colloid and Interface Science* 211 (2): 221-229.
- (62) Belzung, B.; Lequeux, F.; Vermant, J.; Mewis, J. **2000**. Flow-induced anisotropy in mixtures of associative polymers and latex particles. *Journal of Colloid and Interface Science* 224 (1): 179-187.
- (63) Lyon, M. K.; Mead, D. W.; Elliott, R. E.; Leal, L. G. **2001**. Structure formation in moderately concentrated viscoelastic suspensions in simple shear flow. *Journal of Rheology* 45 (4): 881-890.
- (64) Won, D.; Kim, C. **2004**. Alignment and aggregation of spherical particles in viscoelastic fluid under shear flow. *Journal of Non-Newtonian Fluid Mechanics* 117 141-146.

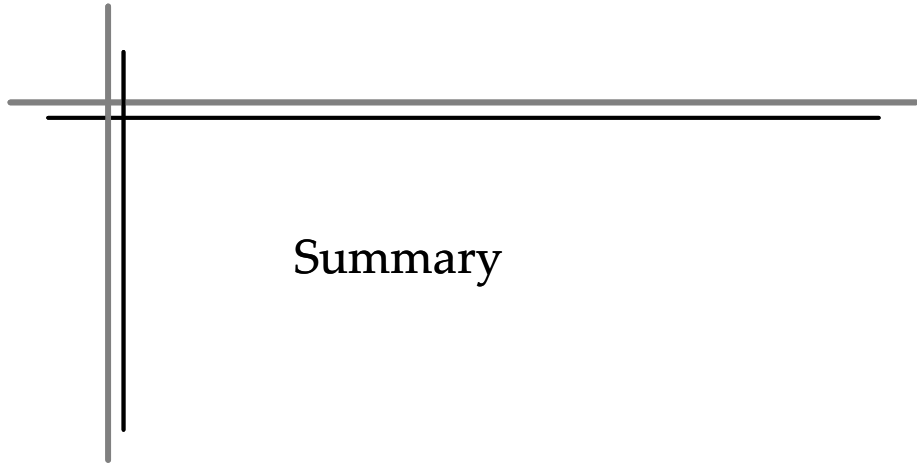
- (65) Scirocco, R.; Vermant, J.; Mewis, J. **2004**. Effect of the viscoelasticity of the suspending fluid on structure formation in suspensions. *Journal of Non-Newtonian Fluid Mechanics* 117 (2-3): 183-192.
- (66) Hashimoto, T.; Matsuzaka, K.; Moses, E.; Onuki, A. **1995**. String phase in phase-separating fluids under shear-flow. *Physical Review Letters* 74 (1): 126-129.
- (67) Wolf, B.; Frith, W. J. **2003**. String phase formation in biopolymer aqueous solution blends. *Journal of Rheology* 47 (5): 1151-1170.
- (68) Migler, K. B. **2001**. String formation in sheared polymer blends: Coalescence, breakup, and finite size effects. *Physical Review Letters* 86 (6): 1023-1026.
- (69) Hobbie, E. K.; Migler, K. B. **1999**. Vorticity elongation in polymeric emulsions. *Physical Review Letters* 82 (26): 5393-5396.
- (70) Montesi, A.; Pena, A. A.; Pasquali, M. **2004**. Vorticity alignment and negative normal stresses in sheared attractive emulsions. *Physical Review Letters* 92 (5): (058303-)1-4.
- (71) Butler, P. **1999**. Shear induced structures and transformations in complex fluids. *Current Opinion in Colloid and Interface Science* 4 (3): 214-221.
- (72) Radulescu, O.; Olmsted, P. D.; Decruppe, J. P.; Lerouge, S.; Berret, J. F.; Porte, G. **2003**. Time scales in shear banding of wormlike micelles. *Europhysics Letters* 62 (2): 230-236.
- (73) Vermant, J. **2001**. Large-scale structures in sheared colloidal dispersions. *Current Opinion in Colloid and Interface Science* 6 (5-6): 489-495.
- (74) Saito, S.; Hashimoto, T. **2001**. Critical conditions for structure formation in semidilute polymer solutions induced under continuous shear flow. *Journal of Chemical Physics* 114 (23): 10531-10543.
- (75) Eiser, E.; Molino, F.; Porte, G.; Diat, O. **2000**. Nonhomogeneous textures and banded flow in a soft cubic phase under shear. *Physical Review E* 61 (6): 6759-6764.
- (76) Ackerson, B. J.; Pusey, P. N. **1988**. Shear-induced order in suspensions of hard-spheres. *Physical Review Letters* 61 (8): 1033-1036.
- (77) Onuki, A. **1995**. Effects of shear-flow and viscosity difference on phase-separation. *International Journal of Thermophysics* 16 (2): 381-390.
- (78) Wang, S. Q. **1991**. Growth of dynamic polymers (micelles) in shear flow. *Macromolecules* 24 (10): 3004.
- (79) Grand, C.; Arrault, J.; Cates, M. E. **1997**. Slow transients and metastability in wormlike micelle rheology. *Journal De Physique Ii* 7 (8): 1071-1086.
- (80) Le Meins, J. F.; Tassin, J. F. **2001**. Shear-induced phase separation in an associating polymer solution. *Macromolecules* 34 (8): 2641-2647.

- (81) De Groot, J. V.; Macosko, C. W.; Kume, T.; Hashimoto, T. **1994**. Flow-induced anisotropic SALS in silica-filled PDMS liquids. *Journal of Colloid and Interface Science* 166 (2): 404-413.
- (82) Michele, J.; Patzold, R.; Donis, R. **1977**. Alignment and aggregation effects in suspensions of spheres in non-Newtonian media. *Rheologica Acta* 16: 317-321.
- (83) Wolf, B.; Frith, W. J.; Singleton, S.; Tassieri, M.; Norton, I. T. **2001**. Shear behaviour of biopolymer suspensions with spheroidal and cylindrical particles. *Rheologica Acta* 40 (3): 1435-1528.
- (84) Forster, S.; Konrad, M.; Lindner, P. **2005**. Shear thinning and orientational ordering of wormlike micelles. *Physical Review Letters* 94 (1): 17803-1-4.
- (85) Ganapathy, R.; Sood, A. K. **2006**. Tuning rheochaos by temperature in wormlike micelles. *Langmuir* 22 (26): 11016-11021.
- (86) Peighambardoust, S. H.; Van der Goot, A. J.; Hamer, R. J.; Boom, R. M. **2004**. A new method to study simple shear processing of wheat gluten-starch mixtures. *Cereal Chemistry* 81 (6): 714-721.
- (87) Macosko, C. W. **1994**. In *Rheology: Principles, measurements, and applications*; Wiley-VCH, New York: 550.
- (88) De Kruif, C. G. **1998**. Supra-aggregates of casein micelles as a prelude to coagulation. *Journal of Dairy Science* 81 (11): 3019-3028.
- (89) Dickinson, E.; Semenova, M. G.; Belyakova, L. E.; Antipova, A. S.; Il'in, M. M.; Tsapkina, E. N.; Ritzoulis, C. **2001**. Analysis of light scattering data on the calcium ion sensitivity of caseinate solution thermodynamics: Relationship to emulsion flocculation. *Journal of Colloid and Interface Science* 239 (1): 87-97.
- (90) Lucey, J. A.; Srinivasan, M.; Singh, H.; Munro, P. A. **2000**. Characterization of commercial and experimental sodium caseinates by multiangle laser light scattering and size-exclusion chromatography. *Journal of Agricultural and Food Chemistry* 48 (5): 1610-1616.
- (91) Hobbie, E. K.; Lin-Gibson, S.; Wang, H.; Pathak, J. A.; Kim, H. **2004**. Ubiquity of domain patterns in sheared viscoelastic fluids. *Physical Review E* 69 (6): (061503-)1-5.
- (92) Jaspe, J.; Hagen, S. J. **2006**. Do protein molecules unfold in a simple shear flow? *Biophysical Journal* 91 (9): 3415-3424.
- (93) Maa, Y. F.; Hsu, C. C. **1996**. Effect of high shear on proteins. *Biotechnology and Bioengineering* 51 (4): 458-465.
- (94) Van der Veen, M. E.; Van Iersel, D. G.; Van der Goot, A. J.; Boom, R. M. **2004**. Shear-induced inactivation of  $\alpha$ -amylase in a plain shear field. *Biotechnology Progress* 20 (4): 1140-1145.



- (95) Peighambardoust, S. H.; Van der Goot, A. J.; Hamer, R. J.; Boom, R. M. **2005**. Effect of simple shear on the physical properties of glutenin macro polymer (GMP). *Journal of Cereal Science* 42 (1): 59-68.
- (96) Peighambardoust, S. H.; Van der Goot, A. J.; Van Vliet, T.; Hamer, R. J.; Boom, R. M. **2006**. Microstructure formation and rheological behaviour of dough under simple shear flow. *Journal of Cereal Science* 43 183-197.
- (97) Van den Einde, R.; Van der Linden, E.; Van der Goot, A. J.; Boom, R. **2004**. A mechanistic model of the relation between molecular structure of amylopectin and macromolecular degradation during heating-shearing processes. *Polymer Degradation and Stability* 85 (1): 589-594.
- (98) Van den Einde, R. M.; Akkermans, C.; Van der Goot, A. J.; Boom, R. M. **2004**. Molecular breakdown of corn starch by thermal and mechanical effects. *Carbohydrate Polymers* 56 (4): 415-422.
- (99) Farrer, D.; Lips, A. **1999**. On the self-assembly of sodium caseinate. *International Dairy Journal* 9 (3-6): 281-286.
- (100) Ikeda, S.; Nishinari, K. **2000**. Intermolecular forces in bovine serum albumin solutions exhibiting solidlike mechanical behaviors. *Biomacromolecules* 1 (4): 757-763.
- (101) Larson, R. G. **1999**. In *The structure and rheology of complex fluids*; Oxford University Press, New York: 664.
- (102) Bimbenet, J.J.; Schubert, H.; Trystram, G. **2007**. Advances in research in food process engineering as presented at ICEF 9. *Journal of Food Engineering* 78 (2): 390-404.





## Summary

## **Introduction and objective**

Both health and sustainability are drivers for the increased interest in the creation of novel foods comprising a high protein content. Key challenge is the formation of an attractive, stable and palatable food texture. The perception of food texture is mainly influenced by the food structure.

The creation of food structures involves deformation to organize and assemble ingredients. In addition, solidification of the structures obtained is required to entrap these structures and to create products with a certain consistency. In general, food structure formation is the result of both ingredients and processing. The application of new ingredients in existing processes has been the focus in structure formation rather than the development of new processes. This has led to limitations with respect to the creation of innovative food structures. Therefore, the objective of this thesis is to explore new processing routes based on flow to create innovative protein structures, and in parallel to gain insight in the relevant mechanisms involved in structure formation of dense protein dispersions.

## **Structure formation of protein dispersions**

Random flow (mixing) and well-defined flow (shear flow) are applied to induce structures in dense sodium caseinate and calcium caseinate dispersions (> 10% w/w), ranging from isotropic to anisotropic structures. In most cases, a dispersed fat phase is included to mimic the complexity of food products. Enzymatic crosslinking using transglutaminase provides solidification of the created structures.

### ***Mixing and solidification***

**Chapter 3** describes the properties of sodium caseinate dispersions (10-30%) that are mixed and enzymatically crosslinked in the presence of palm fat. Changing the order of fat addition and solidification influences the structural properties of the protein-fat products to a large extent. Adding fat at the start of the process to the protein phase yields strong homogeneous products, as emulsification through mixing and solidification occurs simultaneously. Adding fat after mixing and

solidifying the protein phase first leads to a brittle structure because protein granules are formed, and subsequently surrounded by a concentrated fat phase.

### ***Well-defined flow and solidification***

The application of well-defined flow and enzymatic crosslinking induces fibrous structures in calcium caseinate dispersions (30%) in the absence of a dispersed phase (**Chapter 4**). The fibrous materials show anisotropy on both macroscale (visually) and microscale (fibers of ~100-200 nm). Both shear and crosslinking prove essential for creating fibrous protein structures, as only shearing yields a slightly anisotropic layered structure. Crosslinking in the absence of flow or during mixing results in products without alignment.

In the presence of fat, an additional scale (i.e. mesoscale) of structuring was induced in calcium caseinate dispersions (25-30%) using shearing and crosslinking (**Chapter 5**). The shear rate is an essential process parameter to control the formation of fibrous structures and the degree of fibrousnesses. Prolonged shear time results in the transition from a fibrous structure into a damaged structure accompanied by syneresis. The ratio between the solidification rate, in this case the crosslinking rate, and the shear rate influences the formation of fibrous structures, therewith indicating the importance of the subtle interplay between ingredient properties and process conditions for structure formation.

This conclusion is confirmed when calcium caseinate is replaced by sodium caseinate. The latter dispersion (30%) yields an isotropic material instead of a fibrous structure after shearing and crosslinking (**Chapter 6**).

### **Parallels between protein dispersions and model systems**

Parallels with model systems provide insight in the rheological properties of isotropic materials created from dense sodium caseinate dispersions in the presence of a dispersed phase. In addition, the formation of anisotropic structures from dense calcium caseinate dispersions using well-defined flow is compared with shear-induced structure formation of polymer systems.

### ***Isotropic protein structures: effect of a dispersed phase***

Models describing the effect of filler particles in composite materials prove useful to explain the rheological and mechanical properties of sodium caseinate products (30%) comprising various dispersed phases, being palm fat and glass spheres (**Chapter 2**). The products are prepared by mixing the ingredients at 40°C. The structural properties of the isotropic products are mostly influenced by the volume fraction of the dispersed particles. The type of particles, the (average) particle size and the surface properties hardly affect the rheological properties of the structures obtained. The interactions between sodium caseinate and the dispersed particles play an important role in the mechanical properties of the structures. It can be concluded that the relatively simple models comprising the relevant parameters can be applied for designing foods comprising a dispersed phase.

### ***Anisotropic protein structures***

Comparing the structure formation of calcium caseinate dispersions (15-30%) with polymer systems yields the factors that are essential for creating anisotropic structures using well-defined flow (**Chapter 6**): both the rheological properties and the thermodynamic properties of the systems are important for shear-induced structure formation. Exactly these properties provide insight in the difference between the structures obtained for calcium caseinate (anisotropic structures) and sodium caseinate (isotropic structures) after shearing and concurrent crosslinking.

The thermodynamic and rheological properties of protein dispersions provide parameters that can be applied to modify the susceptibility of protein dispersions to exhibit structure formation using well-defined flow. In addition, since the same parameters influence the rheological properties of ingredients in general, rheological measurements can prove useful to predict the structure formation.

### **Future outlook**

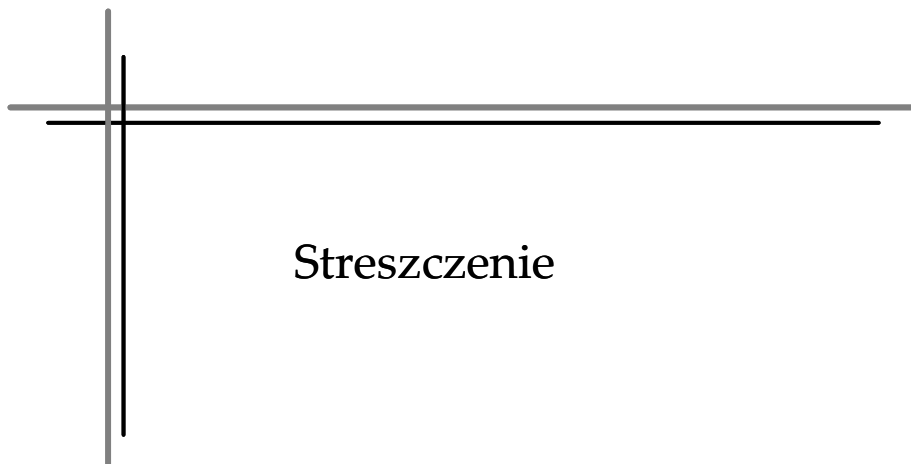
Matching the use of well-defined flow and specific initial ingredient properties will yield innovation in food structuring. Dedicated structuring equipment based on well-defined flow, therewith enabling the use of shear rate as design parameter, appears promising not only for acquiring scientific insights but also for producing

innovative food products (**Chapter 7**). The rheological and thermodynamic properties of the protein dispersions appear successful tools to estimate their performance during shearing. Therefore, future research should be devoted to characterize, quantify and understand these properties of dense protein dispersions in relation to their structure formation capabilities. Apart from further development of dedicated structuring equipment, also analytical techniques suitable to investigate dense protein dispersions should be extended, therewith enabling further exploration of parallels with polymer systems. Then, increasing scientific insights can be acquired and applied to create innovative foods.

## *Summary*

---





## Streszczenie

## **Wstęp i cel pracy**

Zarówno zdrowotność, jak i trwałość, są elementami, które powodują zwiększenie zainteresowania wytworzeniem nowych produktów spożywczych o wysokiej zawartości białka. Kluczowym zadaniem jest kształtowanie atrakcyjnej, stabilnej i smakowitej tekstury tych wyrobów. Odczuwanie cech tekstury jest w głównej mierze uzależnione od struktury żywności.

Kształtowanie struktury produktów spożywczych obejmuje uszkodzenie pierwotnej oraz ukształtowanie nowej struktury przez przegrupowanie składników funkcjonalnych żywności. W dodatku, zestalenie uzyskanej struktury jest niezbędne do jej utrwalenia oraz do kształtowania produktów o określonej konsystencji. Generalnie stwierdzić można, iż proces formowania struktury produktu jest wynikiem zarówno doboru składników, jak i metod jej kształtowania. Zastosowanie nowych składników w istniejącym procesie technologicznym zazwyczaj jest częściej stosowane w celu kształtowania struktury niż opracowywanie nowych technologii. Takie podejście musiało ograniczyć kreowanie innowacyjnej struktury produktów żywnościowych. Biorąc to pod uwagę, głównym celem prezentowanej rozprawy było opracowanie nowego procesu technologicznego opartego na zjawisku przepływu umożliwiającego kształtowanie innowacyjnej struktury białkowej i równolegle wnikliwe poznanie mechanizmów zaangażowanych w formowanie struktury skoncentrowanych dyspersji białkowych.

## **Wpływ deformacji oraz stężenia na kształtowanie struktury dyspersji białkowych**

Przepływ swobodny (mieszanie) oraz ściśle zdefiniowany (przepływ ścinający) zostały zastosowane do kształtowania struktury w skoncentrowanych dyspersjach kazeinianu sodu oraz kazeinianu wapnia (> 10% w/w), zmieniając strukturę izotropową na anizotropową. W większości przypadków do układu zostaje włączona rozproszona faza tłuszczowa w celu imitacji złożoności produktów żywnościowych. Enzymatyczne usieciowienie z zastosowaniem transglutaminazy umożliwia zestalenie i utrwalenie ukształtowanej struktury wewnętrznej.

### ***Mieszanie i zestalanie***

W **Rozdziale 3** opisano właściwości roztworu kazeinianu sodowego (10-30%) poddawanego mieszaniu oraz enzymatycznemu usieciowieniu w obecności tłuszczu palmowego. Zmiany spowodowane dodatkiem tłuszczu i procesem sieciowania miały duży wpływ na właściwości strukturalne produktów białkowo-tłuszczowych. Dodatek tłuszczu do frakcji białkowej na początku procesu umożliwił uzyskanie niezwykle jednorodnych produktów, zaś emulsyfikacja podczas mieszania oraz zestalanie produktu przebiegały równocześnie. Dodatek tłuszczu po wymieszaniu i zestaleniu fazy białkowej powodował w pierwszym etapie utworzenie kruchej struktury spowodowanej uformowaniem agregatów białka, a następnie ich otaczanie przez skoncentrowaną fazę tłuszczową.

### ***Określone warunki przepływu oraz stężenie***

Zastosowanie ściśle określonych warunków przepływu oraz enzymatycznego usieciowania spowodowało powstanie włóknistej struktury roztworu kazeinianu wapnia (30%) i brak fazy rozproszonej (**Rozdział 4**). Materiały włókniste wykazują charakter anizotropowy zarówno w skali makro (widzialna), jak również w mikroskali (włókna o długości ~100-200 nm). Zarówno siły ścinania, jak i usieciowanie wpływają w głównej mierze na tworzenie włóknistej struktury białkowej, jednakże tylko siły ścinania wywołują powstanie w niewielkim stopniu warstwowej struktury anizotropowej. Usieciowanie przy zastosowaniu niskich sił ścinających lub w czasie mieszania uniemożliwia uzyskanie wyrównanego produktu.

W obecności tłuszczu proces strukturyzacji 25-30% roztworów kazeinianu wapnia w tzw. mezoskali indukowano przez zastosowanie ścinania oraz usieciowania (**Rozdział 5**). Gradient szybkości ścinania jest zasadniczym parametrem umożliwiającym ściśle określone kontrolowanie formowanej struktury włóknistej oraz stopnia zwłóknienia. Wydłużenie czasu ścinania wpływa na zniszczenie struktury włóknistej, której towarzyszy zjawisko synerezy. Stosunek pomiędzy szybkością zestalania, w tym wypadku indeksem usieciowania, a indeksem ścinania (szybkością ścinania) wpływa na tworzenie struktury włóknistej, ze szczególnym uwzględnieniem ważnych wzajemnych oddziaływań pomiędzy

właścivościami składników i warunkami przetwarzania stosowanymi do kształtowania struktury.

Zależność ta została zaobserwowana również wtedy, gdy zamiast kazeinianu wapnia zastosowano kazeinian sodu. Roztwór tej drugiej substancji (30%) powoduje utworzenie materiału izotropowego w przeciwieństwie do pierwotnej struktury włóknistej po zastosowaniu ścinania i usieciowienia (**Rozdział 6**).

### **Analogie pomiędzy skoncentrowanymi roztworami białek a systemami modelowymi polimerów**

Porównanie z systemami modelowymi umożliwia zagłębienie się w zagadnienia związane z właściwościami reologicznymi materiałów izotropowych utworzonych ze stężonych roztworów kazeinianu sodu w obecności fazy rozproszonej. W dodatku formowanie struktury anizotropowej z roztworów kazeinianu wapnia o wysokiej lepkości z zastosowaniem ściśle określonych warunków przepływu jest porównywalne z wykorzystującym siły ścinania formowaniem struktury systemów polimerowych.

#### ***Struktura izotropowa białek: wpływ fazy rozproszonej***

Modele opisujące wpływ cząstek wypełniaczy w materiałach kompozytowych umożliwiają dokładne wyjaśnienie właściwości reologicznych i mechanicznych kazeinianu sodu (30%) w zależności od obecności fazy rozproszonej, którą może być tłuszcz palmowy oraz kulki szklane (**Rozdział 2**). Materiały są przygotowywane przez mieszanie składników w temperaturze 40°C. Cechy strukturalne otrzymanych produktów izotropowych zależały głównie od objętości frakcji rozproszonych cząstek. Rodzaj cząsteczek, ich wymiary liniowe i cechy powierzchniowe w zdecydowany sposób wpływały na właściwości reologiczne otrzymanej struktury. Interakcje pomiędzy kazeinianem sodu i fazą rozproszoną miały istotny wpływ na mechaniczne cechy otrzymanej struktury. W podsumowaniu stwierdzić można, iż relatywnie prosty model, obejmujący istotne parametry, może być z powodzeniem zastosowany do projektowania cech żywności zawierającej fazę rozproszoną.

### ***Anizotropowa struktura białek***

Porównując formowanie struktury przez roztwór kazeinianu wapnia (15-30%) z systemami polimerów uwidaczniają się czynniki, które są istotne podczas kreowania struktury anizotropowej z zastosowaniem zdefiniowanych warunków przepływu (**Rozdział 6**): zarówno właściwości reologiczne, jak i cechy termomechaniczne systemów są ważne podczas procesu kształtowania struktury spowodowanego działaniem sił ścinających.

Właśnie te właściwości decydują o zróżnicowaniu wewnętrznej struktury otrzymanej dla kazeinianu wapnia (struktura anizotropowa) oraz kazeinianu sodu (struktura izotropowa) po ścinaniu oraz równoczesnym usieciowieniu.

Termodynamiczne i reologiczne cechy roztworów białkowych warunkują dobór parametrów, które mogą być zastosowane w celu zmodyfikowania podatności roztworów białka na specyficzne kształtowanie struktury z zastosowaniem ściśle zdefiniowanych warunków przepływu ścinającego. Dodatkowo, dopóki identyczne parametry mają wpływ na cechy reologiczne ogółu składników, pomiary właściwości reologicznych mogą umożliwić sprawne ukształtowanie założonej struktury.

### **Spojrzenie w przyszłość**

Zastosowanie odpowiednio dobranych określonych warunków przepływu oraz specyficznych własności składników może być wykorzystane w aspekcie innowacyjności w strukturyzacji żywności. Zalecane wyposażenie wykorzystywane do kształtowania struktury, oparte na zasadzie zdefiniowanych warunków przepływu, umożliwiające zastosowanie indeksu ścinania jako głównego parametru, wydaje się obiecujące nie tylko w warunkach laboratoryjnych, ale także przy produkcji innowacyjnej żywności funkcjonalnej (**Rozdział 7**). Poznanie reologicznych i termomechanicznych właściwości dyspersji białkowych może stać się użytecznym narzędziem do określenia ich zachowania podczas ścinania. Oprócz tego dalsze badania powinny zostać poświęcone scharakteryzowaniu, określeniu ilościowemu i zrozumieniu tych cech skoncentrowanych roztworów białkowych, które warunkują zdolność formowania różnorodnej struktury.

Oprócz dalszego rozwoju aparatury umożliwiającej kształtowanie struktury żywności, powinny rozwijać się również metody analityczne przydatne w badaniach dyspersji białkowych o dużej lepkości, które mogą posłużyć do dalszego identyfikowania podobieństw z tworzywami sztucznymi. W wyniku tego pogłębi się naukowe podejście do problemu, zaś jego rozwiązanie może być wykorzystane do kreowania cech żywności innowacyjnej.



## Samenvatting

## Eiwitrijke producten

Veel levensmiddelen bevatten eiwitten. De hoeveelheid eiwit in een product kan sterk variëren, maar in sommige natuurlijke producten zoals kaas en vlees is het eiwitgehalte hoog (20-30%). Dit hoge eiwitgehalte zorgt ervoor dat het product min of meer vast is en dus een zekere consistentie heeft.

Vanwege de hoge kostprijs van eiwitten wordt het eiwitgehalte in producten vaak zo laag mogelijk gehouden. Echter, recentelijk zijn er aanwijzingen gevonden dat er aan de consumptie van eiwitrijke producten gezondheidsvoordelen verbonden zijn. Zo zouden consumenten sneller een verzadigd gevoel krijgen van eiwitrijk voedsel (belangrijk in verband met overgewicht) en zou het spiernmassaverlies bij ouderen beperkt kunnen worden. Vanuit dit oogpunt zou de consumptie van bijvoorbeeld kaas en vlees gestimuleerd moeten worden.

Echter, kaas en vlees hebben ook hun nadelen. Kaas bevat veel vet en de lange rijpingstijd tijdens de kaasproductie is vanuit een bedrijfseconomisch oogpunt niet gunstig. De productie van vlees vereist veel natuurlijke hulpstoffen zoals granen en water. Bovendien is een overmatige vleesconsumptie niet gezond. Zo ontstaat er dus een behoefte aan nieuwe eiwitrijke producten die gezonder zijn en slimmer geproduceerd kunnen worden. Tegenwoordig zijn er al een aantal eiwitrijke producten op de markt zoals vleesvervangers en eiwitrijke repen voor sporters. Helaas voldoen deze producten nog niet aan de wensen van de consumenten. Vleesvervangers hebben vaak nog geen goede beet en de eiwitrijke repen worden als droog en niet lekker beoordeeld.

Er zijn dus nieuwe methoden nodig om kwalitatief goede en lekkere eiwitrijke producten te maken. Het onderzoek dat beschreven staat in dit proefschrift laat een aantal nieuwe mogelijkheden zien om zulke producten te maken. In dit proefschrift is ook geprobeerd om meer inzicht te krijgen in deze nieuwe productiemethodes, omdat huidige processen voor de productie van levensmiddelen vaak empirisch van aard zijn. Dat wil zeggen dat deze processen proefondervindelijk verbeterd worden, maar dat ze tegelijkertijd niet helemaal begrepen worden en dus een 'black box' blijven.

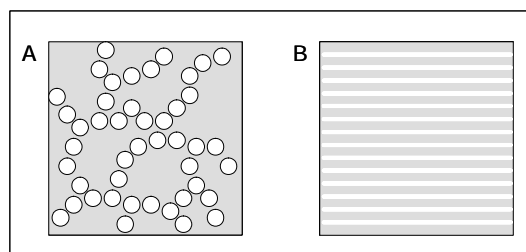


## De titel van het proefschrift

Nu de rol van eiwitten in dit proefschrift is toegelicht, zijn er nog twee kernwoorden in de titel van dit proefschrift, '**Het structureren van geconcentreerde eiwitoplossingen door vervorming**', die een nadere uitleg vragen, te weten *structureren* en *vervorming*.

### Structureren

Als de consument een product beoordeelt, wordt er vaak over de textuur van het product gesproken. Hoewel textuur een breed begrip is, hangt textuur nauw samen met de structuur van het product. De structuur van het product kan op verschillende groottes bekeken worden. De vorm en de uiterlijke kenmerken van een product die met het oog zichtbaar zijn (groter dan 1 mm) vormen de macrostructuur. Wat in de mond ervaren wordt, hangt samen met de mesostructuur (0.001 tot 1 mm) van het product. Deze mesostructuur wordt bepaald door nog kleinere bouwstenen: de microstructuur (kleiner dan 0.001 mm). Op deze schaal spelen moleculaire effecten een rol.



**Figuur 1** Schematische weergave van de netwerkstructuur van kaas (**A**) en de vezelstructuur van vlees (**B**).

Dit onderzoek richt zich vooral op de structuren op mesoschaal. Op deze schaal zijn er verschillende structuren mogelijk. In het geval van kaas is er sprake van een netwerkstructuur (Figuur 1A). De vetbolletjes lopen als een soort draad door de structuur. Voor de perceptie in de mond is de ordening van deze bolletjes belangrijk, wat verklaart dat het verwijderen van het vet tot sensorische veranderingen leidt. De structuur van vlees kenmerkt zich door lange vezels

(Figuur 1B). De vezels zorgen ervoor dat de eigenschappen van vlees niet in alle richtingen gelijk zijn. Dat laatste wordt anisotropie genoemd.

Structureren is uiteindelijk niets anders dan het aanbrengen van de structuur in het product. In de keuken gebeurt dat met roeren, kneden, hakken, etc. In industriële processen gaat het in principe op dezelfde wijze.

### ***Vervorming***

Producten moeten dus vervormd worden om de juiste ordening van ingrediënten plaats te laten vinden. Het bewerken van ingrediënten door middel van vervorming is terug te vinden in industriële apparaten zoals mixers en extruders. Als er gekeken wordt naar hoe het materiaal in zo'n industrieel apparaat vervormd wordt, dan blijkt dat de vervorming afhankelijk is van de positie van het materiaal in het apparaat. Hierdoor wordt niet alleen de uitkomst onvoorspelbaar, maar ook wordt wellicht de functionaliteit van ingrediënten in het product niet volledig benut. Indien we de vervorming van het product nauwkeurig kunnen instellen, zou dit hier meer mogelijkheden kunnen bieden.

Deze aanpak wordt al toegepast in het gebied van de reologie. Dat is de leer van de stroming van vloeistoffen en de vervorming van vaste materialen. Om reologische eigenschappen van materialen te meten, zoals viscositeit en stevigheid, wordt een nauwkeurige vervorming opgelegd. Dit wordt mogelijk gemaakt door het gebruik van speciaal ontworpen meetcellen waarin bijvoorbeeld een constante vervormingsnelheid (ofwel afschuifsnellheid) ingesteld kan worden. In dit proefschrift is deze reologische aanpak als uitgangspunt gebruikt om meer begrip te krijgen van de vervorming van eiwitrijke oplossingen en producten.

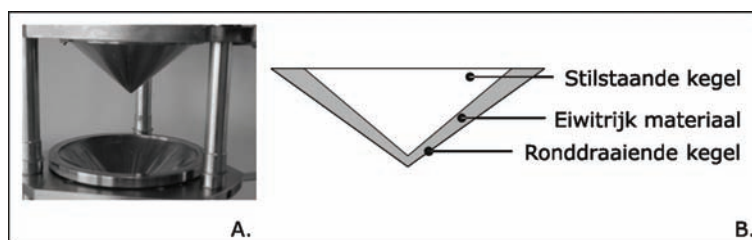
Er is nog een ander aspect dat een rol speelt bij het vervormen van producten. Het aanbrengen van structuur kan alleen als het product nog min of meer vloeibaar is. Als het product al te vast is, leidt vervorming tot schade aan het product. Het is dus zaak om het fixeren van een product en het structureren goed op elkaar af te stemmen. Bij het bakken van brood is dit dilemma opgelost door het structureren in een min of meer vloeibare fase te laten gebeuren (tijdens kneden). Door het bakken (verhitten) wordt de structuur vastgelegd in het eindproduct waarbij de eiwitten een belangrijke rol spelen.

Het structureren van eiwitoplossingen met een hoog eiwitgehalte (meer dan 10%) door vervorming is uitdagend omdat deze oplossingen erg stroperig (visceus) zijn. Bovendien stollen (geleren) veel eiwitten bij verhitting. Ze vereisen dus een bijzondere aanpak om verwerkt te worden tot producten met aantrekkelijke structuren.

### *Doel en aanpak onderzoek*

In dit proefschrift zijn nieuwe manieren voor het vervaardigen van structuren verkend om van geconcentreerde eiwitoplossingen innovatieve eiwitrijke producten te maken. Tegelijkertijd is geprobeerd inzicht te verkrijgen in de mechanismen die van belang zijn tijdens de structuurvorming van deze geconcentreerde eiwitoplossingen.

Het melkeiwit caseïnaat in een concentratie van 10-30% in water is als het uitgangsmateriaal gekozen. Naast twee types caseïnaat (natrium-caseïnaat en calcium-caseïnaat) is ook een plantaardig vet (palmvet) gebruikt om de complexiteit van echte levensmiddelen te benaderen. Het product is op twee manieren vervormd: door mengen en met behulp van goedgedefinieerde afschuiving zijn eiwitrijke structuren gemaakt. Om afschuiving toe te passen op stroperige eiwitoplossingen is een speciale afschuifreactor, de zogenaamde shear cell, ontwikkeld. De shear cell bestaat uit twee kegels waartussen het materiaal in een spleet van ongeveer 5 mm zit en waarvan de onderste kegel ronddraait (Figuur 2). Net als bij reologische meetcellen kan de afschuifsnelheid bij de shear cell ingesteld worden en wordt de weerstand (het koppel) gemeten.



**Figuur 2** Foto van de twee kegels van de shear cell (A) en een schematische weergave van de shear cell (B). De diameter van de ronddraaiende kegel is ongeveer 15 cm.

## Variatie in structuur door mengen

Verschillende structuren zijn bereid door het mengen van het eiwit natrium caseïnaat (concentratie 30%) en palmvet in een menger die normaal gesproken voor synthetische polymeren gebruikt wordt. Naast palmvet zijn ook glasbolletjes met verschillende groottes toegevoegd aan het eiwit om de invloed van modeldeeltjes op de structuur te bestuderen.

**Hoofdstuk 2** laat zien dat de aanwezigheid van beide type deeltjes, zowel vet als glasbolletjes, bijdraagt aan de stevigheid van de gehele structuur, mits er sprake is van goede hechting tussen het eiwit en de deeltjes. Modellen die vaak gebruikt worden om de invloed van deeltjes op de eigenschappen van composietmaterialen (zoals rubber en beton) te beschrijven blijken ook geschikt om de eigenschappen van deze eiwitrijke structuren te beschrijven.

**Hoofdstuk 3** beschrijft wat er gebeurt wanneer de vervorming en het fixeren van een product op elkaar afgestemd worden. Hiervoor zijn natrium-caseïnaatoplossingen (concentratie 10-30%) weer vervormd in een menger, samen met palmvet en het enzym transglutaminase. Het enzym geleert het eiwit natrium-caseïnaat, waardoor de structuur wordt vastgelegd. Door het veranderen van de volgorde van het geleren van het eiwit en het mengen van het palmvet met het eiwit zijn verschillende structuren verkregen. Zowel sterke, goedgemengde structuren als brosse structuren konden gemaakt worden door het aanpassen van de procesvolgorde. De verkregen brosse structuur vertoonde overeenkomsten met de netwerkstructuur van kaas.

## Nieuwe technologie: afschuiven

Een belangrijk resultaat van dit proefschrift is de toepassing van een nieuwe technologie om producten te maken die een vezelstructuur hebben. **Hoofdstuk 4** laat zien dat geconcentreerde oplossingen van calcium-caseïnaat (30%) na een behandeling van goedgedefinieerde afschuiving en gelering tot vezelstructuren leiden. De vezelige producten zijn niet alleen op het oog anisotroop, maar ook met de elektronenmicroscopie zijn vezels waargenomen die ongeveer 100 tot 200 nanometer dik zijn. Zowel afschuiving als gelering met het enzym transglutaminase blijken essentieel om deze nieuwe vezelstructuren te maken.

**Hoofdstuk 5** laat zien dat de toevoeging van palmvet aan de calcium-caseïnaatoplossing ervoor zorgt dat er na afschuiving en gelering lagen van palmvet en bundels van eiwitvezels gevormd worden. Dit is waargenomen op de mesoschaal. Tijdens het afschuiven blijkt de afschuifsnelheid in grote mate de vorming van de vezelstructuren te bepalen. De vezeligheid neemt toe wanneer de afschuifsnelheid toeneemt.

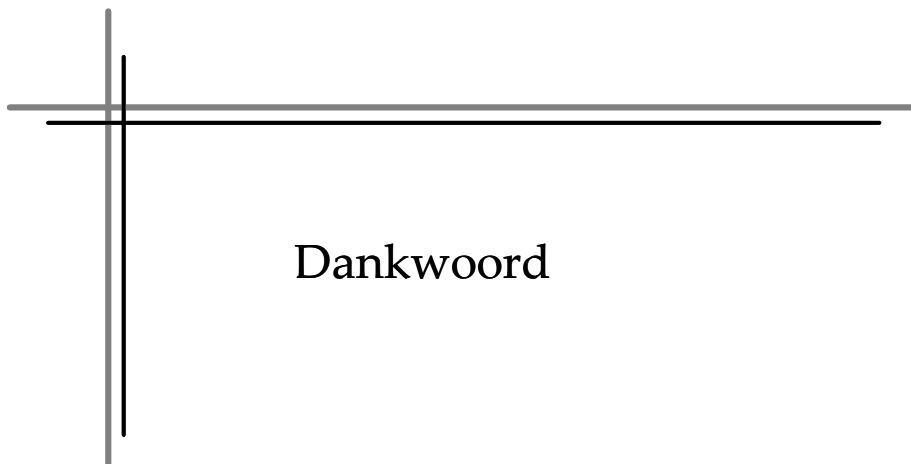
Wanneer calcium-caseïnaat vervangen wordt door natrium-caseïnaat blijkt hetzelfde proces van afschuiven en geleren niet tot vezelstructuren te leiden, maar tot goedgemengde structuren zonder enige ordening die met het oog waargenomen kan worden. **Hoofdstuk 6** laat zien dat specifieke eigenschappen van een eiwitoplossing belangrijk zijn voor de vorming van geordende vezelstructuren. Dit lijkt in overeenstemming te zijn met waarnemingen die gedaan zijn voor synthetische polymeeroplossingen.

## Hoe verder?

In toekomstig onderzoek kunnen juist deze specifieke eigenschappen, die sterk bepaald worden door moleculaire effecten van de eiwitten, beïnvloed worden om zo structuurvorming beter te controleren en te begrijpen. In deze benadering is het belangrijk dat de procescondities nauwkeurig worden afgestemd op de eigenschappen van het uitgangproduct. Dit maakt het proces wat gecompliceerder, maar het wordt wel mogelijk om optimaal gebruik te maken van de ingrediënten. Het laatste kan verder ondersteund worden door het uitbreiden van de wetenschappelijke basis waarbij we inzicht krijgen in wat er eigenlijk gebeurt tijdens nieuwe maar ook huidige structureringsprocessen (zoals afschuiven en mengen).

Naast het voortzetten van het leggen van een wetenschappelijke basis voor de structurering van eiwitrijke producten, dient ook de ontwikkeling van procesapparatuur gestimuleerd te worden. **Hoofdstuk 7** laat zien dat een nieuwe generatie procesapparatuur op basis van afschuiving bij zal dragen aan wetenschappelijke inzichten én aan de ontwikkeling van innovatieve producten. Al deze ontwikkelingen zullen ervoor zorgen dat we het maken van structuren beter gaan begrijpen en dat we in staat zijn om nieuwe aantrekkelijke producten te maken.





Dankwoord

Na iets meer dan vier jaar komt er toch echt een einde aan mijn promotieonderzoek... en dit proefschrift is daar het bewijs van! Voordat ik iedereen wil bedanken die in meer of mindere mate bijgedragen heeft aan mijn promotietijd, ben ik allereerst de lieve Heer dankbaar voor alle goede dingen die Hij mij elke dag weer geeft.

Al snel na mijn afstuderen kwam dit promotieonderzoek op mijn pad, en ik wil mijn begeleiders Atze Jan van der Goot en Remko Boom bedanken dat ik hieraan kon gaan werken. Atze Jan, heel erg bedankt voor je enthousiaste en motiverende begeleiding. Op de juiste momenten stimuleerde je me, remde je me wat af en plaatste je alles in het juiste perspectief. Ongelooflijk hoe je altijd weer tijd maakte om manuscripten snel van commentaar te voorzien. Ik heb er veel van geleerd en ik kijk met veel plezier terug op onze discussies over mijn onderzoek. Verder wil ik Anita en jou bedanken voor de gezellige etentjes die we met de Food Structuring groep bij jullie thuis hadden. Remko, je enthousiasme voor het onderzoek werkt aanstekelijk. Daarbij vind ik je creativiteit en je kijk op engineering erg inspirerend! Na de besprekingen met jou en Atze Jan had ik altijd een positief gevoel over mijn resultaten, hartelijk bedankt voor je inbreng en je motivatie.

Mijn promotieonderzoek is mogelijk gemaakt door Friesland Foods in het kader van een EET project. In het bijzonder wil ik Marcel Paques, Jaap de Slegte, Frank Jeurissen en Tjeerd Jongsma van Friesland Foods bedanken voor de prettige samenwerking. Ook de Food Physics groep van Wageningen Universiteit maakte deel uit van het EET project. Hilde, ik vond het leuk dat je tegelijkertijd met mij je promotieonderzoek deed. Bedankt voor het delen van ervaringen en alvast veel succes met je verdediging. Ik wil je begeleiders Paul Venema en Erik van der Linden bedanken voor inhoudelijke discussies tijdens de projectbesprekingen.

Zonder mijn studenten, Loes Hulshof, Ivo Kretzers, Lieke van Riemsdijk en Elsbeth van der Zalm zou dit proefschrift nooit zo dik geworden zijn! Heel erg bedankt voor jullie enthousiaste inzet en voor jullie mooie resultaten die bijna allemaal een plek hebben gevonden in dit proefschrift! Loes en Ivo werden experts op het gebied van composietmaterialen (Hoofdstuk 2) terwijl Lieke en Elsbeth verrassende resultaten boekten met calcium caseïnaat (Hoofdstukken 5 en 6). Ernesto Altman, thank you for your work on transglutaminase; it inspired us for



Chapter 3. Elsbeth, bedankt voor je opmerkzaamheid toen je proefjes aan het doen was: het vinden van de vezelstructuren heeft veel teweeggebracht!

Veel mensen hebben ervoor gezorgd dat ik experimenten kon doen. De mannen van de werkplaats, in het bijzonder Jan, Hans en André, bedankt voor het bouwen van de shear cell en voor jullie geweldige service. Harry Baptist, Adriaan van Aelst, Boudewijn van Veen, Jos Sewalt, Bas Kuipers, Christopher Klein en iedereen die meegewerkt heeft bij het opzetten en uitleggen van experimenten en (meet)apparaten: bedankt! Hylke, bedankt voor de mooie foto's die je van de eiwitstructuren gemaakt hebt. Gerrit en Pieter, bedankt voor de PC ondersteuning.

Ik wil mijn (oud-)collega's van de Food Structuring groep bedanken voor de enthousiaste sfeer en voor de discussies over shear cellen, shear leader en structureren. Mark, eerst was je mijn begeleider, later mijn collega. Ik zag je toen een beetje als mijn voorbeeld! René, bedankt voor alle weetjes over de shear cell. Saskia, ik vond het leuk om samen in het begin van mijn onderzoek nieuwe apparatuur te leren kennen/ontwikkelen. Bedankt voor al je hulp in het lab. Het samen uitlopen van de Nijmeegse wandel vierdaagse in 2004 was een mooie ervaring! Cynthia, we begonnen tegelijkertijd met studeren in Wageningen, en jij bent nu de volgende die bij Atze Jan gaat promoveren. Bedankt voor de gezelligheid tijdens cursussen en buitenlandse congressen. Ik vind het erg leuk dat je mijn paranime wilt zijn! Michel, veel succes in je loopbaan! Hadi, I enjoyed our discussions about doing experiments and interpreting data. Edwin, I appreciate your sincerity and our nice conversations about work- and non-work-related topics. Elsbeth en Lieke, ik vind het leuk dat jullie collega's zijn geworden, veel succes met jullie onderzoeken!

We also had guest scientists in the Food Structuring group. Donatella Peressini, thank you for your advice on rheological measurements. Agnieszka Wojtowicz, thank you very much for translating the summary into Polish. Chcę Ci bardzo gorąco podziękować, że znalazłaś trochę czasu na przetłumaczenie tekstu na język polski. Jestem Ci bardzo wdzięczna. Mile wspominam nasze spotkanie u Ciebie w Lublinie i Twoją wizytę u nas na Uniwersytecie. Jeszcze raz dziękuję Ci za pomoc i gościnność.

Ik heb vier jaar in de mooiste aio-kamer van de 6<sup>e</sup> verdieping gezeten en ik wil al mijn kamergenoten, Marieke B., Janneke, Judy, Hadi, Jan en Edwin bedanken voor

de gezellige sfeer. Judy, ik vond de etentjes en de sportieve avonden erg gezellig! Jan, je bent de beste plantenverzorger die ik ken! Edwin and Hadi, I enjoyed the fact that you brought an international atmosphere to our room!

Ik heb me de afgelopen vier jaar thuis gevoeld bij Proceskunde. Ik wil daarvoor *iedereen* van Proceskunde bedanken! Alle borrels, labuitjes en We-days waren ontzettend leuk. Ik vond het gezellig om het labuitje (met het mooiste weer!) in 2004 te organiseren met Martin, Saskia en Gerben. De aio-reizen naar Canada en Denemarken/Zweden waren super. Ik heb erg genoten van de reis die we (Sandra, Cynthia, Marleen, Janneke, Jan, Daniel, Olivier en Hylke, bedankt!) na het officiële programma in Canada gemaakt hebben. Ik had geen gebrek aan sportieve activiteiten met collega-aio's. Sebastiaan H. en Gerben, het was lastig om te winnen met squash, maar het was wel erg leuk! Het hardlopen met Judy en Tim was kortstondig maar gezellig; later heb ik het lopen opgepakt met Marieke K. wat voor de nodige ontspanning gezorgd heeft tijdens 'de laatste loodjes'.

Buiten het onderzoek doen, was er gelukkig ook ruimte voor andere dingen. Hilde, Paula en Ruth, bedankt voor de gezellige avondjes en weekendjes weg! Het is altijd leuk om bij een spelletje en glaasje wijn bij te komen! Marieke, ik vind onze bijkletsavondjes heel gezellig. Alle huisgenoten van Herenstraat 14: bedankt voor de gezelligheid thuis! Iedereen van de Bijbelgroep van de R.K. Kerk in Wageningen: bedankt voor de inspirerende discussies.

Lieve Ma en Pa, bedankt voor alles... voor jullie liefde, steun en stimulans om door te leren en iets te bereiken. De avondjes thuis zijn heerlijk. Hanna, bedankt voor de gezellige uitjes (concerten!) en het kletsen over alles en niks. Sylwester, met jou kan ik een beetje meepraten over technische zaken! Ik ben blij dat je mijn paranimf wilt zijn. Moniek, bedankt voor je gezelligheid! Familie van Oosten, bedankt voor de leuke tijd die we in Brazilië hebben gehad en voor jullie gastvrijheid.

Lieve René, bedankt voor je luisterende oor, voor je scherpheid en vooral voor je liefde! Mijn promotietijd is er alleen maar mooier van geworden omdat ik het grootste gedeelte met jou heb kunnen delen. Ik ben daar heel dankbaar voor en ik kijk uit naar alles wat we samen nog mogen meemaken!

*Julita\**



Publication List

Training Activities

Curriculum Vitae

## Publication List

Manski, J.M.; Van der Goot, A.J.; Boom, R.M. **2007**. Advances in structure formation of anisotropic protein-rich foods through novel processing concepts. *Submitted*.

Manski, J.M.; Van Riemsdijk, L.E.; Van der Goot, A.J.; Boom, R.M. **2007**. Factors influencing shear-induced anisotropy in dense caseinate dispersions. *Submitted*.

Manski, J.M.; Van der Zalm, E.E.J.; Van der Goot, A.J.; Boom, R.M. **2007**. Influence of process parameters on formation of fibrous materials from dense caseinate dispersions and fat. *Food Hydrocolloids*: in press.

Manski, J.M.; Van der Goot, A.J.; Boom, R.M. **2007**. Formation of fibrous materials from dense caseinate dispersions. *Biomacromolecules*: in press.

Manski, J.M.; Van der Goot, A.J.; Boom, R.M. **2007**. Influence of shear during enzymatic gelation of caseinate-water and caseinate-water-fat systems. *Journal of Food Engineering* 79 (2): 706-717.

Manski, J.M.; Kretzers, I.M.J.; Van Brenk, S.; Van der Goot, A.J.; Boom, R.M. **2007**. Influence of dispersed particles on small and large deformation properties of concentrated caseinate composites. *Food Hydrocolloids* 21 (1): 73-84.

Manski, J.M.; Matsler, A.L.; Siebenmorgen, T.J. **2005**. The influence of storing high moisture content rough rice on subsequent drying characteristics and milling quality. *Cereal Chemistry* 82 (2): 204-208.

### Conference proceeding

Manski, J.M.; Van der Goot, A.J.; Boom, R.M. **2006**. Influence of processing on rheology and microstructure of caseinate composites. *Proceedings 4<sup>th</sup> International Symposium on Food Rheology and Structure* (ISFRS), Zurich: 251-255.

### Book chapter

Van der Goot, A.J.; Manski, J.M. **2007**. Creation of novel microstructures through processing: structure formation in (semi-)solid food materials. In *Understanding and controlling the microstructure of complex foods*; McClements, D.J., Ed., Woodhead Publishing Limited, Cambridge: in press.

### Patent

Manski, J.M.; Van der Zalm, E.E.J.; Boom, R.M.; Van der Goot, A.J.; Nieuwenhuijse, J.A.; Paques, M. **2006**. *Fibrous food material*. P78438EP00.

## Training Activities

### *Discipline specific courses*

Unified Approach to Mass Transfer (OSPT, 2003)

Particle Based Modelling of Transport Phenomena (OSPT, 2003)

Industrial Proteins (VLAG, 2003)

Numerical Methods in Chemical Engineering (OSPT, 2004)

Polymer Processing (OSPT, 2004)

Macroscopical Physical Chemistry (Han-sur-Lesse Winterschool, 2005)

Rheological Measurements (KU Leuven, 2005)

Introduction to Star CD (CD Adapco, 2005)

### *General courses*

Scientific Writing (Wageningen University, 2004)

Organising and Supervising M.Sc. Thesis Projects (Wageningen University, 2004)

Philosophy and Ethics of Food Science and Technology (VLAG, 2006)

Career Perspectives (Wageningen Graduate Schools, 2006)

### *Meetings*

Brainstorm Week Food and Bioprocess Engineering (2003 and 2005)

Ph.D. Study Tour Canada (2004)

Ph.D. Study Tour Denmark and Sweden (2006)

3<sup>rd</sup>, 4<sup>th</sup>, 5<sup>th</sup>, 6<sup>th</sup> Netherlands Process Technology Symposium (2003, 2004, 2005 and 2006\*)

4<sup>th</sup> International Symposium on Food Rheology and Structure (Switzerland, 2006\*)

3<sup>rd</sup> Annual European Rheology Conference (Crete, 2006\*)

\*Oral presentation

## **Curriculum Vitae**

Julita Maria Manski werd op 15 juni 1979 geboren te Kartuzy in Polen. In 1997 behaalde zij haar Gymnasium diploma aan het Reynaertcollege te Hulst. In datzelfde jaar begon ze met de studie levensmiddelentechnologie aan Wageningen Universiteit. Ze specialiseerde zich in de richtingen Levensmiddelenproceskunde en Meet-, Regel- en Systeemtechniek. In 2001 voerde ze een stage uit aan de University of Arkansas in Fayetteville (Arkansas, U.S.A.). In 2002 liep ze stage bij de Research en Development afdeling van H.J. Heinz Company in Pittsburgh (Pennsylvania, U.S.A.). In november 2002 behaalde ze haar ingenieursdiploma. Van februari 2003 tot en met mei 2007 voerde ze een promotieonderzoek uit bij de sectie Proceskunde aan Wageningen Universiteit. De resultaten hiervan zijn beschreven in dit proefschrift.

Julita Maria Manski was born in Kartuzy in Poland on the 15<sup>th</sup> of June in 1979. In 1997 she graduated from secondary school, the Reynaertcollege in Hulst. In the same year she enrolled in the Food Science and Technology program at Wageningen University. She specialized in Food Process Engineering and in Systems and Control. In 2001 she conducted an internship at the University of Arkansas in Fayetteville (Arkansas, U.S.A.). In 2002 she completed an internship at the Research and Development department of H.J. Heinz Company in Pittsburgh (Pennsylvania, U.S.A.). In November 2002 she graduated from Wageningen University with a M.Sc. degree. From February 2003 until May 2007 she worked as a Ph.D. student in the Food and Bioprocess Engineering group at Wageningen University. The results of her Ph.D. research are described in this thesis.

This research was supported with a grant of the Dutch Programme EET (Economy, Ecology, Technology), a joint initiative of the Ministries of Economic Affairs, Education, Culture and Sciences and of Housing, Spatial Planning and the Environment. The programme is managed by the EET Programme Office, SenterNovem.

